SPI Scientific Team Meeting

CESR - Toulouse, June 11-13, 2003

How and Where getting in touch with the Participants

				
ATTIE D.	CEA	(33) 1 69 08 15 47	(33) 1 69 08 65 77	attie@cea.fr
BLAY P.	GACE	(34) 96 354 36 79	(34) 96 354 36 77	pere.blay@uv.es
BOUCHET L.	CESR	(33) 5 61 55 86 03	(33) 5 61 55 66 51	bouchet@cesr.fr
CAMERO A.	GACE	(34) 96 354 36 11	(34) 96 354 32 61	Ascension.Camero@uv.es
CORDIER B.	CEA	(33) 1 69 08 27 92	(33) 1 69 08 65 77	bcordier@cea.fr
DIEHL R.	MPE	(49) 89 30000 3850	(49) 89 30000 3569	rod@mpe.mpg.de
DUBATH P.	ISDC	(41) 22 950 9124	(41) 22 950 9133	dubath@obs.unige.ch
DUROUCHOUX Ph.	CEA	(33) 1 69 08 33 76	(33) 1 69 08 65 77	pdurouchoux@ cea.fr
JEAN P.	CESR	(33) 5 61 55 67 44	(33) 5 61 55 66 51	jean@cesr.fr
KNODLSEDER J.	CESR	(33) 5 61 55 66 63	(33) 5 61 55 67 01	knodlseder@cesr.fr
LARIGAUDERIE C.	CNES	(33) 5 61 28 21 99	(33) 5 61 28 23 50	larigauderie@cnes.fr
LELEUX P.	Univ. Louvain	(32) 10 47 32 29	(32) 10 45 21 83	leleux@fynu.ucl.ac.be
LONJOU V.	CESR	(33) 5 61 55 66 47	(33) 5 61 55 66 51	lonjou@cesr.fr
MANDROU P.	CESR	(33) 5 61 55 66 42	(33) 5 61 55 66 51	mandrou@cesr.fr
MAURIN D.	CEA			dmaurin@cea.fr
ROQUES J.P.	CESR	(33) 5 61 55 64 53	(33) 5 61 55 66 51	roques@cesr.fr
SCHANNE S.	CEA	(33) 1 69 08 15 47	(33) 1 69 08 65 77	schanne@hep.saclay.cea.fr
SCHÖNFELDER V.	MPE	(49) 89 30000 3578	(49) 89 30000 3606	vos@mpe.mpg.de
SIZUN P.	CEA	(33) 1 69 08 27 92	(33) 1 69 08 65 77	sizun@discovery.saclay.cea.fr
SKELTON T.	UCSD	(1) 858 534 09 62	(1) 858 534 22 94	rskelton@ucsd.edu
SKINNER G.	CESR	(33) 5 61 55 85 61	(33) 5 61 55 66 51	skinner@cesr.fr
STRONG A.	MPE	(49) 89 30000 3575	(49) 89 30000 3606	aws@mpe.mpg.de
STURNER S.	GSFC	(1) 301 286 8447	(1) 301 286 1684	sturner@swati.gsfc.nasa.gov
TEEGARDEN B.	GSFC	(1) 301 286 5277	(1) 301 286 1684	bonnard@lheamail.gsfc.nasa.gov
TEXIER D.	ESA	(41) 22 950 91 48	(41) 22 950 91 33	Damien.Texier@rssd.esa.int
VON BALLMOOS P.	CESR	(33) 5 61 55 66 47	(33) 5 61 55 66 51	pvb@cesr.fr
VON KIENLIN A.	MPE	(49) 89 30000 3514	(49) 89 30000 3606	azk@mpe.mpg.de
WEIDENSPOINTNER G.	CESR (GSFC)		(33) 5 61 55 66 51	georg.weidenspointner@cesr.fr
WUNDERER C.	MPE	(49) 89 30000 3858	(49) 89 30000 3606	cow@mpe.mpg.de

RAMON P. *SPI Project Assistant*	*(33) 5 61 55 66 88*	*(33) 5 61 55 66 51*	*Pascale.Ramon@cesr.fr*

AGENDA

Wednesday 11 - 14h00/17h00

A & A Special Issue

- Status report on the paper on :

- SPI instrumental lines	10'	G. Weidenspointner
- SPI background	10'	P. Jean
- Maximum entropy imaging	10'	A. Strong
- SPI Simulations and Response Generation	10'	S. Sturner
- Determining Imaging performance for extended emission and high-energy sources with the SPI Test Setup	10'	C. Wunderer
- SPI GRB detection capabilities - GRB030320	10'	A. von Kienlin
- Galactic diffuse continuum emission	10'	A. Strong
- SPI ground calibrations	10'	D. Attié
- SPIROS	10'	G. Skinner
- First results from GPS - SPI input	10'	A. Strong
- SPI data analysis methods	5'	R. Diehl
- Neutron-induced reactions and degradation	Email + Paper Copy	From P. Leleux

- SPI Authors list philosophy

Thursday 12

Hardware status

9h30 – 9h50	Camera status and next annealing	J.P. Roques
9h50 – 10h05	ACS status	A. von Kienlin
10h05 – 10h15	PSD status	J. Knödlseder
10h15 – 10h25	PSD status from PSD designers	UCSD
10h25 – 10h35	onboard PSD setup and actions for the future	J.P. Roques/all
10h35 – 10h45	Telemetry usage	S. Schanne
10h45 – 11h05	*Coffee Break*	
11h05 – 11h15	Telemetry reduction	C. Larigauderie

ISDC and ISDAG Status

11h15 – 11h30	Status of the ISDC SPI analysis software	P. Dubath
11h30 – 11h35	Analysis Software: Status and Maintenance	R. Diehl
11h35 – 11h40	Data Access for Analyses	R. Diehl

Calibration & Instrument Performances

11h40 – 11h55	SPI Spectral Analysis: Comparison of Methods	S. Sturner
11h55 – 12h10	Energy calibration and scientific validation (incl.misalignement)	P. Dubath
12h10 – 12h25	Report on pointing offset	G. Skinner/L. Bouchet
12h25	*Lunch*	
14h00 – 15h10	Energy response :	

- New results at low energy from BLC calibrations	15'	B.Cordier
- New version of the response	15'	S. Sturner
- Crab spectrum stability	15'	L. Bouchet
- Spectral analysis problem	15'	B. Cordier
- SPI/ISGRI spectral comparison	10'	B. Cordier

15h10 – 15h25	Justification for new crab observation	All
15h25 – 15h40	Energy calibration	Ph. Paul
15h40 – 15h50	Background line studies, energy resolution	R. Diehl
15h50 – 16h05	The distribution of SPI background events in lines and continuum for the singles and the multiples	C. Wunderer for E.Kalemci
16h05	*Coffee Break + Discussion*	

Friday 13

Scientific results

9h30 – 9h40	GCDE 26Al	R. Diehl
9h40 – 9h50	GRB Analysis	A. von Kienlin
9h50 – 10h00	Galactic Diffuse Emission	A. Strong
10h00 – 10h10	GCDE investigations with SPIROS: Line Sources in 44Ti	A. von Kienlin
10h10 – 10h20	Diffuse Line Emission, 26Al and 60Fe	C. Wunderer
10h20 – 10h30	Preliminary results of a search for the galactic 60Fe line	A. von Kienlin for G. Lichti
10h30 – 10h50	*Coffee Break*	
10h50 – 11h10	Diffuse gamma-ray line emission	J. Knödlseder
11h10 – 11h25	Galactic 511 keV line results	P. Jean

MGGPOD Code: Update

Two additional quantities are available for each energy deposit:

- **The kinetic energy of the primary cosmic-ray proton to assess variation with the solar cycle.**
  For radioactive decays, this energy is determined from a probability distribution that is created during the simulation of activation.
- **The physical time-scale of the process that resulted in an energy deposit to assess short and long term variations, e.g. of the instrumental 511 keV line.**
  For prompt processes this time is set to 1 ns.
  For radioactive decays this time is set to the half-life of the parent isotope.

Status of Line Identifications

Progress since last meeting:

- **Processed data with stable instrument configuration to allow meaningful determination of line count rates and quantitative comparisons with simulations.**
- **To better resolve blends, many isotope which give rise to more than one line have been simulated individually. These isotope templates are now used to define line ratios and to resolve line blends.**
- **A new line list should be available soon.**

A&A Special Edition contributions:

1. SPI Imaging with Maximum Entropy method

2. Diffuse Galactic continuum emission

3. GPS (SPI input)

A&A special: Diffuse Galactic Continuum Emission

Original title:
Diffuse Continuum from Cygnus region
but seems to be little continuum in Cygnus (concentrated to inner Galaxy)

Proposed title:
First results on Diffuse Continuum from the inner Galaxy
(agreed by Chris Winkler)

Signal is large, spectrum robust.
Consistent with previous experiments.

A&A special:
Maximum Entropy Skymapping

1. Describe method

2.1 Illustrate with simulations

2.2 BLC example:
2 sources:

2.3 Flight data examples

Cygnus region: test case

GCDE: many sources,
good test, illustrates performance

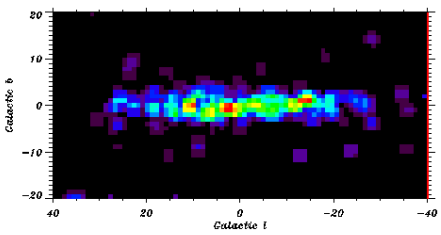

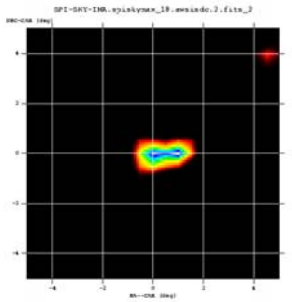

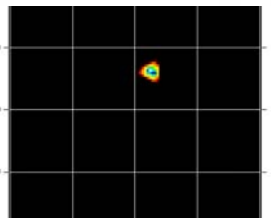

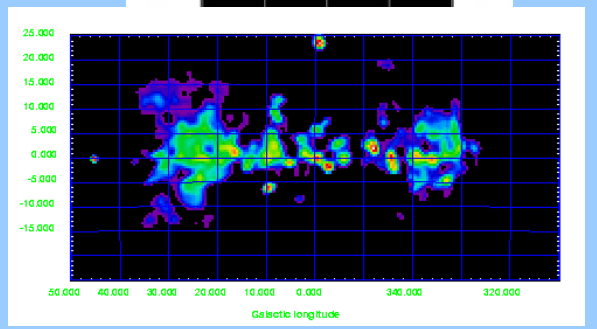

A&A special GPS

Winkler et al.
GPS revolution 25 - 51; SPI results on consolidated data
Input from SPI:
spiros (Beckmann) source list, >3σ, source map

Results from 8 combined GPS scans, with in total 87 pointings and 190ksec ONTIME.
Sources located in a single energy bin from 20.0 to 40.0 keV

no	source		(ph/cm2/sec)	sigma	(L-deg)	(B-deg)
2	1516-569	C	0.5611E-02	4.6	-37.882	0.038
8	2CG_135+01	C	0.6570E-02	9.0	134.892	2.075
10	2CG_311-01	C	0.4286E-02	4.2	-47.612	1.234
11	3C_111	C	0.4848E-02	3.0	161.674	-8.817
18	Cen_X-3	C	0.5056E-02	5.9	-67.910	0.336
19	Crab	C	0.1538	113.9	-175.442	-5.784
20	Cyg_X-1	C	0.7415E-01	50.4	71.335	3.067
21	Cyg_X-2	C	0.7092E-02	4.0	87.329	-11.316
22	Cyg_X-3	C	0.2273E-01	17.7	79.846	0.700
23	GRO_J0422+32	C	0.2972E-01	4.9	165.881	-11.913
24	GRO_J1008-57	C	0.2961E-02	3.7	-77.002	-1.822
30	GS_0834-43	C	0.1366E-01	6.0	-97.982	-1.510
31	GX_301-2	C	0.1263E-01	13.1	-59.902	-0.035
36	Geminga	C	0.3979E-02	3.0	-164.864	4.269
42	H1624-490	C	0.1440E-01	7.3	-25.080	-0.257
43	H1636-536	C	0.1102E-01	6.4	-27.085	-4.818
44	H1705-440	C	0.4701E-01	3.2	-16.678	-2.342
49	OAO_1657-415	C	0.3143E-01	6.2	-15.646	0.311
52	PSR_B1259-63	C	0.3742E-02	4.0	-55.816	-0.996
57	Vela_X-1	C	0.8164E-02	5.7	-96.942	3.930
58	XTE_J1650-500	C	0.1141E-01	5.1	-23.282	-3.427
60	SOURCE-60	N	0.4689E-01	11.5	297.242	16.591
61	SOURCE-61	N	0.7440E-02	7.3	304.748	-10.078
62	SOURCE-62	N	0.8029E-02	6.9	282.633	8.893

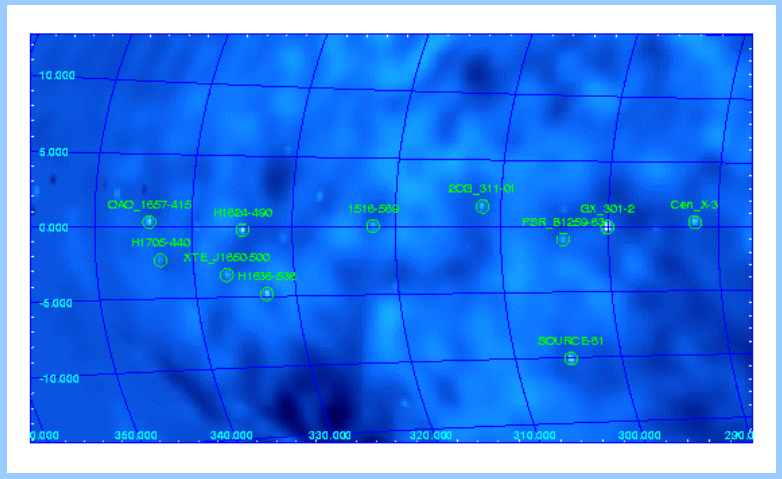

Spiros sources 20-40 keV

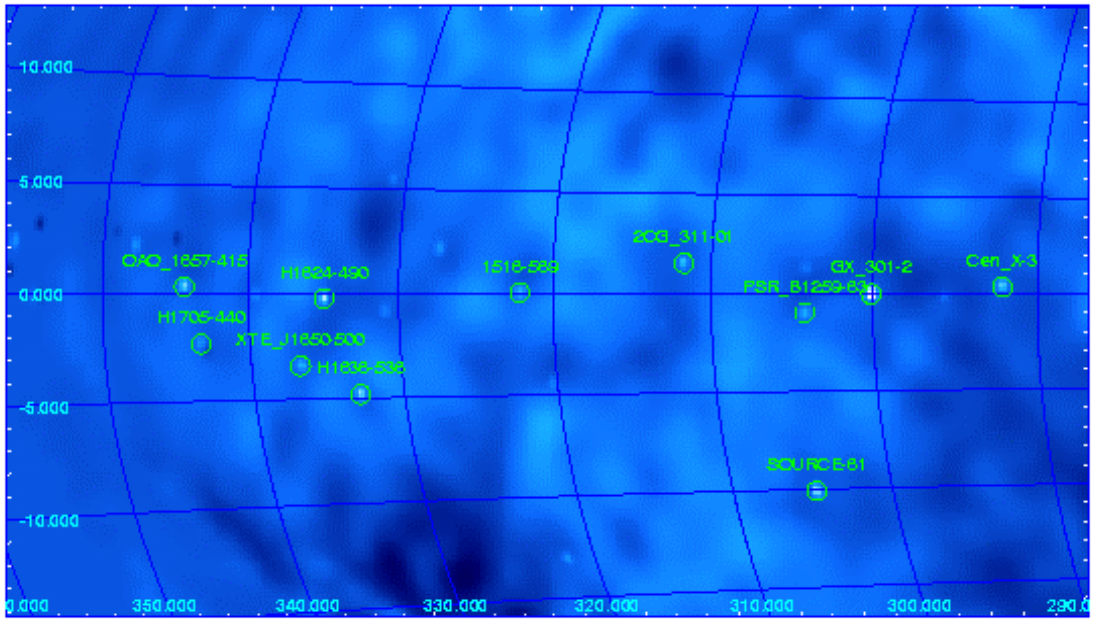

A&A special: GPS

Input from SPI (continued):
12 known sources >5σ,
3 unknown sources which need further study

spiskymax image ? – to illustrate GPS as GCDE extension

Detectability of 511 keV line transients
(Wunderer, Schoenfelder,Beckmann)

Ref.	Line Flux [keV]	Line FWHM [keV]	SPI sens. (optimum) [ph/(cm^{2}s)]	SPI sens. (intermed.) [ph/(cm^{2}s)]	Observed Flux [ph/(cm^{2}s)]
1E1740.7 - Oct 1990 Event					
Bur91	480	240	$7.7 \cdot 10^{-4}$	$10. \cdot 10^{-4}$	$13. \cdot 10^{-4}$
Sun91	410	160	$6.2 \cdot 10^{-4}$	$8.4 \cdot 10^{-4}$	$(9.5 \pm 4.5) \cdot 10^{-4}$
1E1740.7 - Sept 1992 Event					
Cru93	350	170	$5.5 \cdot 10^{-4}$	$7.5 \cdot 10^{-4}$	$4.3^{+2.7}_{-1.4} \cdot 10^{-4}$
1E1740.7 - Oct 1990 and Sept 1992 Events combined					
Cru93	390	190	$6.5 \cdot 10^{-4}$	$8.8 \cdot 10^{-4}$	
Nova Muscae - Jan 1991 Event					
Gol93	461	54	$3.9 \cdot 10^{-4}$	$5.3 \cdot 10^{-4}$	$(6.0 \pm 2.9) \cdot 10^{-4}$

Table 1: SPI estimated sensitivities in one GPS scan to broadened line features at 350–500 keV as observed by SIGMA. See text for details.

Galactic plane is intense source of hard X-rays/soft γ-rays
luminosity 10^{38} erg s^{-1}

Detected by RXTE, ASCA, OSSE

Origin unclear:
* unresolved souces: no known source population
* thermal : too high pressure in ISM
* non-thermal electron bremsstrahlung, energy required ~ 10^{41} erg s^{-1}
because of ionization losses

one possibility: in-situ acceleration of quasi-thermal“ electrons
(e.g. talk by Vladimir Dogiel last year,
Dogiel,Inoue, Masai,Schoenfelder,Strong ApJ 581 2002)

A major goal of INTEGRAL is to study this emission.
AWS is a Responsible Scientist for analysis of Core Time Data on this topic.

First complete GCDE scan available, rev. 46 -66

What can INTEGRAL do better for diffuse continuum emission ?

* identify & remove point sources >100 keV (cf OSSE had no imaging)

* imaging of Galactic ridge > 100 -1000 keV (never done before)

* wide energy range (20 keV - few MeV, cf RXTE 3-30 keV)

* high energy resolution: spectral features (better than OSSE, COMPTEL)

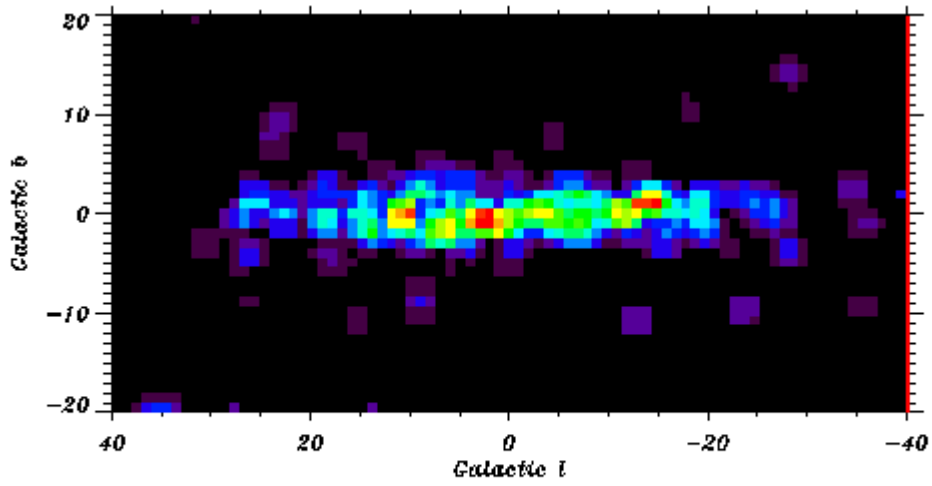

GCDE simulation
200-400 keV

Spectrum of Galactic ridge continuum

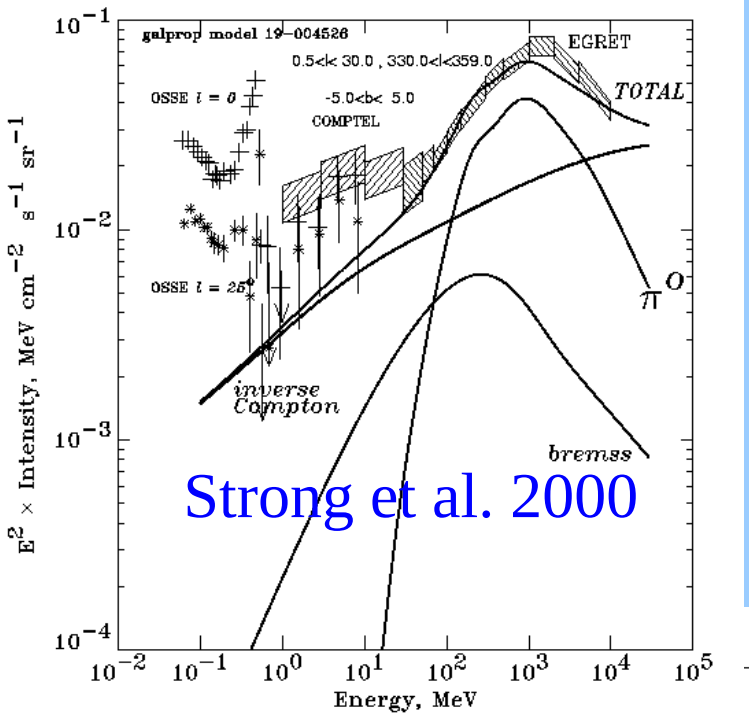

Strong et al. 2000

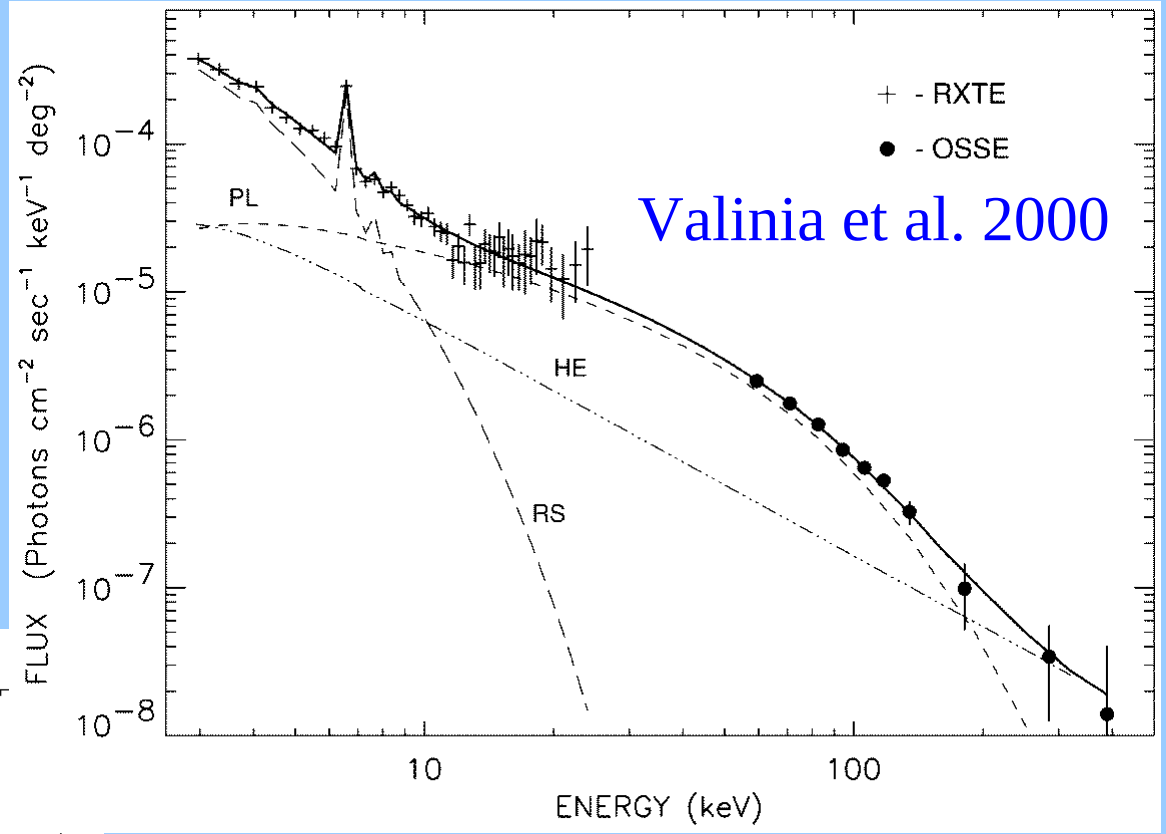

Valinia et al. 2000

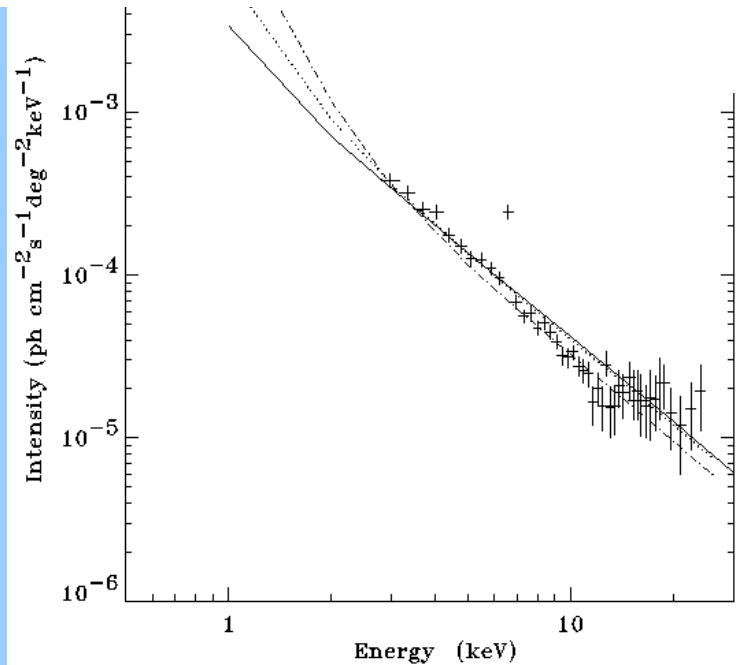

Bremsstrahlung from quasi-thermal electrons

(Dogiel,Inoue, Masai,Schoenfelder,Strong ApJ 581 2002)

Revnivtsev 2003 RXTE

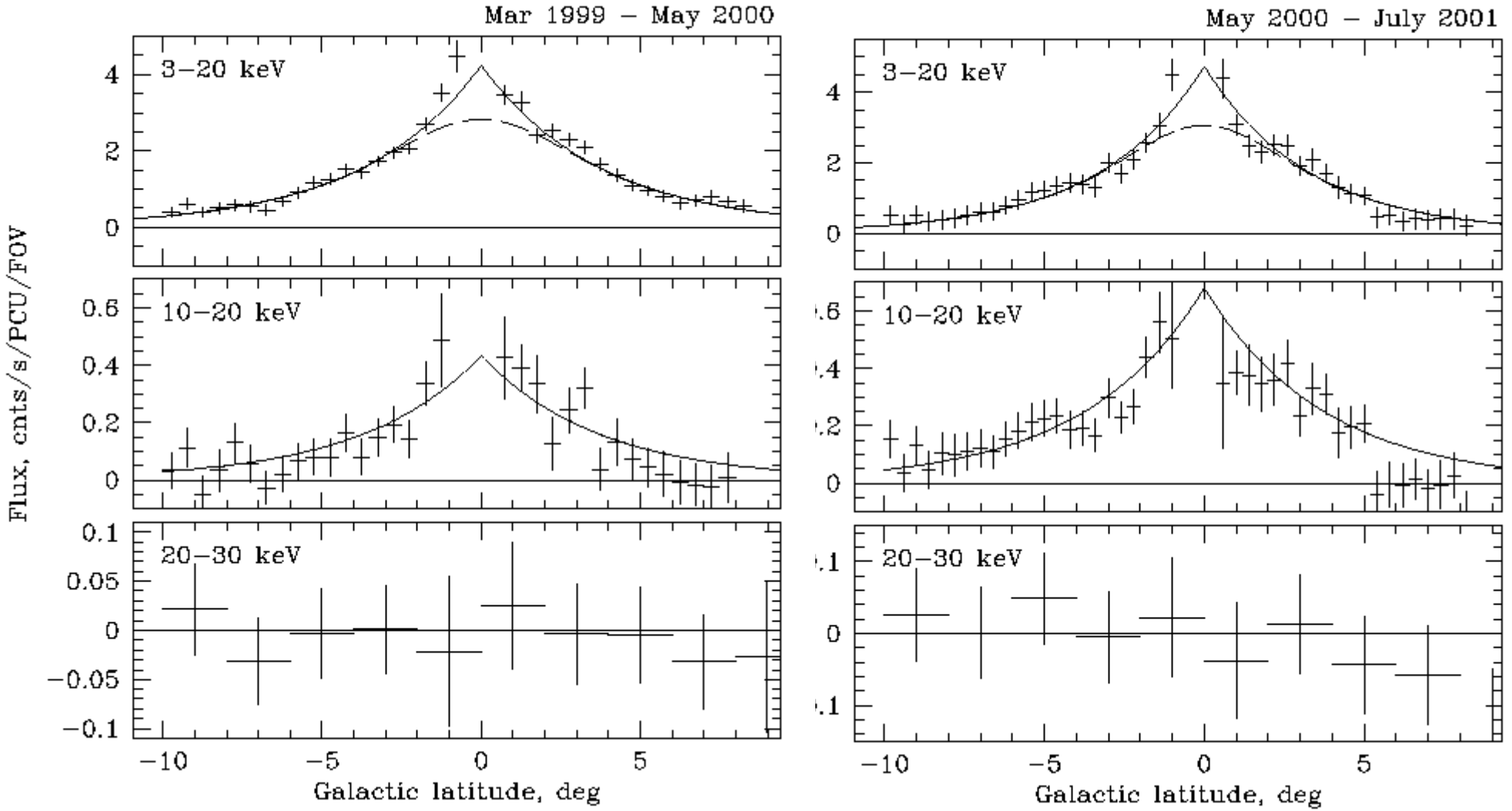

M. Revnivtsev 2003 RXTE

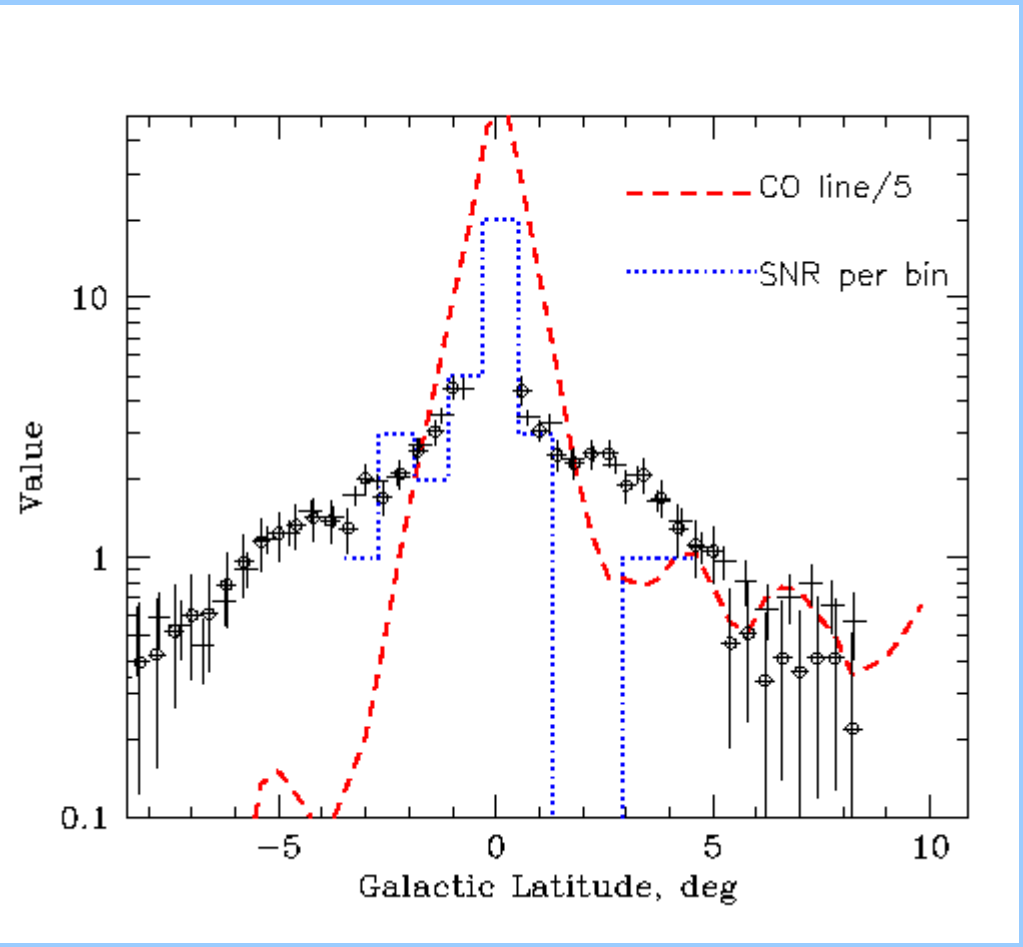

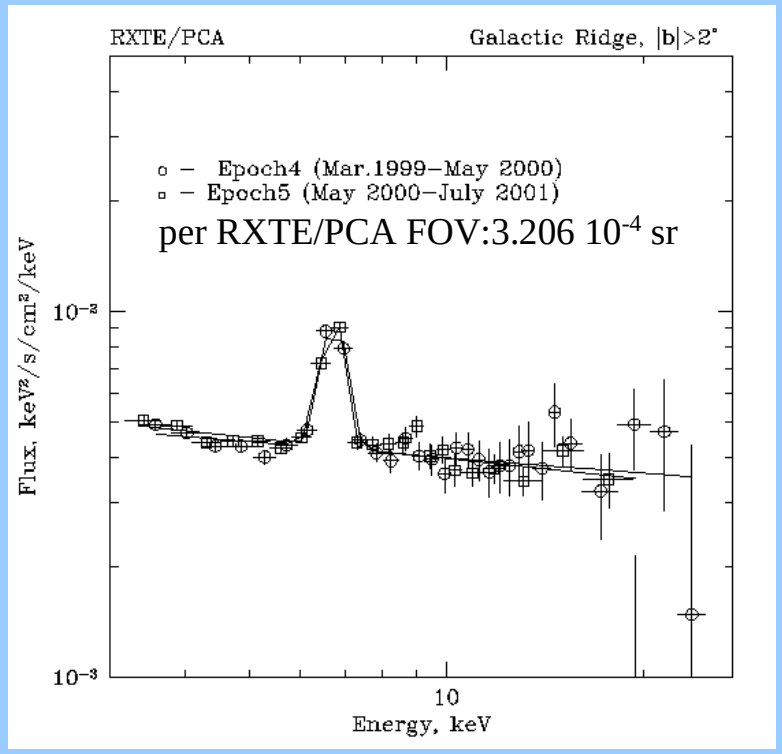

Galactic Centre Deep Exposure (GCDE)

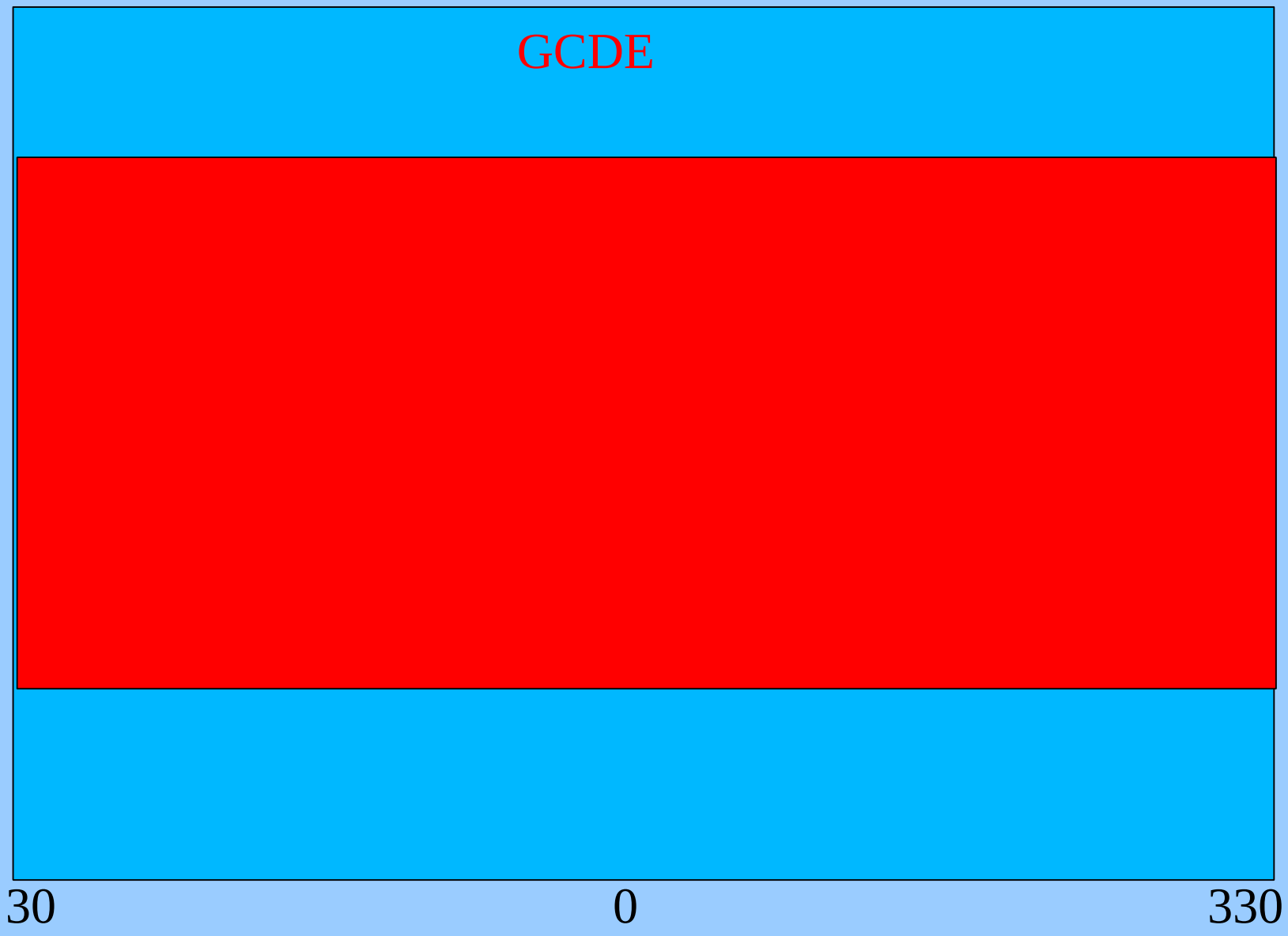

spidiffit PV Phase, Cyg X-1

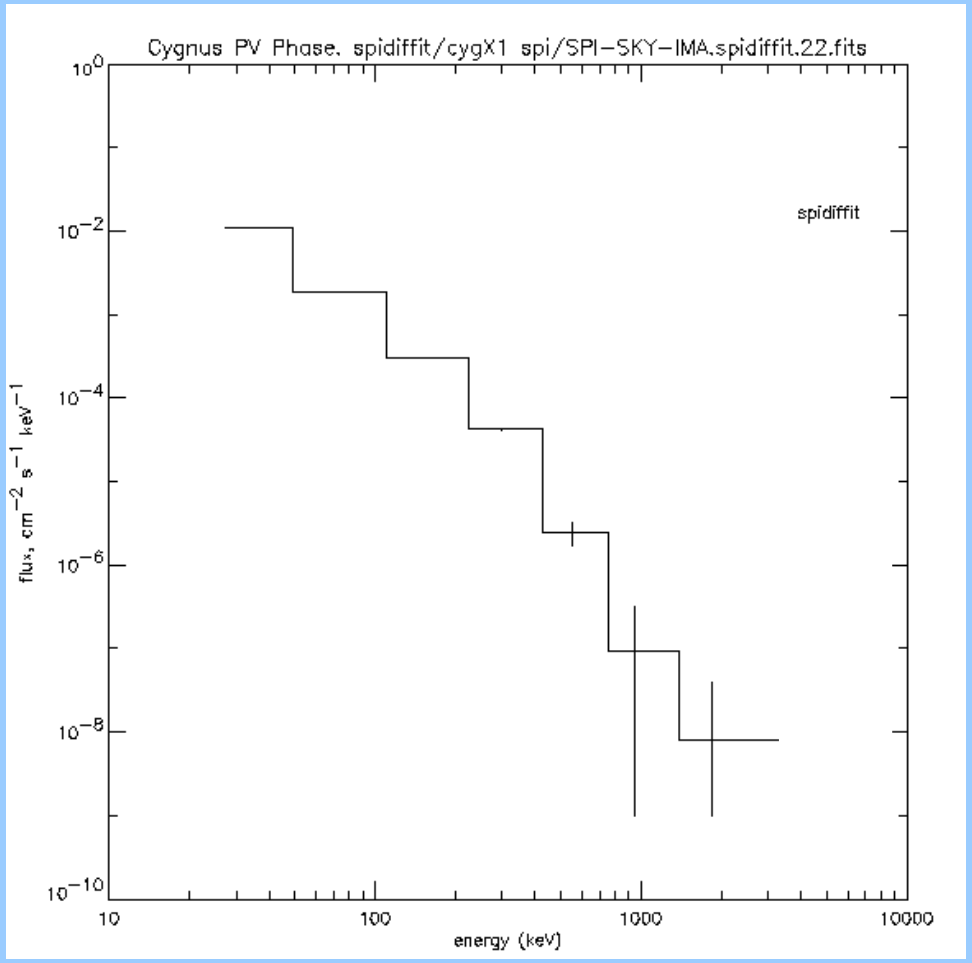

GCDE 4U1700-377

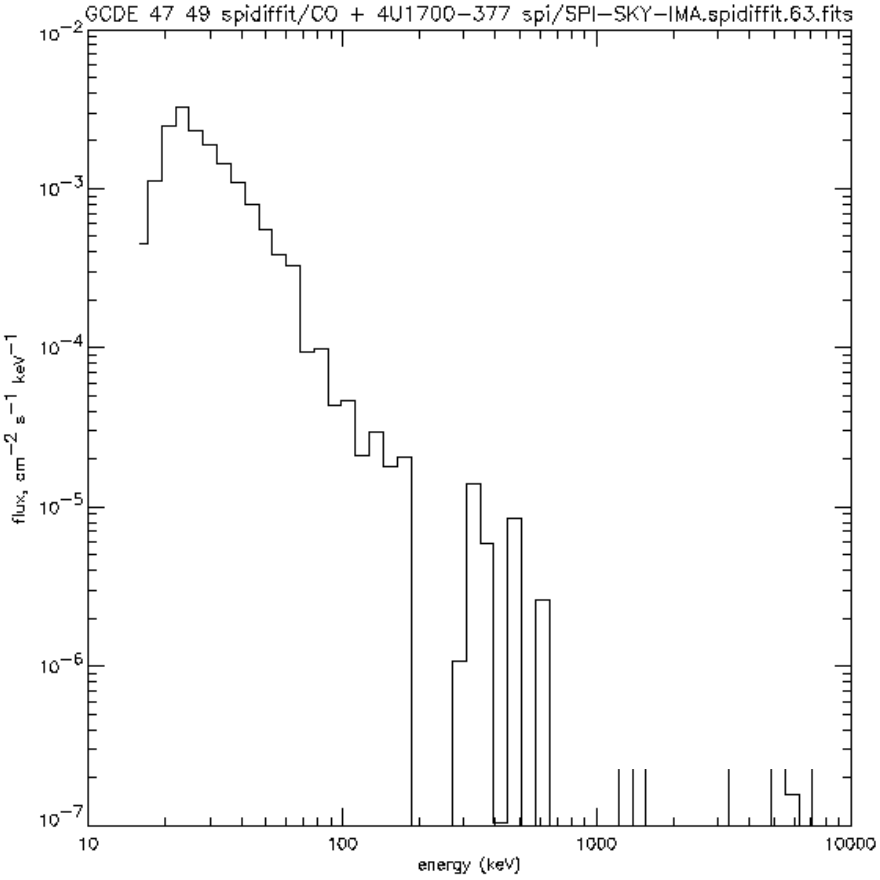

spidiffit PV Phase, Cyg X-1

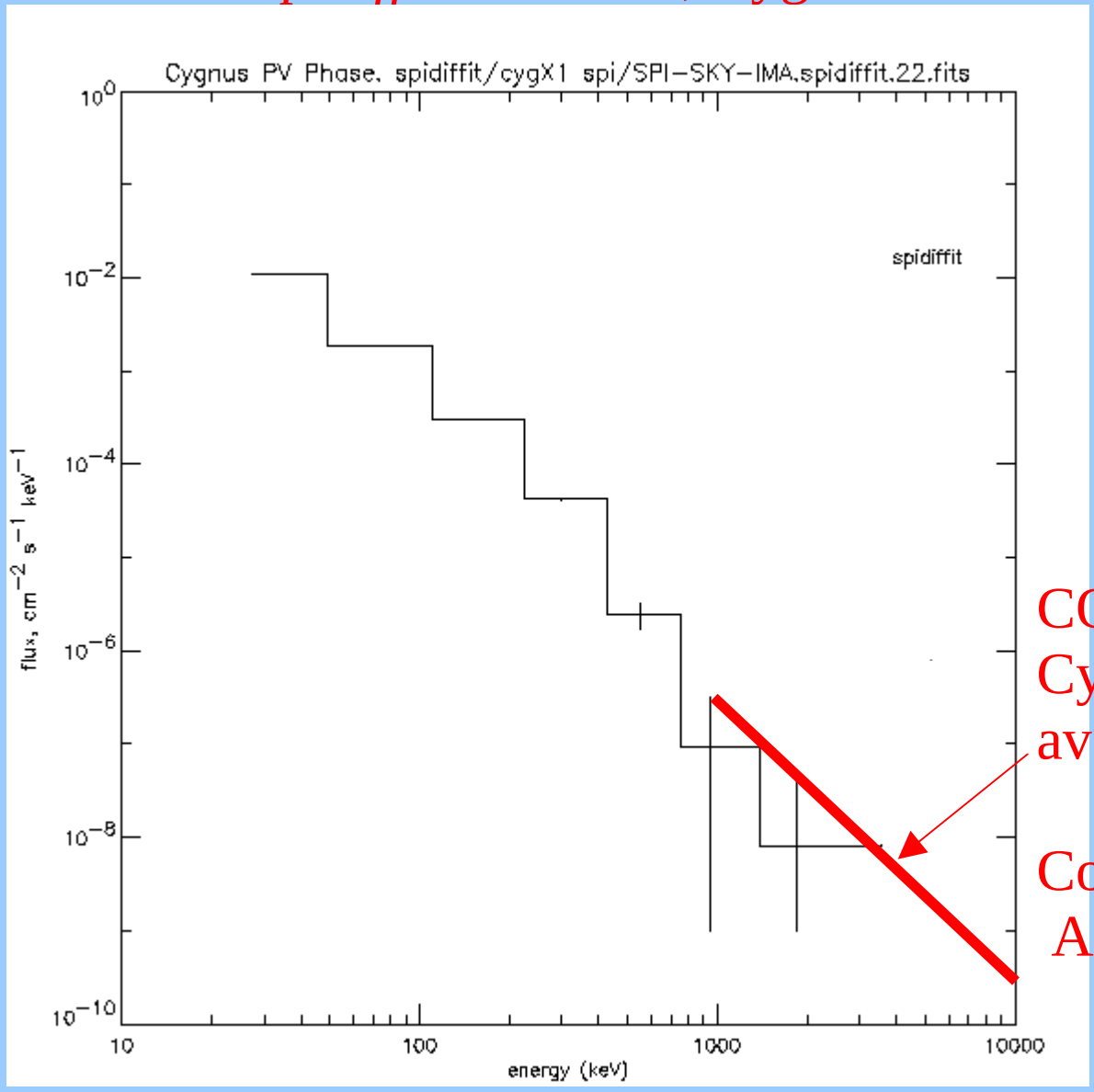

COMPTEL,
Cyg X-1
average hard state

Connell et al. 2002
ApJ 572, 984

Chandra,
quiescent state
Boronson et al.
Astroph/0303277

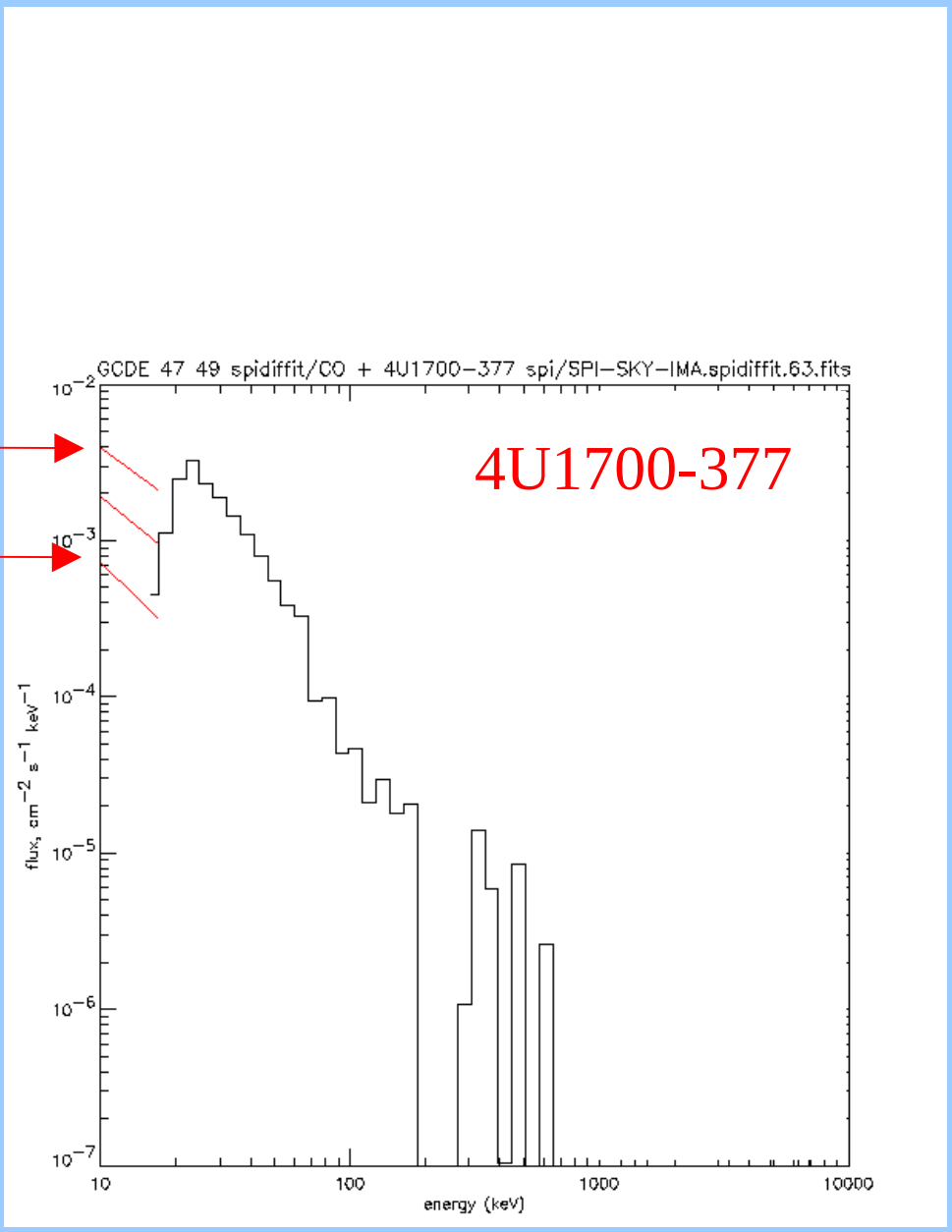

15-40 keV

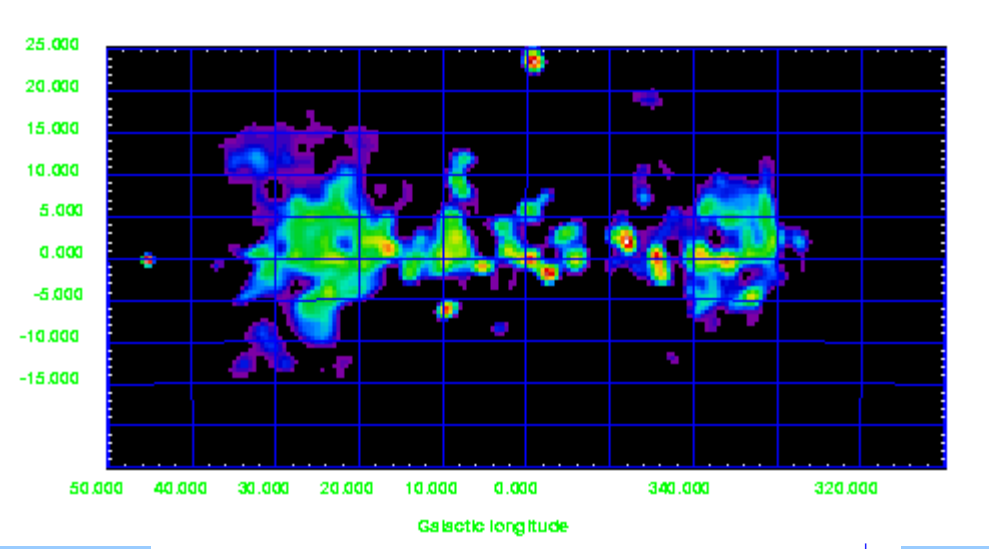

274

40-100 keV

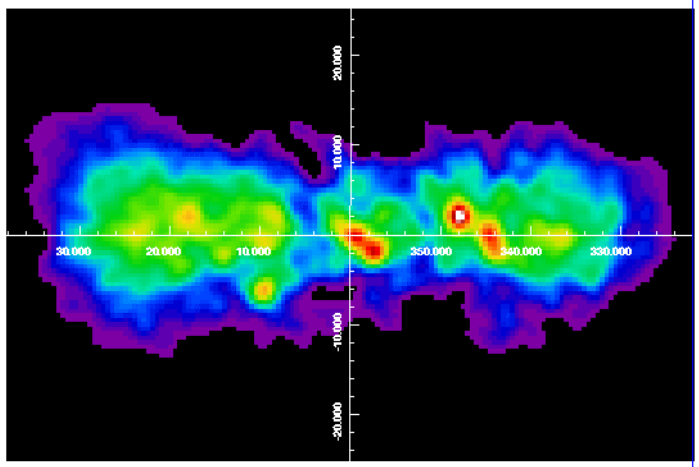

237

100-200 keV

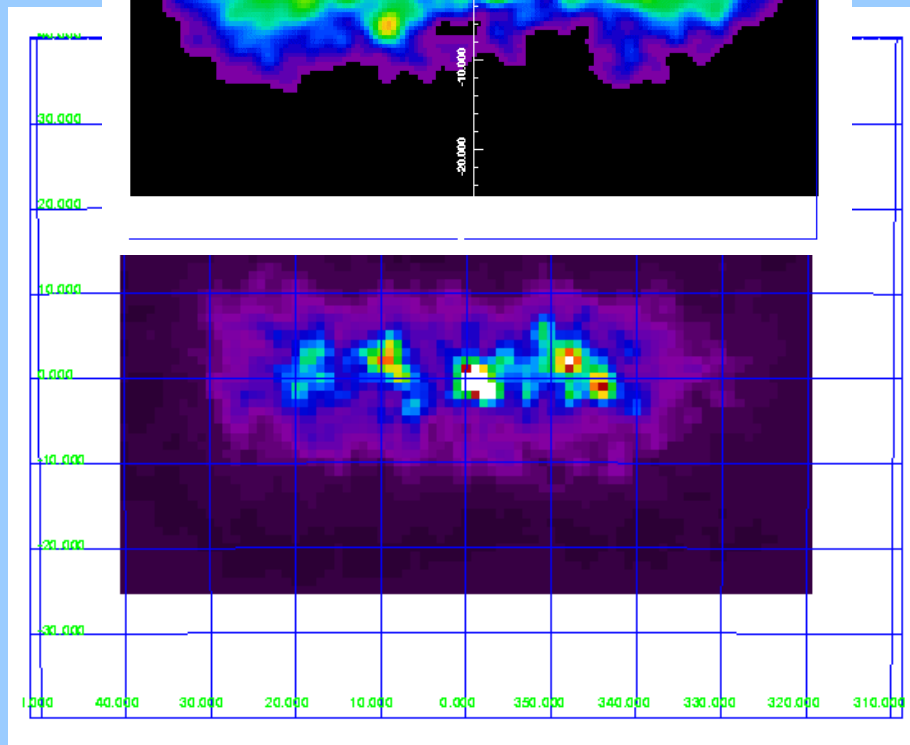

259

spidiffit details

Model skymaps

Response IRF

Background template

For each energy bin

$$d_k = \Sigma_m \Sigma_j \theta_m I_{mj} R_{jk} + \theta_{m'} B_k$$

d_k: Data

θ_m: Model scaling

$\theta_{m'}$: Background scaling (-> time-dependence)

data = sum over components convolved with IRF + background

θ = parameters to be fitted, number = #model skymaps + #science windows

model response matrix S:

$$S_{mk} = \Sigma_j I_{mj} R_{jk}$$

$$d_k = \Sigma_m \theta_m S_{mk} + \theta_{m'} B_k$$

-> input to maximum-likelihood/MCMC analysis

SPI Simulations and Response Generation: Status Report

Steve Sturner

NASA/GSFC, USRA

Calibration Simulations

- Simulations of the BLC calibration were performed at NASA/GSFC using our GEANT3-based package MGEANT.
- A detailed mass model was created based on technical drawings provided by various SPI institutions and from CAD files converted to GEANT readable format.
- Comparison of these simulations with BLC data led to improvements in the simulation software and the mass model.
- We found good agreement between the simulations and BLC data.

SPI Mass Model

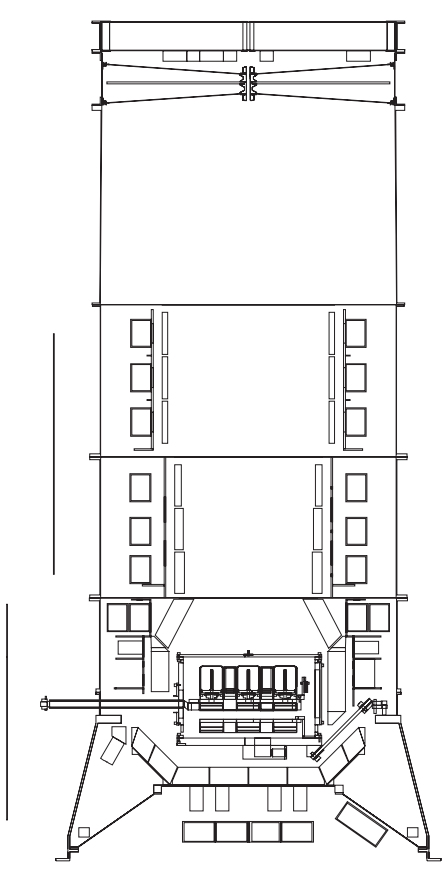

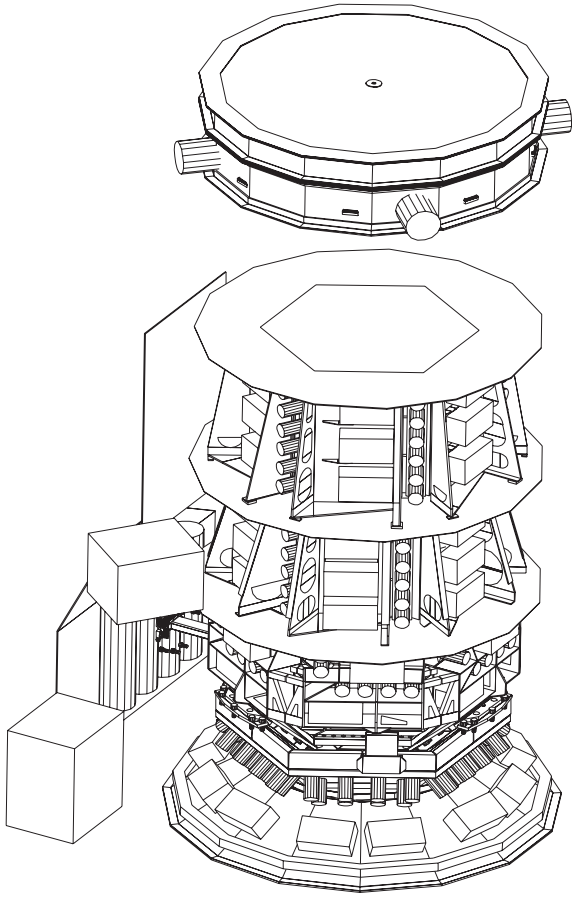

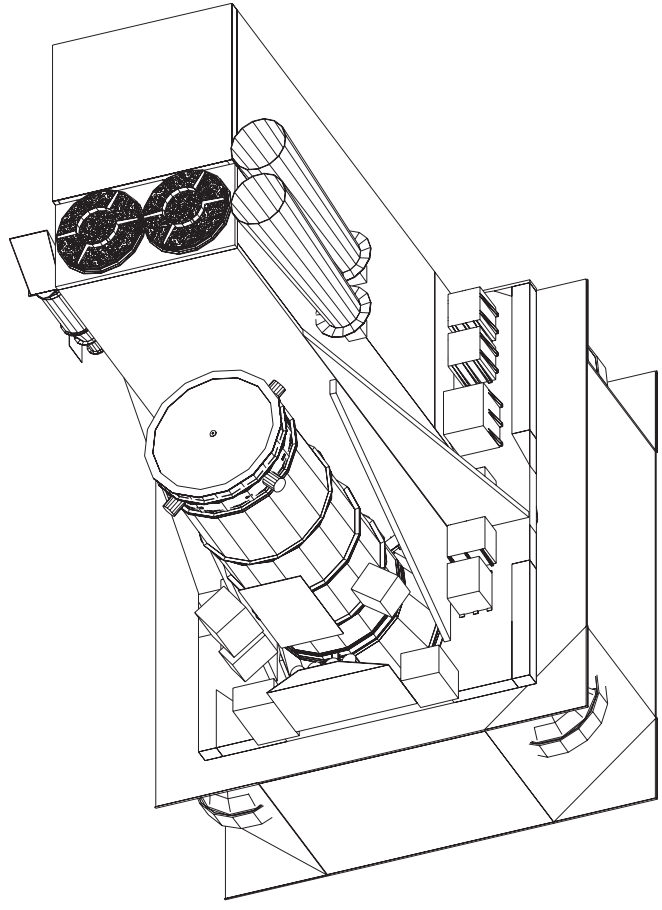

Simulation Results

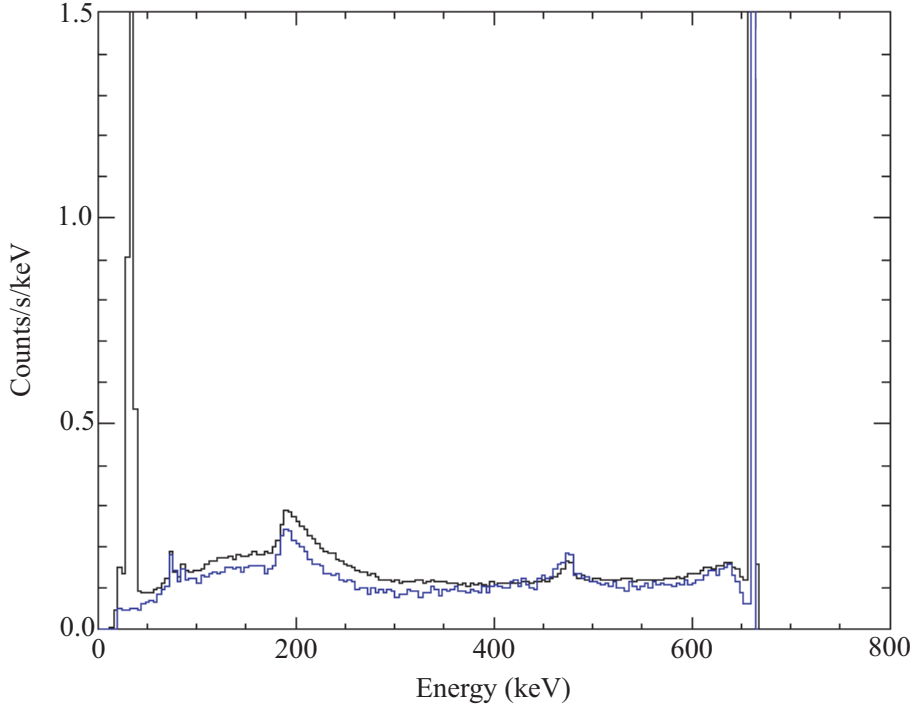

- Comparison of SPI Bruyères-le-Châtel ground calibration data for the ^{137}Cs source (black) and our MGEANT simulation (blue). Note that the low energy line seen in the data was not included in the simulation.

Method of Response Generation

- We determined that a full Monte Carlo calculation of the SPI response was unrealistically CPU and storage intensive.
- This led to a hybrid approach combining ray tracing and Monte Carlo components:
  - Ray tracing for radiation processes outside the cryostat
  - Monte Carlo for radiation processes inside the cryostat

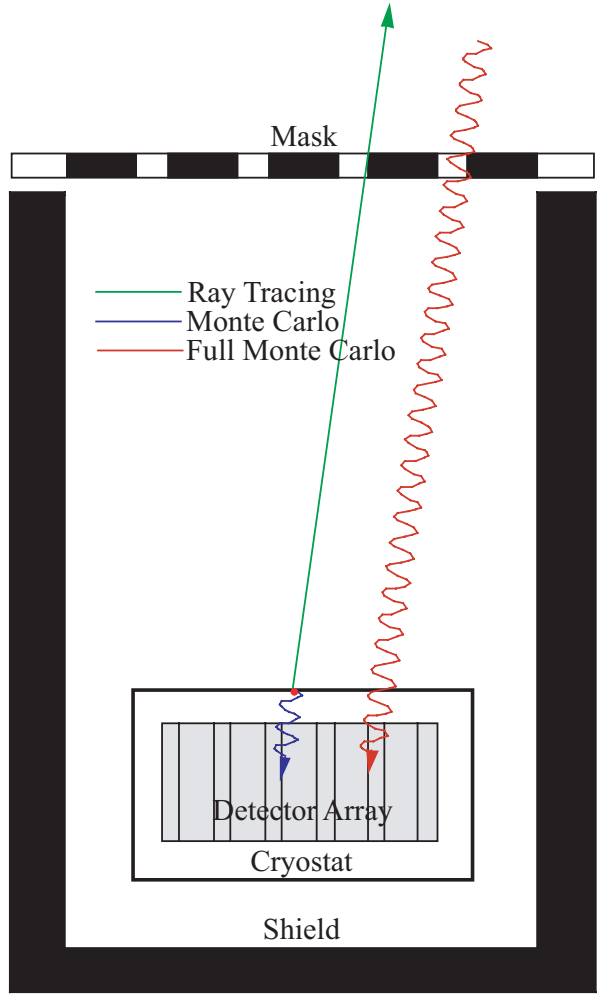

Response Decomposition

- A decomposition of the SPI RMF was implemented to further reduce the number of Monte Carlo photons required to produce an IRF.

- We determined that the count spectrum due to a mono-energetic input spectrum could be well described by the linear combination of 3 shape templates.

- These templates correspond to 3 types of events:
  - Photopeak events
  - Continuum events that interact first in a detector
  - Continuum events that interact first in passive material

- The normalizations for these templates are the values stored in the SPI IRFs. The templates themselves are the SPI RMFs which are currently used in XSPEC-12 spectral analysis.

IRF Correction Factors

- A set of multiplicative correction factors are applied to the MGEANT generated IRFs.

- The correction factors arise from known approximations in the SPI mass model and differences between the SPI data and simulations.

- The correction factors are:
  - Ge mass variation correction
  - Honeycomb mask support correction
  - Photopeak efficiency correction
  - In flight calibration corrections

Detector Mass Variation Correction

- The detector mass in the SPI mass model is set to the average value of 950.91 g for every detector.
- D. Attíe has shown that the variation in detector efficiency across the array follows the variation in mass.
- We apply a correction factor for each detector based on the ratio of its actual mass to the average mass.

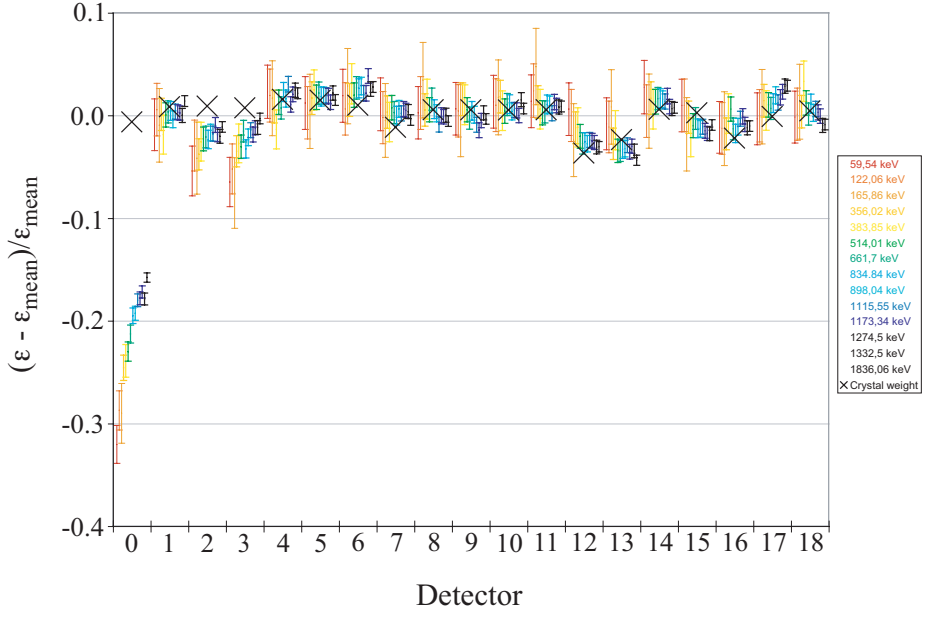

Mask Correction Factor

- The Nomex mask support structure is a honeycomb with 1/8” diameter cells.
- The mask support in the SPI mass model is a uniform slab of the same nominal density.
- This reproduces the transparency of the mask support well on average but exhibits significantly less angular variation at low energies.
- This set of factors corrects for this lack of variation.

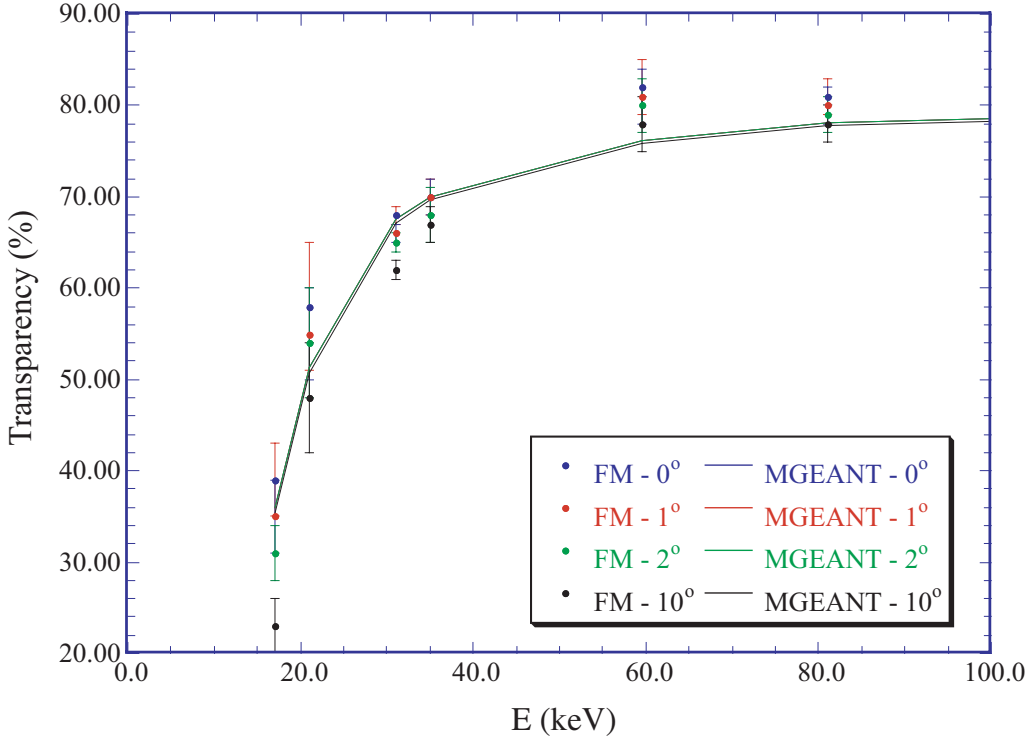

Photopeak Correction Factors

- Analysis of the BLC calibration data indicated that the simulations had a photopeak efficiency ~10% higher than the data.

- We calculated the efficiencies for the 85 pseudo-detectors representing singles, doubles, & triples for both data and simulations.

- The correction factors are the ratio of the efficiencies averaged over all pseudo-detectors for a given multiplicity.

In Flight Corrections

- We have performed spectral analysis of rev 44 data from the Crab Nebula + pulsar using both SPIROS and XSPEC-12.
- The efficiency below ~40 keV was found to be over estimated.
- We derived IRF correction factors by fitting the Crab spectrum above 40-50 keV with a single power-law and then forcing this fit when the low energy channels were included.
- The low energy correction factors are the ratio of the model to the data.

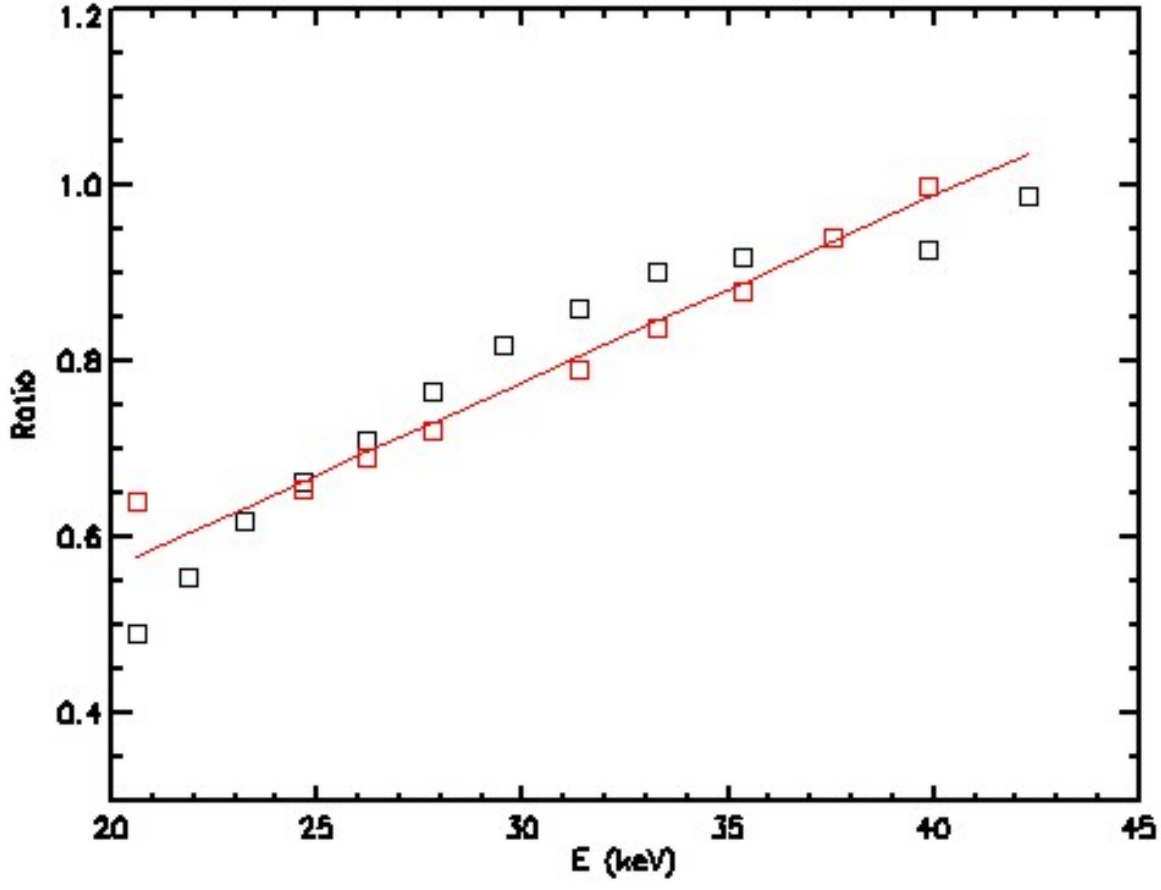

Ratio of Crab data to best-fit power-law model above ~40 keV for SPIROS (black) and XSPEC-12 (red) analyses.

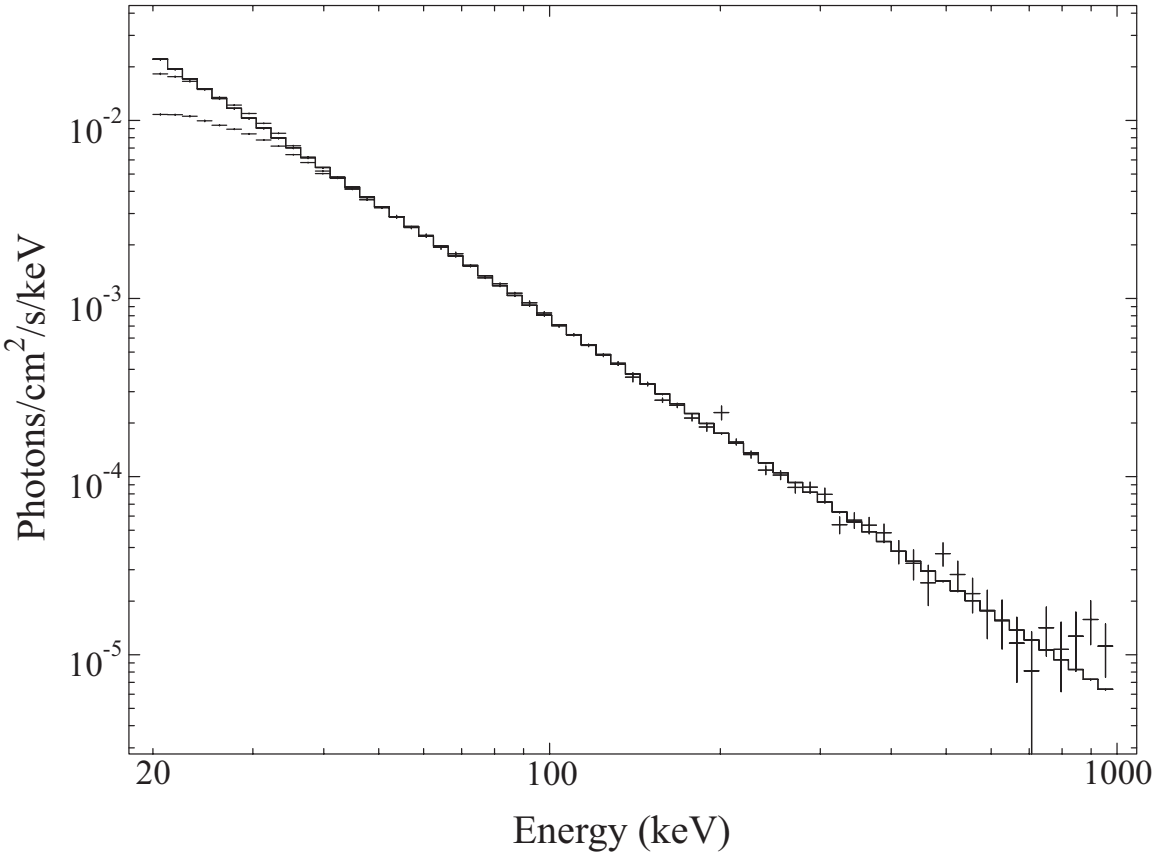

Comparison of SPIROS output using both IRFs corrected at low energies and those not corrected, as well as the best-fit power-law model for data above ~40 keV.

Testing SPI Imaging of High-Energy and Extended Sources

C. B. Wunderer[1], P. Connell[2], J. W. Hammer[3], V. Schönfelder[1], and A. W. Strong[1]

[1] Max-Planck-Institute for extraterrestrial Physics, Giessenbachstr. 1, 85748 Garching, Germany
[2] University of Birmingham, ..., UK
[3] Institut für Strahlenforschung, University Stuttgart, Allmandring 3, xxxx Stuttgart, Germany

Received ; accepted

Abstract. INTEGRAL's main instruments employ coded apertures to obtain directional information on the incoming radiation. In order to experimentally better determine the imaging capabilities of the spectrometer SPI, the SPI Imaging Test Setup (SPITS) has been built at MPE. It consists of the SPI coded mask and two SPI-identical Ge detectors on an XY-table which allows us to move them to cover the 19 Ge detector positions. The SPI flight model imaging calibration only covered the energy range up to 2.7 MeV and did not include extended emission. SPITS was used to explore the performance of such a coded aperture system — combined with the SPI image analysis software — for higher-energy point sources and extended sources. We find that a 2.4^o diameter disk emitting 511 keV emission is reconstructed well. For the high signal-to-noise ratios of laboratory measurements, positions of point sources above 4 MeV could be reconstructed to better than 0.1^o.

Key words. INTEGRAL – spectrometer SPI – imaging – gamma-ray – TBD!!

1. Introduction

The INTEGRAL spectrometer SPI is designed to measure 20 keV – 8 MeV photons with an energy resolution of 2.3 keV at 1.3 MeV using 19 high-purity Ge detectors. A tungsten-alloy coded aperture provides spatial information with an angular resolution of $\sim 2.5^o$ and a 16^o fully coded field of view (Vedrenne et al. 2003).

The technique of using coded apertures, although well established in the X-ray domain (see e.g. Badiali et al. (1985) and references therein), are used by INTEGRAL's instruments for the first time on a space platform up to 10 MeV. Studies of the imaging capabilities of SPI were performed using GEANT and other simulation tools (Connell et al. 1998, Strong et al. 1998, Skinner et al. 1997).

The spectrometer has been calibrated in spring 2001 at the accelerator facility of the CEA at Bruyères-le-Châtel, France (Schanne et al. 2002, Attié et al. 2003). These measurements were subject to strict time constraints. Thus some aspects of SPI performance could not be addressed, among them SPI response to extended sources and the *imaging* performance of the instrument above 3 MeV. SPI imaging above a few MeV is also difficult to test in flight due to low celestial source fluxes at these energies (see Roques et al. 2003).

To complement the SPI calibration data from Bruyères-le-Châtel, the SPI Imaging Test Setup (SPITS) was built at the Max-Planck-Institut für extraterrestrische Physik (MPE). SPITS measurements include imaging data up to 9 MeV taken at the Institut für Strahlenphysik (Univ. Stuttgart, Germany) and measurements with an extended 511 keV source.

Send offprint requests to: C. B. Wunderer

2. The SPI Imaging Test Setup

The SPI Imaging Test Setup (SPITS) consists of two SPI Ge detectors and a SPI-equivalent coded aperture. The Ge detectors are taken from the SPI satellite manufacturing line and mounted in an Al cryostat. For cost reasons, SPITS has only 2 Ge detectors. The 19-Ge detector camera of SPI is emulated by mounting the Ge detectors on an XY-table. The 19 Ge positions are covered in 19 consecutive measurements. This method necessitates constant source activity over the 11 consecutive measurements. Where this condition is not met, measurement times have to be corrected a posteriori based on monitor data or a known source decay rate. The SPITS coded mask is built on the basis of a SPI mask development model made available by the University of Valencia. All mask materials are identical to those of the SPI mask. The development model was extended to the full SPI mask code and mounted in an Al frame.

The test setup has some restrictions, primarily due to the lack of 17 detectors during any one measurement. With SPITS, the SPI "multiple events (ME)" cannot be used - only photopeak interactions in *one* Ge detector are used for image analysis. Figures 1 and 2 show pictures of the SPITS mask and Ge detector assemblies. A more detailed description of the setup can be found in Wunderer et al. (2001).

In general, all SPITS measurements have comparatively low (laboratory) background levels, resulting in much higher S/N-ratios than are expected/seen from celestial γ-ray sources.

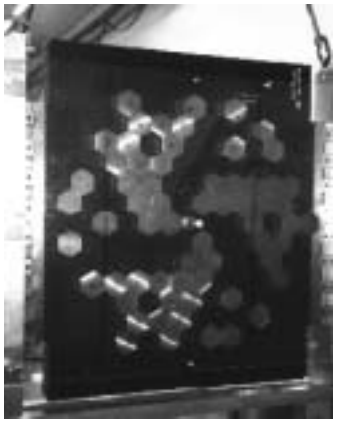

Fig. 1. The SPITS mask with its Al mounting frame.

Fig. 2. The SPITS Ge detectors, mounted with their liquid N_2 dewar on the XY-table.

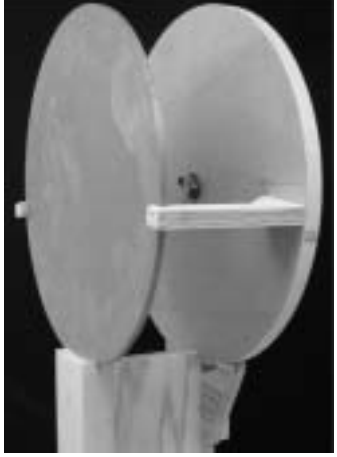

Fig. 3. The Pb disk used as source of extended emission, shown with ^{88}Y source and mounting device.

3. Imaging Algorithms and the SPITS Instrument Response Functions

Since coded aperture instruments do not produce a "conventional" image of the source, but instead record the source distribution information convolved with the mask function, a deconvolution of the data is needed to recover the spatial source distribution. Combining data from several pointings of the instrument close to the source (region) of interest — a stategy called *dithering* — usually allows a more unambiguous source reconstruction especially in the case of diffuse emission or crowded fields. For SPI standard analysis, two image reconstruction algorithms have been developed:

Image entropy is a measure for structure in the image. By maximizing this entropy, *spiskymax* searches the "least-structured" image consistent with the available data (and prior knowledge about the distribution). With increasing number of iterations, *spiskymax* reconstructions get "spikier," and thus especially for extended emission the stopping criterion is an issue. See Strong et al. 2003 for details on *spiskymax*.

spiros (SPI Iterative Removal Of Sources) in its basic version is primarily geared towards point sources. A rough sky image is generated by cross-correlation, the strongest point source is located and subtracted in dataspace, and the process is repeated until all significant sources are localized (Skinner et al. 2003).

In order to reconstruct source images with either algorithm, the instrument response (expected rates in all 19 Ge detectors) to incoming radiation of a given energy has to be known for all possible incident directions. This is stored in Instrument Response Functions (IRFs). For SPI, these IRFs are obtained with MGEANT from a combination of full Monte Carlo simulations and ray-tracing using a complex mass model (????? et al. 2003). For SPITS, different IRFs were needed due to a different mass model. The SPI IRF generation tools could not be used since they assumed parallel-beam sources and SPITS measurements were performed with sources at 9 m. SPITS IRFs were generated instead using a ray-tracing method only (CAPTIF, Connell et al. 1998). The resulting SPITS IRFs agree fairly well with measured data once a correction factor is applied to account for the actual Ge photopeak efficiencies. However, since CAPTIF could not accomodate a full SPITS mass model and the presence of 19 detectors had to be assumed, the accuracy of SPITS IRFs is necessarily somewhat less than that of SPI IRFs. Therefore, the performance parameters obtained here with the Test Setup and its IRFs have to be considered lower limits for SPI (and SPI IRF) performance under the same circumstances.

4. Imaging of Point Sources above 3 MeV

While SPI is designed to image celestial sources up to 8 MeV, it was calibrated on ground with its mask in place only up to 2.7 MeV. At higher energies, precedence was given to a uniform energy and efficiency calibration of the Ge detectors over a test of the imaging performance; for this, the mask was removed. Thus, no imaging measurements exist with SPI above 2.7 MeV. To fill this gap, SPITS imaged proton-capture targets (^{13}C, ^{19}F, and ^{15}N) at the IfS Stuttgart emitting gamma-ray lines up to 9 MeV (Wunderer 2003).

We imaged these "sources" using *spiskymax* and *spiros*. In addition to imaging one target, we combined the data from two observations to generate datasets of "two-target observations". This allowed us to test the capability of SPITS and the imaging algorithm used to separate and correctly locate two close point sources of equal intensity. Since absolute target flux calibrations are difficult and there is no independent way to determine the necessary correction factors for the SPITS IRFs, we limit ourselves to the discussion of source positioning for the accelerator targets.

Figure 4 shows reconstructions of accelerator targets at different photon energies and off-axis angles from SPITS using both *spiskymax* and *spiros* algorithms. Single targets were localized well with the *spiskymax* algorithm in all cases; the location accuracy is 0.1^o or better. Reconstructions with *spiros* were problematic in many instances; these coincide with mea-

surements taken during periods of unstable accelerator performance. The most likely explanation for this is that the flux corrections applied to the 11 SPITS positions composing one SPITS "observation" are not good enough for these periods of instable accelerator operations, resulting — in a sense — in different source fluxes seen by different Ge detectors. This can also be formulated as the IRFs not matching the true instrument response very well (e.g. different efficiencies of the 19 Ge detectors would have a similar effect). Thus, the comparatively worse performance of *spiros* with these datasets can be interpreted as *spiros* being more sensitive to imperfections in the IRFs than *spiskymax*.

Even given these imperfections, two close sources in the field can be separated and localized correctly by the *spiskymax* algorithm for source separations above 1^o, while for separations of 0.5^o, generally the two sources are not resolved. This is similar to the observations made with SPITS for lower-energy point sources. Figure 5 shows *spiskymax* reconstructions of two-target observations for different separation angles and photon energies.

5. Imaging of Extended Emission

To test SPITS' capability to image extended emission, we placed a strong ^{88}Y source behind a lead disk (Figure 3). In this disk, 1.8 MeV photons from the source interact; some produce electron-positron pairs. The positrons in turn annihilate, and as a result, the whole disk "glows" in 511 keV photons. Of course, 511 keV emission from the center of the disk is stronger than from the disk edge. At 9 m from the detectors, the disk appears 2.4^o across. An 8 MBq source was used; it produced 55000 phot/s from the disk or 520 511 keV photons incident on one (non-shaded) Ge detector in an one-hour measurement. The disk was moved horizontally to positions $\pm 2^o$, $\pm 4^o$, 6^o, and 8^o from the instrument axis. These measurements were later combined to emulate a dithered observation of the extended source. A more detailed description of the lead disk and the determination of its 511 keV emissivity can be found in Wunderer 2003. Figure 6 shows the 511 keV emission from the disk predicted by an analytical calculation based on first interactions of the 1.8 MeV photons only.

Dithering, as mentioned above, is especially important for observations of extended emission. But even without dithering, SPI with *spiskymax* can discriminate extended and point source emission given a strong signal and low background. Figures 7 and 8 show reconstructed images of our extended source and a 511 keV point source of equal flux (^{22}Na).

In order to emulate a 5-point dither pattern with pointings separated by 2^o, all available measurements at five Pb disk positions were combined. The measurement durations had to be corrected for the ^{88}Y decay, and an analysis of the resulting dataset in the 1836 keV line of ^{88}Y was used to confirm that this had been done correctly.

Figure 9 shows the results of *spiskymax* reconstruction of the extended source from dithered observations for different numbers of iterations. The source is clearly visible in the images after 10 and 15 iterations. Its intensity, however, is still very much lower in the 10-iteration image than in the 15-iteration image. Here, the flux begins to reach "final" reconstructed levels. Starting at iteration 20 — and very much so at

spiskymax *reconstruction of* ^{13}C*target in the 6.1 MeV line at* 0.0^o.

spiros *reconstruction of* ^{13}C*target in the 6.1 MeV line at* 2.9^o.

spiskymax *reconstruction of* ^{19}F*target in the 6.1 MeV line at* 1.0^o.

spiskymax *reconstruction of* ^{19}F*target in the 6.1 MeV line at* 2.9^o.

Fig. 4. Reconstructions of accelerator targets with *spiskymax* and *spiros*. Photon energies and aspect angles vary.

^{13}C*targets in the 6.1 MeV line at* 0.0^o *and* 1.0^o

^{13}C*targets in the 6.1 MeV line at* 1.1^o *and* 2.9^o

^{19}F*targets in the 6.1 MeV line at* 0.0^o *and* 1.0^o

^{19}F*targets in the 6.1 MeV line at* 1.1^o *and* 2.9^o

Fig. 5. *spiskymax* reconstructions of two targets; photon energies and separation angles vary. Source separation is clearer for the ^{19}Fthan for the ^{13}Ctarget, this is at least in part due to more line photons measured from the ^{19}Ftarget.

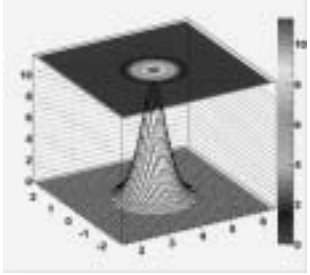

Fig. 6. Predicted emission from the extended 511 keV source. (Diameter: 2.4^o)

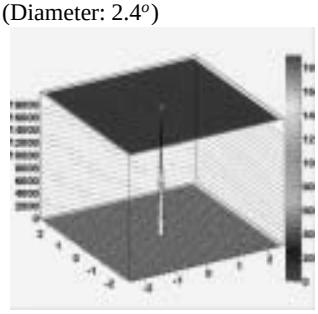

Fig. 7. *spiskymax* reconstruction of a ^{22}Na point source in the 511 keV line from a non-dithered observation. Total 511 keV flux is equal to that from the extended source in Figure 8.

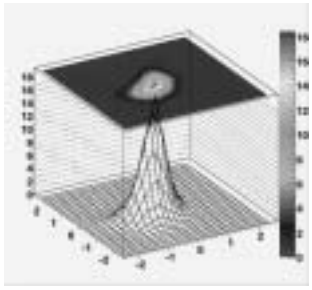

Fig. 8. *spiskymax* reconstruction of the 511 keV extended source from a non-dithered observation. Total 511 keV flux is equal to that from the point source in Figure 7.

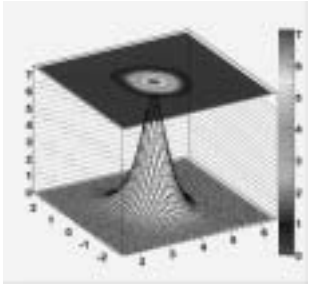

10 iterations

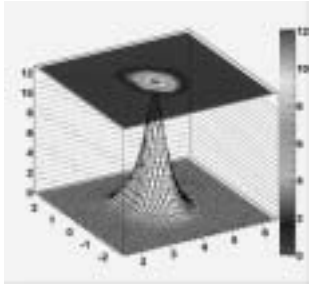

15 iterations

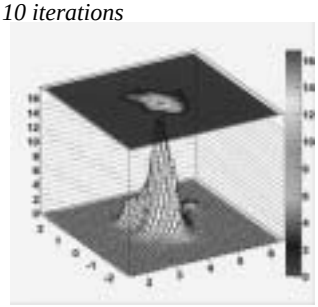

20 iterations

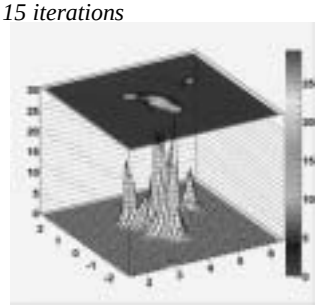

25 iterations

Fig. 9. *spiskymax* reconstruction of the 511 keV extended source from dithered observations. Different iteration stages are shown.

iteration 25 and higher — the *spiskymax*-reconstructed image acquires more structure ("spikyness") than the original source distribution would merit. A (non-normalized) χ^2 comparison of calculated and reconstructed emission shows that the 15 and 20 iteration images best reflect the "true" distribution.

A similar behavior was observed when a simulated dithered observation of such an extended source was deconvolved with *spiskymax*. While for the determination of overall flux levels the number of iterations used is not too crucial, the reconstructed shape of the distribution depends on it. For the SPITS low background case, we found that the evolution of the reconstructed source flux and its significance help to determine a stopping criterion for *spiskymax* (Wunderer 2003).

The 511 keV flux predicted from first interactions of 1.8 MeV photons only in the Pb disk is $6.5 \cdot 10^{-3}$ph/(cm^{2}s) while the reconstructed flux is ~50% higher. In contrast, point source fluxes (from laboratory sources below 2 MeV) have always been reconstructed a few percent below the true flux. The deficiency in calculated flux from the extended source is likely due to a combination of (1) only the first interaction of a 1.8 MeV photon being considered relevant in the calculation, while a once Compton-scattered photon with remaining energy of, say, 1.6 MeV can still pair-produce in the Pb (add ~ 6%); (2) so far, the 2.7 MeV line from ^{88}Y — emitted with 0.7% probability — has been neglected. It becomes non-negligible here due to the higher pair productio cross section (add ~ 5%); (3) pair production interactions of source photons in the concrete wall behind the lead; and (4) 0.2% of ^{88}Y decays are β^+ decays resulting in 511 keV photons (this contributes another ~ 11% to the observeable 511 keV flux). Together, these effects enhance the 511 keV flux from the region of the lead disk by roughly 20% — not accounting for pair production in the surrounding material which is not easyily quantified —, enough to make the observed (0.010±0.001) ph/(cm^{2}s) seem reasonable within the error margin.

6. Conclusions

.

.

.

Acknowledgements. We gratefully acknowledge the help received at the IfS in Stuttgart from both the IfS team and people from MPE, especially A. Zoglauer. In addition, we wish to thank G. Vedrenne (CESR Toulouse) and F. Sanchez (U. Valencia) for making hardware available to SPITS.

References

D. Attié et al. (???), SPI BLC Calibration paper, A&A, this volume, 2003

M. Badiali, D. Cardini, A. Emanuele, M. Ranieri, and E. Soggiu 1985, A&A, 151, 259.

P. Connell and G. K. Skinner, in Proc. Imaging in High Energy Astronomy, eds. L. Bassani and G. di Cocco, 143.

P. Connell, G. K. Skinner, B. G. Teegarden, J. Naya, and S. Sturner 1998, in Proc. of the 3rd INTEGRAL Workshop, eds. A. Bazzano, G. G. C. Palumbo, and C. Winkler, 2, 397.

J. P. Roques et al. (???), SPI In-Flight Calibration paper, A&A, this volume, 2003

S. Schanne et al. (???), SPI BLC paper for SPIE 2002, SPIE, 2002

G. K. Skinner, P. H. Connell, J. Naya, H. Seifert, S. Sturner, B. J. Teegarden, and A. W. Strong 1997, in AIP Conf. Proc. 410, Proc. of the 4th COMPTON Symposium, eds. C.D. Dermer, M. S. Struckman, and J. D. Kurfess, 1544.

G. K. Skinner et al. (???), spiros, A&A, this volume, 2003

A. W. Strong, R. Diehl, P. Connell, and G. K. Skinner 1998, in Proc. of the 3rd INTEGRAL Workshop, eds. A. Bazzano, G. G. C. Palumbo, and C. Winkler, 2, 221.
A. W. Strong et al. (???), spiskymax , A&A, this volume, 2003
G. Vedrenne et al. (???), SPI Description paper, A&A, this volume, 2003
C. B. Wunderer, P. Connell, R. Diehl, R. Georgii, A. v. Kienlin, G. G. Lichti, F. Sanchez, V. Schönfelder, A. Strong, and G. Vedrenne 2001, IEEE Trans. Nucl. Sci, 48, 1053.
=?? not cited yet ??? C. B. Wunderer et al. 2002, SPIE proceedings - TBcontinued!.
C. B. Wunderer 2003, PhD thesis, TU Munich, Germany.
??????? et al. (???), spi response / IRFs , A&A, this volume, 2003

Status of A&A paper
on

SPI Ground calibration

David Attié, et al

CoI meeting SPI (CESR-Toulouse) - June 11,12 & 13, 2003

Summary : status [1/2]

- **Total of pages already written : 10 (+3)**
- **Number of missing page : ~1**

1. Introduction

2. General description of the spectrometer SPI (1p)

2.1. SPI elements

2.2 SPI camera events : Single Events and Multiple Events

3. Calibrations campaigns (1p)

3.1. SPI calibration at Bruyères-Le-Châtel (BLC)

3.1.1. *Low-intensity sources*

3.1.2. *Accelerator measurements: resonance and branching ratios*

3.1.3. *High-intensity sources*

3.2 Payload calibration of *INTEGRAL* at ESTEC

3.2.1. *Cross calibration*

3.2.2. *SPI thermal vacuum test*

4. Camera performance (0.5p)

4.1. Energy calibration

4.2. Energy resolution and temperature evolution [J-P Roques-CESR]

Summary : status [2/2]

5. Anticoincidence system [A. von Kienlin] (?p)
   - 5.1. ACS Threshold calibration
   - 5.2. Self compton mode
   - 5.3. Angular efficiency of ACS
   - 5.4. ACS rejection of single and double escape peaks and background homogeneity on SPI camera

6. **Full-energy peak efficieny of the SPI telescope (3.5p)**
   - 6.1. Full-energypeak efficiency of the SPI camera for the SE
     - 6.1.1. *Efficiency by detector*
     - 6.1.2. *Homogeneity of the camera*
     - 6.1.3. *Full-energy efficiency of the SPI camera for SE*
   - 6.2. Full-energypeak efficiency of the SPI camera for the ME
   - 6.3. Total full-energypeak efficiency of the SPI camera (SE+ME)
   - 6.4. Full-energy peak of SPI telescope

7. **Imaging capabilities [A. Strong, G. Skinner] (1.5p)**
   - 7.1. Angular resolution and Point Spread Function
   - 7.2. Single source localization precision
   - 7.3. Double Separation capability

8. **SPI background (0.75p)** (+ list of instrumental lines (1p))

9. **Conclusion**

Camera efficiency ESTEC vs BLC

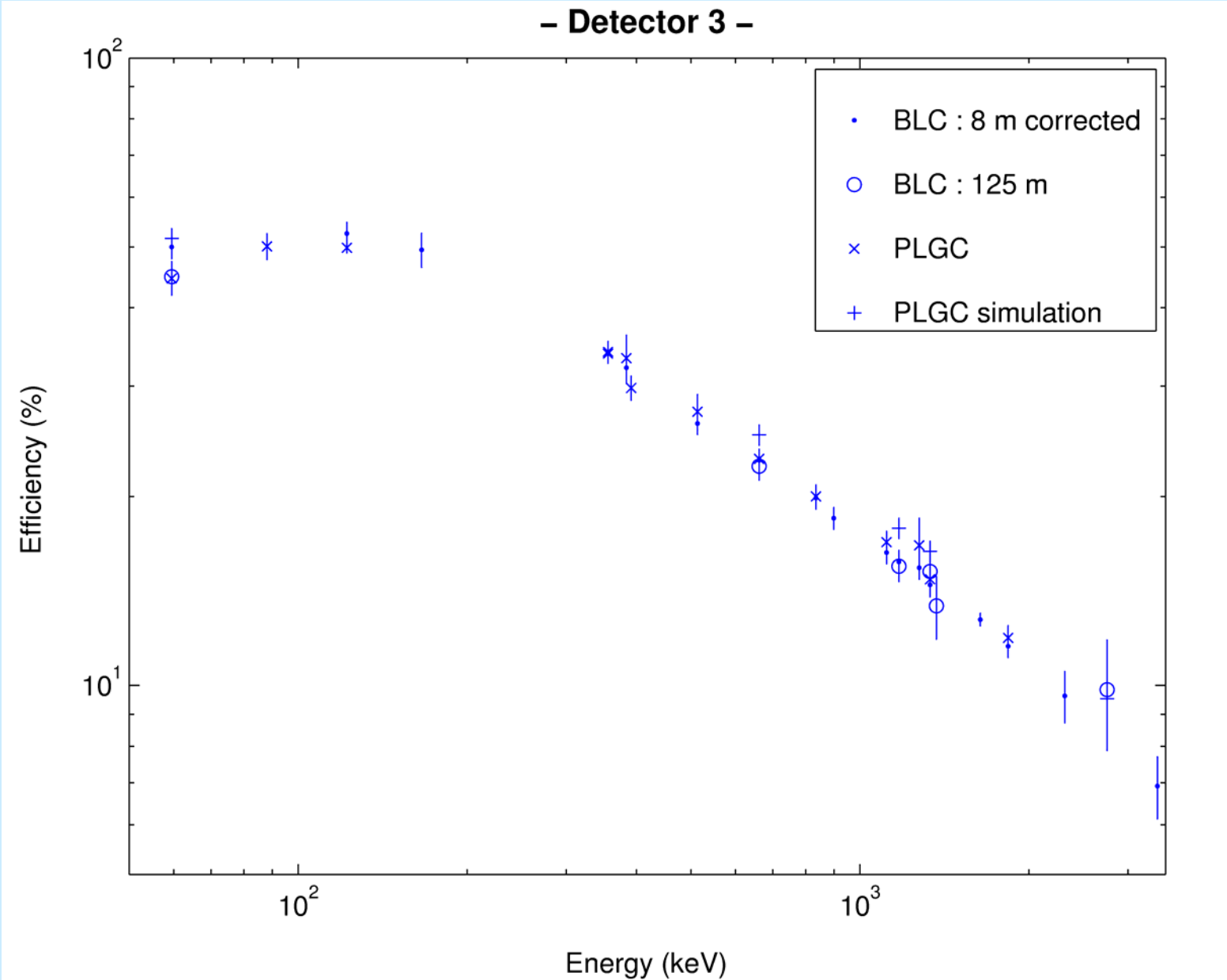

Camera efficiency ESTEC vs BLC

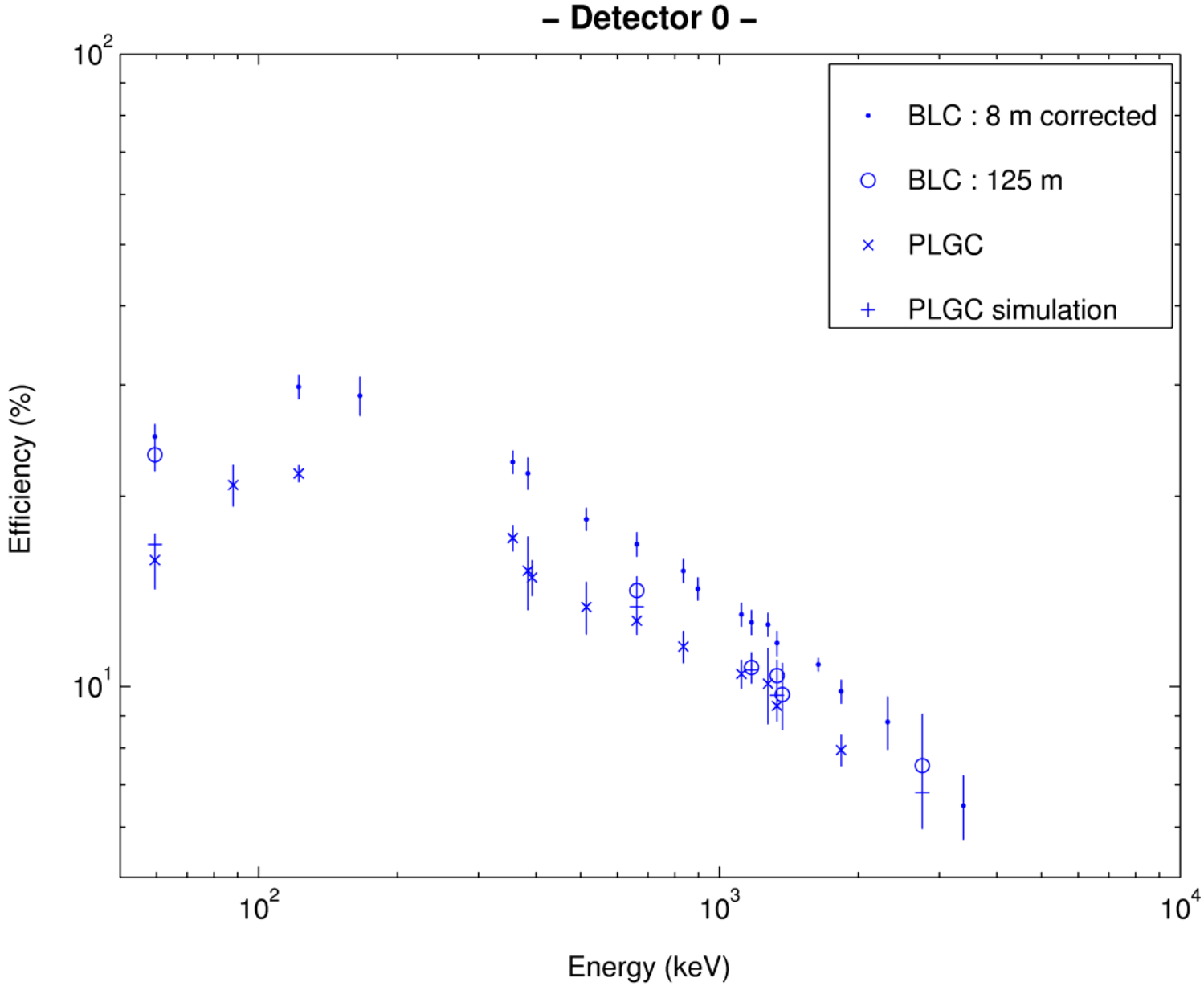

Conclusion

Planning expected

- Deadline for contribution : beginning of May
- Correction by a part or all the team
- Deadline for final article version : June

Comments are welcome …

SPI Team Meeting June 2003 at CESR

Roland Diehl

Papers and Analysis Plans

Papers

INTEGRAL A&A Volume

- ☆ SPI Data Analysis Overview
  - ☞ Draft Available
  - ☞ Contents: Introduce SPI Data Types and Tools, Guide to Special Papers
- ☆ ^{26}Al from the Galaxy
  - ☞ Outline Prepared
  - ☞ Contents: Report Detection of ^{26}Al from Galaxy (~"PV")

Others

- ☆ See R_Sci / Research Group Discussions
  - ☞ ^{26}Al Large-Scale Emission Results
    - line shape
    - spatial distribution
    - specials…
  - ☞ …

SPI Data Analysis Overview (0)

- Structure
  - Introduction: What is SPI, what its Analysis Toolbox
  - Data Preparation: from measurements to data types
  - Response: from event simulations & calibrations to IRF
  - Spectra: types, characteristics, calibrations
  - Imaging: dithering, deconvolutions and fitting
  - Background: types, measures to account for it in analysis
- Key Statements
  - Introduce SPI Data Types (from H/W to Data)
  - Introduce Suite of Analysis Tools
- Figures
  - Instrument's Basic Data Types
  - Observation Database Structure
  - (List of ISSW Tools?)

SPI Data Analysis Overview (1)

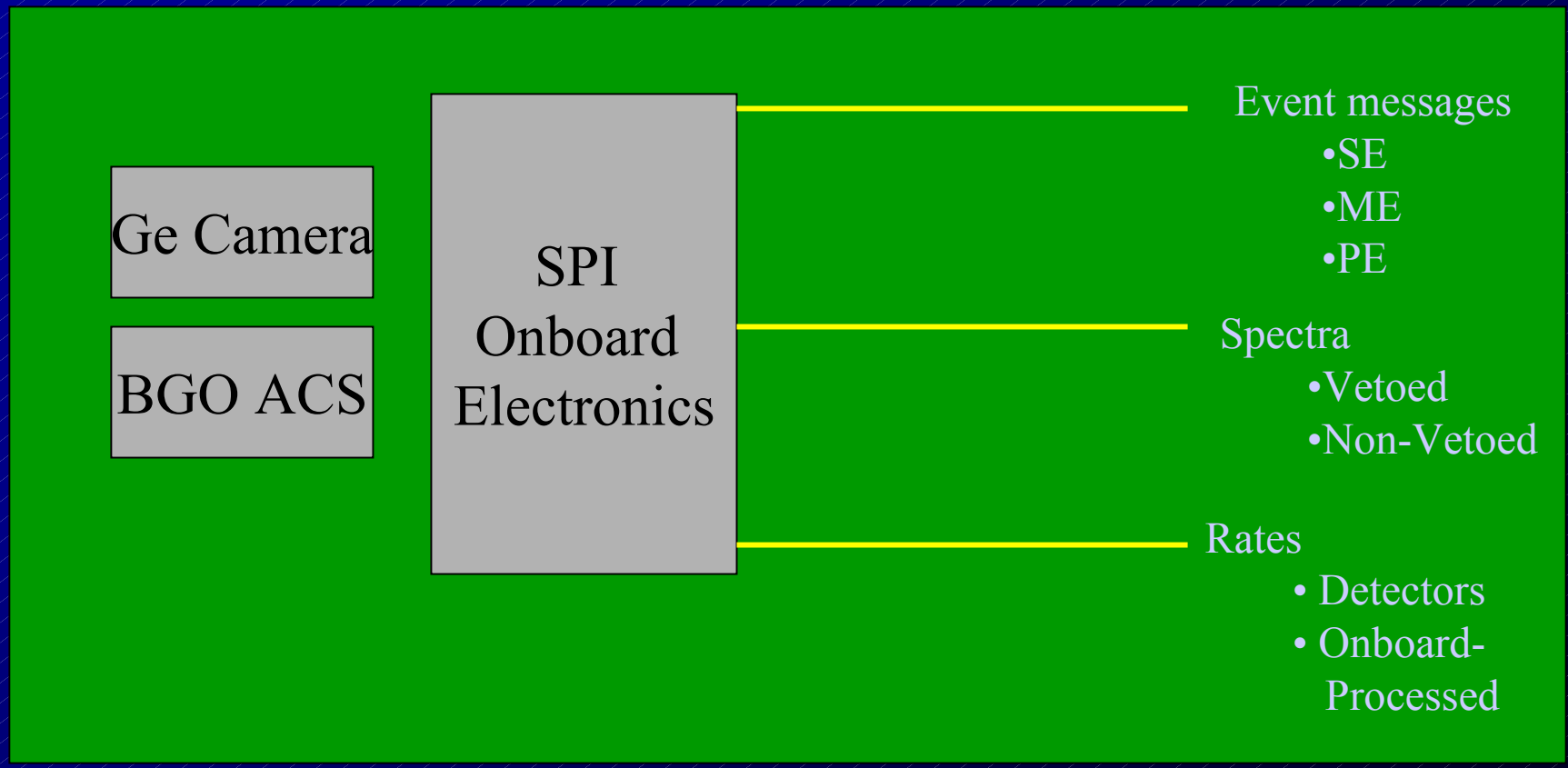

☆ Fig 1: SPI Data Types

SPI Data Analysis Overview (2)

- Observation
  - Set of Pointings
  - (Slews)

- Observation Database
  - Spectra
    - Per pointing
    - Per detector
    - Per event type
  - Pointings
  - Time Intervals
    - Live time
  - Bgd Monitors
    - Pointing
    - Time
    - Detector
    - Type
  - Response
    - Detector
    - Energy
    - Angle

Fig 2: Observation Database

GCDE First ^{26}Al

Goal

- Include ^{26}Al Detection Paper(s) in this A&A Volume (major goal)
- This should be a brief paper, ~2-4 pages.

Outline

- Introduction
  - Science Context
- Observations and Data
  - GCDE and ^{26}Al Line Region
- Results
  - ON/OFF results with Crab bgd
  - SPIDIFFIT and JK model fitting results (with various selections and parameters)
  - line width constraints (preliminary and conservative)
  - no images

Astronomy & Astrophysics manuscript no. "Neutron˙induced nuclear" June 6, 2003
(DOI: will be inserted by hand later)

Neutron-induced nuclear reactions and degradation in Germanium detectors

P. Leleux[1], F. Albernhe[2,3], V. Borrel[2,3], B. Cordier[4], R. Coszach[1⋆], S. Crespin[5], J.M. Denis[1], P. Duhamel[6], P. Frabel[3], W. Galster[1⋆⋆], J.-S. Graulich[1⋆⋆⋆], P. Jean[3], B. Kandel[3], J.P. Meulders[1], G. Tauzin[4], J. Vanhorenbeeck[6], G. Vedrenne[3], and P. von Ballmoos[3]

[1] Institut de Physique Nucléaire, Université catholique de Louvain, B-1348 Louvain-la-Neuve, Belgium
e-mail: leleux@fynu.ucl.ac.be
[2] Institut Universitaire de Technologie, Université Paul Sabatier,
F-31077 Toulouse, France
[3] Centre d'Etude Spatiale des Rayonnements, Université Paul Sabatier,
F-31028 Toulouse, France
[4] CEA-Saclay, DSM/DAPNIA/SAP, F-91191 Gif-sur-Yvette, France
[5] CEA-Bruyères, DAM/DPTA, F-91180 Bruyères-le-Chatel, France
[6] Institut d'Astronomie et d'Astrophysique, Université Libre de Bruxelles, B-1050 Bruxelles, Belgium

Abstract. We have measured cross sections of neutron-induced nuclear reaction leading to the delayed production of γ-ray lines similar to the ones of astrophysical interest. The neutron-induced degradation of Ge detectors was studied vs the neutron energy, the neutron fluence and the detector temperature. The recovery of the detectors was performed for different annealing temperatures.

Key words. neutron-induced background, neutron damage

1. Introduction

In the preceding contribution (Vedrenne 2003), the importance of the BGO shield to the definition of the field-of-view was emphasized. However, a negative consequence of the shield's presence is the abundant production of neutrons resulting from the interactions of primary cosmic rays in BGO. From the cosmic protons energy distribution, Monte Carlo simulations (Jean **?**) predict a neutron energy distribution inside the shield represented in Figure 1 [1]. This contribution reports an experimental study of the neutrons impact to the performance of SPI, in two directions :

i) the neutron-induced delayed production of γ-ray lines at the same energy as the ones from astrophysical sources (Section 2)
ii) the neutron-induced degradation of the Ge detector's energy resolution and the recovery after annealing (Section 3).

2. The background resulting from neutron-induced reactions

2.1. The problem

Neutron interactions in materials located inside the shield will lead to the delayed production of γ-ray lines. Being delayed, these events will not be vetoed by anticoincidence signals in the active shield. Several neutron-induced γ-ray lines coincide with lines of astrophysical interest :

⋆ *Present address*: Office for Scientific, Technical and Cultural Affairs, Brussels, Belgium
⋆⋆ *Present address*: Tohoku University, Sendai, Japan
⋆⋆⋆ *Present address*: CERN, Geneva, Switzerland

[1] Secundary protons are present as well but their abundance is smaller by a few orders of magnitude. Only above an energy of 350 MeV, protons become as abundant as neutrons.

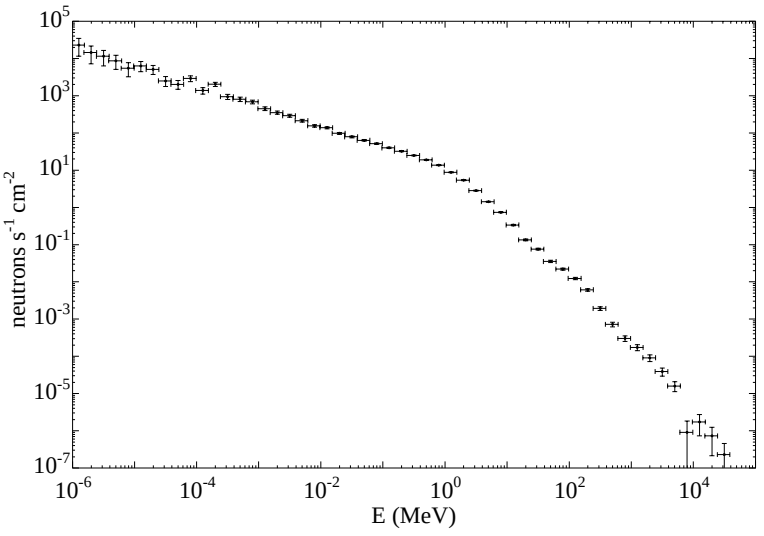

Fig. 1. Neutron energy distribution per sec per cm^2 inside the shield of SPI.

- The 122 keV and 136 keV lines from the decay of ^{57}Co are a signature of a Supernova event. The detection of these lines from SN1987a) was reported by OSSE (Kurfess 1992). Neutrons interacting with Ni nuclei inside the shield will produce the 122 and 136 keV lines through the ^{58}Ni(n,2n)^{57}Ni(β^+)^{57}Co reaction.
- The 478 keV line from ^{7}Be decays is expected from a nova explosion (Hernanz 1996). No positive detection of this line was reported by previous missions. The 478 keV line can result from neutron interaction with Be through the ^{9}Be(n,3n)^{7}Be reaction.
- The 847 keV line from ^{56}Fe was detected from SN1987a) (Matz 1988). The ^{56}Fe(n,p)^{576}Mn(β^-)^{56}Fe reaction leads to the emission of the same line.
- The emission of ^{60}Fe lines at 1173 keV and 1332 keV is expected from supernovae models (Woosley 1994), but no observed until now. The fact that models predict a ratio of ^{26}Al to ^{60}Fe depending on the mass of the progenitor is of particular interest. Both ^{60}Fe γ-ray lines can be produced by neutron interactions with Copper, by the ^{63}Cu(n,α)^{60}Co reaction (the 1332 keV line only), and the ^{63}Cu(n,4n)^{60}Cu reaction (both lines are present).
- Finally, the 1809 keV line from ^{26}Al was detected extensively by several missions, including CGRO, which succeeded to produce a global map of the ^{26}Al activity (Plüschke 2001). In astrophysical sources, this line results in fact from the decay of ^{26}Al to the first excited state of ^{26}Mg, at 1.809 keV above the ground state. Neutrons interactions with aluminium through the ^{27}Al(n,2p)^{26}Na(β^-)^{26}Mg will result in the same line.
  In addition, one should mention that a line at 1811 keV, very close to the ^{26}Al line and in fact within the energy resolution of SPI, can be obtained from the ^{56}Fe(n,p)^{56}Mn reaction reported above.

2.2. The solutions

No pessimistic conclusion about the possibility of detecting the above lines from astrophysical sources should be drawn from the previous section. The first point is that most of the above γ-rays belong to a cascade : if one of the γ-rays in the cascade is detected in the shield, the probability for the event to be vetoed is large. In addition, two complementary solutions exist :

- The first solution (in flight) consists in pointing successively into an astrophysical source emitting a line, and an empty field; this procedure requires the construction of a background model in order to take into account a possible variation of background versus time (or position in orbit).
- The second solution (prior to the flight), consists in performing an extensive simulation of neutron interactions with material inside the SPI shield, and deducing the amount of background produced in the lines of interest.

In the second solution, a most needed ingredient of the simulation is the cross section for neutron interaction in different material present inside the shield. Although nuclear models have been developed to predict such cross sections, the safest way consists to measure some cross sections over the neutron energy range of interest. The present work reports such measurements.

2.3. The experimental set-up

In the Cyclotron Research Center in Louvain-la-Neuve, a collimated neutron beam was produced by the Li(p,n) reaction induced by a proton beam in the 20-80 MeV energy range (Dupont 1985). The sample was placed at 1 m behind the collimator exit, and

irradiated for a period equal to two lifetimes of the nucleide of interest. After the irradiation, the sample was removed from the cave and placed in front of a 90 % HPGe detector which recorded decay gamma-rays, in a well-shielded area. In a particular measurement, i.e. the ^{27}Al(n,2p)^{26}Na reaction, the very short lifetime of the final nucleus ^{26}Na (1.09 s) precluded the above procedure. Instead of it, a fast mobile arm displaced the sample every two seconds in front of a HPGe detector placed 1 m below the neutron beam and strongly shielded. For each sample, measurements were performed for different proton beam energies, i.e. different neutron energies.

2.4. Results

The following reactions were measured :
^{58}Ni(n,np)^{57}Co and ^{58}Ni(n,2n)^{57}Ni(β^+)^{57}Co, from 24 MeV to 69 MeV; ^{9}Be(n,3n)^{7}Be from 25 to 70 MeV; ^{56}Fe(n,p)^{56}Mn from23 to 50 MeV; ^{63}Cu(n,α)^{60}Co and ^{63}Cu(n,4n)^{60}Cu from 24 to 69 MeV; ^{27}Al(n,2p)^{26}Na from 20 to 65 MeV. A detailed report on these measurement can be found in several publications (Duhamel 1998, Coszach 2000, Coszach 2001).

A minimal model was developed to extrapolate data to higher energies, up to 100 MeV. Some of these data were already incorporated in simulations yielding some predictions. In particular the ^{9}Be(n,3n)^{7}Be reaction was found to affect significantly the maximal distance from which 478 keV ^{7}Be γ-rays will be detected in SPI : the cross section for this reaction is indeed about 0.3 mb above 20 MeV neutron energy, and a large amount of Be (4.7 kg) is located very close to the detectors.

3. The neutron-induced degradation and recovery of HPGe detectors

3.1. The problem

It has been known experimentally for decades, that Ge detectors are subject to damages when exposed to fast neutrons. Lattice defects acting as charge carrier traps are in fact created in germanium crystals, leading to an increase of the energy resolution of the detector.

In the present geometry of the detectors, i.e. cylindrical, n-type Ge detectors are less sensitive to neutron damage, as holes - the most sensitive carrier type - are collected in the external surface and their average range in the crystal is small. For n-type detectors, significant damage is expected for integrated neutron fluences of about 10^{9} cm^{-2}. Simulations of the neutrons inside the shield of SPI predict this integrated fluence to be obtained in less than two years, i.e. the nominal lifetime of the instrument. It was thus decided from the early design of SPI, to embark onboard a heating system able to anneal the detectors in order to repair the damage.

The study reported in the present section aimed at answering the several questions regarding the damage and the recovery.

3.2. Experimental procedure

- Three different neutron beams were used : two monoenergetic beams of 5 MeV and 16 MeV, produced in Bruyères-le-Chatel (France) by the D(d,n)^{3}He and the T(d,n)^{4}He reaction, respectively and a continuous beam from 6 to 70 MeV with a 27 MeV mean energy produced in Louvain-la-Neuve (Belgium) by the p + ^{9}Be interaction at 65 MeV energy. The latter beam simulates quite well the neutron energy distribution to which detectors will be submitted in orbit. In addition, neutrons below 70 MeV represent 96 % of the whole neutron fluence in orbit.
- Flight model detectors were irradiated with different neutron fluences ranging from 3.6×10^{8} cm^{-2} to 1.6 x 10^{9} cm^{-2} in different neutron beams. The lower fluence is the one expected during one year in orbit. Detectors were irradiated with high-voltage (HV) ON.
- The parameters used to estimate the damage were the ratio of the Full-Width-at-Tenth-of-Maximum (FWTM) to the Full-Width-at-Half-Maximum (FWHM), and the relative increase of the FWTM or the FWHM. The ^{60}Co peak at 1332 keV was selected for that purpose.
- Annealings were performed with the detector capsule being pumped down to a pressure of a few 10^{-6} Torr.

3.3. Results

3.3.1. Damage versus neutron fluence and neutron energy

Data for both problems are reported in Figure 2.

For 16 MeV neutrons, the degradation versus the neutron fluence was measured up to 5×10^{9} n/cm^{2}. No saturation of the damage is appearing for either measured variable, i.e. the relative increase of the FWHM and the FWTM. In the same figure, the degradation versus the neutron energy was also plotted ; it shows the extreme sensitivity of both variables to the neutron energy. In particular, the relative increase of the FWTM is rising very quickly for high-energy neutrons, prohibiting to submit the detector to fluences larger than 6×10^{8} n/cm^{2}. Let us recall that the energy distribution of the 6-70 MeV neutrons is close to the

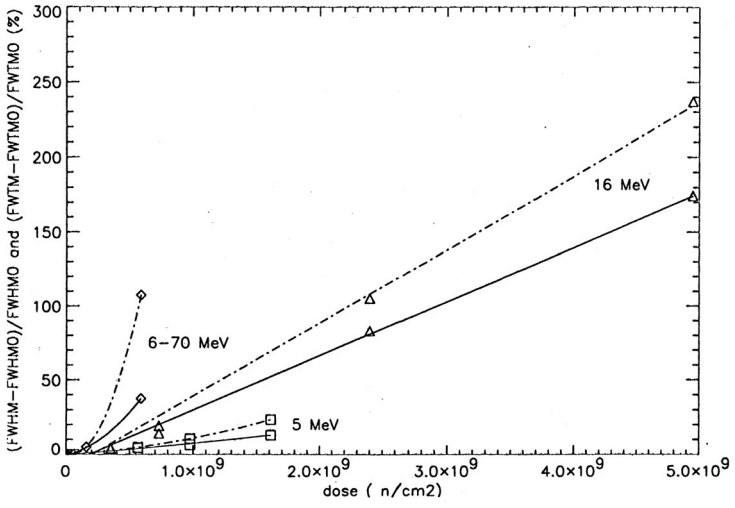

Fig. 2. Degradation of a Ge detector vs the neutron fluence, for different neutron beams (5 MeV, 16 MeV, 6-70 MeV). Two parameters are measuring the degradation : the relative increase of the FWHM (solid line) and the relative increase of the FWTM (dot-dashed line).

one expected in orbit. From the data of figure 2, an annealing in orbit appears mandatory after a fluence of about 6 x 10^8 n/cm^2 at most. A detailed report of these measurement can be found in ref. (Borrel 1999).

3.3.2. Damage versus detector temperature

Although unlikely, a failure of a cryocooler in orbit cannot be excluded. Such a failure would cause an increase of the Ge detectors temperature. Two detectors were irradiated while they were at different temperatures, i.e. 91 K and 110 K. Clearly the damage in the ”hot” detector was more important and it increased faster at lower fluences. However, when cooled down to a lower temperature, this detector showed a partial recovery of the energy resolution. See ref. (Kandel 1999) for more data on this work.

3.3.3. Annealings

The strategy was the following : a detector was first submitted to a neutron fluence of 3.6×10^8 n/cm^2 in the 6-70 MeV energy range. One day after the irradiations the detector activity had decreased enough for a resolution measurement to be done, and the initial degradation to be estimated. Then the detector was warmed up to the annealing temperature. The annealing was interrupted after each period of about 24 h in order to measure the detector energy resolution with a ^{60}Co source, and then started again ; this sequence was repeated several times. The parameter of interest was the annealing temperature. In fact, when these measurements were performed, the temperature of the annealings in orbit was not yet decided and it was interesting to measure beforehand the loss of observation time caused by an annealing. Annealings were performed at three different temperatures, 94 ° C, 100° C and 105° C. Results are reported in Fig. 3. The parameter measured here is the ratio of the FWTM to the FWHM of the 1332 keV ^{60}Co peak, which should be equal to 1.82 for a Gaussian peak. Data indicate that an annealing at 94 ° C does not provide with a full recovery after 8 days ; in fact an additional period of a few days at 100 ° C was requested in order to complete the return to the original resolution. At the other extreme, the annealing at 105 ° C yielded a fast recovery. A full account of the measurements related to annealings is in ref. (Albernhe 2002).

4. Conclusions

The impact of neutrons on the performance of the SPI Ge detectors was studied experimentally in two fields, the neutron-induced background in the gamma-ray lines, and the neutron-induced degradation and recovery of the detectors. It the first domain, cross section measurements aiming at a better accuracy of the simulations were performed. In the second case, the degradation was measured versus the neutron fluence and the detector temperature, and the recovery was obtained for different annealing temperatures.

It should be noted that since the launch of INTEGRAL, a first annealing of the SPI detectors was performed, on Feb. 6, 2003, i.e. after 110 days in orbit. At that time, the FWHM of the detectors had increased on average by 15 % w.r.t. the original values. The annealing temperature of 105.7°, was maintained for 36 h. A complete recovery of the resolution was found after annealing, as expected from our data in Fig. 3.

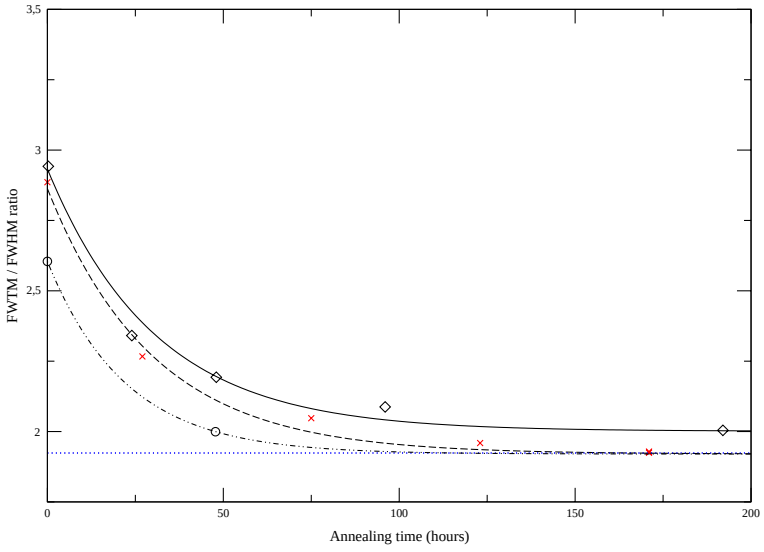

Fig. 3. Recovery of a detector vs the annealing time. The parameter used to quantify the recovery is the FWTM/FWHM ratio, which is equal to 1.82 for a perfect detector (horizontal dotted line). Annealings were performed at three different temperatures : 94° C (diamonds fitted with the solid line) ; 100° C (crosses fitted with the dashed line), and 105° C (open dots fitted with the dot-dashed line).

This work was granted by a PRODEX budget from the Office for Scientific, Technical and Cultural Affairs, Brussels. P.L. is a Research Director of the National Fund for Scientific Research, Brussels.

References

Vedrenne, G. et al. 2003, A&A, this volume
Kurfess, J.D. et al. 1992, Ap. J. Lett., 399, L137
Hernanz, M. et al. 1996, Ap. J. Lett., 465, L27
Matz, S. et al. 1988, Nature, 331, 416 ; Teegarden, B.J. et al. 1989, Nature, 339, 122
Woosley, S.E. and Weaver, T.A. 1994, Ap. J., 423, 371
Plüschke, S. 2001, Ph.D. Thesis, Technische Universiät München, MPE-Report 276
Dupont, C. 1985, Nucl. Phys, A445, 13
Duhamel, P. et al. 1998, Nucl. Instr. Meth. Phys. Res., A404, 143
Coszach, R. et al. 2000, Phys. Rev., C61,064615
Coszach, R. et al. 2001, in ”Exploring the Gamma-Ray Universe”, ESA-SP459, 557
Borrel, V. et al. 1999, Nucl. Instr. Meth. Phys. Res., A430, 348
Kandel, B. et al. 1999, Nucl. Instr. Meth. Phys. Res., A430, 363
Albernhe, F. et al. 2002, Nucl. Instr. Meth. Phys. Res., A492, 91

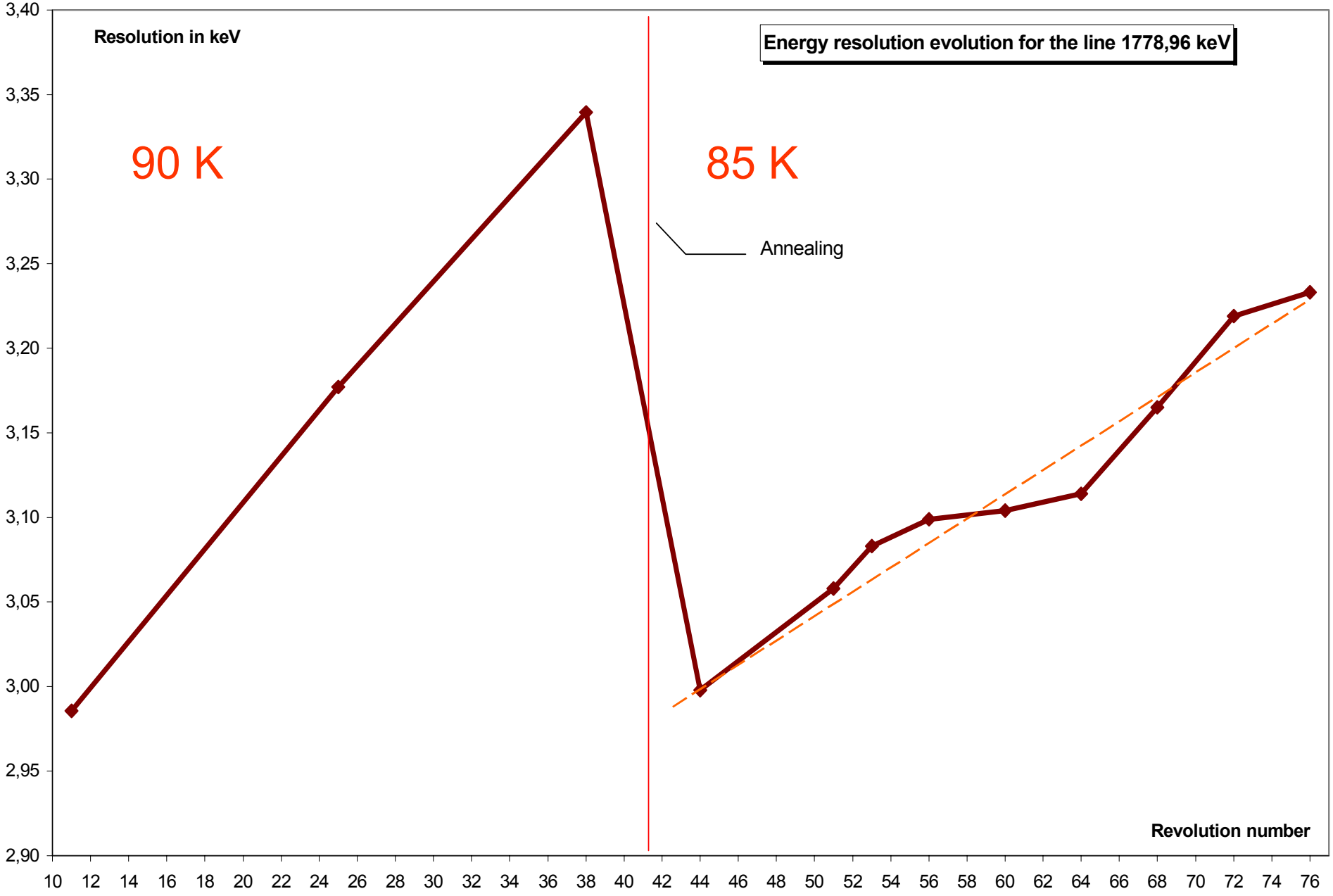
Energy resolution evolution for the line 1778,96 keV
Resolution in keV
90 K
85 K
Annealing
Revolution number
3,40
3,35
3,30
3,25
3,20
3,15
3,10
3,05
3,00
2,95
2,90
10 12 14 16 18 20 22 24 26 28 30 32 34 36 38 40 42 44 46 48 50 52 54 56 58 60 62 64 66 68 70 72 74 76

Line	198,4 keV	882,5 keV	1107 keV	1117,4 keV	1764,3 keV	1778,96 keV	2754 keV
Date	Energy resolution in keV						
13th – 18th Nov (around rev 10-12)	1,82	2,29	2,66	2,51	2,90	2,99	4,03
27th Dec – 2nd Jan (rev 25-26)	1,79	2,34	2,71	2,69	3,03	3,18	4,43
5th – 6th February (rev 38)	1,85	2,47	2,83	2,88	3,13	3,34	4,66
After annealing : rev 45	1,83	2,32	2,66	2,71	2,90	2,97	4,01
dégradation en 15 révolutions	0,0%	1,9%	2,1%	6,9%	4,3%	6,4%	10,1%
dégradation en 27 révolutions	1,7%	7,6%	6,7%	14,6%	8,1%	11,9%	15,7%
rev 44-45	**1,83**	**2,31**	**2,65**	**2,72**	**2,90**	**3,00**	**4,04**
rev 51	1,83	2,31	2,66	2,74		3,06	4,01
rev 53	1,83	2,34	2,68	2,76		3,08	4,11
rev 56-57	1,83	2,34	2,69	2,8	2,97	3,10	4,15
rev 60-61	1,83	2,35	2,70	2,85	3,01	3,10	4,17
rev 64-65	1,83	2,34	2,73	2,87	3,01	3,11	4,23
rev 68-69	1,83	2,34	2,72	2,899	3,02	3,17	4,29
rev 72-73	1,84	2,39	2,75	2,939	3,05	3,22	4,30
rev 76-77	**1,83**	**2,42**	**2,75**	**2,976**	**3,04**	**3,23**	**4,39**
dégradation en 16 révolutions	0,1%	1,4%	2,0%	4,8%	3,5%	3,5%	3,3%
dégradation en 32 révolutions	-0,1%	4,5%	4,0%	9,4%	4,5%	7,8%	8,6%

NEXT ANNEALING
based on 90K operation

- Degradation before 1st annealing was 10% at 1.3 MeV.
- Doing a linear extrapolation 20% degradation will be obtained in August.

NEXT ANNEALING
Temperature dependance

- Warming up a degradated detector degradates the FWHM
- How much from 85K to 90K ?
- Worst case same degradation than 90K operation

NEXT ANNEALING
Based on 85 K operation

- At 85 K degradation is 0.7 slower compared to 90K
- If we assume all linear and wait 20% damage at 85K it is equivalent to a 30%damage at 90 K

NEXT ANNEALING

- At 85 K degradation is 30 % slower than at 90 K
- But the dose is the same
- Before next annealing we need 24 Hr at 90K in order to ‘unfreeze’ the damages and to return to our 90K reference
- First annealing was after 3 monthes
- To be secure about the result next annealing need to be performed around August 15

ACS status:

Count rate stability of the last 100 days:

Answers to:

drifts, gain stability ?

controls needed ?

tunning needed ?

ACS health and performance monitoring

- Short-term monitoring ➡ ISDC
  - Automatic monitoring of ACS HK-data
  - Automatic alert generation in case of:
    - count rate of single FEE, or ACS overall count rate exceeds upper or lower alert limit
    - FEE or VCU malfunction (e.g HV, LV outside nominal range)
  - Indirect monitoring via ACS burst-alert system
    - Sensitive to count-rate changes in the 50 ms to 100 s range
    - Unusual increase of ACS GRB alert rate will trigger a health check
- Long-term monitoring (> 3 days) ➡ MPE
  - Gain drifts and stability
  - HK data:
    - single FEE count rates
    - ACS overall count rate
    - ACS temperatures
  - Tool: OSM averaged HK data (available after completion of orbit)
  - Decision on HV or threshold adjustment (tuning)

ACS
overall count rate of 100 days: 27.02 - 06.06.2003

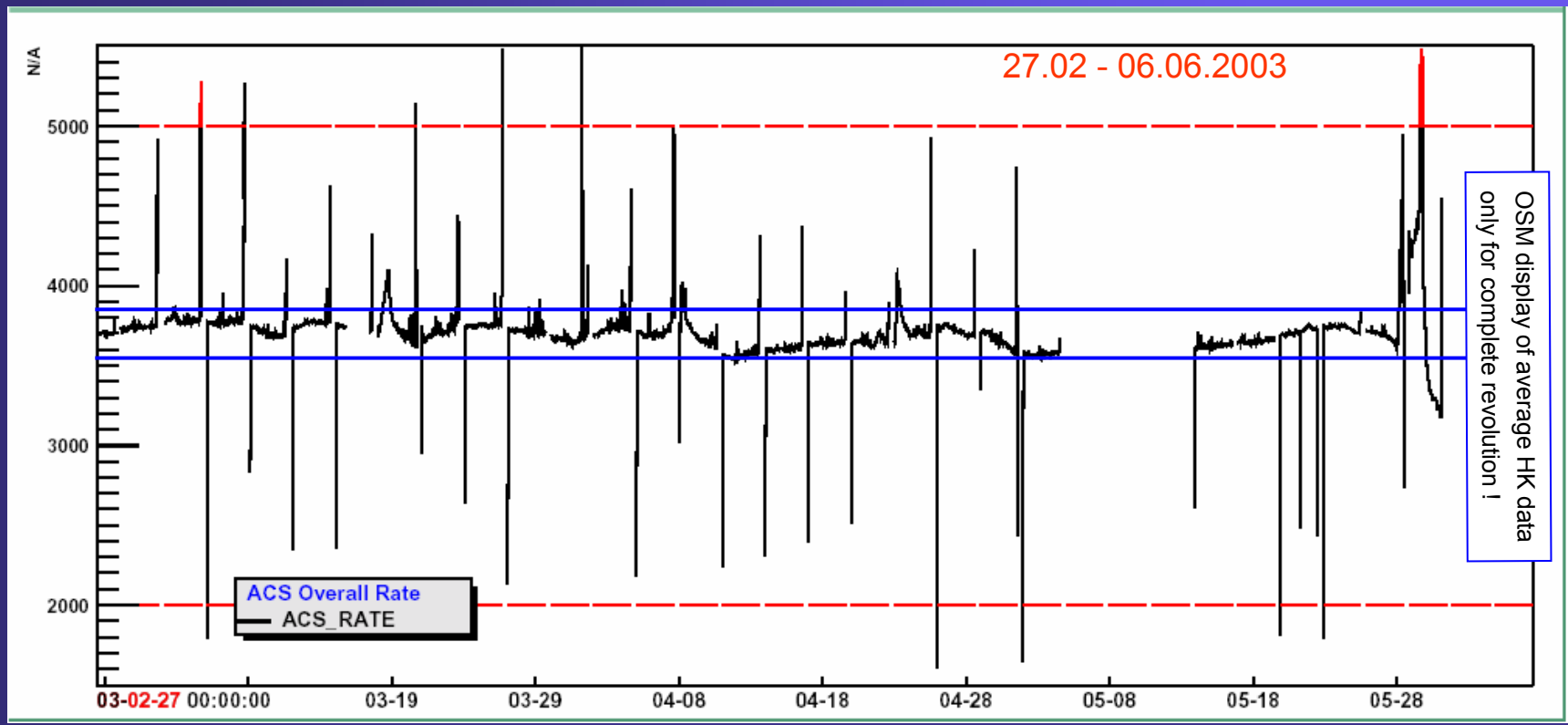

PSAC count rate:

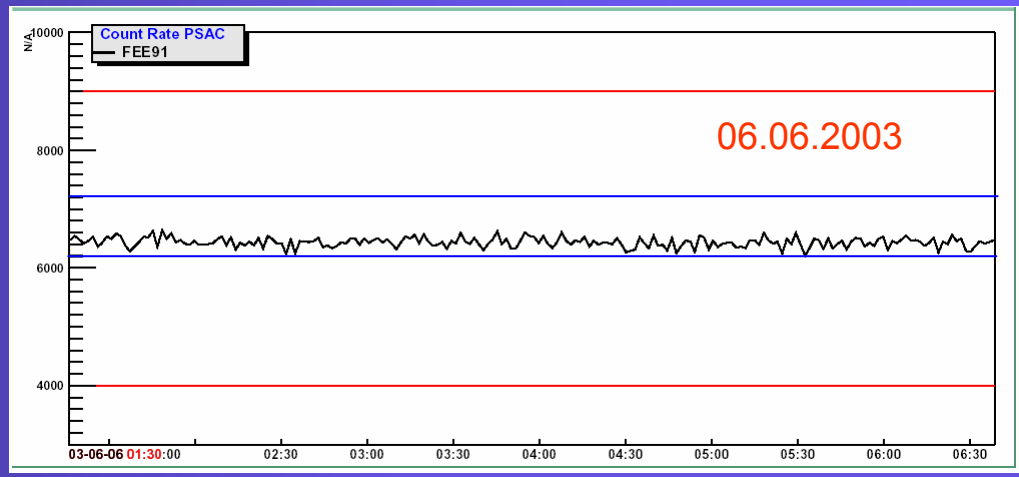

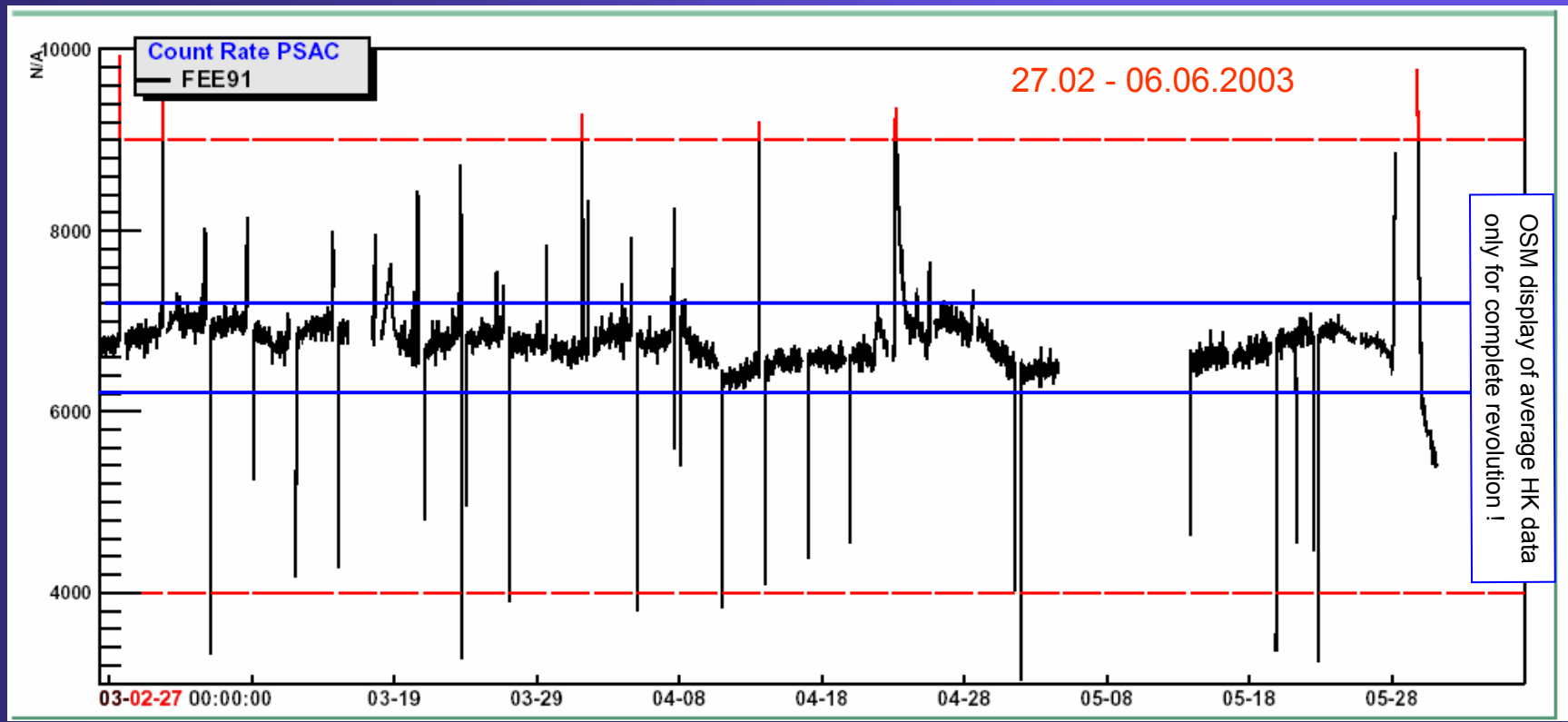

UCR count rates: 27.02 - 06.06.2003

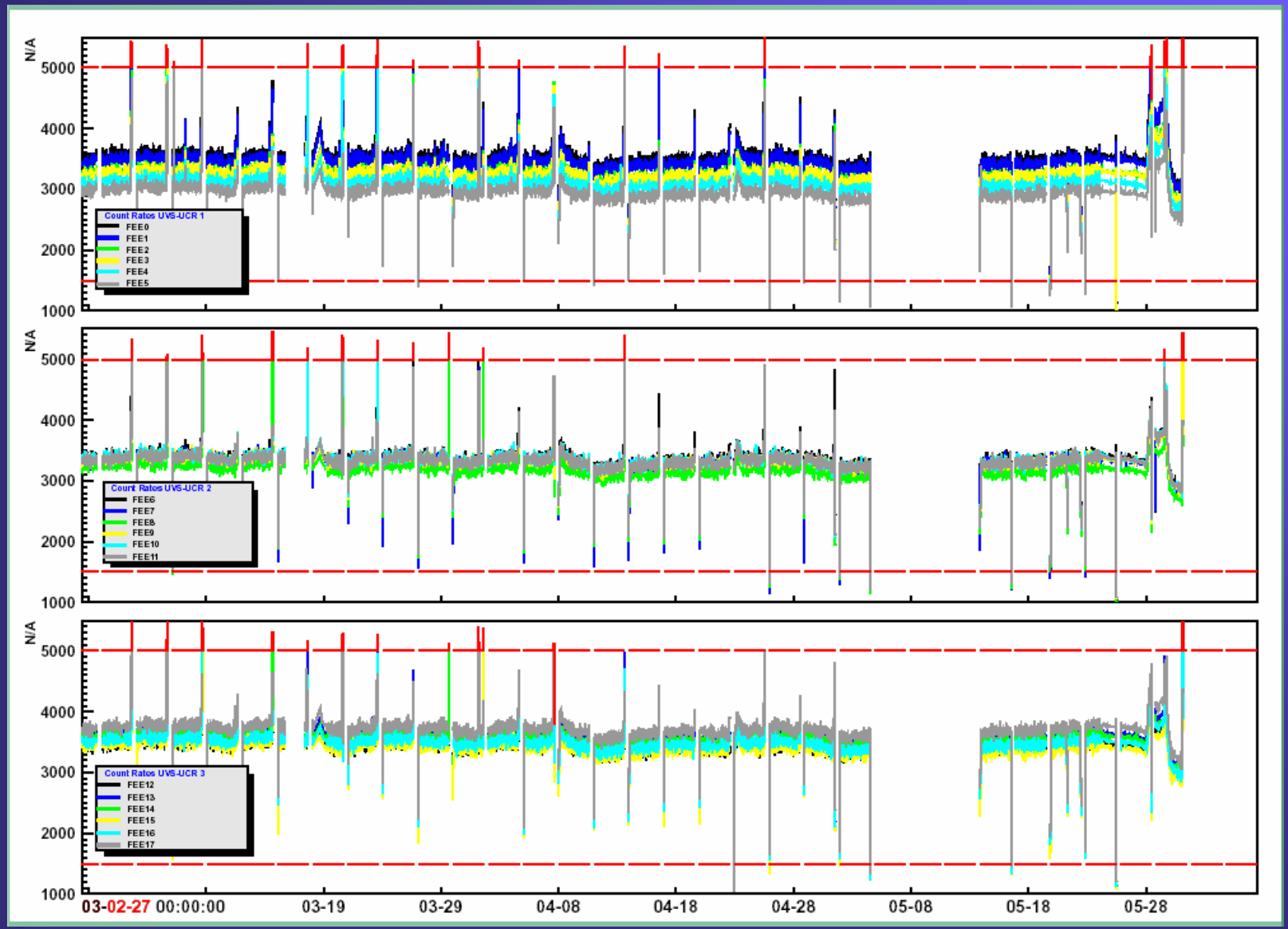

LCR count rates: 27.02 - 06.06.2003

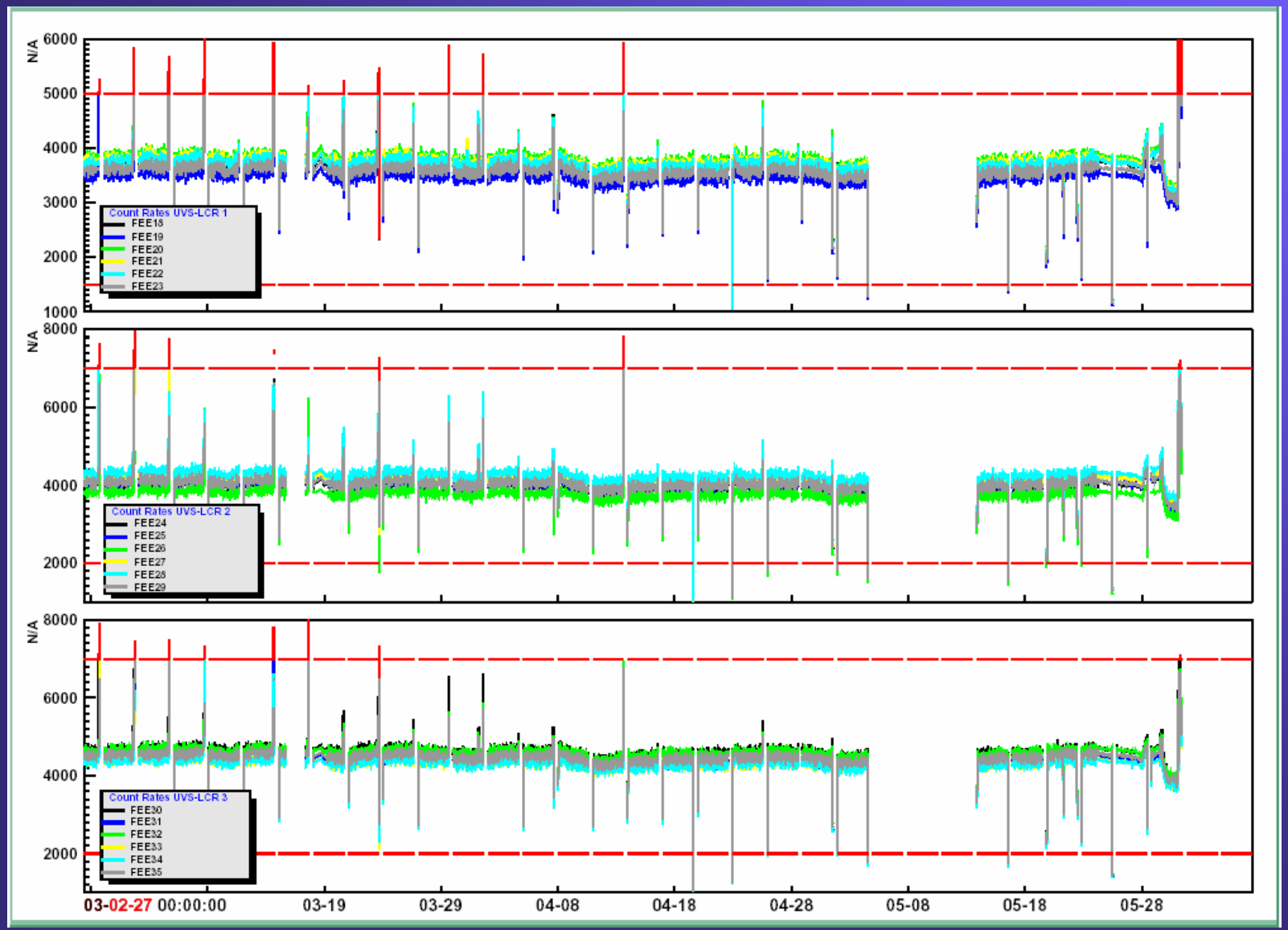

SSA count rates: 27.02 - 06.06.2003

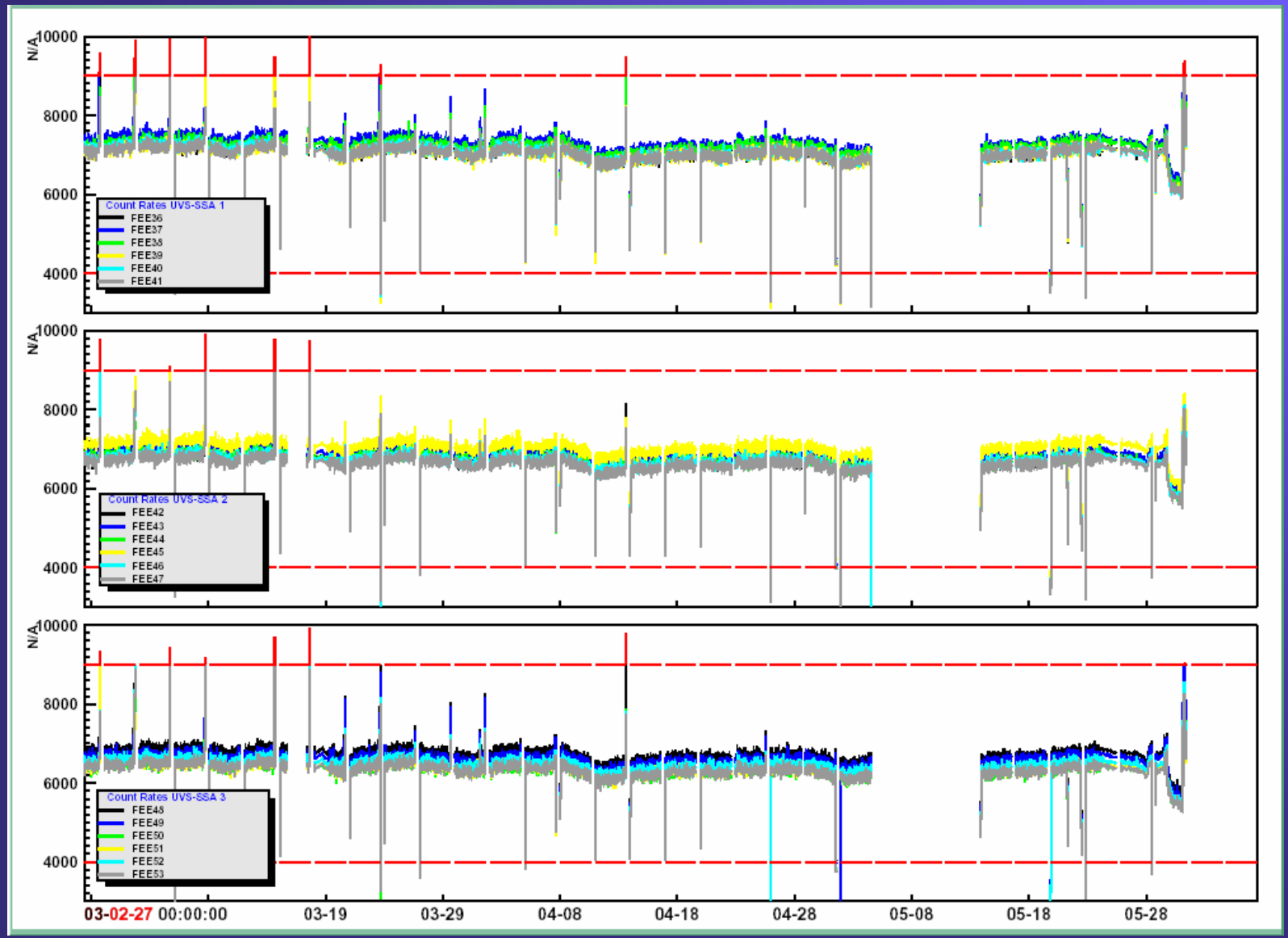

RST count rates: 27.02 - 06.06.2003

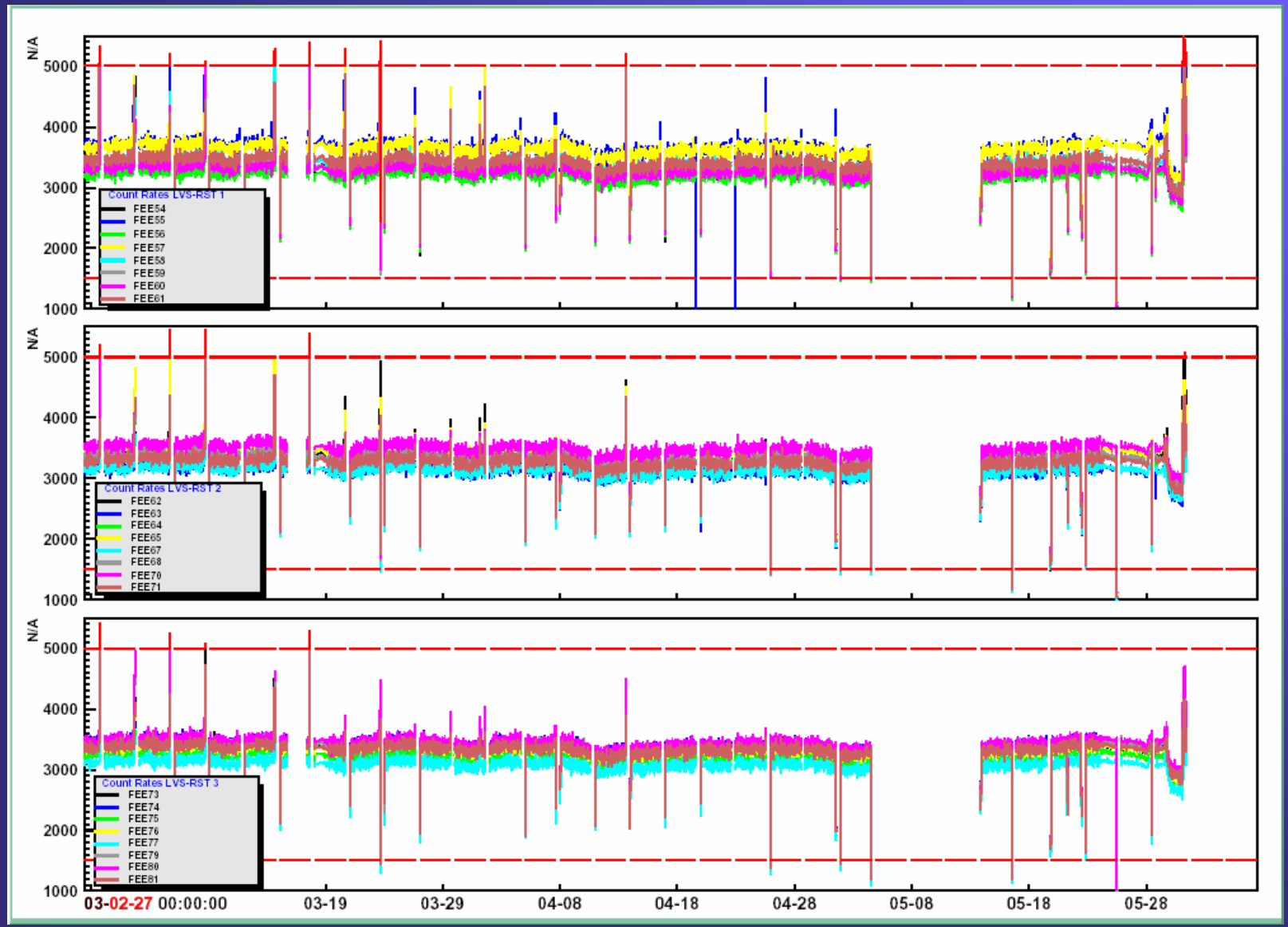

RSP count rates: 27.02 - 06.06.2003

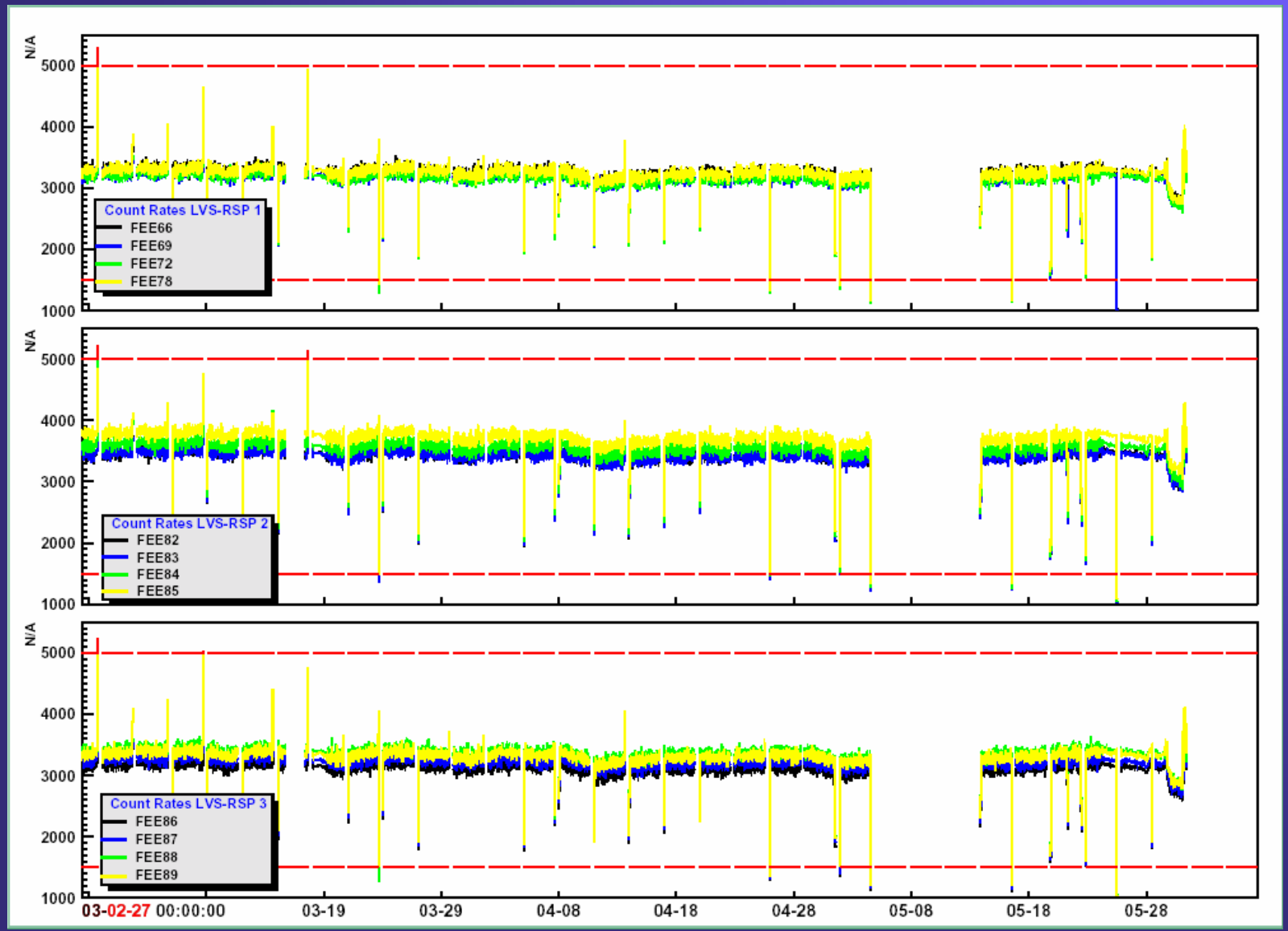

SCS count rates: 27.02 - 06.06.2003

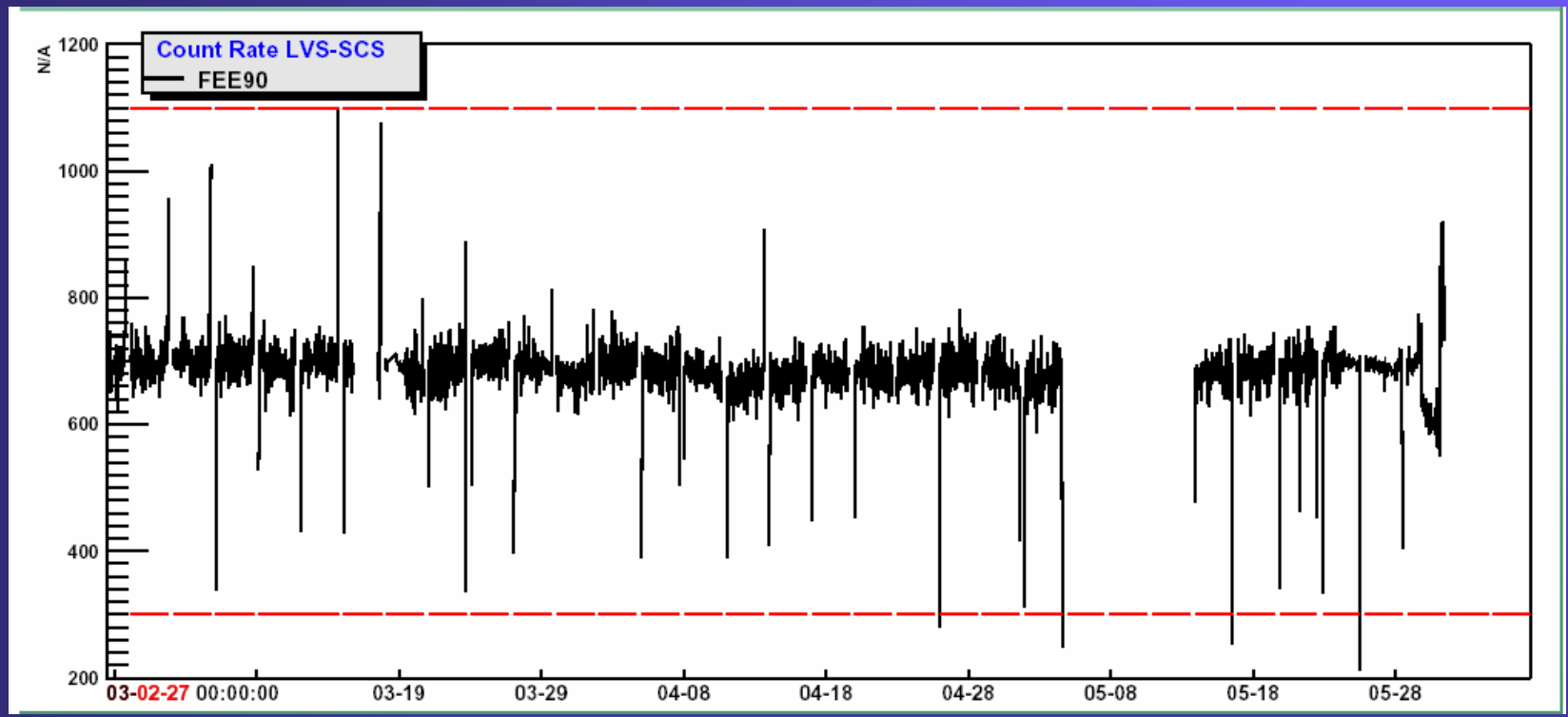

ACS temperatures: 27.02 - 06.06.2003

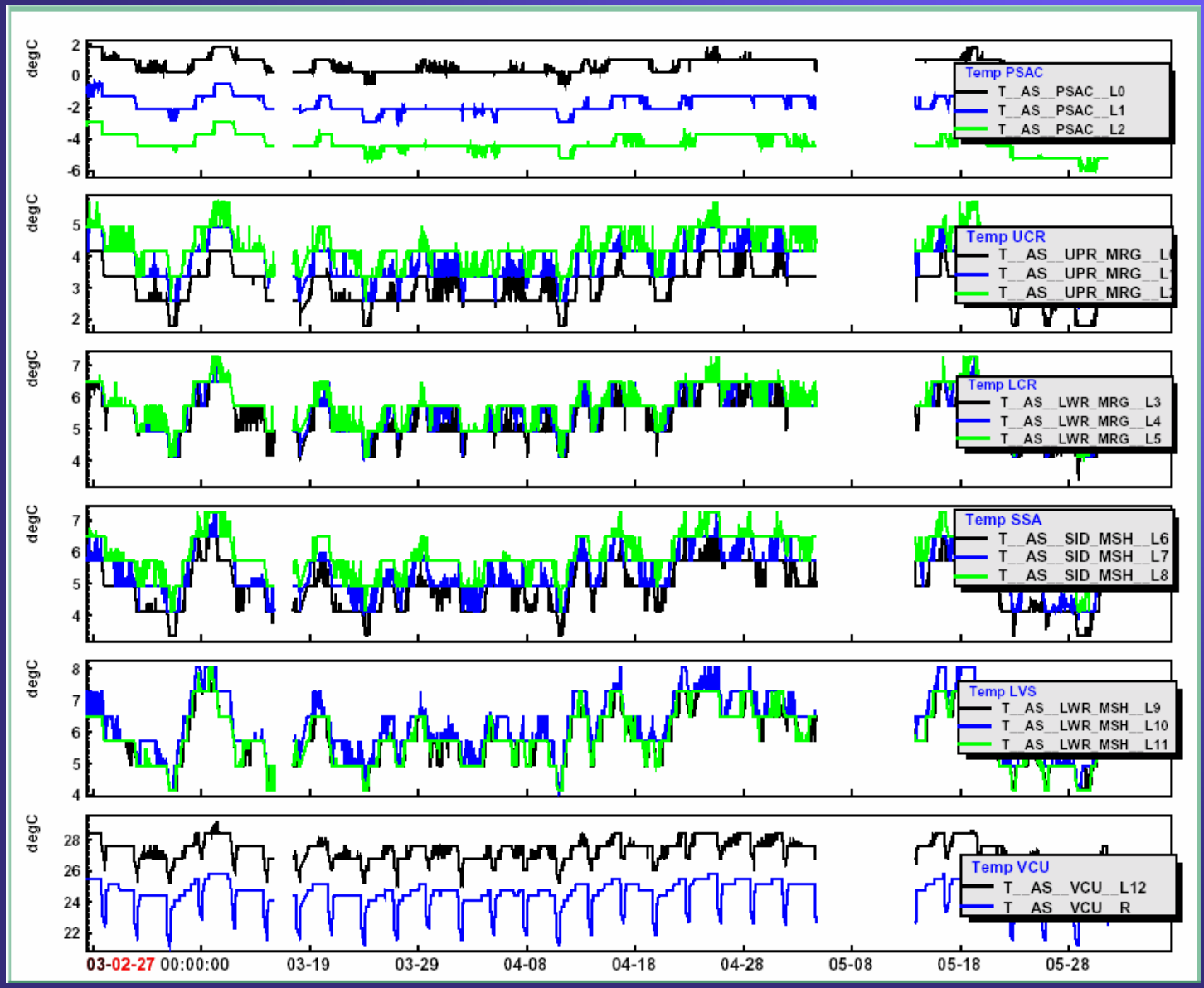

Conclusion

- Up to now
  - No major gain drifts observed

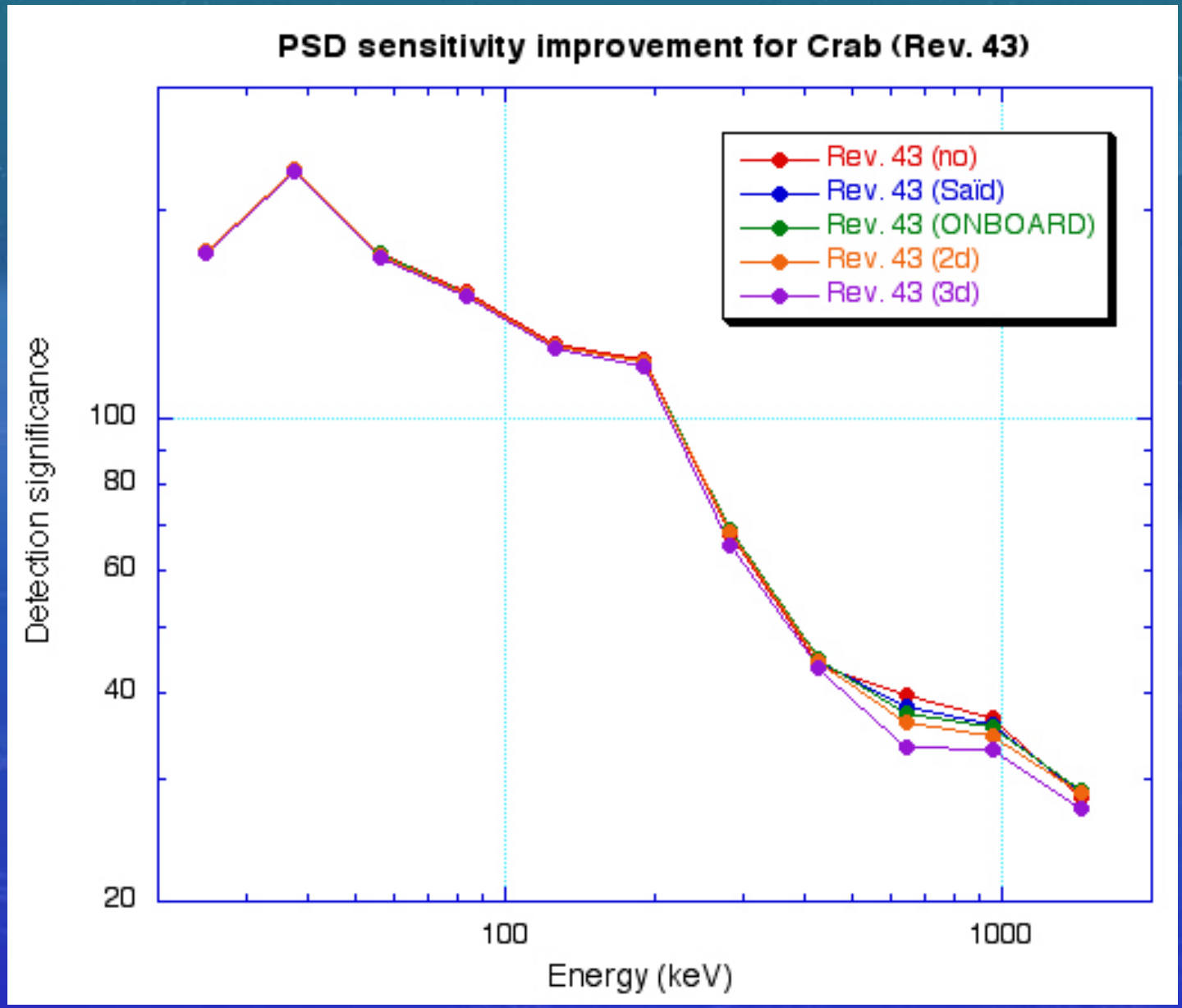
PSD sensitivity improvement for Crab (Rev. 43)
Rev. 43 (no)
Rev. 43 (Saïd)
Rev. 43 (ONBOARD)
Rev. 43 (2d)
Rev. 43 (3d)
Detection significance
100
80
60
40
20
100
1000
Energy (keV)

SPI Scientific Team Meeting

held in Toulouse, June 12, 2003

SPI in flight telemetry need
SPI data loss due to telemetry limitation
SPI in flight telemetry allocation
Solutions by DPE reprogramming

Stéphane Schanne
CEA Saclay / DAPNIA / Bât. 709, F-91191 Gif sur Yvette
Schanne@hep.saclay.cea.fr

Standard Acquisition without data loss

- SPI data acquired on 15th of November 2002, PktAll.000638, packets 429781 to 444622.
  (just before the SPI Activity Card 290)
  - nominal SPI configuration (SE, ME, PE, no On-Board-Spectra)
  - PST = 140 Packets / 8 s
  - no data loss

- Packet statistics:

input	apid	pkt count	count/8s
spacecraft	**0**	**68**	0.43
	129	**636**	4.04
	640	**447**	2.84
SPI-HKt	**1024**	**160**	1.02
	1025	**187**	1.19
SPI-PhPh	**1088**	**12604**	80.11
SPI-HKs	**1120**	**158**	1.00
	1121	**158**	1.00
	1122	**158**	1.00
	1123	**158**	1.00
	1124	**158**	1.00
SPI-total with Spectra off			*87.34*

- With On-Board-Spectra OFF, SPI needs a TM allocation of 87.5 Packets / 8 s
- With On-Board-Spectra ON, SPI needs up to 92.5 Packets / 8 s (depends on Spectra mode)

- Standard pre-launch TM allocation: 36 Packets / 8 s

SPI TM allocations used and data losses

Source	PV	Crab	GCDE	GCDE	GCDE	now
PktAll reference number	638	723	00:00	764	828	931
observation start date	15/11/02	19/2/03 19:28	3/3/03 6:49	27/3/03 15:51	23/4/03 15:16	7/6/03 13:13
observation duration (s)	1258	40910	63011	54781	51014	42398
	pkt/8s	*pkt/8s*	*pkt/8s*	*pkt/8s*	*pkt/8s*	*pkt/8s*
Telemetry allocation	140.00	100.00	59.00	69.00	74.00	98.00
Telemetry use (APID)						
1024 CSSW HK	1.02	1.00	1.00	1.00	1.00	1.00
1025 IASW HK	1.19	1.16	1.16	1.16	1.16	1.16
1088 Science Data	80.15	82.27	47.99	58.43	63.78	79.74
1104 Spectra	0.00	0.83	0.85	0.00	0.00	0.00
1120 Science HK1	1.00	1.00	1.00	0.99	1.00	1.00
1121 Science HK2	1.00	1.00	1.00	0.99	1.00	1.00
1122 Science HK3	1.00	1.00	1.00	0.99	1.00	1.00
1123 Science HK4	1.00	1.00	1.00	0.99	1.00	1.00
1124 Science HK5	1.00	1.00	1.00	0.99	1.00	1.00
used packets	87.38	90.30	56.00	65.55	70.94	86.90
unused packets	52.62	9.70	3.00	3.45	3.06	11.10
Science Data loss / PV	0.00%	-2.64%	40.13%	27.10%	20.42%	0.51%

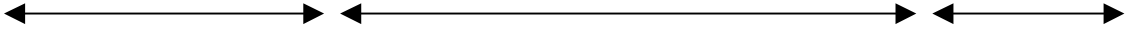

•no Data Loss
•strong source like Crab needs ~3 Packets more

•Data Loss
•Not using ~3 allocated Packets (for an unknown reason)

•no Data Loss

SPI Telemetry allocation vs time

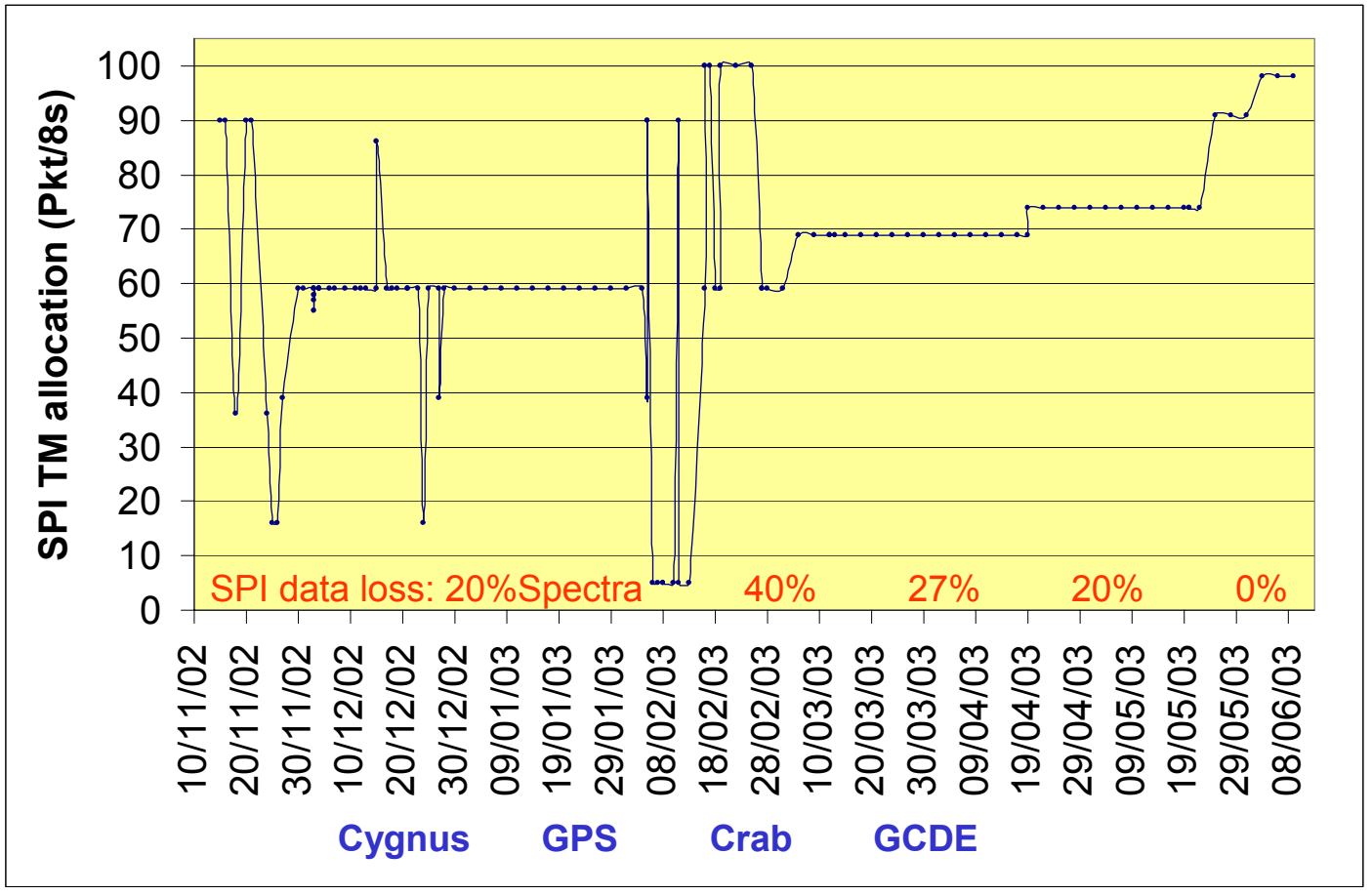

SPI Mode: PE, ME, SP-NV → SE, ME, PE

Spectra losses — Data losses (data gaps) — No data losses

S.Schanne@cea.fr

Reduction of SPI telemetry need by on board filtering (DPE reprogramming)

- **ME reduction (MEr23) by rejection of higher multiplicity ME and compression of Doubles&Triple**
  - On board removal of detector 19 (PSD inside ME tables)
  - From this ME tables keep only:
    - Double ME, coded on 3 words with time resolution 409.6 μs (instead of 102.4 μs)
    - Triple ME, coded on 4 words with time resolution 819.2 μs (instead of 102.4 μs)
  - ***gain = 11.4 TM Pkt/8s***

- **SE reduction (SEr) by line filtering**
  - ***gain < 19.6 TM Pkt/8s***

•we have to decide which bands to reject

• rejected bands are still present inside the On-Boad-Spectra (if switched on!)

	Eband lo	Eband hi	Ewidth	SE/Eband	SE fraction	data-w/TF	data-pkt/8
	0	9000	9000	558500	100.00%	110.90	*33.1*
1	21	28	7	21238	3.80%	4.22	*1.2*
2	50	71	21	156512	28.02%	31.08	*9.2*
3	90	106	16	36526	6.54%	7.25	*2.1*
4	137	144	7	41730	7.47%	8.29	*2.4*
5	193	203	10	73592	13.18%	14.61	*4.3*
total selected lines			61	329598	**59.01%**	65.45	*19.5*

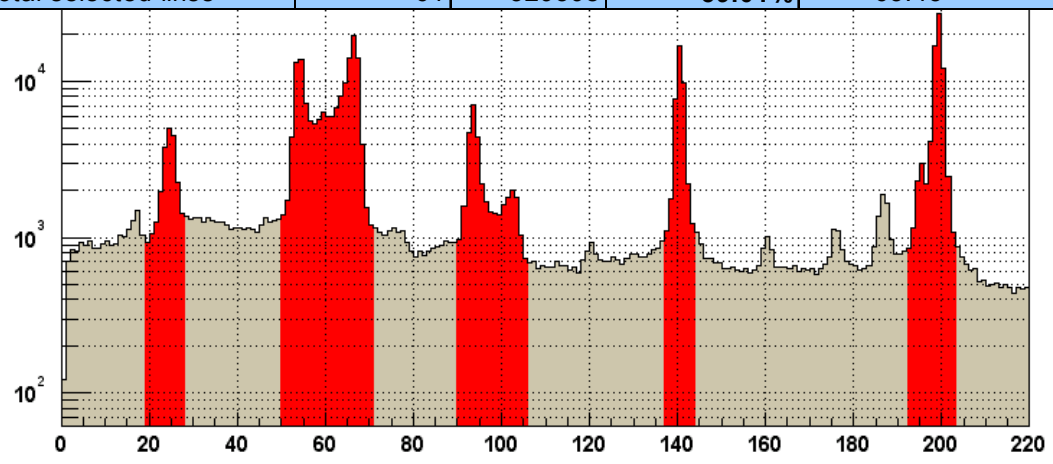

- **Planning:**
- *The DPE software company should deliver soon a version of the new software.*
- *Tests will be performed at CESR using the SEM and data provided by CEA.*

S.Schanne@cea.fr

Integral Spectrometer

IASW status

Anomalies still open

- **INT-002083**: IASW tasks killed by CSSW: heavy operational consequences, need to switch OFF/ON the DPE and restore SPI configuration, but only one occurrence since launch.

- **INT-002024**: Fixed point overflow detected by CSSW. No operational consequence.

These 2 anomalies seems to be related to the same kind of cause, investigation is on going by CSSW developer.

Integral Spectrometer

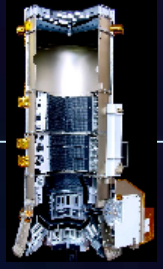

IASW status

Anomalies still open

- **INT-002082**: TM slot lost, not identified at this time. Can be 3 TM slots lost each 8 seconds! The behaviour is checked currently by MOC (PST structure, TM synchronisation, CPU load...).

The review board of MPVR decided to organize the assistance of Mike Rennie (DEIMOS) to solve this anomaly.

Integral Spectrometer

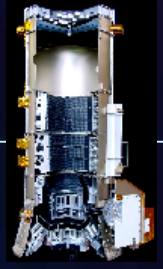

TM reduction study

In the conditions of April 2003, in order to have no data loss, the telemetry need of SPI is around 94 TM packets/8s.
In the future, closer to solar minimum, the background is expected to increase, and so will the telemetry need.
A possibility of reprogramming the on board software in order to compress the Multiple Events and to reduce the Single Events by line filtering before transmission to ground is currently under investigation in the SPI
A realistic schedule was to start the modification implementation in May.

8 weeks are necessary to implement and test the modifications. If everything is well (no CPU overload for example), this new version could be uploaded by July, 2003.

Integral Spectrometer

New IASW release 4.3.0

5 Change Request already accepted by CNES and the PI, to be implemented in next IASW version 4.3.0

- **CR 567rev1**

  Spectra and photon relative priority(better operability)

- **CR 568rev1**

  Multiple events reduction in order to lower the SPI TM need (timing of double-ME should be 409.6 μs, 819.2 μs for triple-ME, more than 11 packets/8s saved)

- **CR 572**

  Line filtering in the SE table (6 to 10 more packets/8s saved, depending on lines filtered), configurable (parameters or patch)

Integral Spectrometer

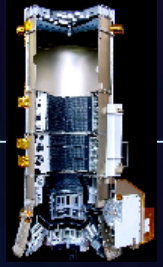

New IASW release 4.3.0

- **CR 575**

  Photon processing configuration (to choose by conf parameter which kind of CR to implement (CR 572: line filtering or/and CR 568: ME reduction) or nothing!

- **CR 576**

  New synchronisation word (if the ME block was processed by the ME reduction algorithm (new format: 7670 d48c 7670 d48c) or not (old format: 7670 d48b 7670 d48b)). This "mark" in the data itself indicates which kind of data organisation is delivered by the SPI IASW and so which kind of de-commutation software should be used.

Integral Spectrometer

New IASW release 4.3.0

ESA CR to be submitted as soon as first test are OK, this CR will gather at least all CR presented here. We expect to submit this CR in the middle of June.

Integral Spectrometer

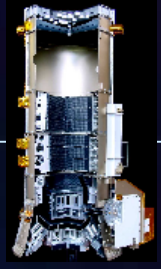

New IASW release 4.3.0 preliminary schedule

15/05/03 to 16/06/03: map modification, CR 567rev, CR 568rev1 and CR 576. Test on an intermediate version. ESA CR to be emitted.

17 to 27/06/03: beginning of CR 572, finalisation of CR 575 implementation and first integration test.

30/06/03 to 04/07/03: Complete validation test on SEM

07 to 11/07/03: Documentation update

15 to 18/07/03: Production of formal delivery to MOC.

Status of ISDC analysis s/w

- POIN: spipoint okay
- GTI level: solved remaining problems with mode handling
- DEAD: spidead minor changes (keywords etc.)
- COR: spi_gain_cor can handle time dependent gain coefficients; will be implemented as soon as the calibration files are ready
- bugs in PSD tools (SPR 2906) - low priority (?)
- BIN_I: spihist (NASA/GSFC) performance slightly improved
- BKG_I: DFEE option working fine in photon/photon mode. ACS/IREM option limited (needs DATA_GAPS in spigti)
- CAT_I: cat_extract okay
- RSP_I: PSD tool problem
- IMA: spiros/spibham minor updates
- spiskymax 29.0: after update of spi_science_analysis working in pipeline!

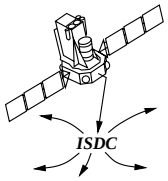

Status of ISDC analysis s/w

- SPI script with advanced GUI
- SPI simulator (spi_osim 1.2) updated (based on gensky, spisimprep, and spiskycnv by Andrew Strong)
- New response delivered by NASA/GSFC including Crab results.
- Information about GPS/GCDE and other data up-to-date (including lists for NRT/Cons. data) under isdc.unige.ch/Instrument/spi

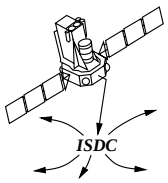

Next steps

- GTI tool to exclude times of strong solar activity / radiation belt effects (important for standard analysis)
- spihist needs further improvement (too long processing times)
- spiback update (especially for multiple detectors)
- scientific validation (study hardening of the spectra, misalignment, etc.)
- documentation update (no input for several tools from instrument team; does this mean that documentation is okay?)
- next software release by ISDC: July 2003

SPI Team Meeting June 2003 at CESR

Roland Diehl

ISDAG Items

ISDAG Items (1)

Data Processing Issues

- Energy Calibration
  - Problems/Systematics at Energies < 400 keV
  - Multiple Events' Calibration?
  - "Good" Calibrations for 511/^{44}Ti/^{60}Fe/^{26}Al Different?
- Livetime / Data Consistency
  - Find Measured Counts where Livetime=0 (!?!)
  - Find low countrates where livetime is high (!?!)
  - Apply a "Data Filter" in Imaging Analysis Tools

  - What is the Origin?
  - What is an Appropriate Treatment?
- More such Issues?
  - We need exchanges of processing experiences

ISSW Status

- ISSW Inventory

task	package	current version	last release	first release	developing site
calibration	spihisto	8.1	10.03.2003	18.07.2000	CESR
calibration	spiline	3.2	10.03.2003	18.07.2000	CESR
calibration	spicali	1.2	07.01.2002	18.07.2000	CESR
calibration	spi_gain_corr	1.4.1.	22.01.2003	17.05.2001	CESR
aux data	spipoint	1.6	02.12.2002	31.08.2000	ISDC
aux data	spigti	3	23.04.2003	31.08.2000	GSFC
aux data	spi_gti_creation	1.8	04.03.2003	06.03.2002	ISDC
data preparation	spidead	2.2.1	12.03.2003	06.07.2000	ISDC
data preparation	spibounds	1.2	29.04.2003	27.11.2000	GSFC
data preparation	spihist	3.0.7	29.04.2003	27.11.2000	GSFC
data preparation	spisumhist	2	10.01.2003	01.10.2001	MPE
data preparation	spiaddobs	4	08.01.2003	17.07.2002	MPE
response handling	spirespgen	not yet	00.01.1900	00.01.1900	GSFC
response handling	spi_psd_optimise	2.0.1	22.01.2003	02.09.2002	CESR
response handling	spi_psd_respgen	2.0.1	22.01.2003	02.09.2002	CESR
response handling	spiarf	1.4.0	18.10.2002	18.10.2002	GSFC
response handling	spirmf	1.3.0	18.10.2002	18.10.2002	GSFC
background handling	spibham	4.3.1	29.04.2003	28.06.2000	Ubham
background handling	spiback	4.7	23.04.2003	26.02.2001	Ubham
background handling	spi_obs_back	1.2.1	19.02.2003	19.02.2003	CESR
imaging	spiskymax	29.0	30.04.2003	15.09.2000	MPE
imaging	spiros	4.3.1	29.04.2003	13.10.2000	Ubham
imaging	spisimprep	3	23.09.2002	01.10.2001	MPE
imaging	spiskycnv	16	29.09.2002	28.10.2000	MPE
imaging	spidiffit	3	12.07.2002	17.12.2001	MPE
tools	spi_toolslib	2.0.2.	03.02.2003	24.06.2002	CESR
tools	spi_osm	1.3.	16.12.2002	04.05.2001	ISDC
tools	spi_scripts	1.4	24.04.2003	16.10.2001	ISDC

More ISDAG Items (2) (for team discussion)

- Maintenance of Analysis Tools
  - ISDC Leadership (Distribution of ISSW)
  - Developer Responsibility
  - Issues
    - Basic Tools: Maintain Stability and Ease-of-Use
      - Data Preparations and Response
      - SPIROS
      - Spectra Tools?
    - Advanced Tools
      - Rapid Evolution by Developer/SPI Team Desirable
      - Ordered Releases to the Community Desirable
- Sharing and Access to Data
  - SPI Bgd&Performance Database: Access?Maintenance?
  - Important for Surveys, Large-Scale Emission Studies
  - Agreements from PI's of 'pointed/pnt src' Observations
  - Issues: Practical Implementation at/with ISDC?

SPI Spectral Analysis: Comparison of Methods

Steve Sturner

NASA/GSFC, USRA

Spectral Analysis Methods

- We have analyzed data for the Crab from revolutions 42, 44, & 45.
- Analysis from the POIN level to the RSP_I level was performed using the ISDC OSA analysis package.
- Source spectra were then derived using 2 different methods:
  - SPIROS + XSPEC-11
  - XSPEC-12

SPIROS + XSPEC-11 Method

- In this method an efficiency corrected, background subtracted, source spectrum is calculated using SPIROS in spectral mode.

- This “photon” spectrum is then fit in XSPEC-11 (this can also be done in XSPEC-12) using a “SPIROS” RMF.

- The “SPIROS RMF” was derived by analyzing the SPIROS derived spectra for a set of simulated mono-energetic input spectra covering the SPI energy range (Gerry Skinner).

XSPEC-12 Method

- In this method the SPIHIST-derived raw count spectra are fit directly in XSPEC-12 without the use of SPIROS. SPIHIST is run in PHA mode.
- The XSPEC-12 ARFs are derived from the IRFs and the SPI.-OBS.-PNT table, and user-specified source positions using SPIARF.
- The XSPEC-12 RMFs are component template RMFs computed at NASA/GSFC and available at the ISDC. They are resampled to the appropriate spectral resolution using SPIRMF.
- The background is treated as a separate source model with a separate (unitary) response.
- A template for the background model is derived from the spectra in detectors with the highest degree of shadowing.

XSPEC-12 Method (cont.)

- XSPEC-12 then solves for the source and background models by simultaneously fitting the count spectra for all detectors and all SCWs.
- During the fitting process small amplitude (~10-15%) channel-to-channel variations in the background model are allowed.
- Initially, a single (constant) background spectrum is obtained. Then, detector-to-detector variations are allowed utilizing the XSPEC data grouping capabilities.
- Prior to the anticipated August 03 α-release, a more sophisticated background modeling approach, which can exploit information generated by SPIBACK, or other tools, will be implmented.
  - See: <http://heasarc.gsfc.nasa.gov/docs/xanadu/xspec/xspec12/>

Crab Results - SPIROS+XSPEC-11

- Spectrum above ~40 keV fit to a single power-law
- Best fit = $14.30 \pm 0.34\ E^{-2.15 \pm 0.006}$ with $\chi_\nu^2 = 8.67$. The 50-100 keV model flux is 8.56e-9 erg/cm^2/s.
- Efficiency problem below ~40 keV, corrected in revised IRFs. If due to absorption in passive material, it requires 10-30 μm of Ge or 0.2-0.8 mm of Al.
- There is an apparent excess at energies ⩗300 keV for which we do not have an explanation.

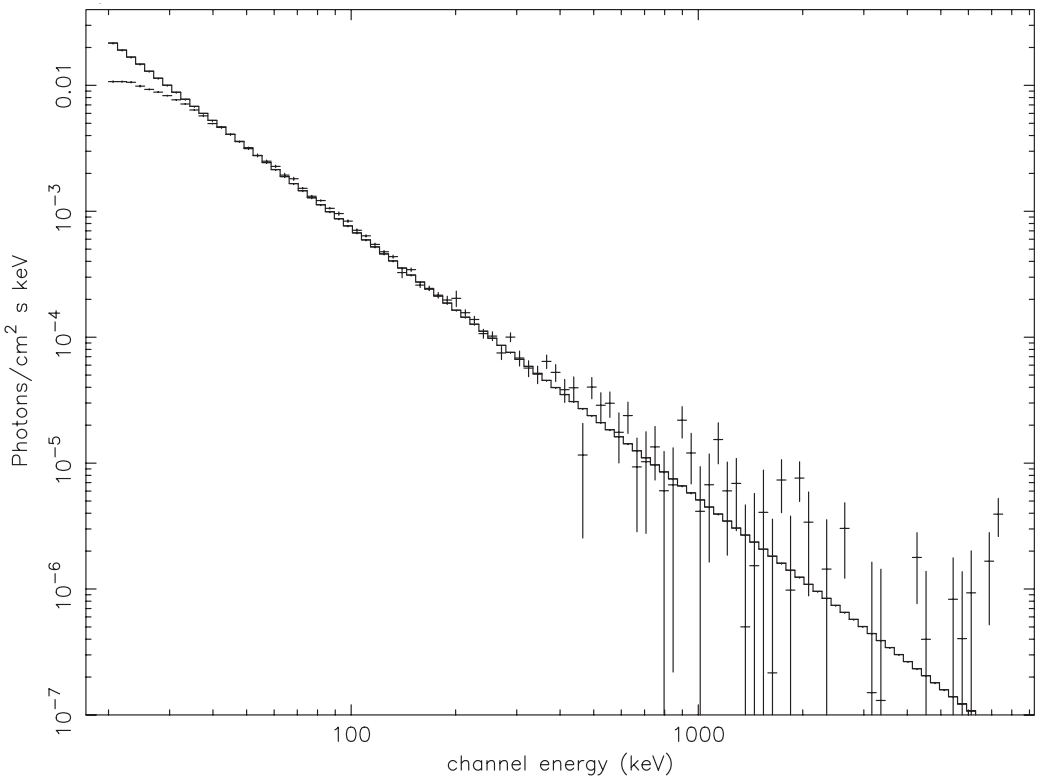

XSPEC-12 Results

- XSPEC-12 data and folded model are shown here using the low E corrected IRFs.

- There are two model curves depicted (source and background). The best fit model is:

  $11.9\ E^{-2.14\pm0.01}$, $\chi_\nu^2=1.91$

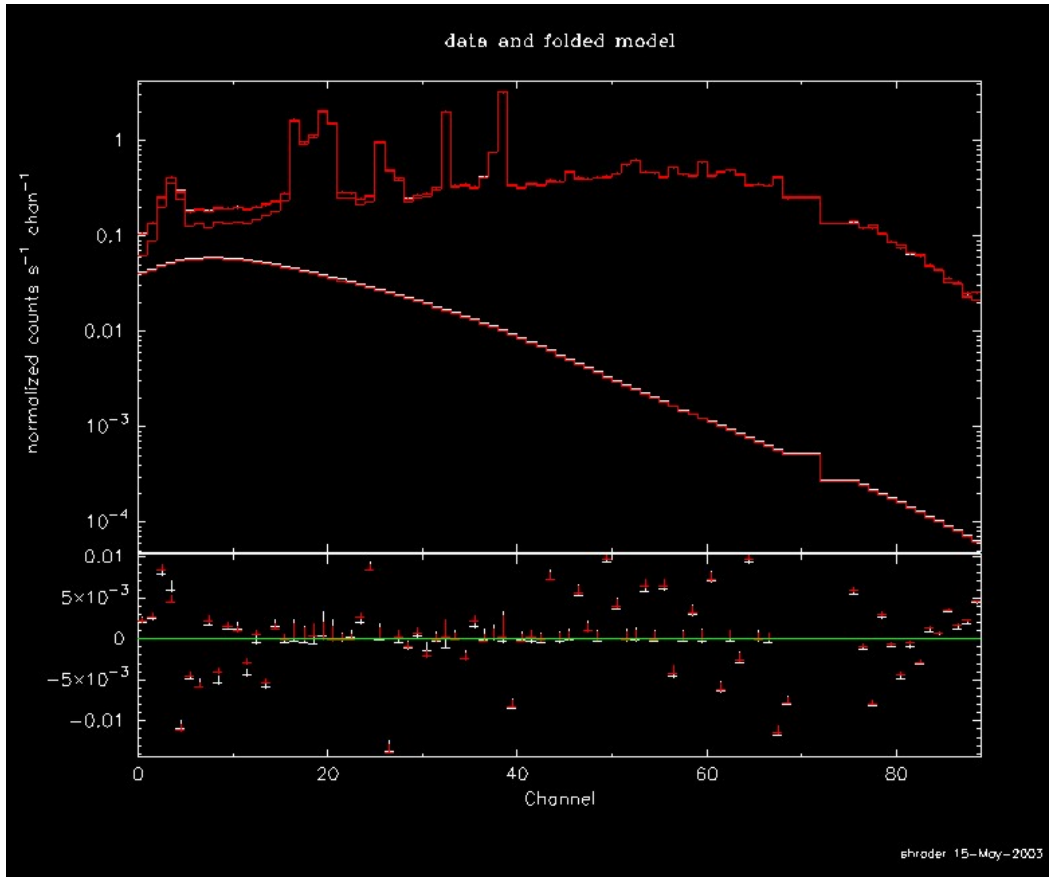

XSPEC-12 Results

- The same fit is depicted here in photon space.

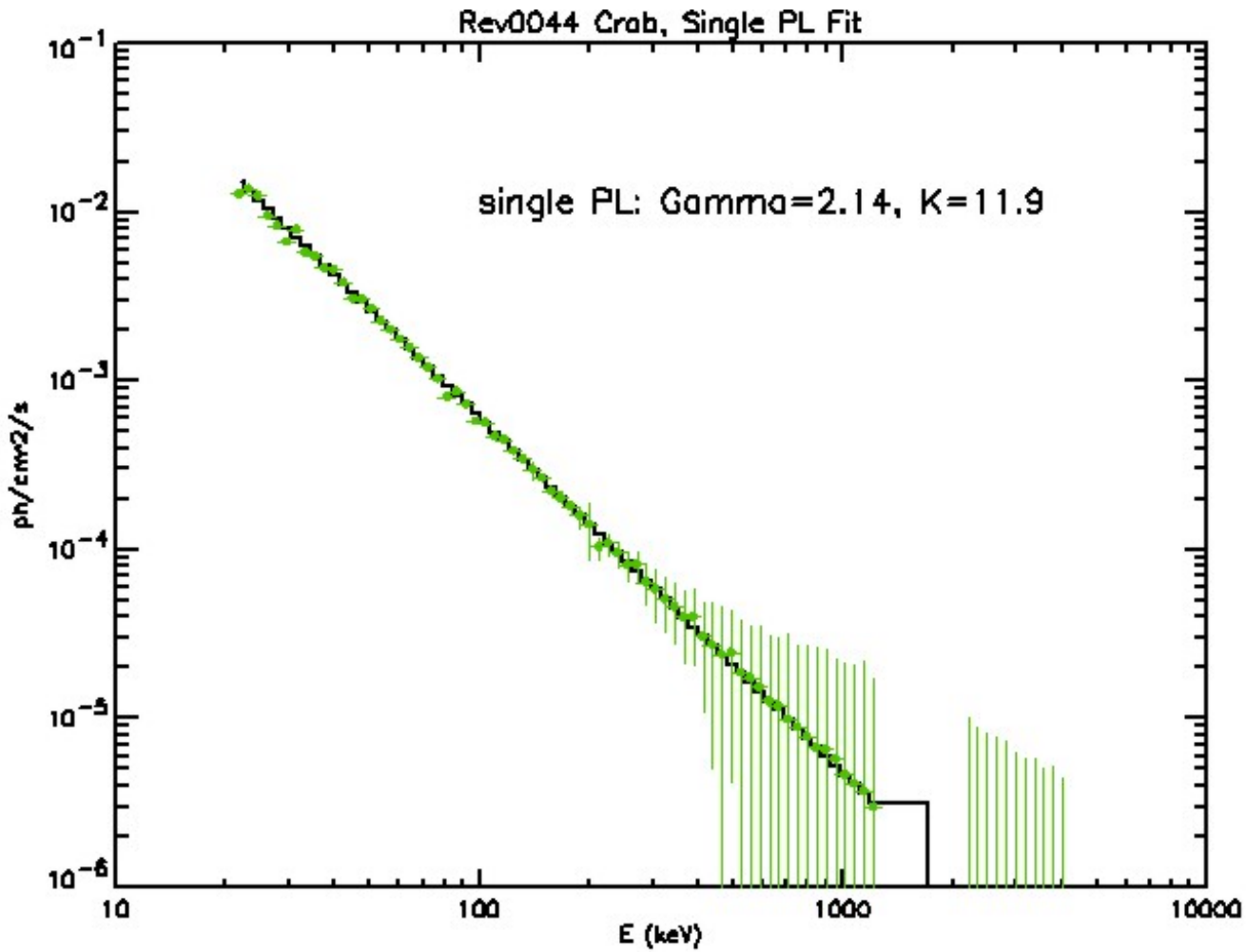

Testing SPIROS & XSPEC-12 with Simulated Crab Data

- We simulated the first 44 SCWs of the Rev 44 Crab data using MGEANT. The input spectrum was 8.0 $E^{-2.12}$ from 20-8000 keV (GRIS results).
- The event data was histogrammed and formatted in ISDC format.
- A background, based on SPI blank field observations, was added to some analyses.
- We then overwrote the inflight SPI.-OBS.-DSP table with this simulated data table and proceeded with SPIROS and XSPEC-12 analyses.

Crab Simulation Results - SPIROS

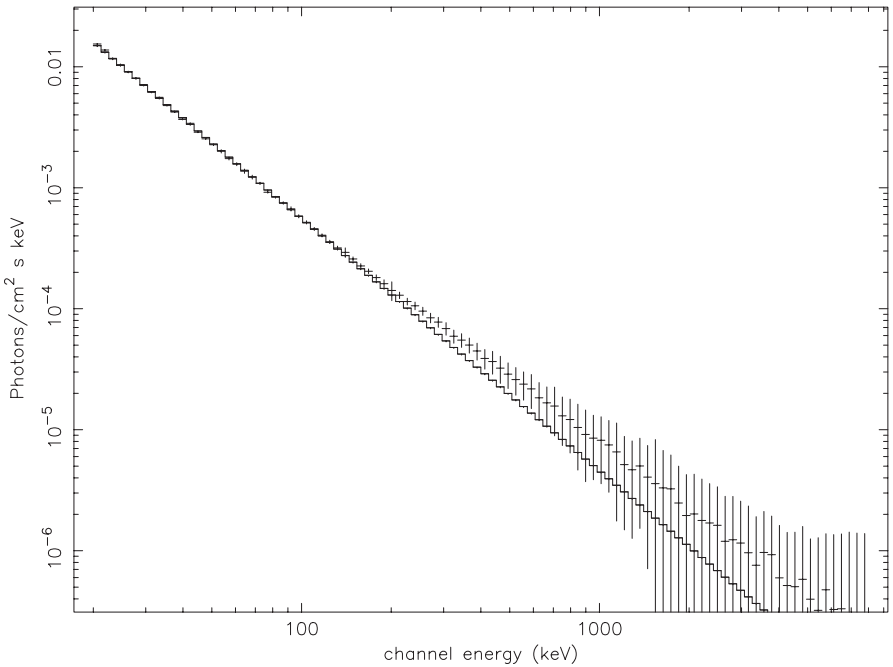

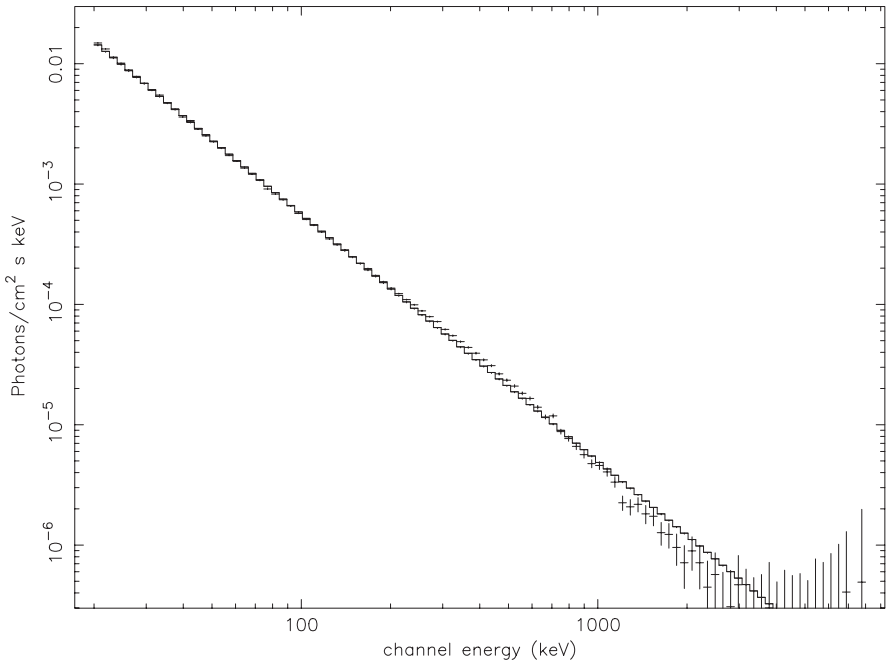

Simulation with background added

Best fit = $8.20 \pm 0.14\ E^{-2.08 \pm 0.005}$

$Flux_{50\text{-}100} = 6.36\text{e-}9$ erg/cm^2/s

Simulation without background

Best fit = $7.11 \pm 0.03\ E^{-2.05 \pm 0.001}$

$Flux_{50\text{-}100} = 6.35\text{e-}9$ erg/cm^2/s

Summary of Crab Results

Method.	Data	BKG	Norm.	Index	Index Constrained	Flux 50-100 (erg/cm^2/s)
SPIROS	Flight	Yes	14.3	2.15	No	8.56e-9
	Flight	Yes	12.9	2.12	Yes	8.61e-9
XSPEC-12	Flight	Yes	12.0	2.14	No	7.35e-9
	Flight	Yes	10.0	2.12	Yes	6.67e-9
SPIROS	Sim	No	7.1	2.05	No	6.35e-9
	Sim	No	9.3	2.12	Yes	6.22e-9
	Sim	Yes	8.2	2.08	No	6.36e-9
	Sim	Yes	9.3	2.12	Yes	6.22e-9
XSPEC-12	Sim	No	6.8	2.07	No	5.61e-9
	Sim	No	8.4	2.12	Yes	5.60e-9
	Sim	Yes	7.7	2.11	No	5.36e-9
	Sim	Yes	8.1	2.12	Yes	5.40e-9
Model			8.0	2.12		5.34e-9

Comparison with CGRO, GRIS Results

- Single PL fits, with the corrected IRFs are now slightly steeper than GRIS, but still flatter than OSSE.

- Broken PL fits have also been attempted.

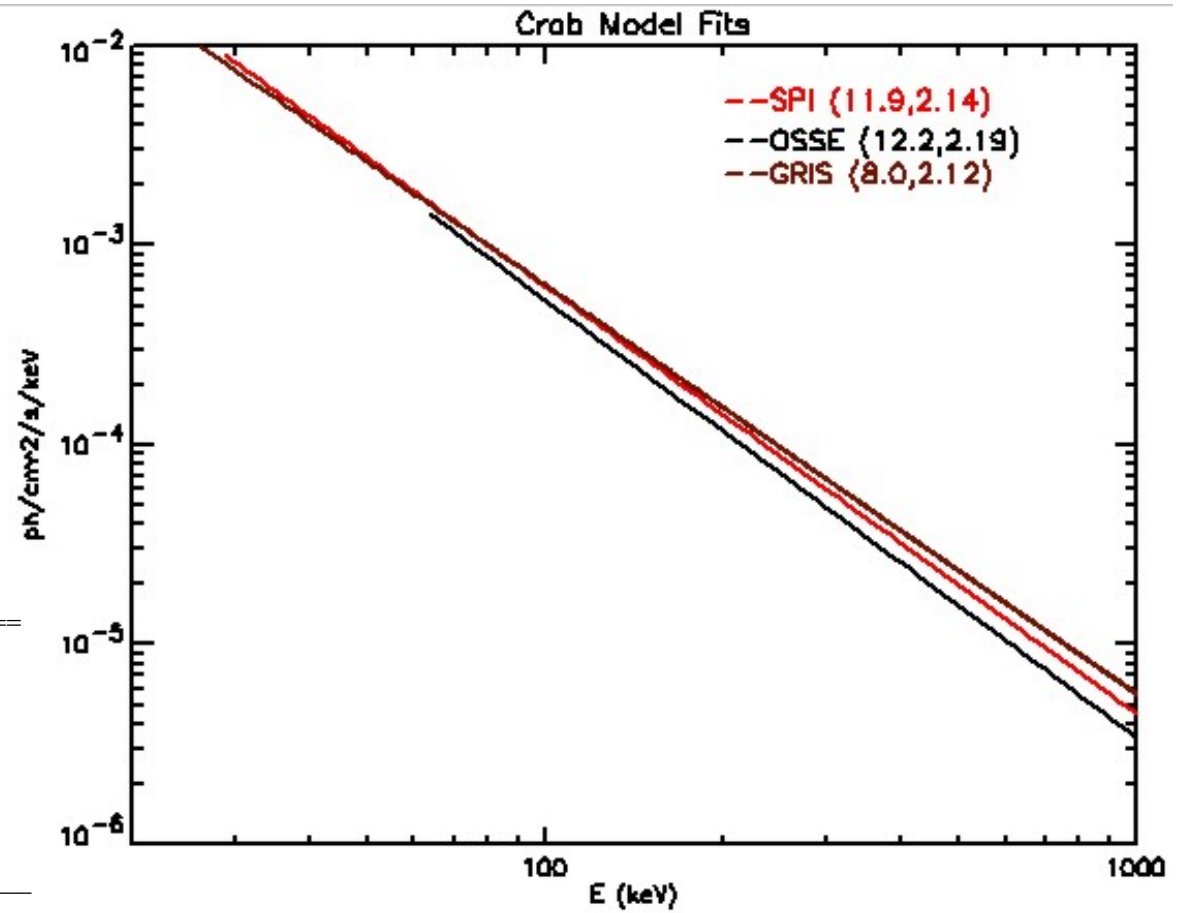

==========

Model crab:bknp Fit to Data Group: 1 Source No.: 1
Model Component Name: bknpower Number: 1

N	Name	Unit	Value		Sigma
1	PhoIndx1		2.0915E+00	+/-	5.2952E-03
2	BreakE	keV	1.5074E+02	+/-	1.4702E+02
3	PhoIndx2		2.2198E+00	+/-	1.9515E-01
4	norm		9.6231E+00	+/-	1.8944E-01

Chi-Squared = 7.3109750E+04 using 36575 PHA bins.
Reduced chi-squared = 2.0038304E+00 for 36485 degrees of freedom

Extrapolation to Higher Energies

- Extrapolation of both the single PL fits, and broken PL fits thus far obtained, still over predict the higher energy points of COMPTEL and EGRET.

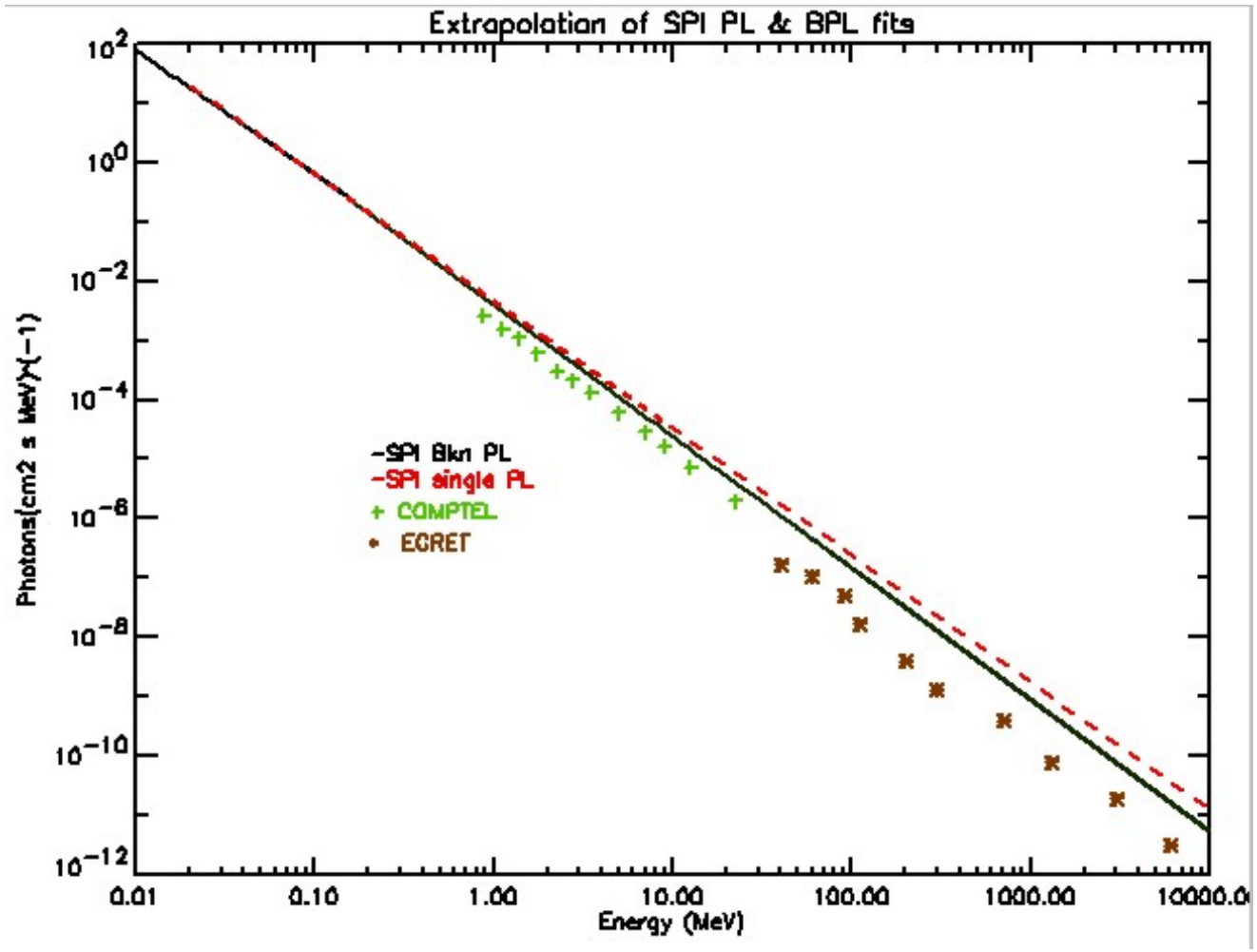

GRS 1915+105

- Additional evidence for cross-calibration differences across methods & instruments has recently emerged in a joint GSFC/Saclay effort to model GRS 1915, during it s rev 57 & 62 outbursts.

- In this RXTE/PCA, SPI & IBIS composite, there are normalization differences, not only between XSPEC-12 & SPIROS SPI models, but are evident with IBIS also.

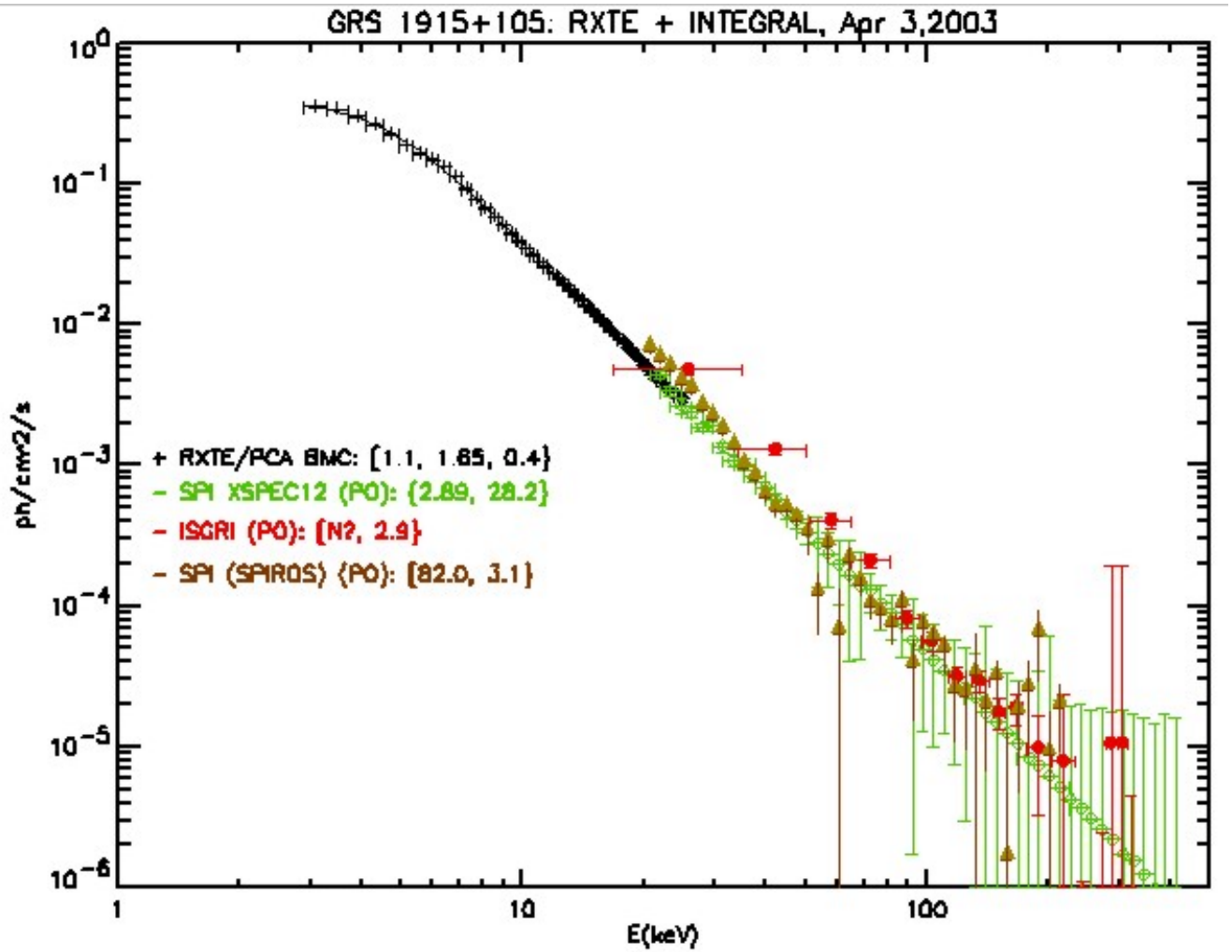

Results Summary

- On Crab flight data, the SPIROS & XSPEC-12 methods consistently produce very similar spectral indices but substantially different normalizations (~15%).

- On simulated data, the SPIROS & XSPEC-12 methods again produce very similar spectral indices but SPIROS overestimates the incident flux by ~16-19% while the XSPEC-12 flux is within 5% of the model.

- The turnover at low energies seen in the analysis of Crab flight data is not seen in the simulated data analyses. Thus we determined that there was an IRF calibration problem which has been corrected. This was not unexpected considering the lowest energy used to calibrate the IRFS was 59.5 keV.

- The excess above ~300 keV observed in SPIROS output, is only seen in data which contain background. (It was not present in the simulated data without background results.) We do not currently have an explanation for this. XSPEC-12 does not produce such an excess, however, it may in fact over-subtract the high-energy background (as revealed in recent work on GRS 1915+105 w/Saclay group).

Misalignment

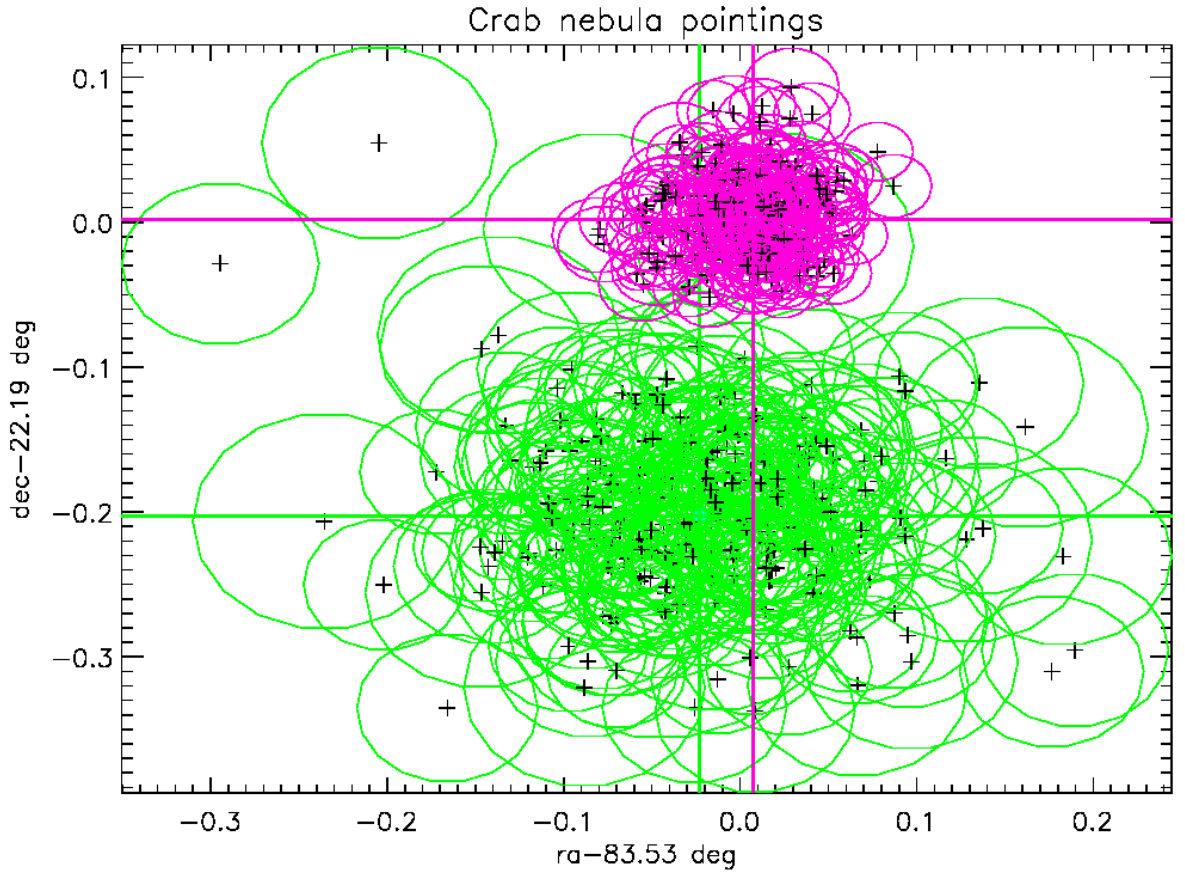

Raw data

3 x 3 rotation matrix has been applied

Offset vs source angular distance from pointing axes

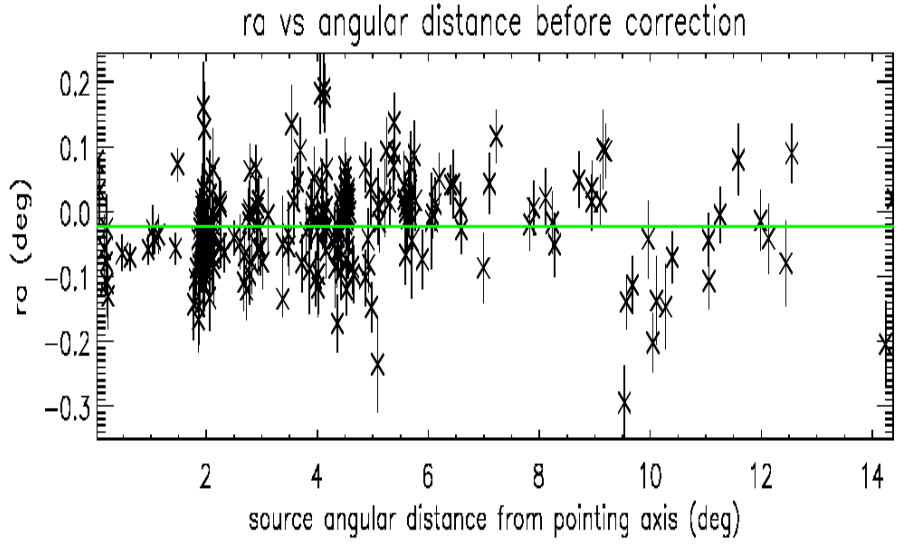

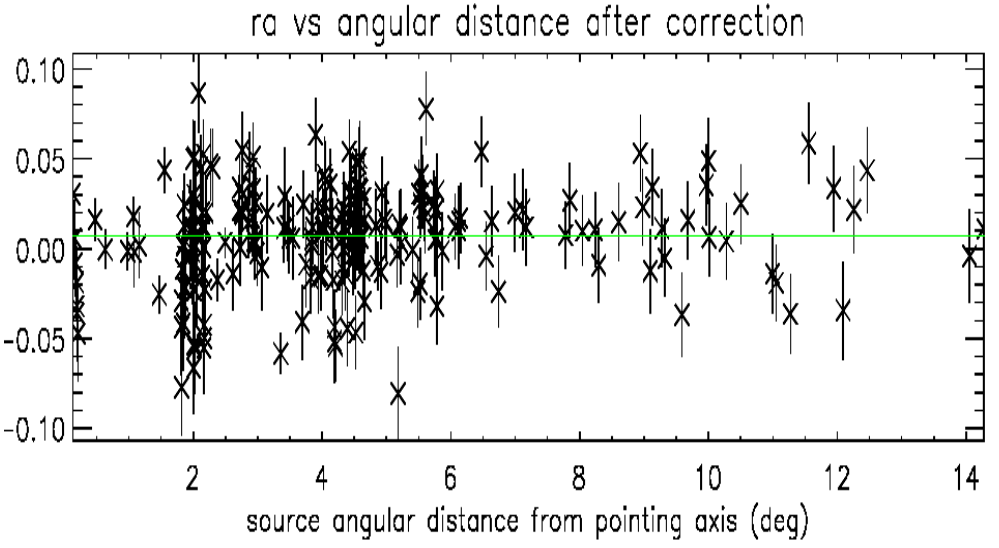

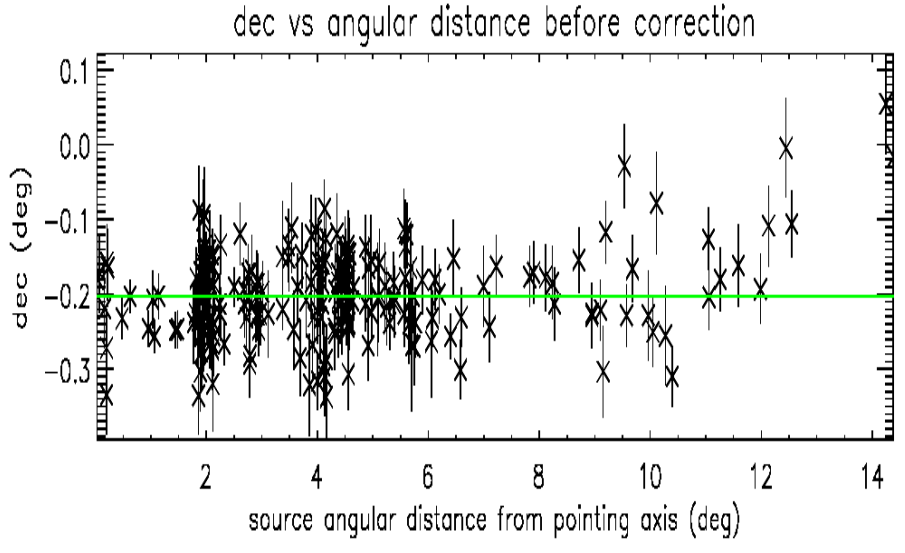

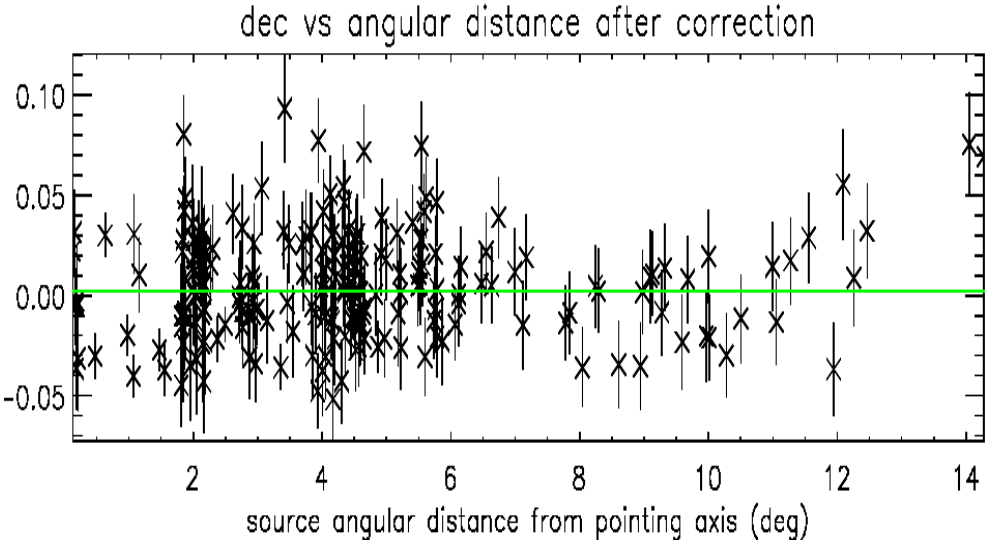

New results at low energy from BLC Calibration

Motivation: Is there a problem at low energy (<40 keV) in the IRF?

In the IRF computation, the low-energy correction was just a constant extrapolation from the 241-Am (59.5 keV) correction.

We observe problems in the low-energy range of the Crab spectrum

→ Need of calibrated data below 40 keV

Solution: Revisiting the BLC data and analyzing the low-energy lines from ^{133}Ba (30,6-30,9)keV and (34,9-35,8) keV.

New results at low energy from BLC Calibration

Calculation of the full energy peak effective area in imaging mode at 30 and 35 keV.
The method is described in the « SPI Ground calibration » paper (Attie et al.)

We use the ^{133}Ba data at (30,6-30,9) keV and (34,9-35,8) keV corrected
By the mask absorption measured by the University of Valencia.

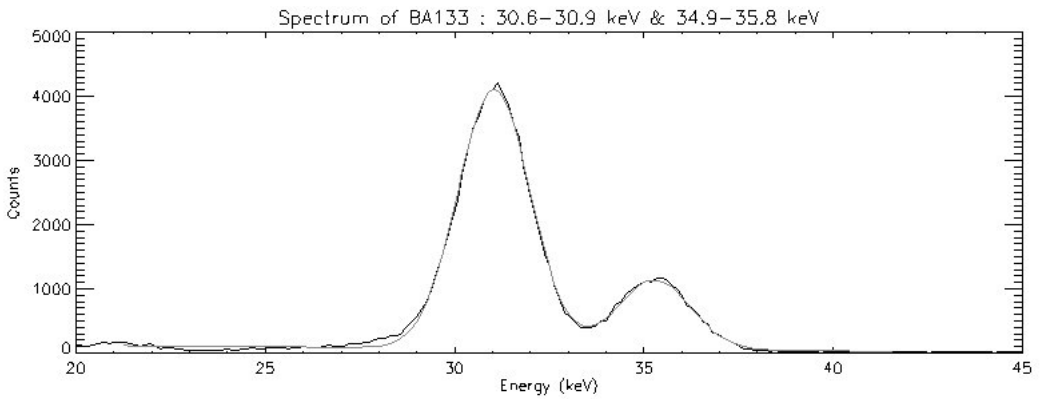

New results at low energy from BLC Calibration

We compare the full energy peak effective area in imaging mode with the Arf1 (photoelectric peak) values
Computed for a science window with the source on axes.

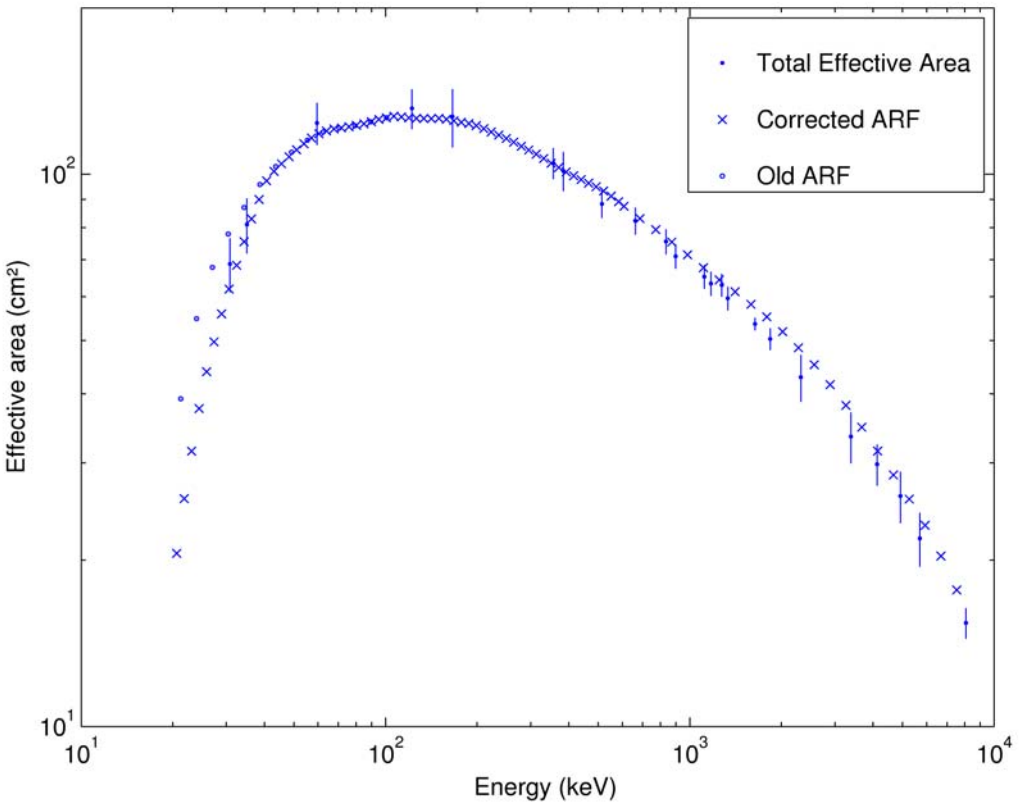

The new Arf (computed by GSFC) is more compatible with the low-energy measurements
Over corrected?

In-Flight Response Corrections

Steve Sturner

NASA/GSFC, USRA

Crab Analysis

- We have performed spectral analysis of rev 44 data from the Crab Nebula + pulsar using both SPIROS and XSPEC-12.
- We found an efficiency problem below ~40 keV. If due to absorption in passive material, it requires 10-30 μm of Ge or 0.2-0.8 mm of Al.
- This was not unexpected.
- There is an excess at energies ⩗300 keV for which we do not have an explanation.

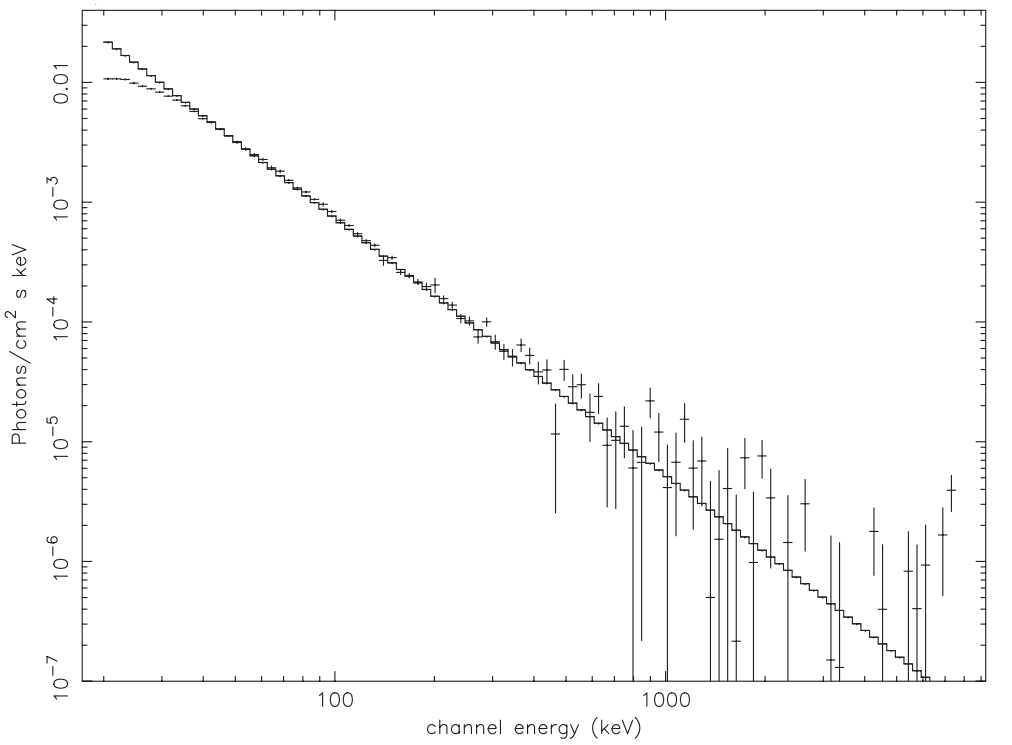

SPIROS unfolded spectrum and model

Low-Energy Correction Factors

- We derived IRF correction factors by fitting the Crab spectrum above 40-50 keV with a single power-law and then forcing this fit when the low energy channels were included.

- The low-energy correction factors are derived from a fit to the model-to-data ratios for both XSPEC-12 and SPIROS analyses.

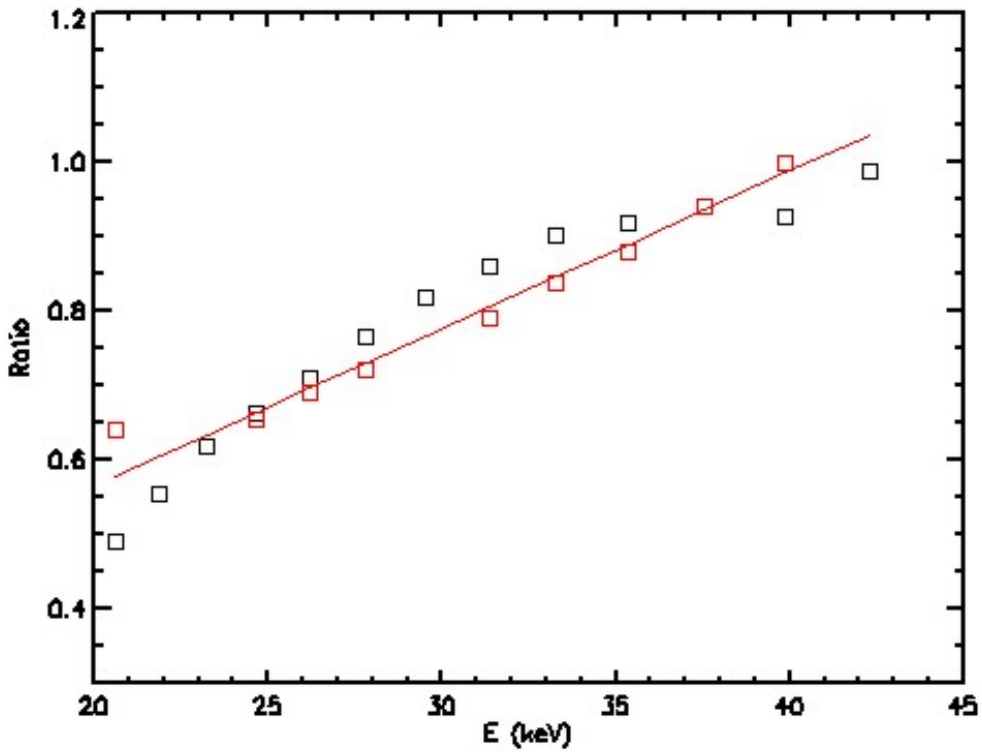

Ratio of Crab data to best-fit power-law model above ~40 keV for SPIROS (black) and XSPEC-12 (red) analyses.

New Results - SPIROS

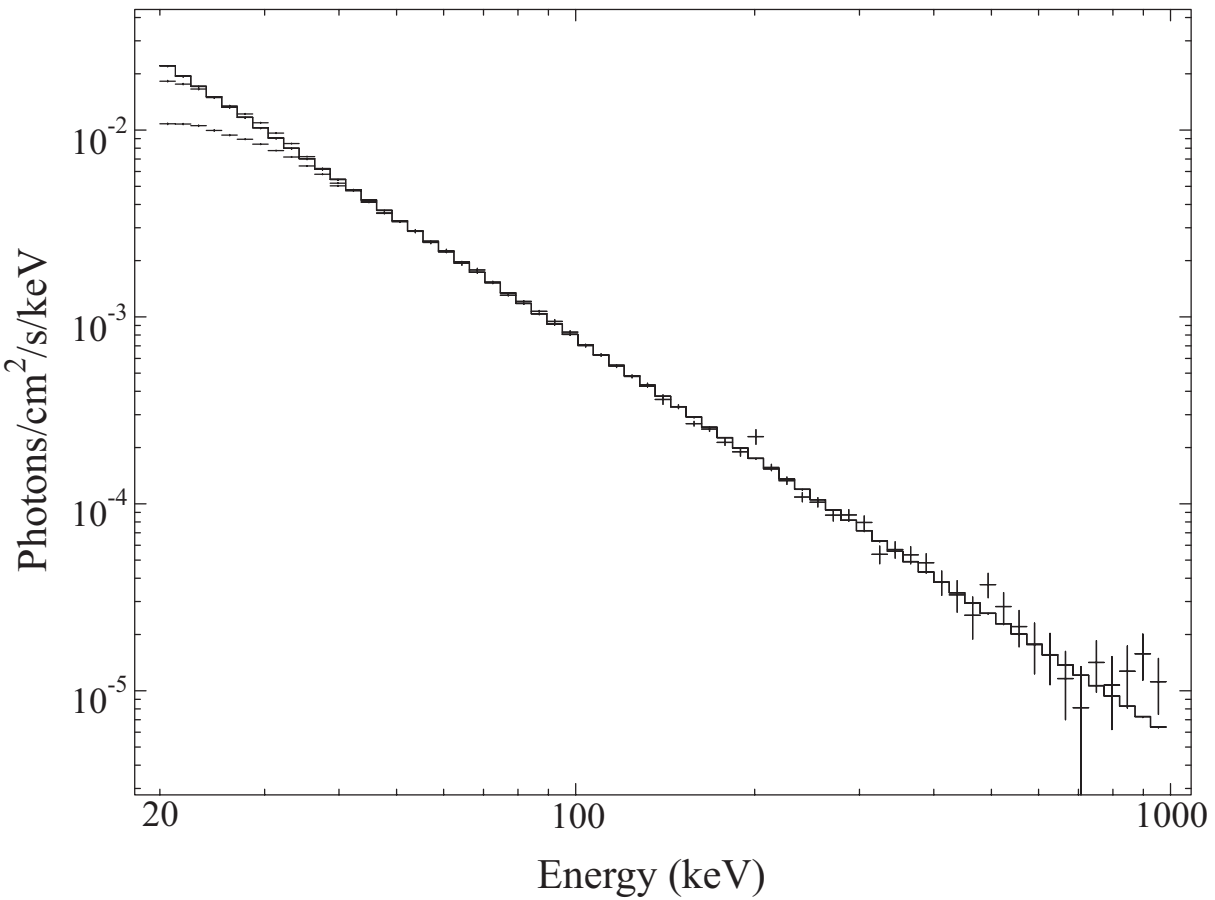

Comparison of SPIROS output using both IRFs corrected at low energies and those not corrected, as well as the best-fit power-law model for data above ~40 keV.

New Results - XSPEC-12

- XSPEC-12 data and folded model are shown here using the low E corrected IRFs.

- There are two model curves depicted (source and background). The best fit model is:

  $11.9\ E^{-2.14\pm0.01}$, $\chi_\nu^2=1.91$

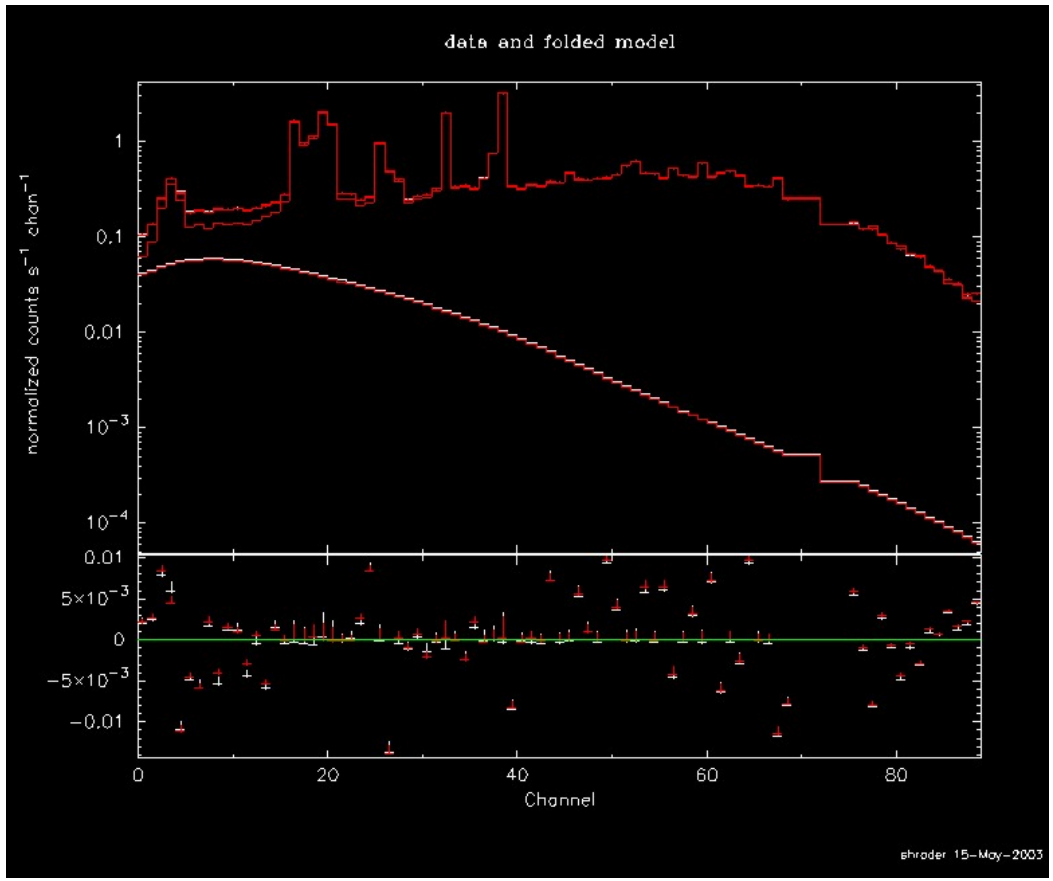

New Results - XSPEC-12

- The same fit is depicted here in photon space.

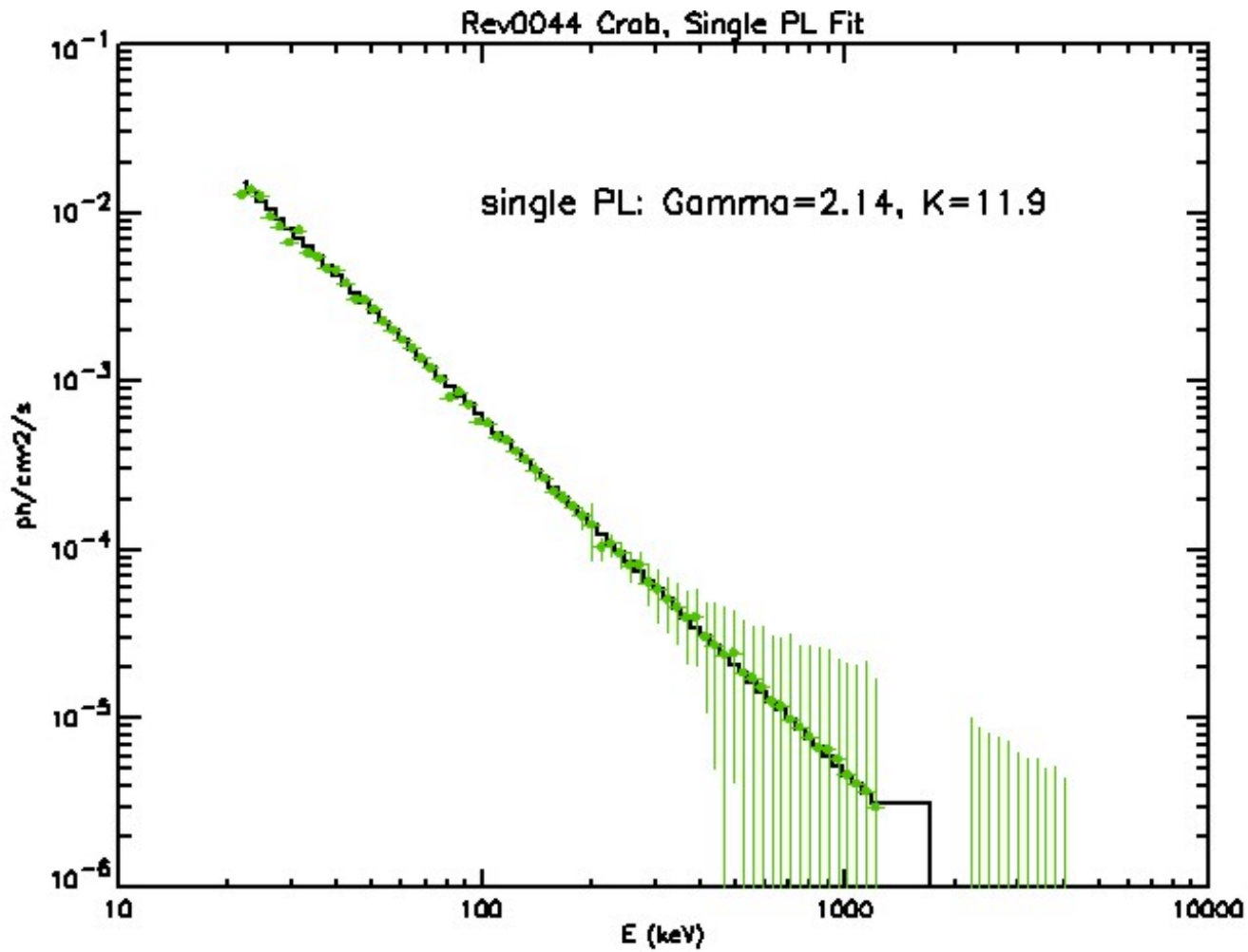

Normalization Problem?

Method.	Data	BKG	Norm.	Index	Index Constrained	Flux50-100 (erg/cm^2/s)
SPIROS	Flight	Yes	14.3	2.15	No	8.56e-9
	Flight	Yes	12.9	2.12	Yes	8.61e-9
XSPEC-12	Flight	Yes	12.0	2.14	No	7.35e-9
	Flight	Yes	10.0	2.12	Yes	6.67e-9
SPIROS	Sim	No	7.1	2.05	No	6.35e-9
	Sim	No	9.3	2.12	Yes	6.22e-9
	Sim	Yes	8.2	2.08	No	6.36e-9
	Sim	Yes	9.3	2.12	Yes	6.22e-9
XSPEC-12	Sim	No	6.8	2.07	No	5.61e-9
	Sim	No	8.4	2.12	Yes	5.60e-9
	Sim	Yes	7.7	2.11	No	5.36e-9
	Sim	Yes	8.1	2.12	Yes	5.40e-9
Model			8.0	2.12		5.34e-9

GRS 1915+105

- Additional evidence for cross-calibration differences across methods & instruments has recently emerged in a joint GSFC/Saclay effort to model GRS 1915, during it s rev 57 & 62 outbursts.

- In this RXTE/PCA, SPI & IBIS composite, there are normalization differences, not only between XSPEC-12 & SPIROS SPI models, but are evident with IBIS also.

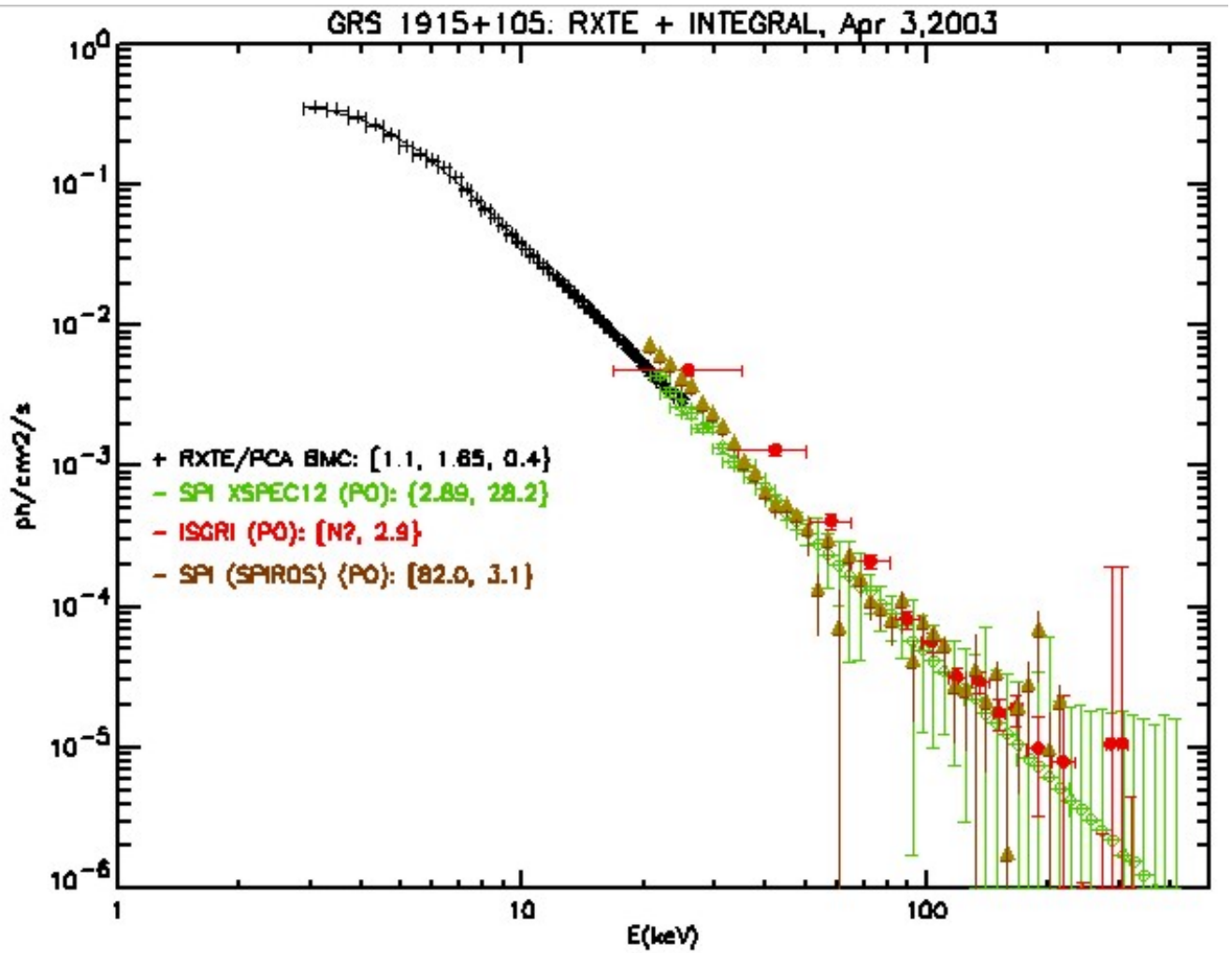

Open Issues

- How does the work on the low energy ^{133}Ba BLC data agree with in-flight Crab analysis?

- On Crab flight data, the SPIROS & XSPEC-12 methods consistently produce very similar spectral indices but substantially different normalizations (~15%). Why? Need for SPIROS ARF?

- The excess above ~300 keV observed in SPIROS output, is only seen in data which contain background. (It was not present in the simulated data without background results.) We do not currently have an explanation for this. XSPEC-12 does not produce such an excess, however, it may in fact over-subtract the high-energy background (as revealed in recent work on GRS 1915+105 w/Saclay group).

Crab counts spectra in mode 2
(19 detectors background to be fitted)

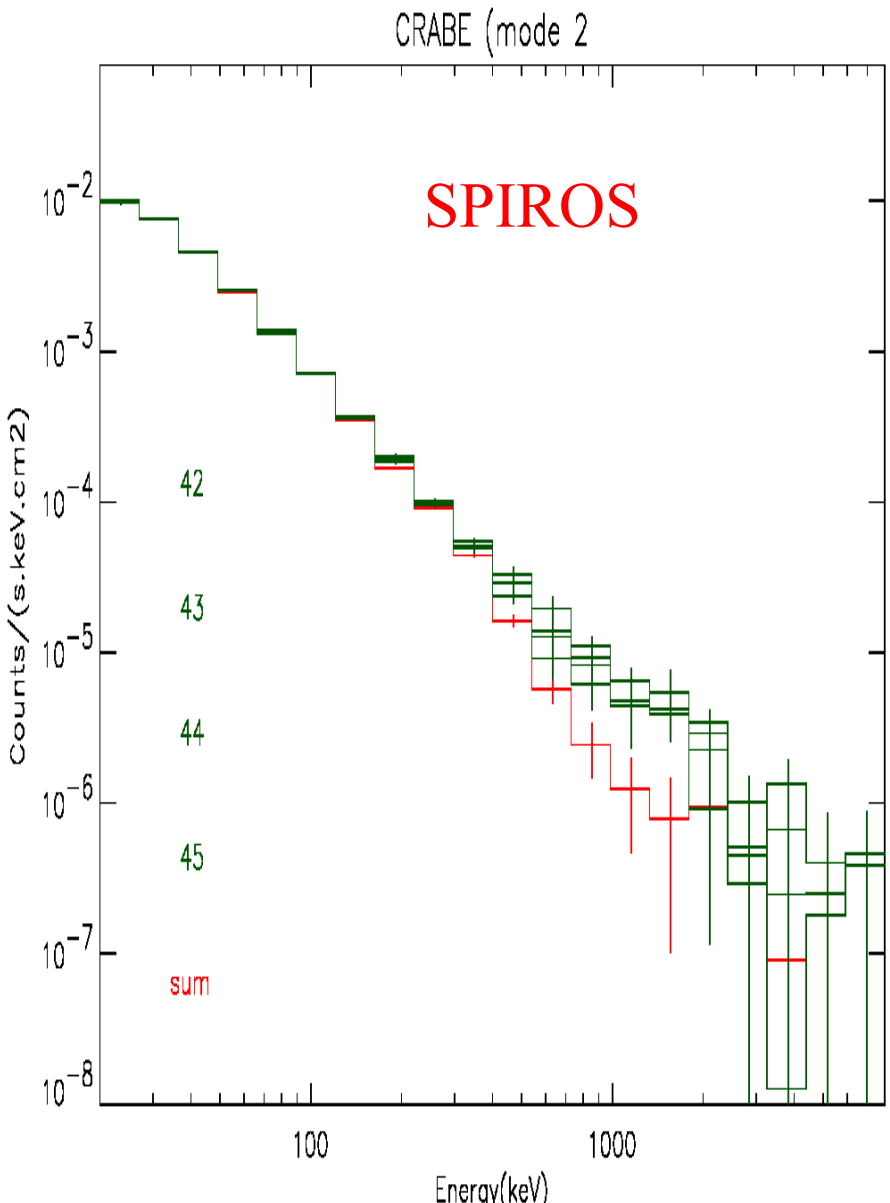

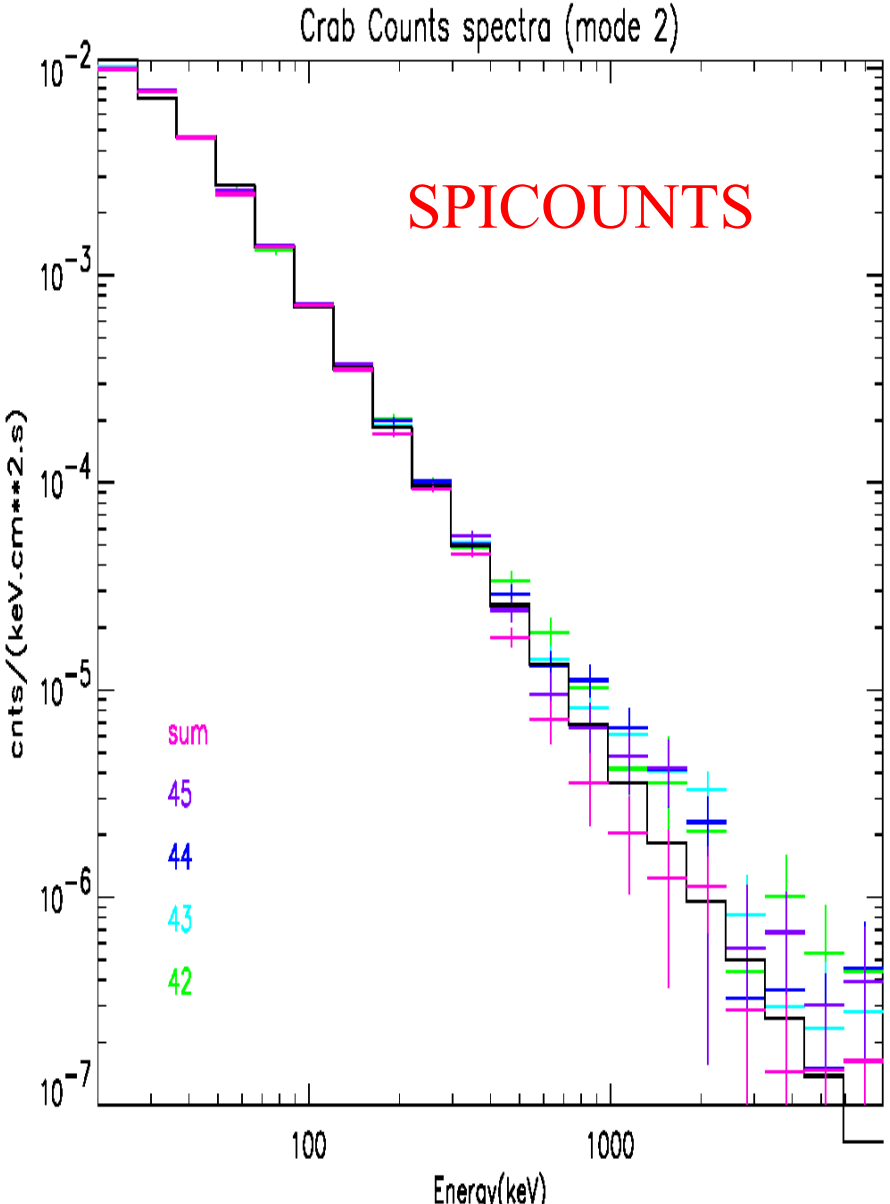

Crab counts spectrum in mode 3
(One amplitude parameter for the background to be fitted)

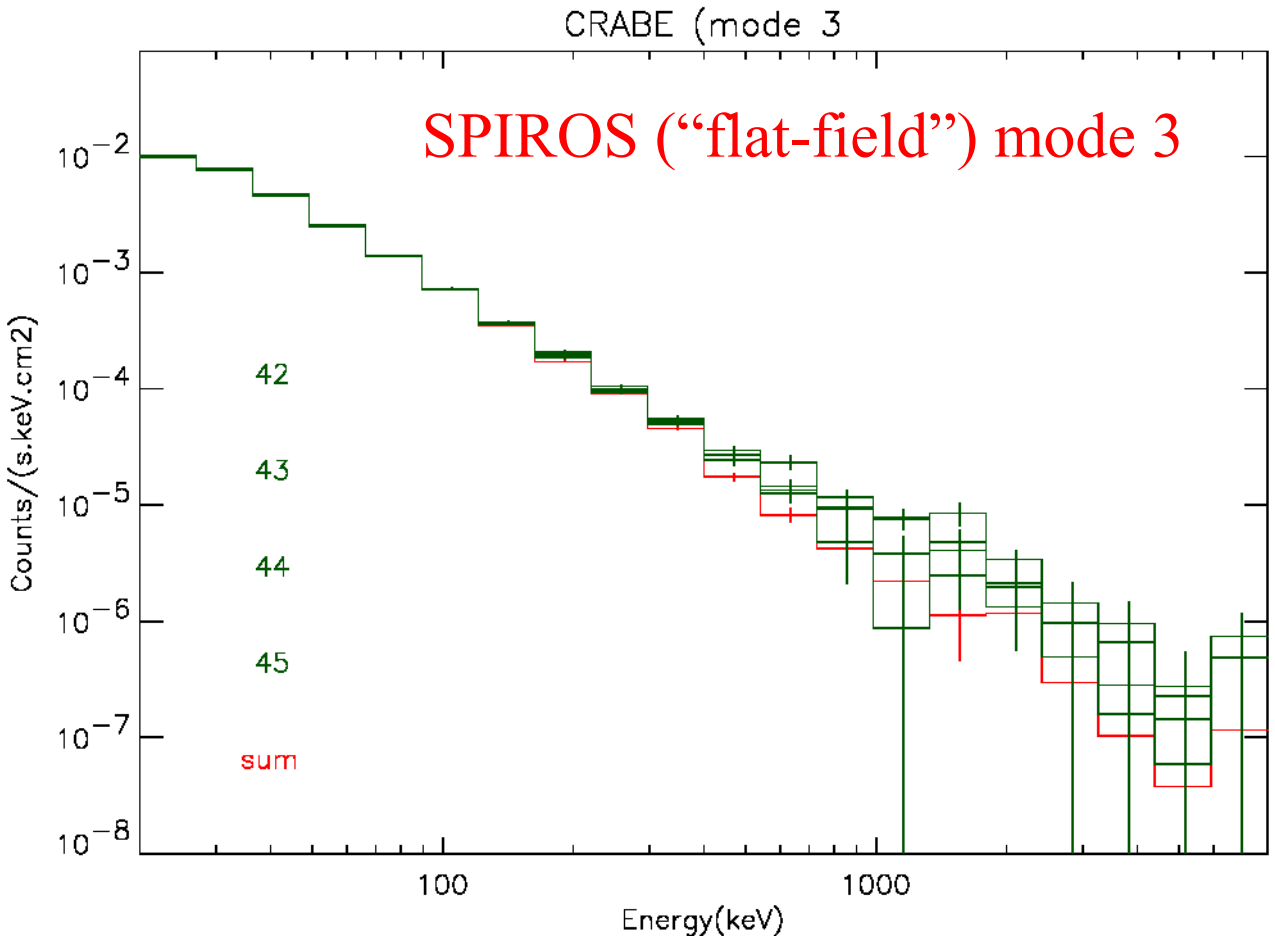

Crab counts and photons spectra in mode 4
("Flat-field" and One amplitude parameter per pointing to be fitted)

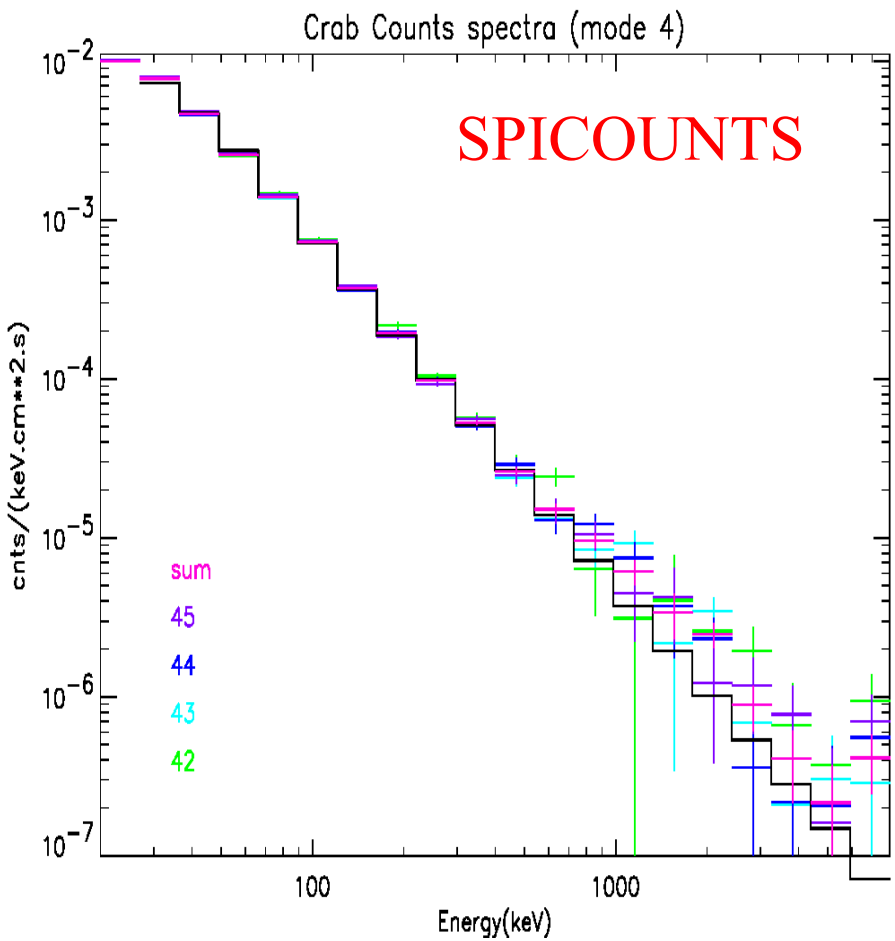

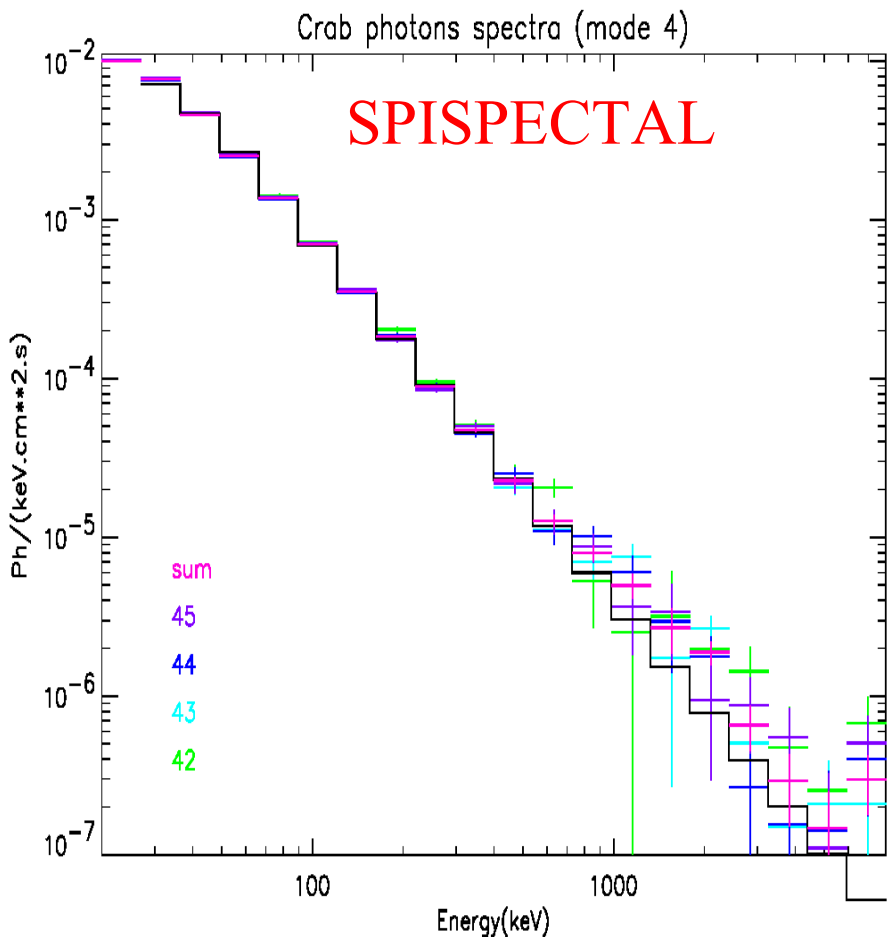

Crab light curve (rev 42-45)

IROS pointing pointing by pointing (20 -163 keV) (mode 3- “flat-field”)

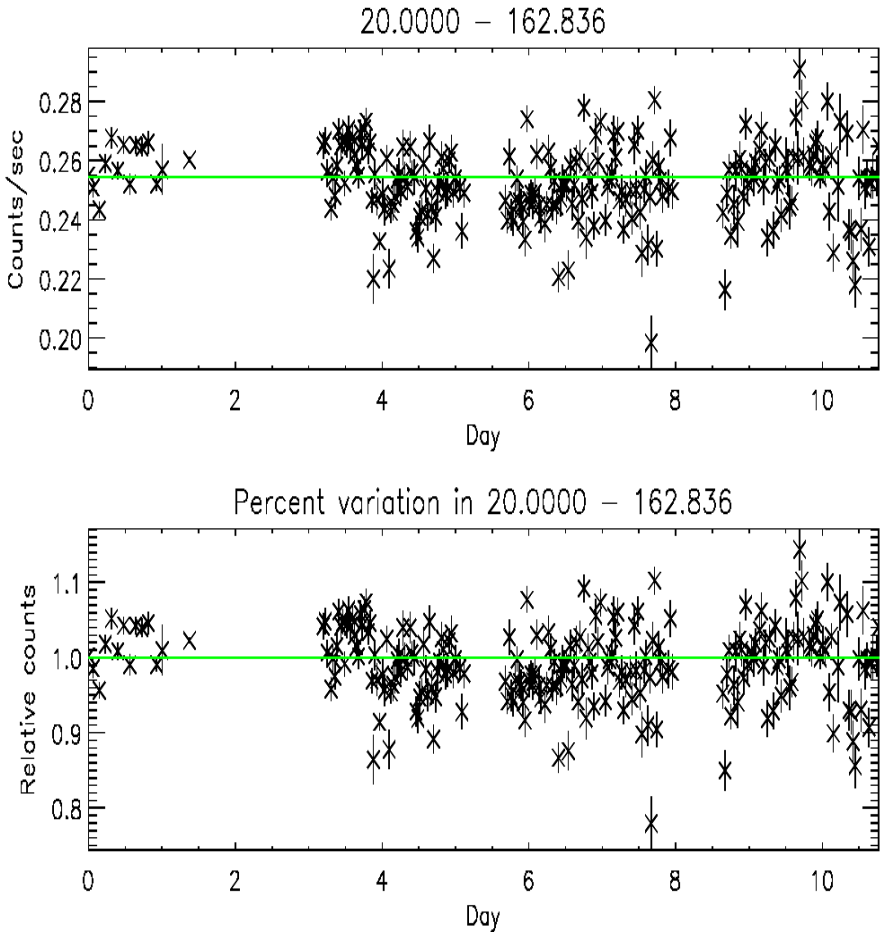

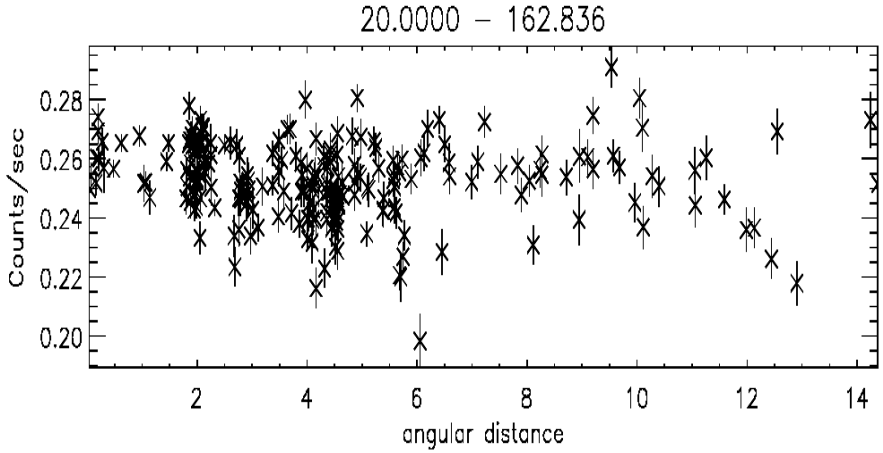

Crab light curve (rev 42-45)

IROS 4 pointings by 4 pointings (20 -163 keV) [boxcar average] (mode 2)

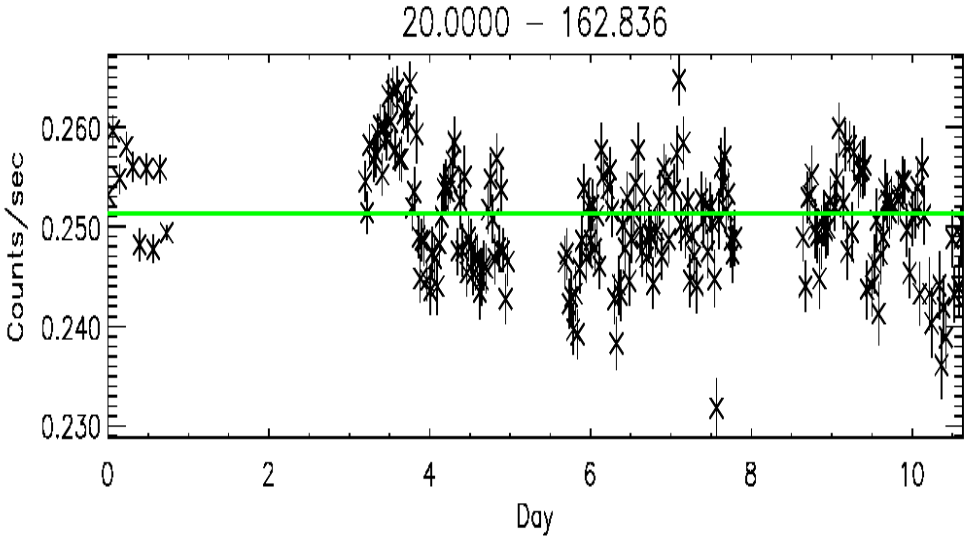

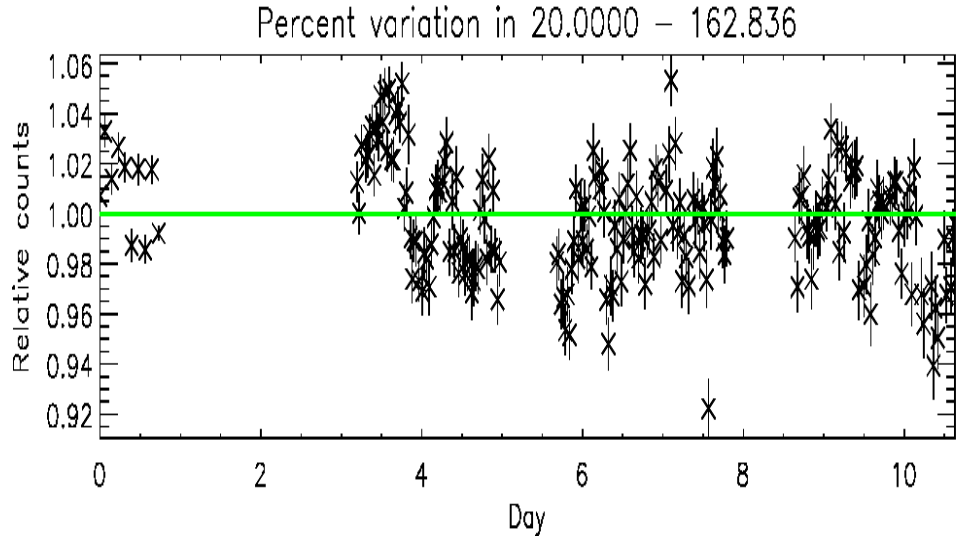

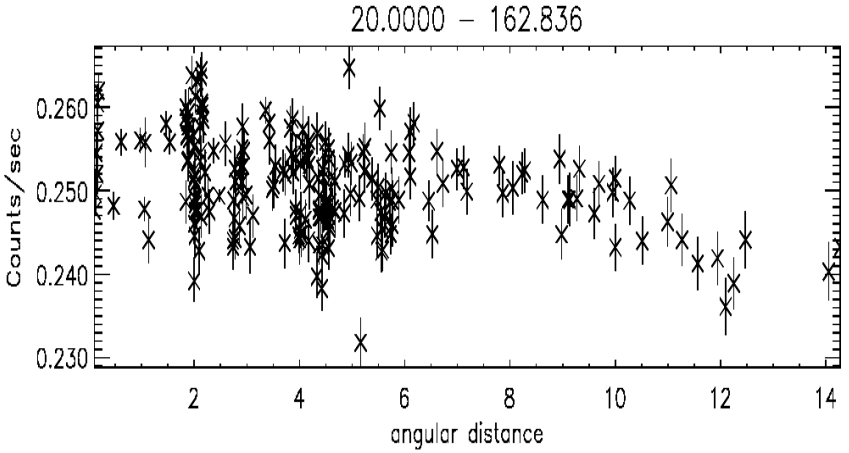

Spectra and background

IROS pointing by pointing (20 -163 keV) (mode 3 - “flat-field”)

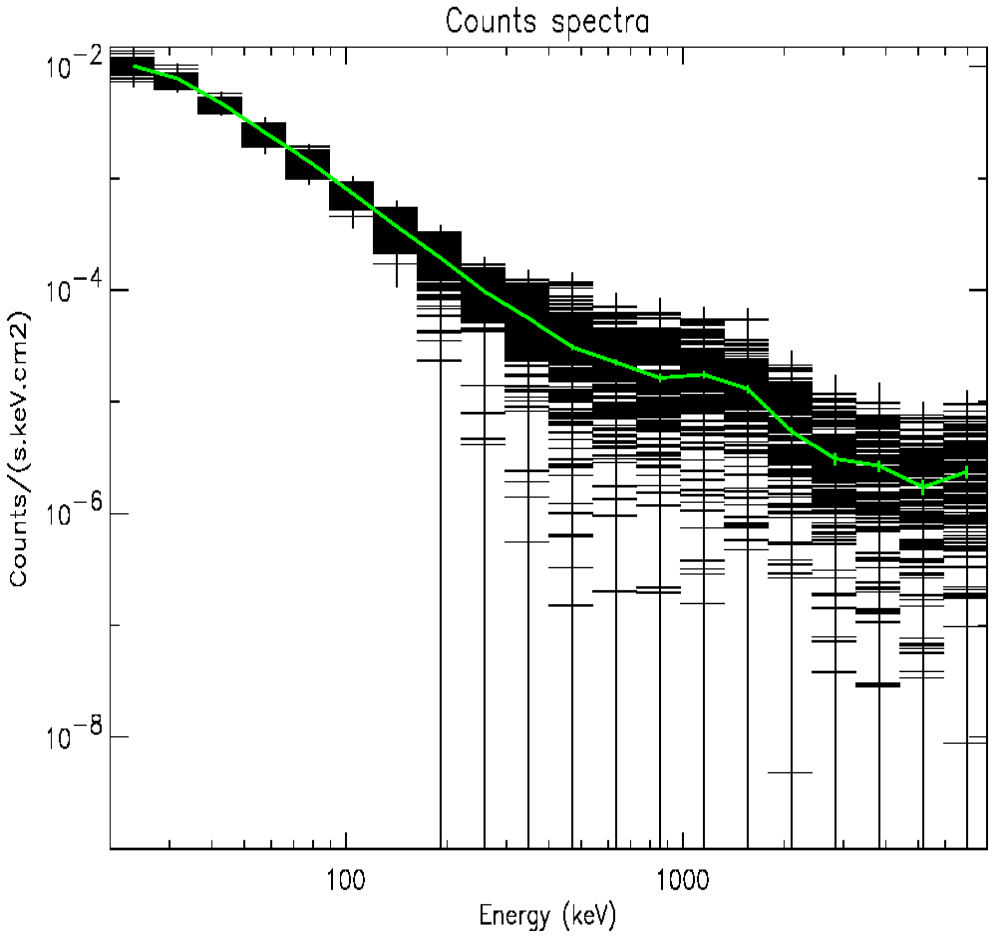

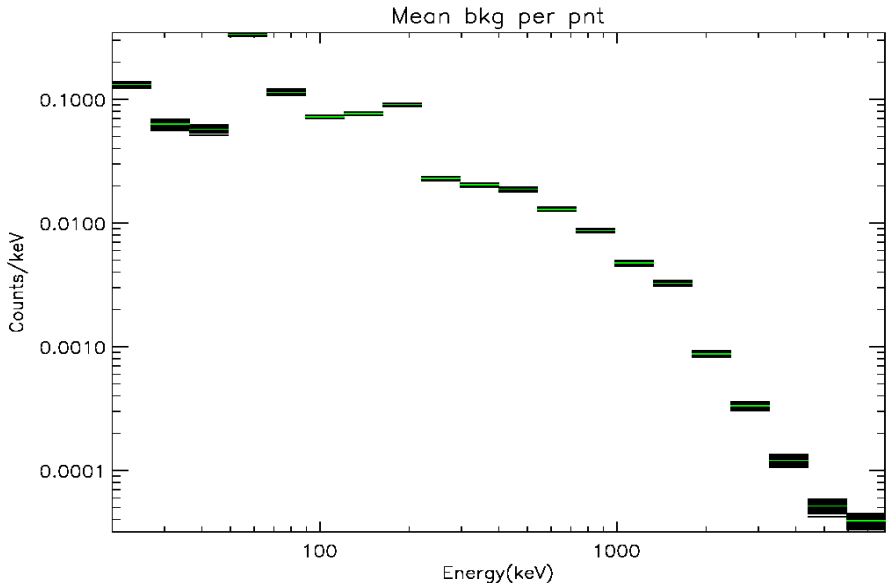

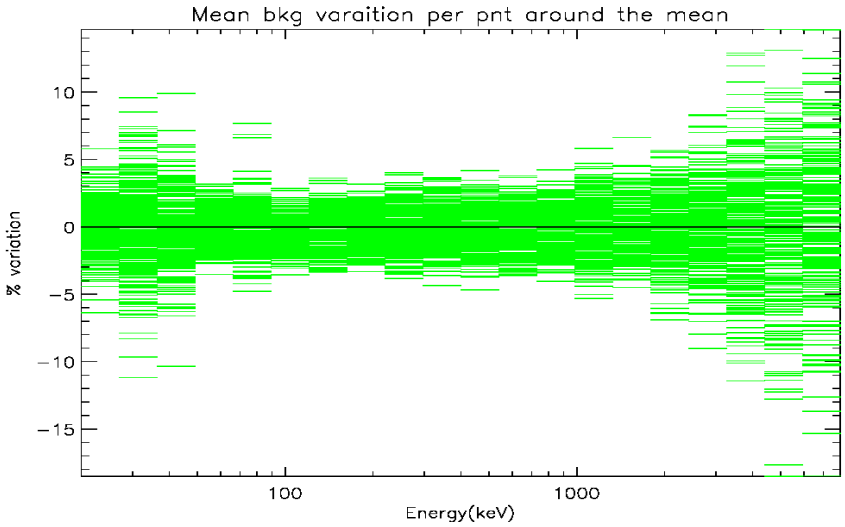

Spectra and background

IROS 4 pointings by 4 pointings (20 -163 keV) [boxcar average] (mode 2)

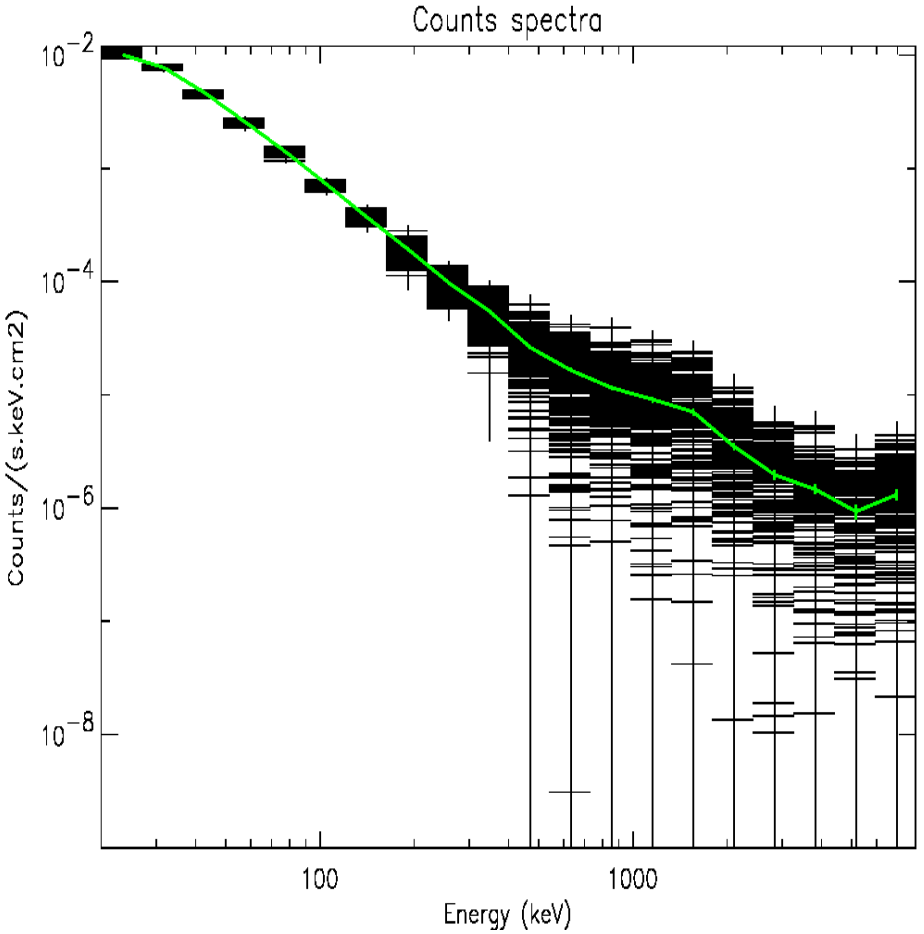

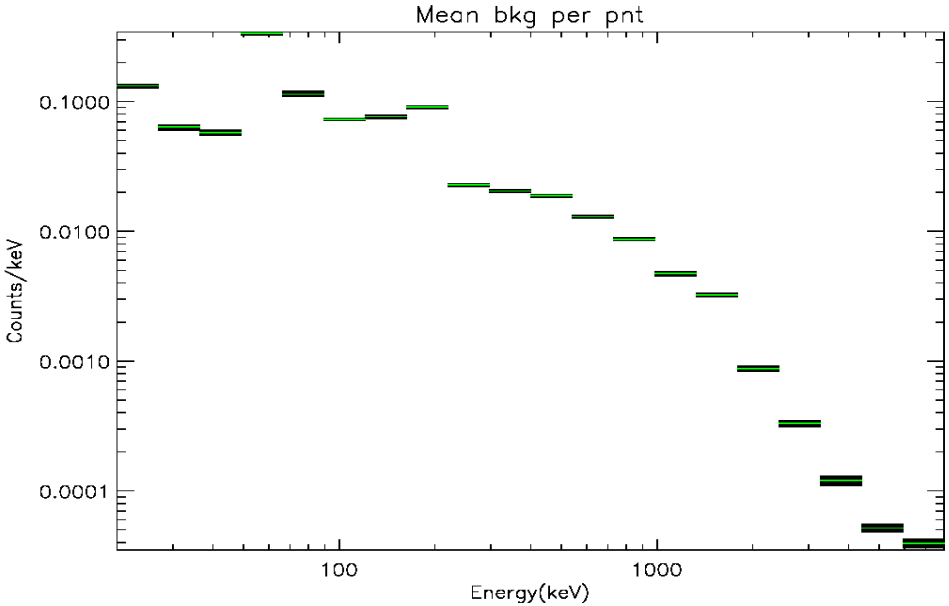

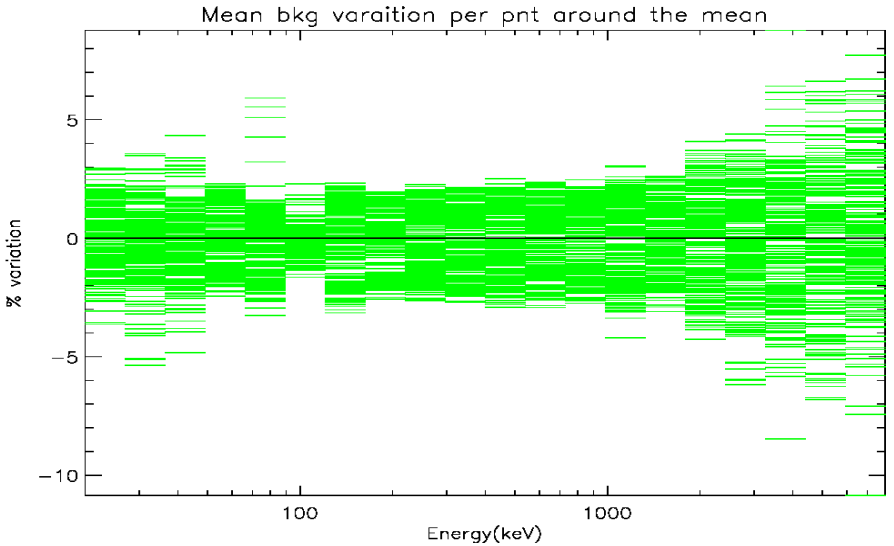

Crab light curve (rev 42 - 45)

IROS 4 pointings by 4 pointings (20 -163 keV) [boxcar average]

MODE 2

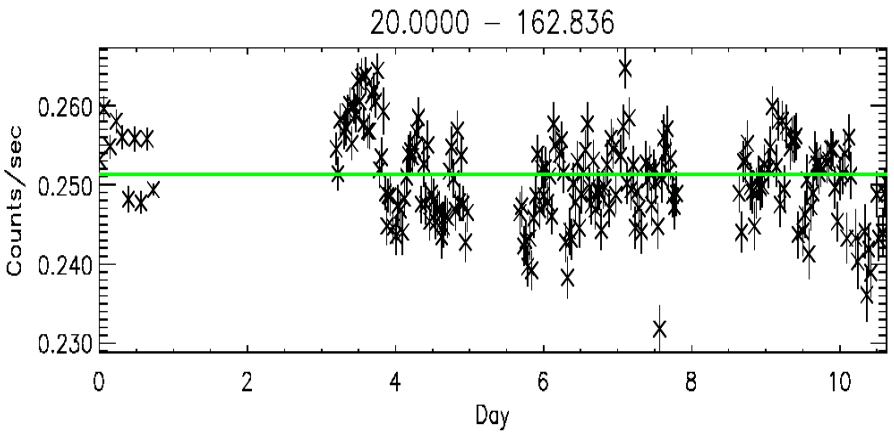

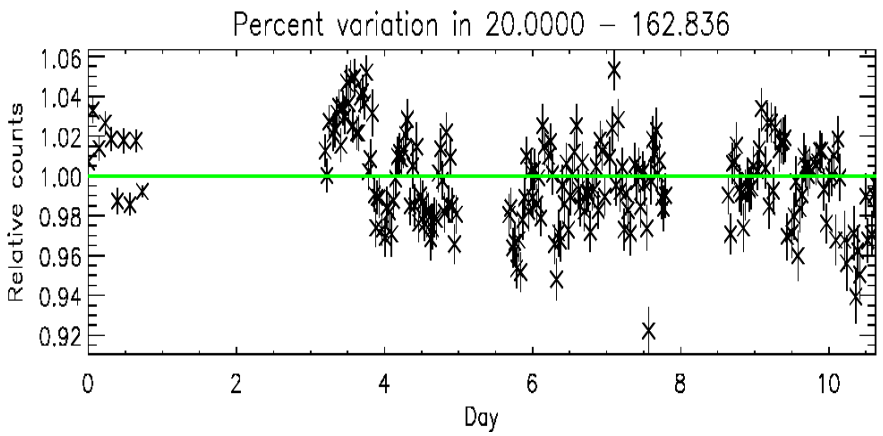

MODE 3

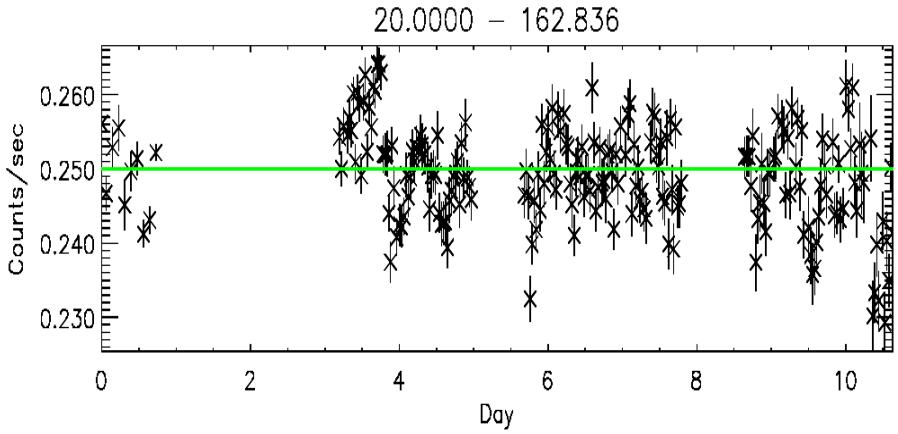

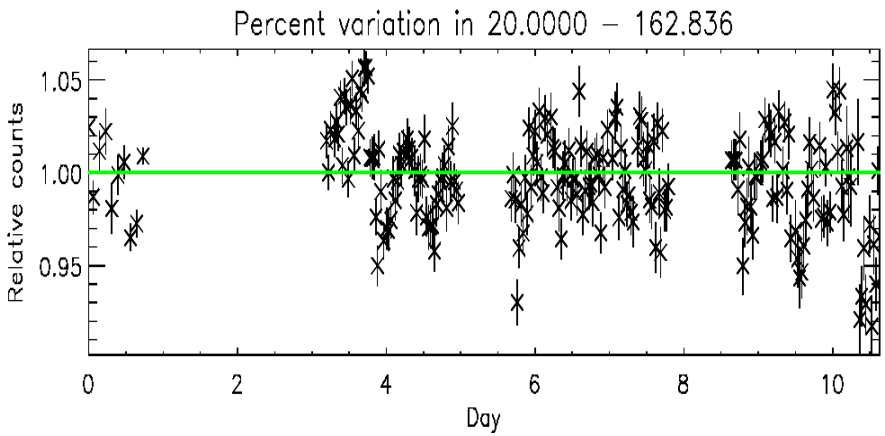

Spectra and background

IROS 4 pointings by 4 pointings (20 -163 keV) [boxcar average]

Mode 2

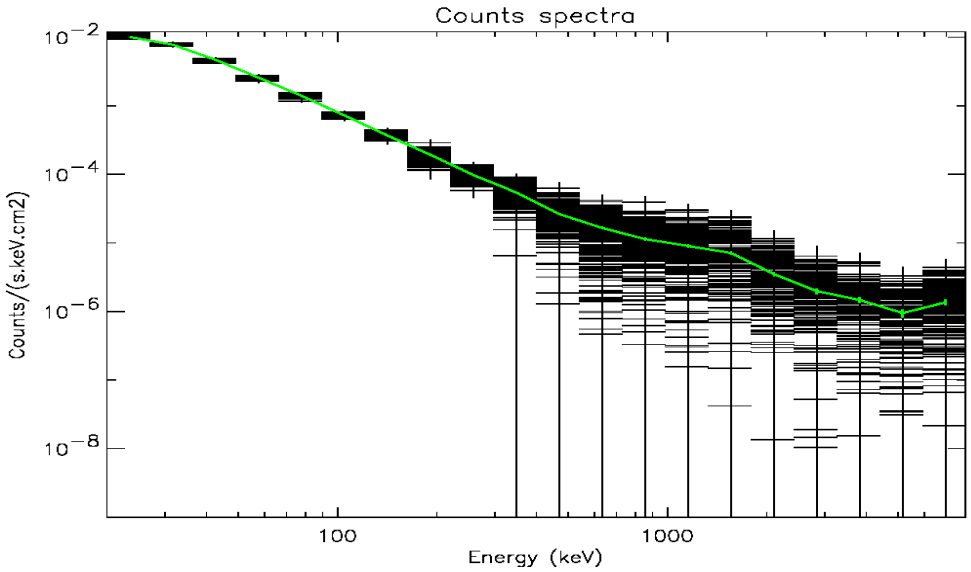

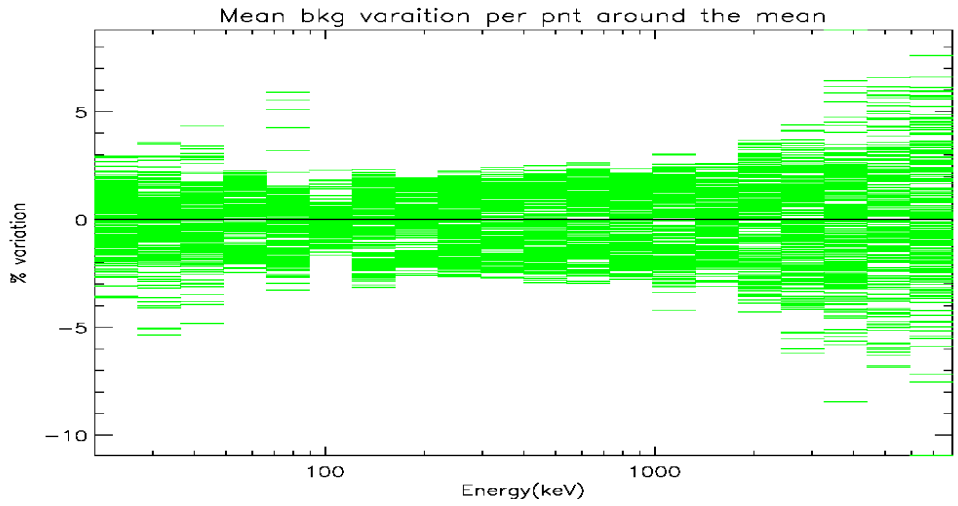

Mode 3

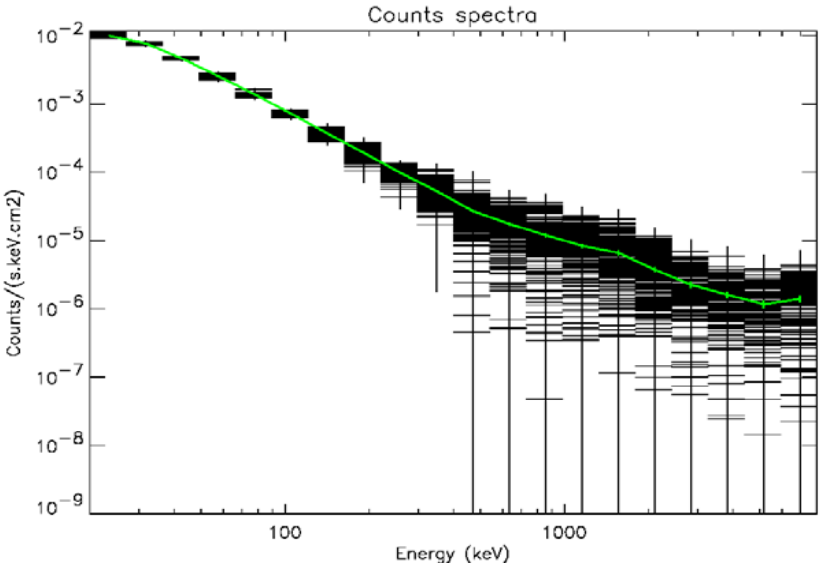

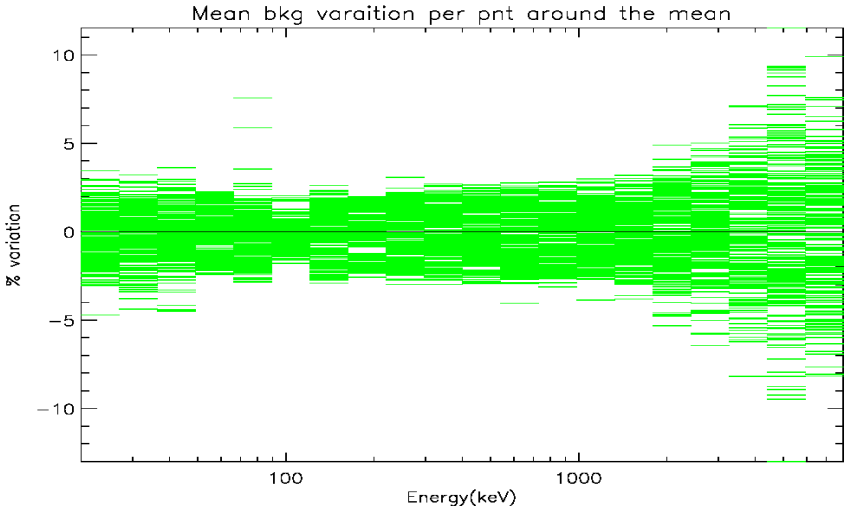

Light curve and background

IROS pointing by pointing (mode 3 - ”flat-field”)

20-49 keV SPIROS Mode 3

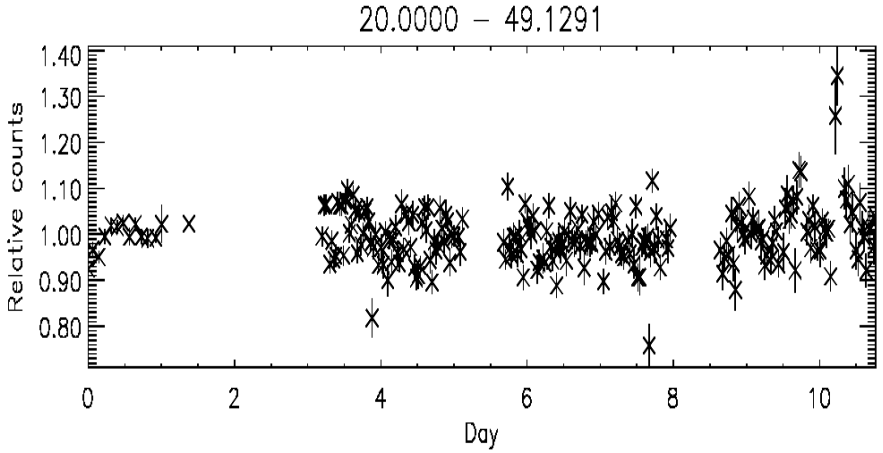

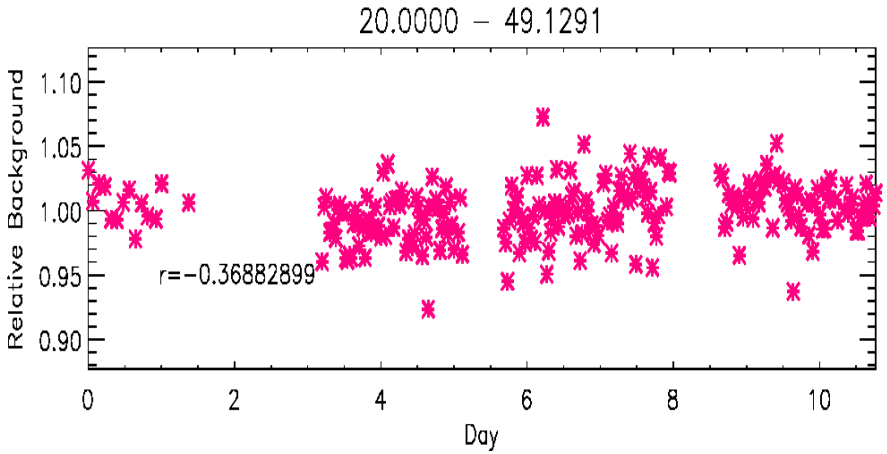

1326 - 8000 keV SPIROS Mode 3

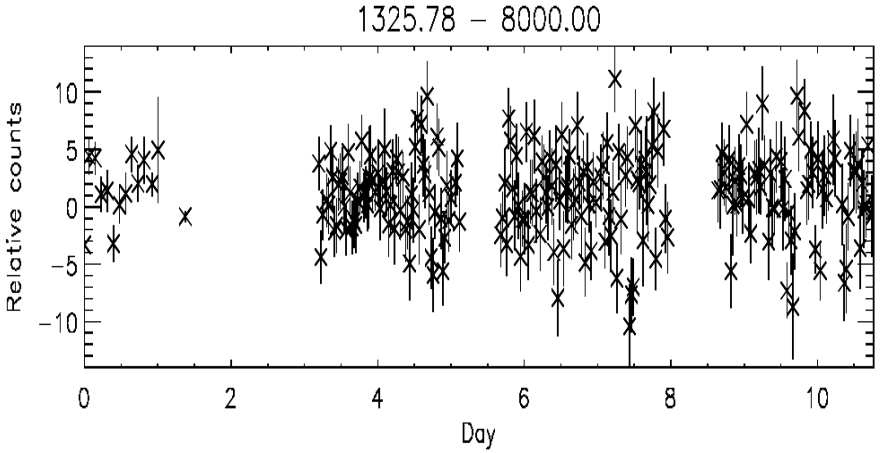

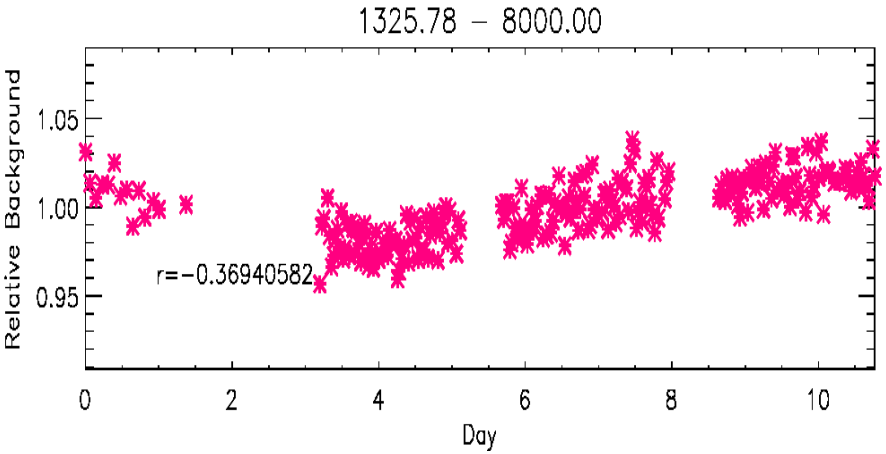

Light curve and background

IROS 4 pointings by 4 pointings (20 -49 keV) [boxcar average]

SPIROS Mode 2

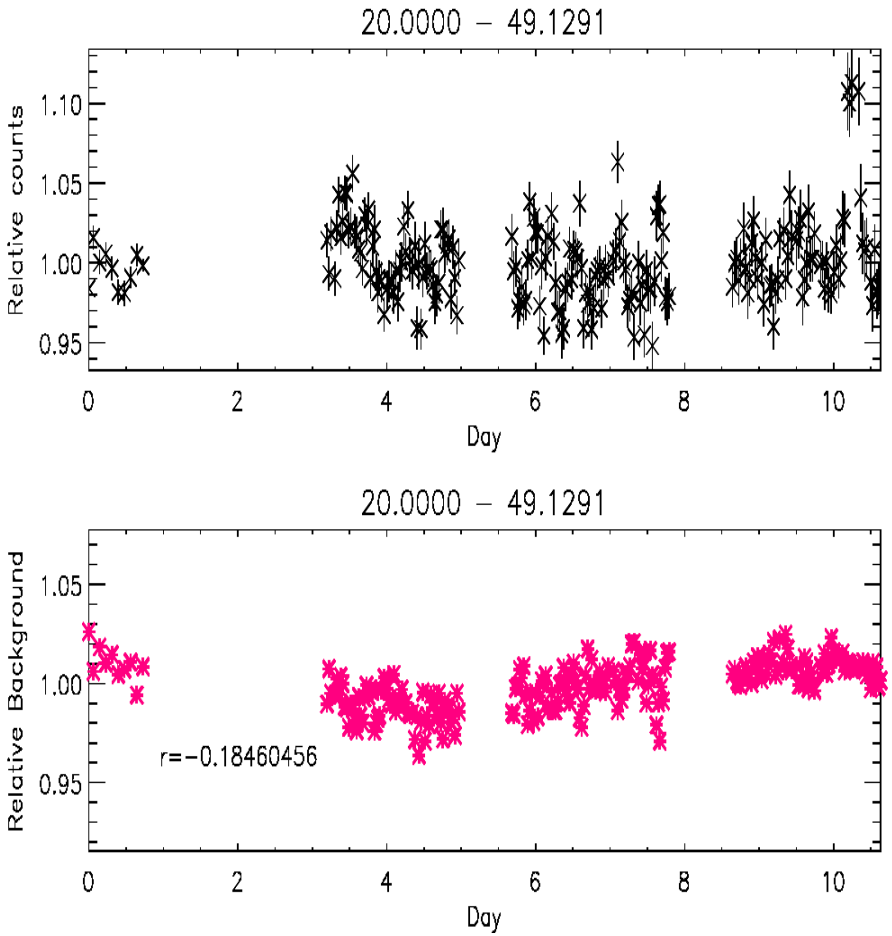

SPIROS Mode 3

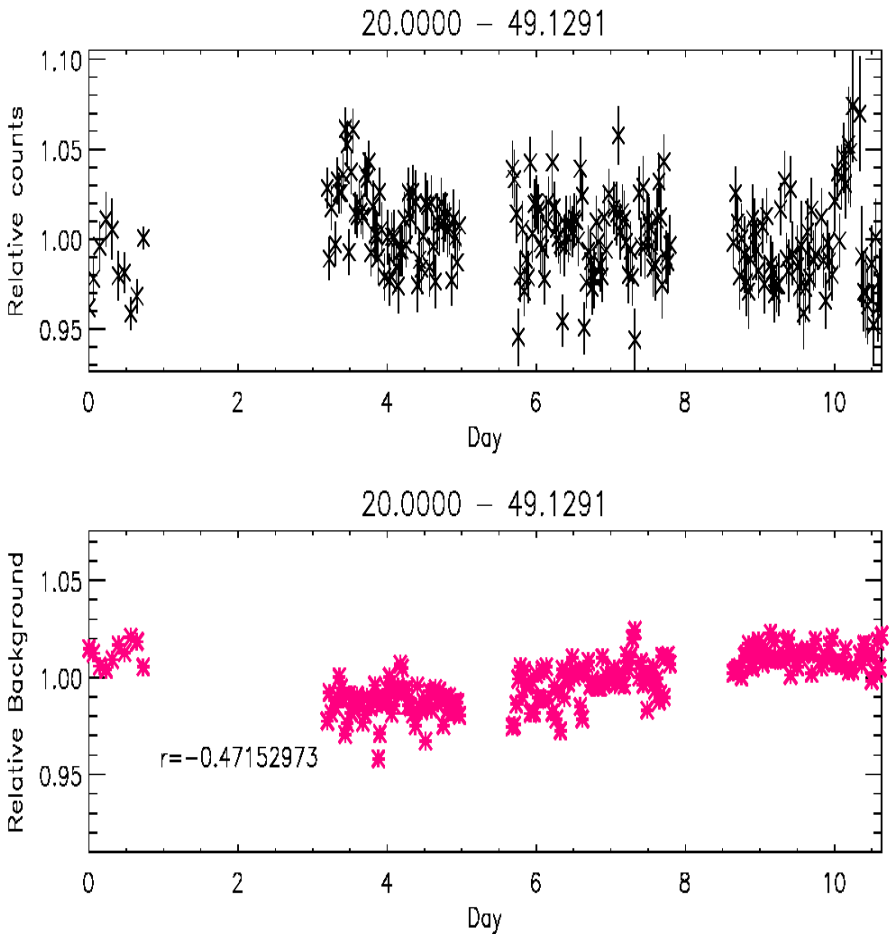

Light curve and background

IROS 4 pointings by 4 pointings (1326 -8000 keV) [boxcar average]

SPIROS Mode 2

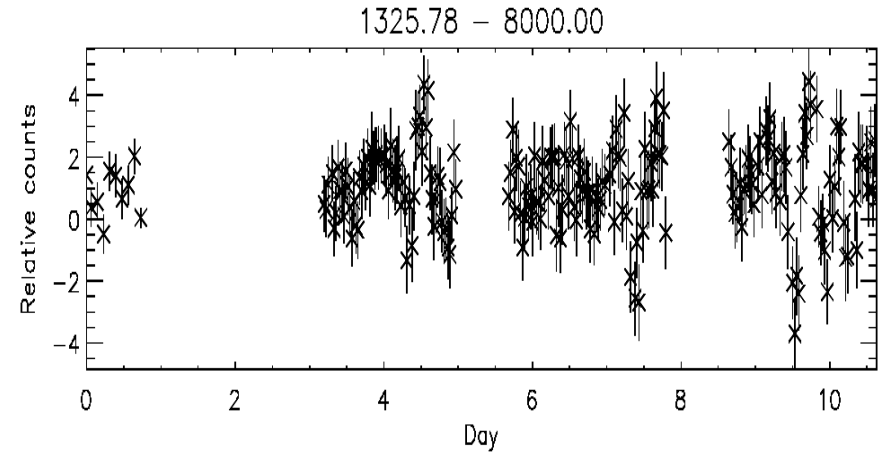

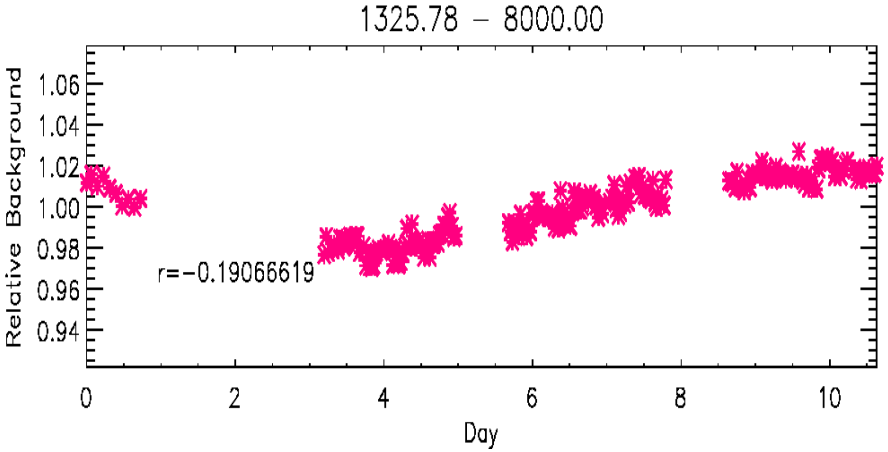

SPIROS Mode 3

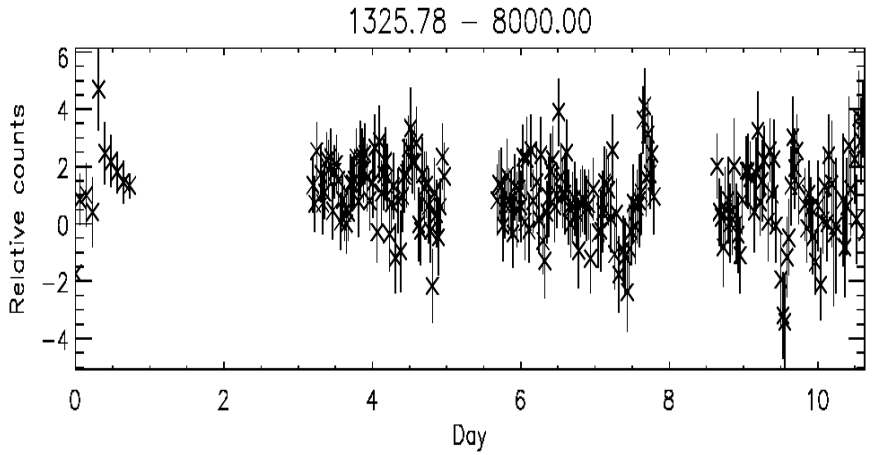

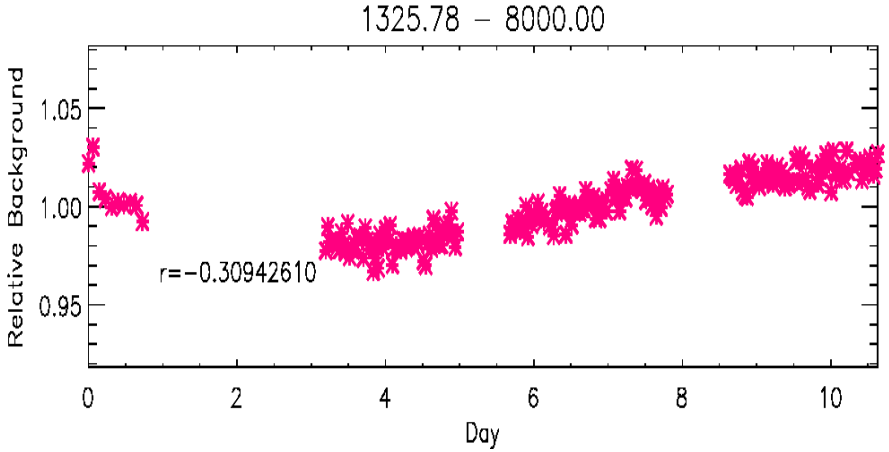

Background stability

SPIROS Mode 3 -"flat-field"

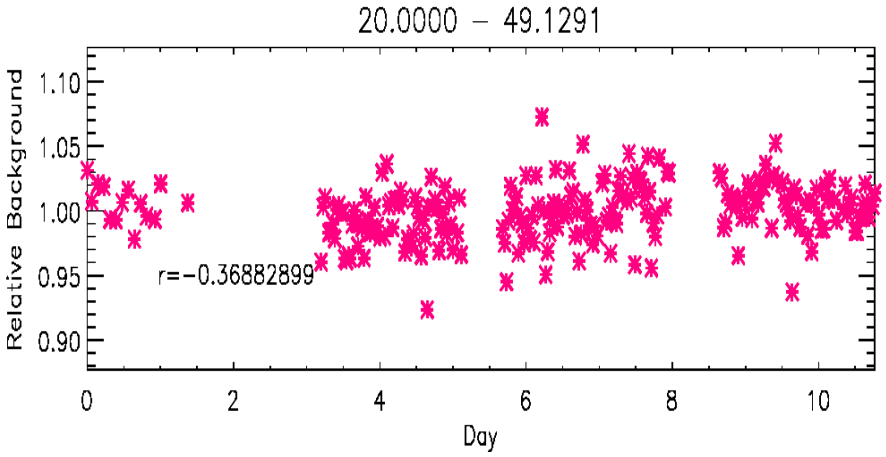

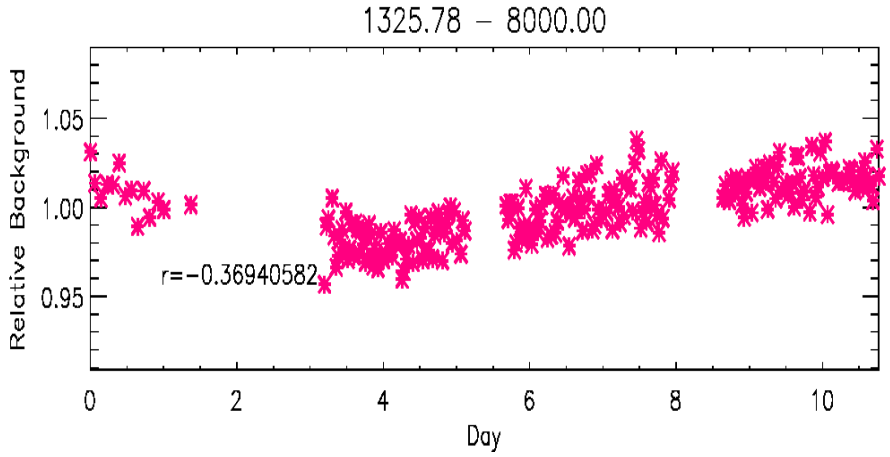

SPIROS Mode 2 - (4 pointings by 4 pointings

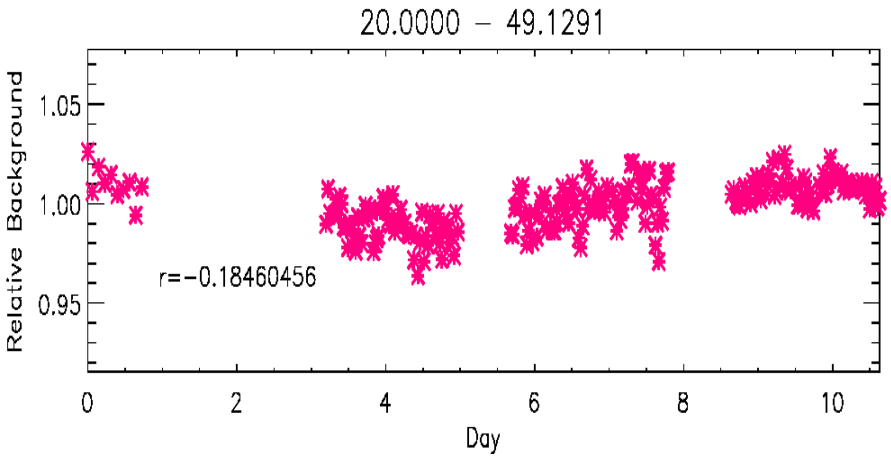

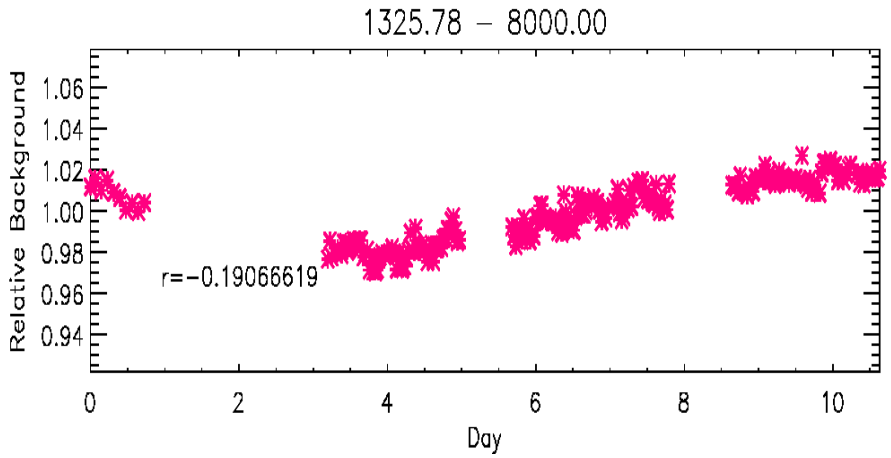

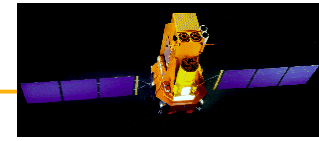

SAp

SPI Team Meeting, Toulouse, 2003 06 12

- **ISGRI-SPI spectra comparison**
- **SPIROS background methods**
- **Data analysis problems encountered in Saclay**

Patrick Sizun, CEA Saclay

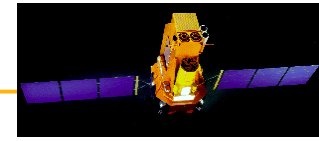

SAp

ISGRI VS SPI : Crab rev 44

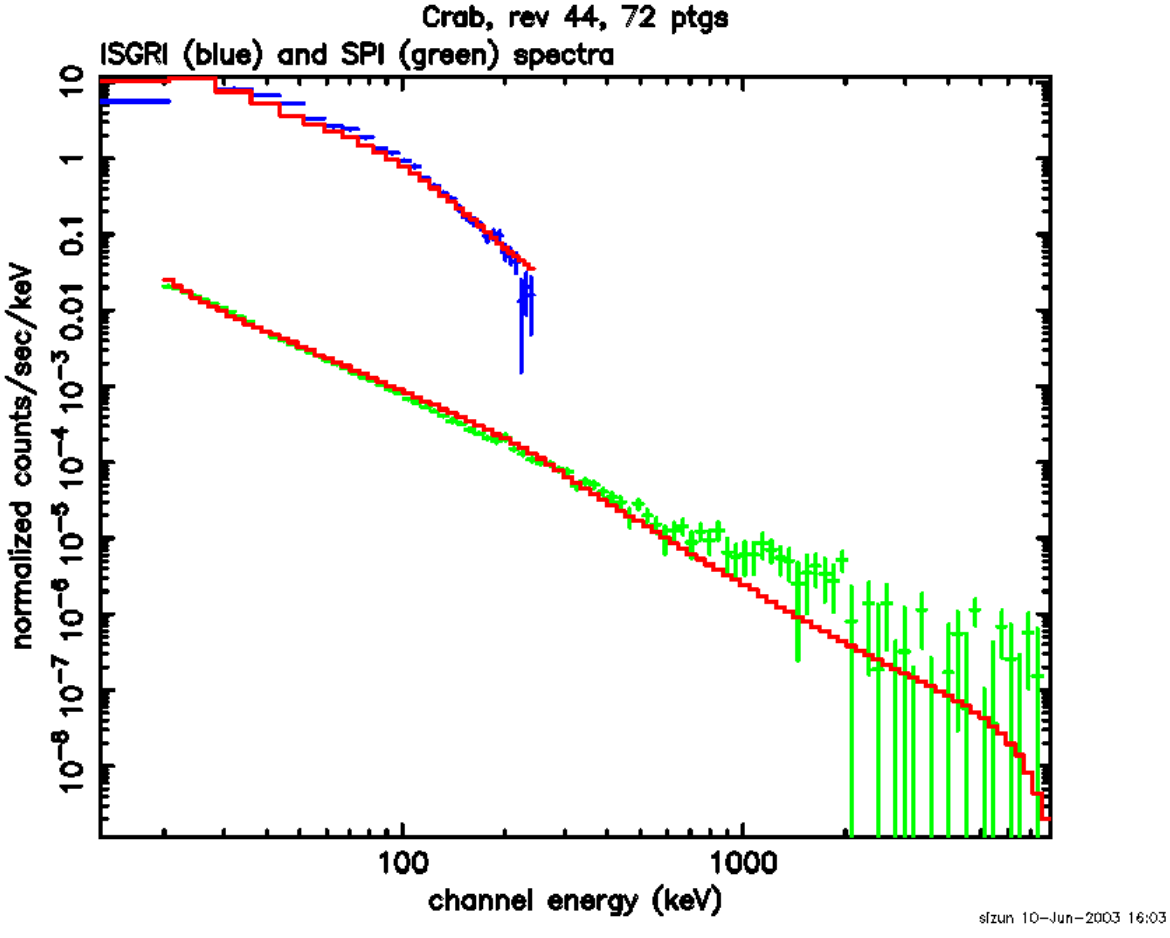

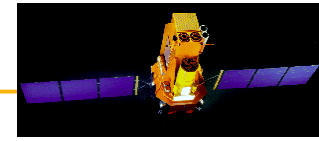

SAp

ISGRI VS SPI : Crab rev 44

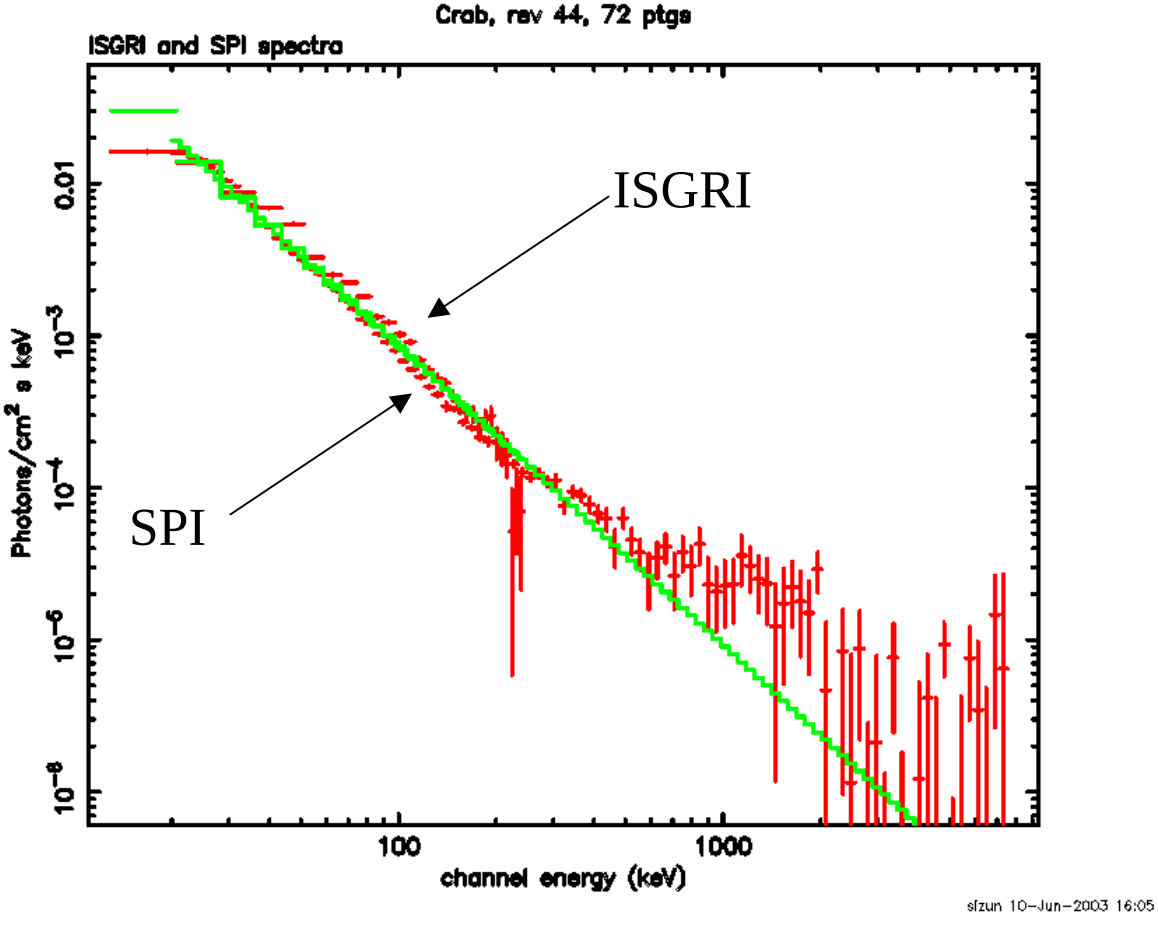

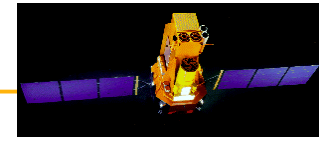

SAp

ISGRI VS SPI : Crab rev 44

- spectra are compatible in their common energy range
- same slope
- different normalization
- used C. Shrader's new IRF for SPI spectrum
- ISGRI Saclay team still working on a new ISGRI IRF

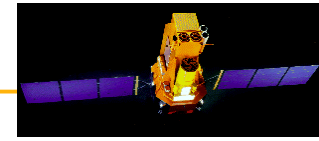

SAp

ISGRI VS SPI : GRS 1915+105 rev 57

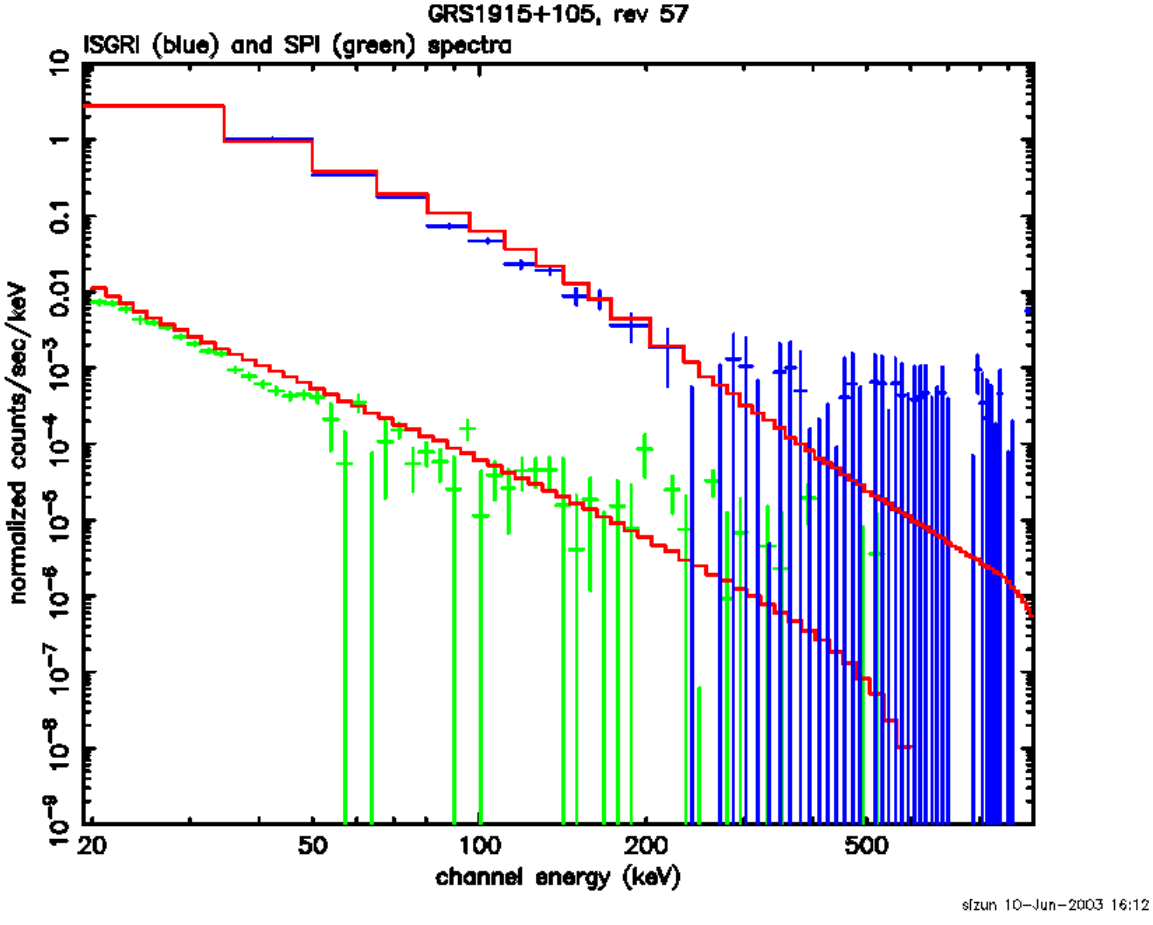

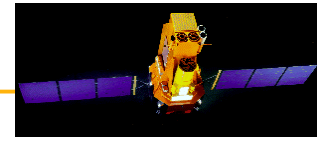

SAp

ISGRI VS SPI : GRS 1915+105 rev 57

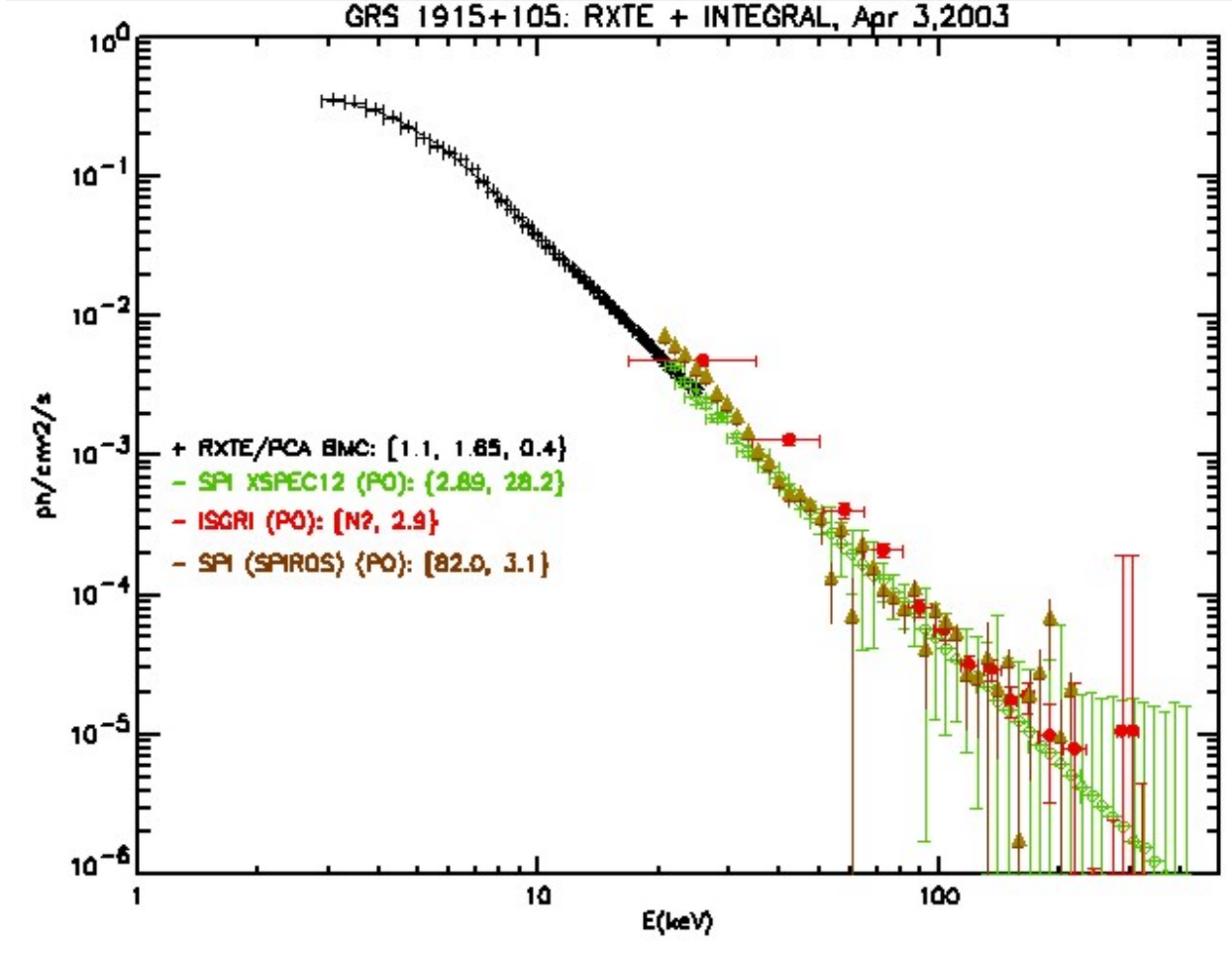

C. Shrader

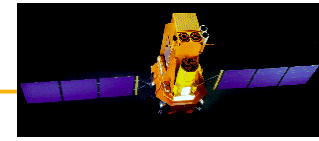

SAp

old IRF VS new IRF : Crab rev 44

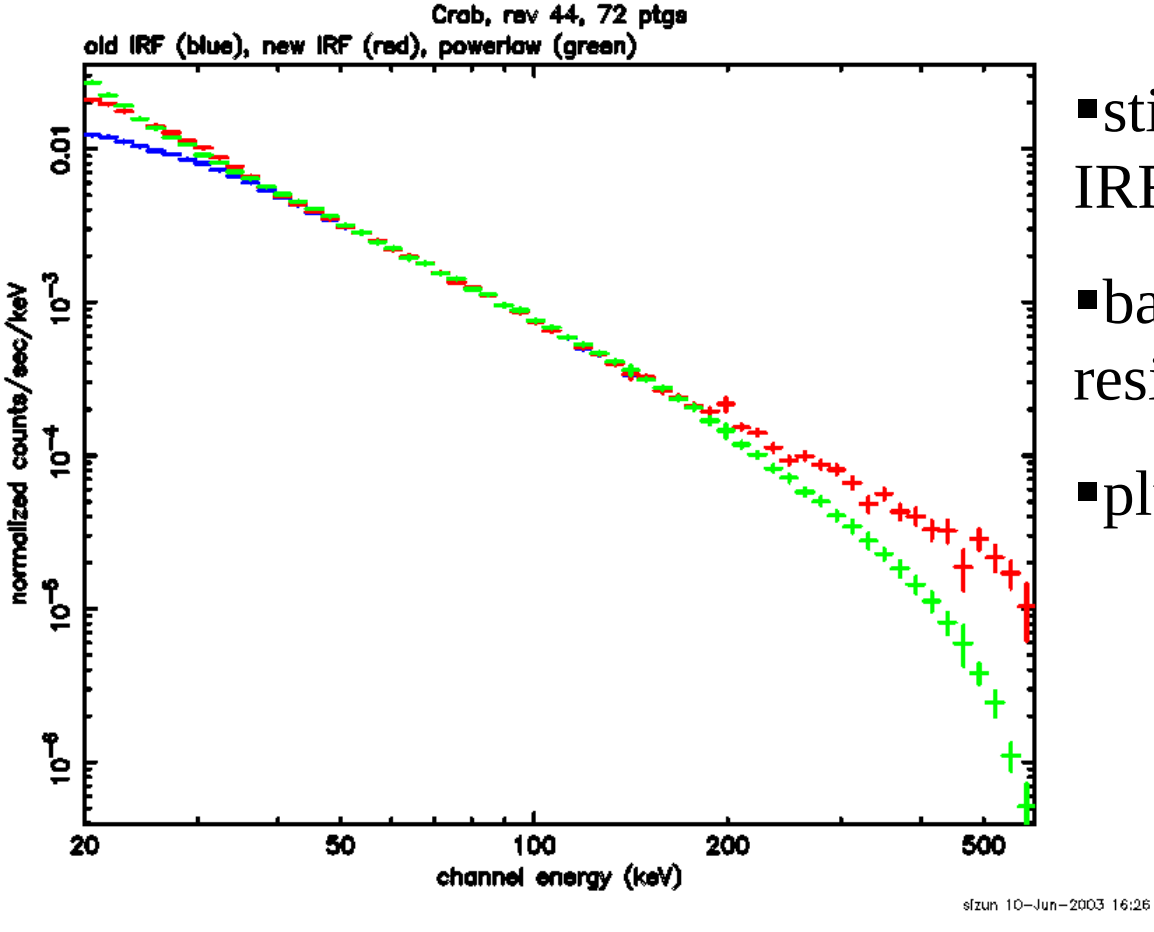

- still a problem with IRF at 20 keV ?
- background residuals
- plus pb with spiros

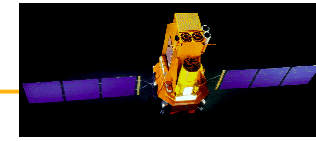

background methods : method 2 ok

SAp

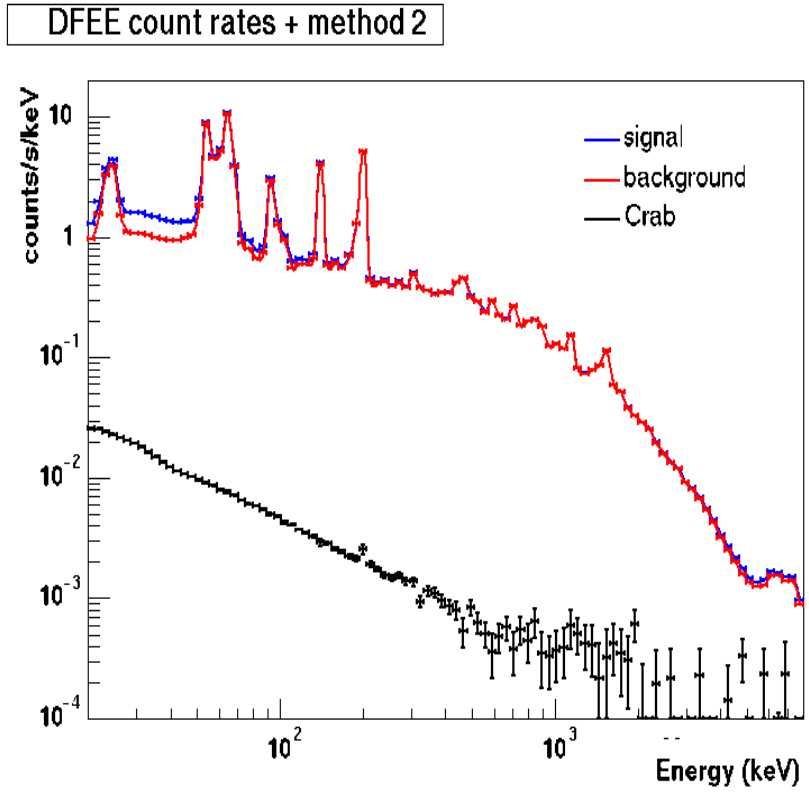

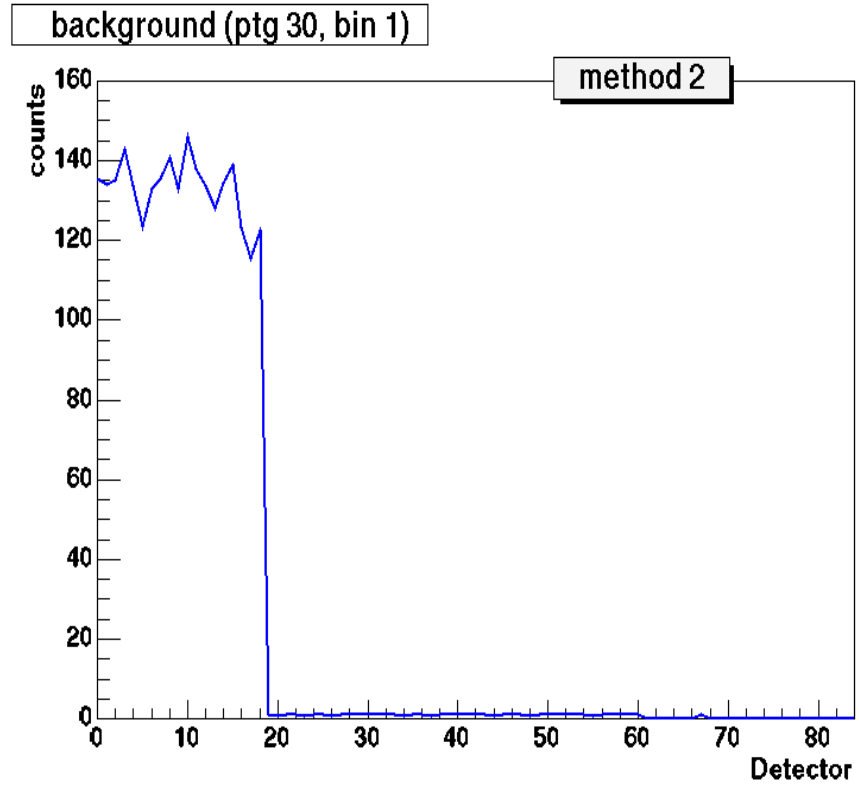

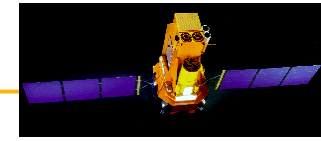

background methods : method 3

SAp

background model (ptg 30, bin 1)

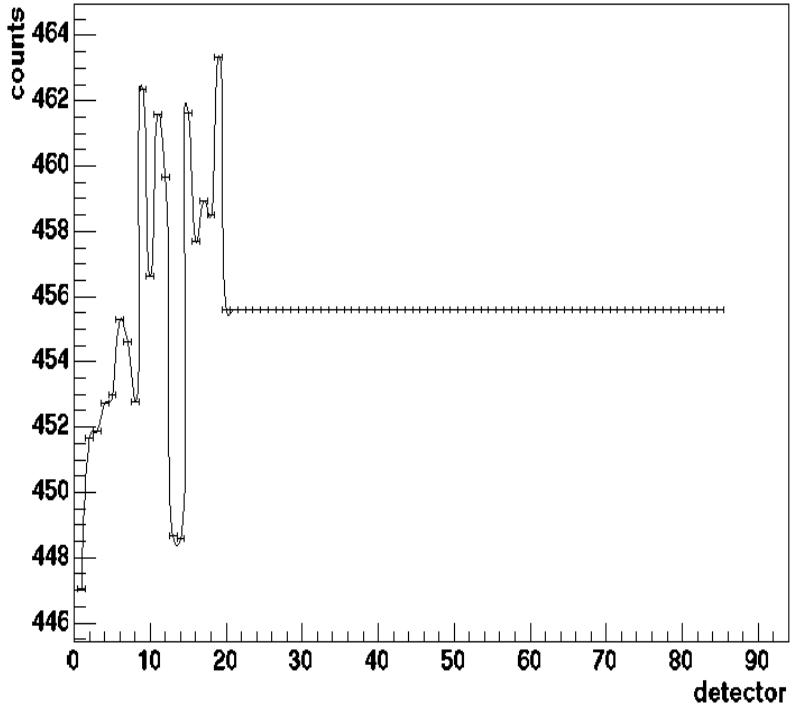

DFEE count rates + method 3

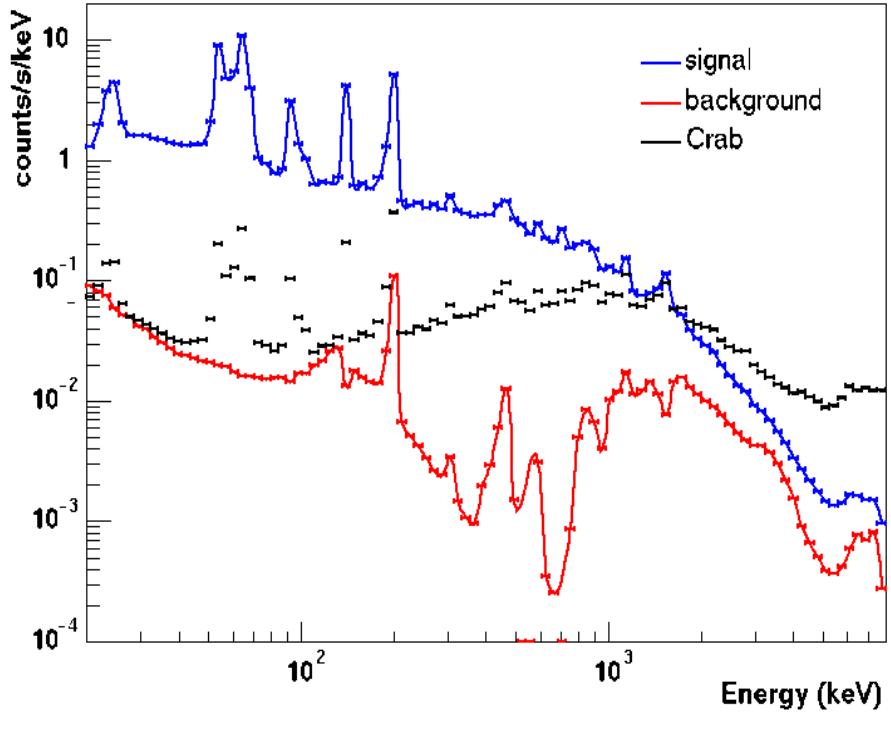

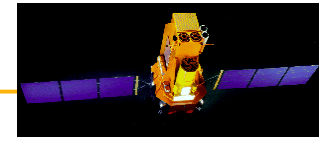

empty field + background method 3 : still not perfect

SAp

background model

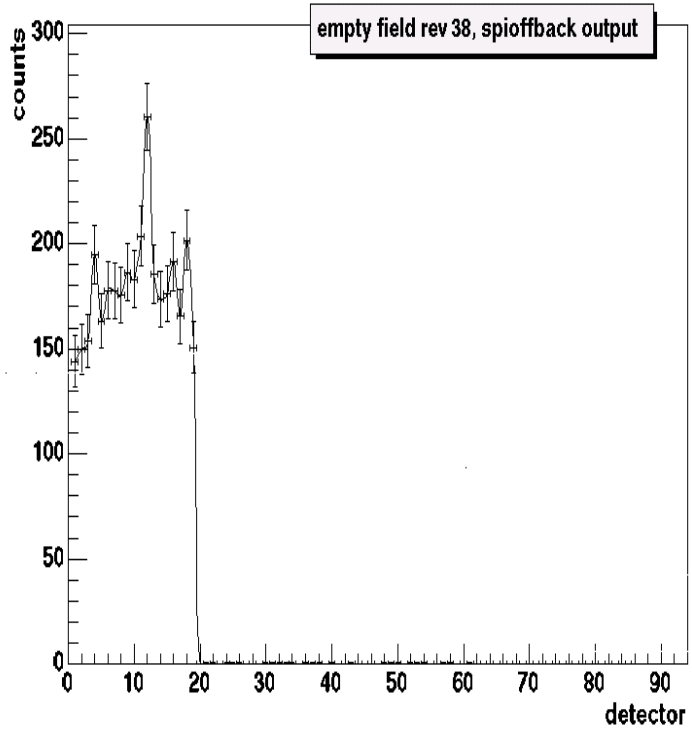

empty field + method 3

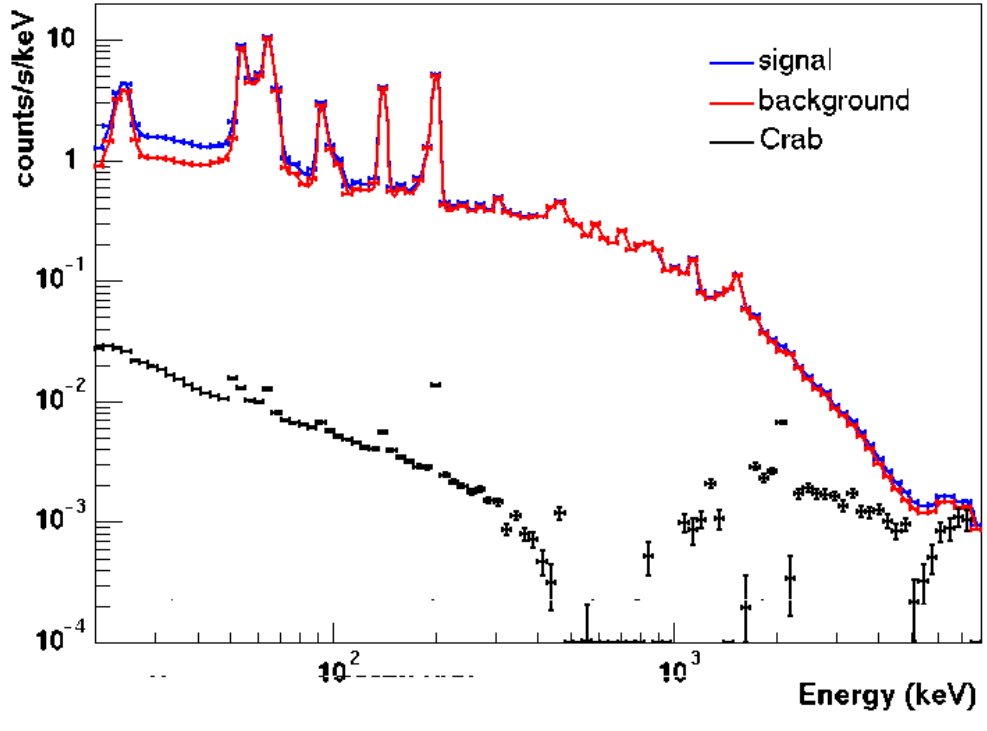

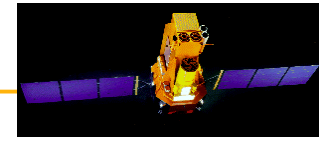

SAp

Cygnus X-1 : high energy problems

- analysis parameters :
  - ✓ rev 20 on axis, consolidated data, only ptgs with a good χ^2
  - ✓ public OSA release 1.0
  - ✓ ISDC keV-chan file, DFEE count rates, method 2
- result :
  - ✓ kT = 100 keV !
  - ✓ unlike L. Bouchet & C. Shrader ?
  - ✓ like ISGRI ?

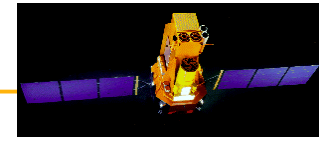

SAp

Cygnus X-1 : high energy problems

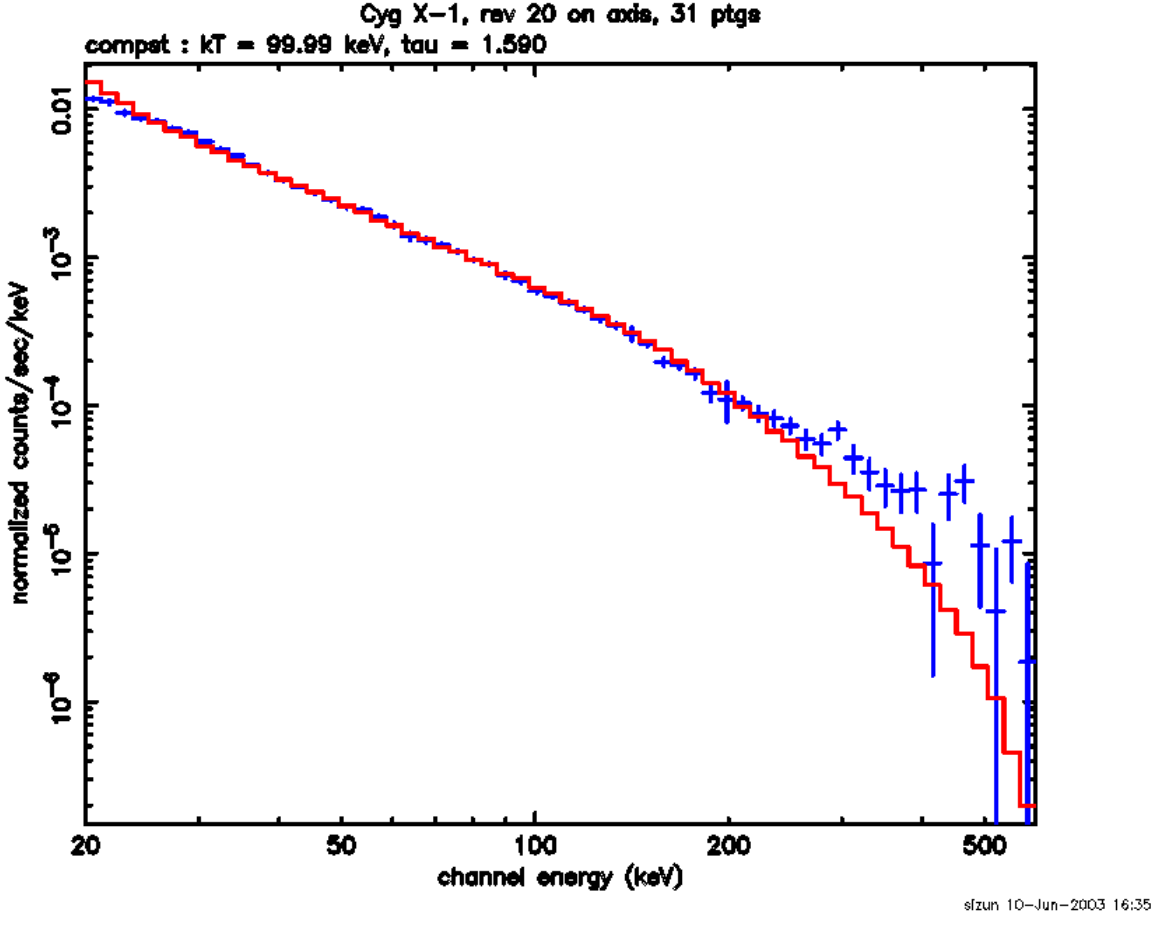

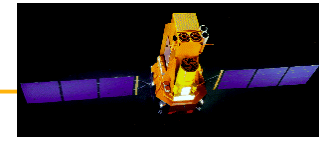

SAp

Cygnus X-1 : high energy problems

- conclusions :
  - ✓ 8 arcmin offset
  - ✓ usual problem with bad background substraction
  - ✓ problem specific with early revolutions ?
  - ✓ problem with public software release

ENERGY CALIBRATION

(Low energy range)

PURPOSE :

FOR ONE REVOLUTION :

- DETERMINE CAMERA LINEARITY

- DETERMINE ENERGY CALIBRATION :
(EACH CALIBRATION COEFFICIENT)

DATA SETUP

Conditions :

Long Live time acquisition

Very Good detector temperature stability ($\Delta T << 1K$)

Stable AFEE saturation flux

REVOLUTION CHOICE : 22 Duration : 2.14 days

CONFIGURATION : NOMINAL

TEMPERATURE COLD PLATE STABILITY

AFEE SATURATION FLUX STABILITY

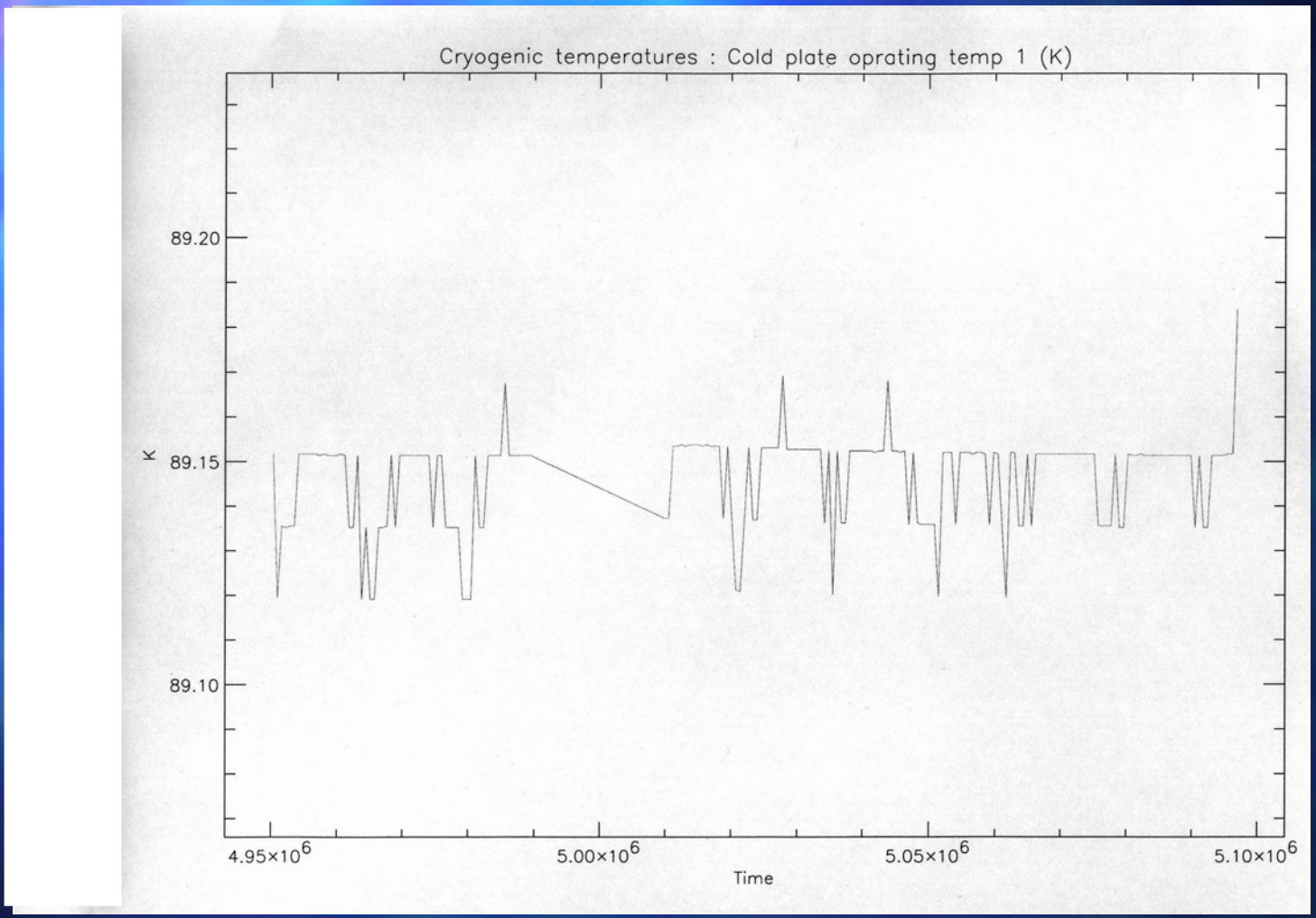
Cryogenic temperatures : Cold plate oprating temp 1 (K)
89.20
89.15
89.10
K
4.95×10^6
5.00×10^6
5.05×10^6
5.10×10^6
Time

$\Delta T = 0.06$ K

AFEE SATURATION FLUX

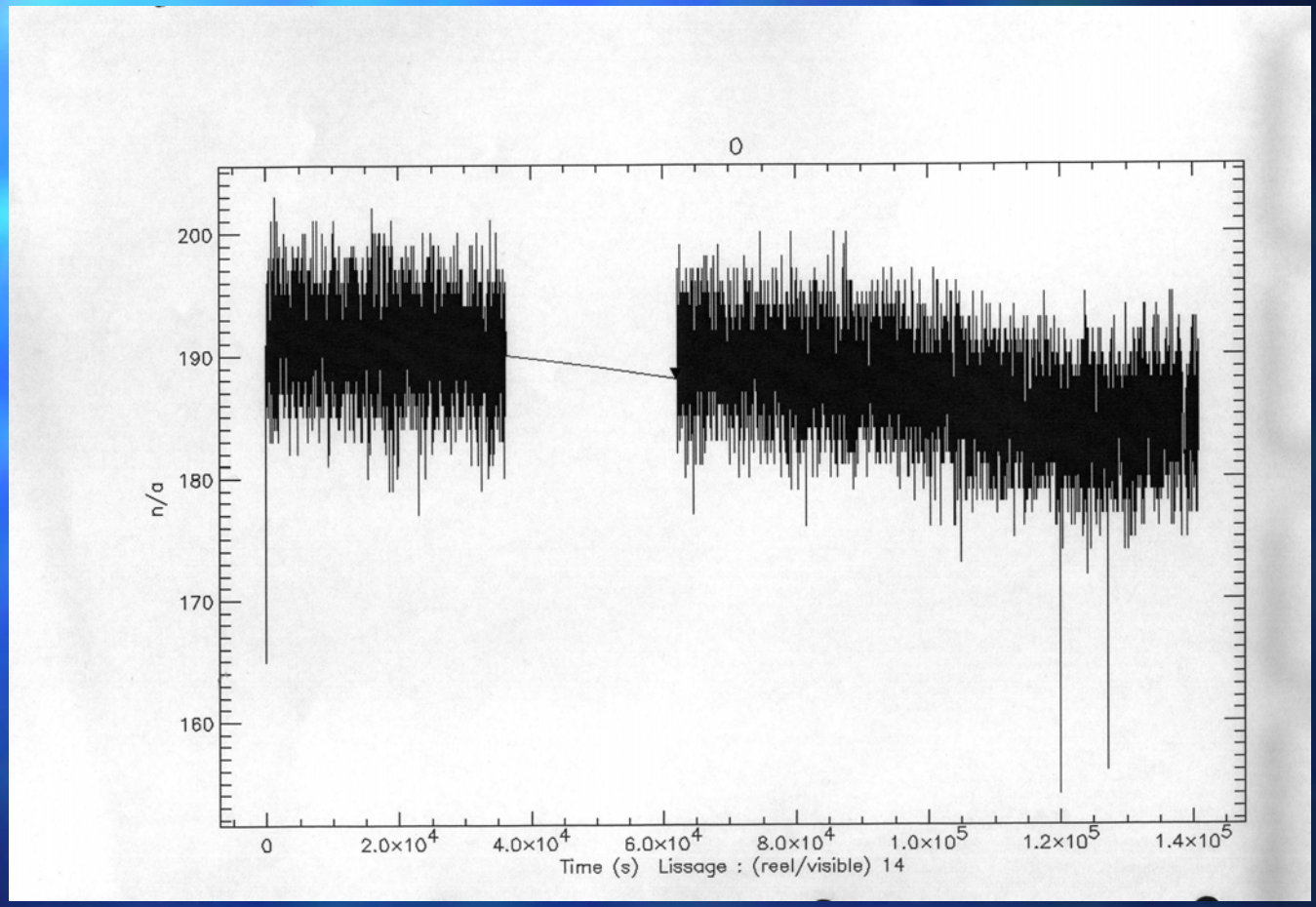

CALIBRATION LINES USED : 23 lines

Energy (keV)	Status
23,43	In ME spectra $^{70}Ge(n,\gamma)^{71*}Ge$
139,68	Always measured at 139.8796 keV
174,90 (ME)	Ok
185,72	Two lines mixed
194,06	One line
198,34	One line $^{70}Ge(n,\gamma)^{71*}Ge$
271,24	One line
309,86	One line
438,6	One line $^{69*}Zn$
511,004	One line
574,11	Two lines mixed
584,48	Two lines mixed
810,75	Two lines mixed
817,86	One line
825,2	One line
882,35	One line ^{69}Ge
1014,4	Two lines
1117,1	One line blended with above
1124,5	Problem with statistics
1336,6	Two lines mixed
1368,53	4 lines mixed
1764,3	Two lines mixed
1778,9	One line blended with above $^{28*}Al$

CAMERA LINEARITY DETERMINATION

Low energy range

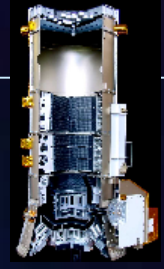

Calibration lines : 198.34 keV, 438.6 keV, 882.35 keV, 1778.9 keV.

Fitting function :

$$\frac{C}{E} = A_0 + \frac{A_1}{E}$$

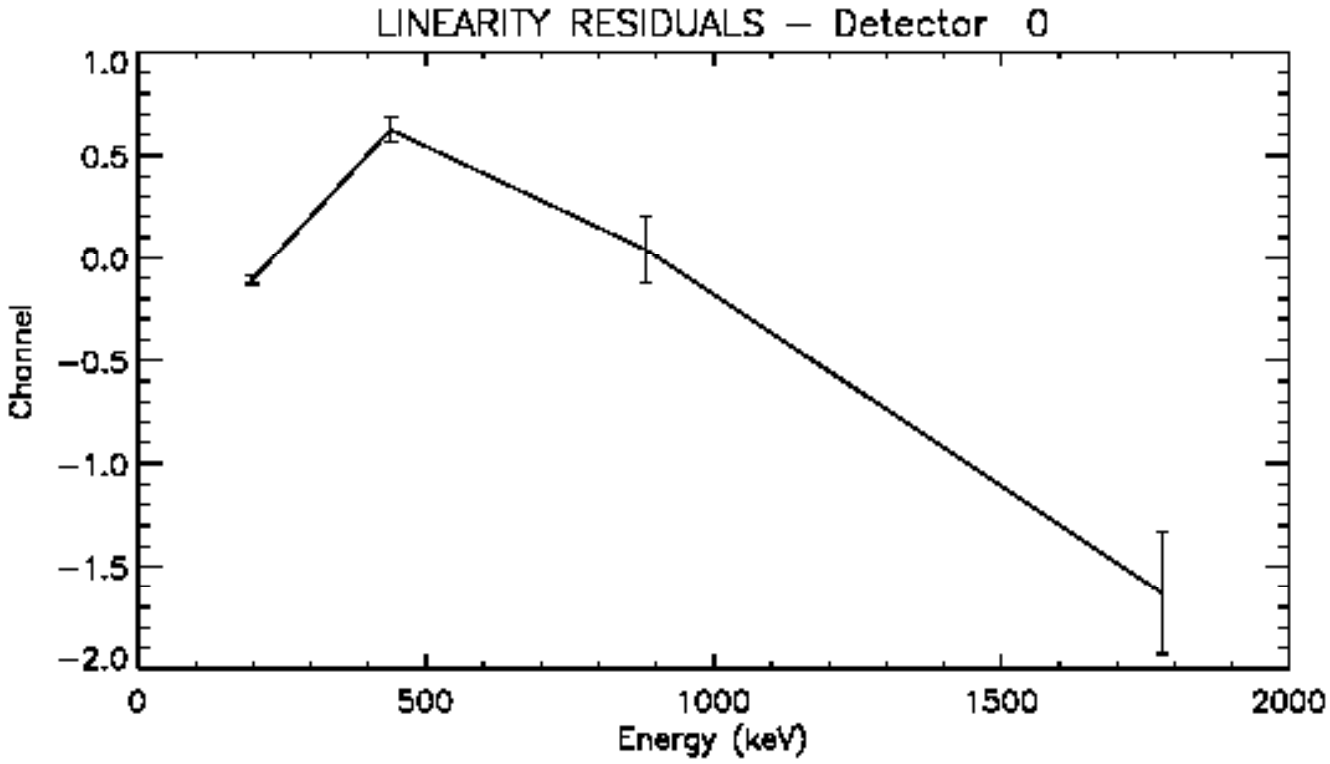

Linearity residuals for the detector 0 (1st order polynomial)

Revolution 22.

LINEARITY RESIDUALS FOR THE DETECTOR 0

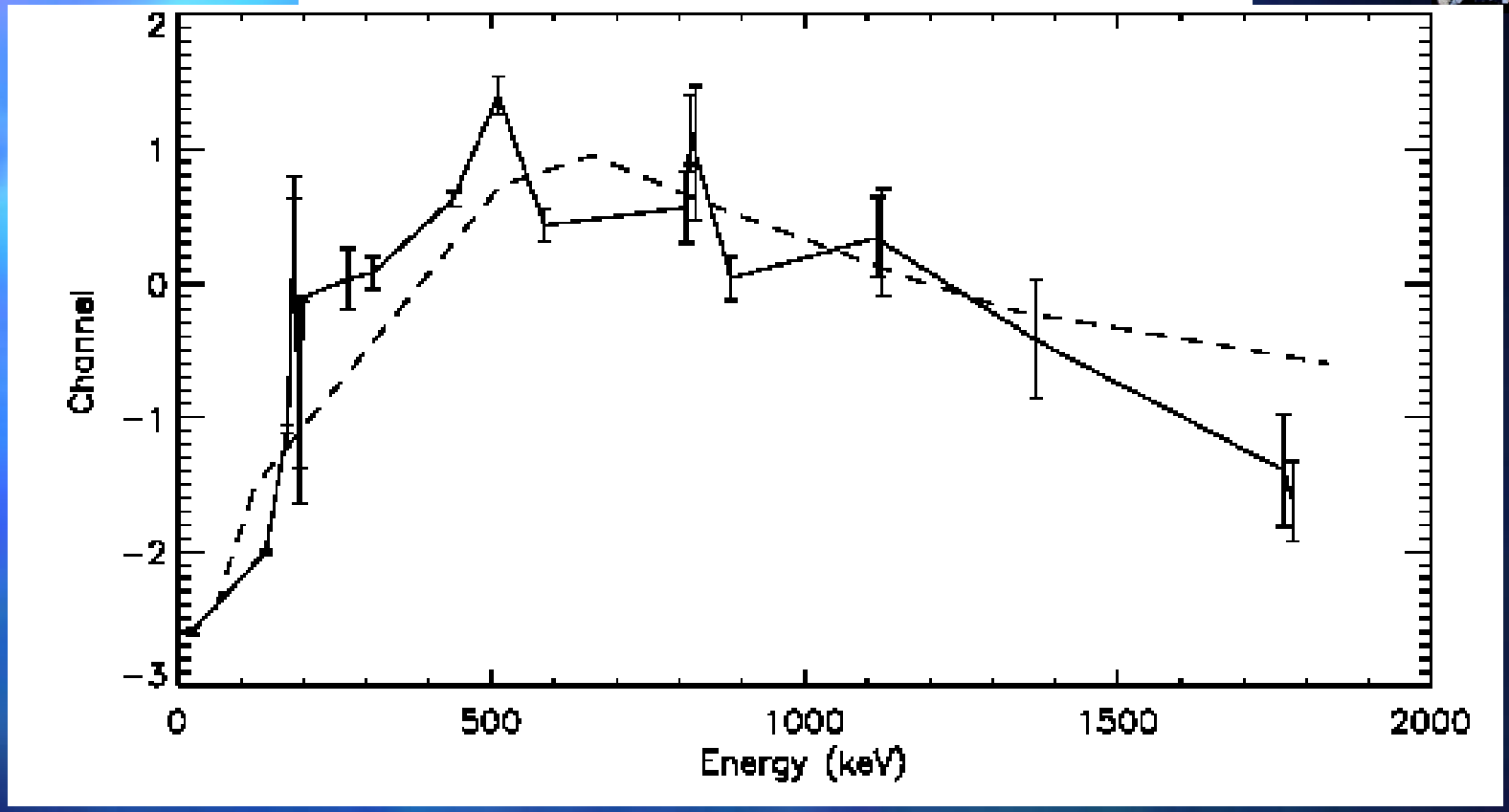

Linearity residuals for the detector 0 (1st order polynomial). Line dashed: data from BLC calibration campaign.Continuous line: 20 gamma ray lines used, 4 calibration lines to compute linearity response (198.34 keV, 438.6 keV, 882.35 keV, 1778.9 keV), revolution 22.

QUESTION : Which parts of the acquisition chain induced its none linearity?

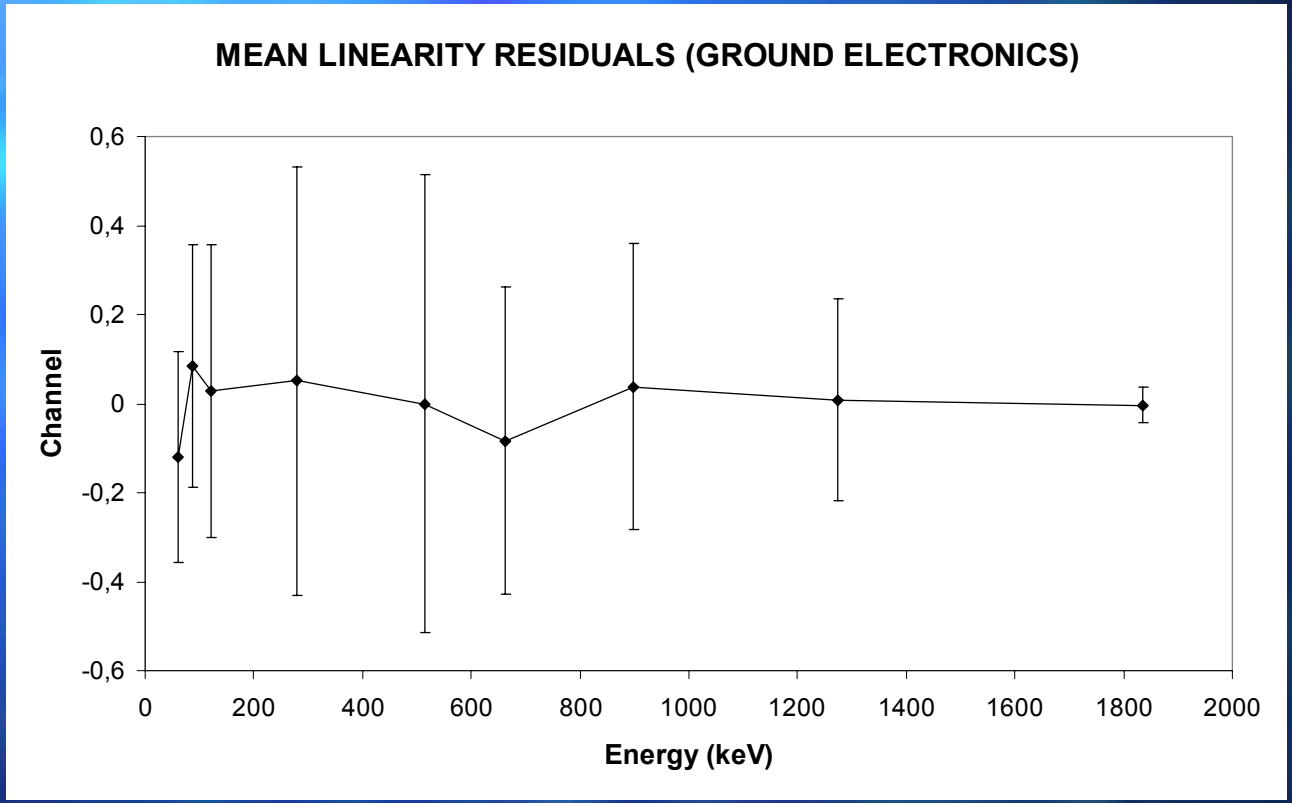

Camera means linearity residuals for ground electronics (Banc de Test).
These measurements had been performed during the SPI camera calibration

ENERGY CALIBRATION

FITTING FUNCTION : 3 rd order polynomial

$$\frac{C}{E} = A_0 + \frac{A_1}{E} + \frac{A_2}{E^2} + \frac{A_3}{E^3}$$

$$\frac{E}{C} = f\left(\frac{1}{C}\right)$$

Inversion numerically the fitting function : The inversion error is less than 0.0001 keV.

CALIBRATION RESIDUALS FOR ALL LINES – DETECTOR 0

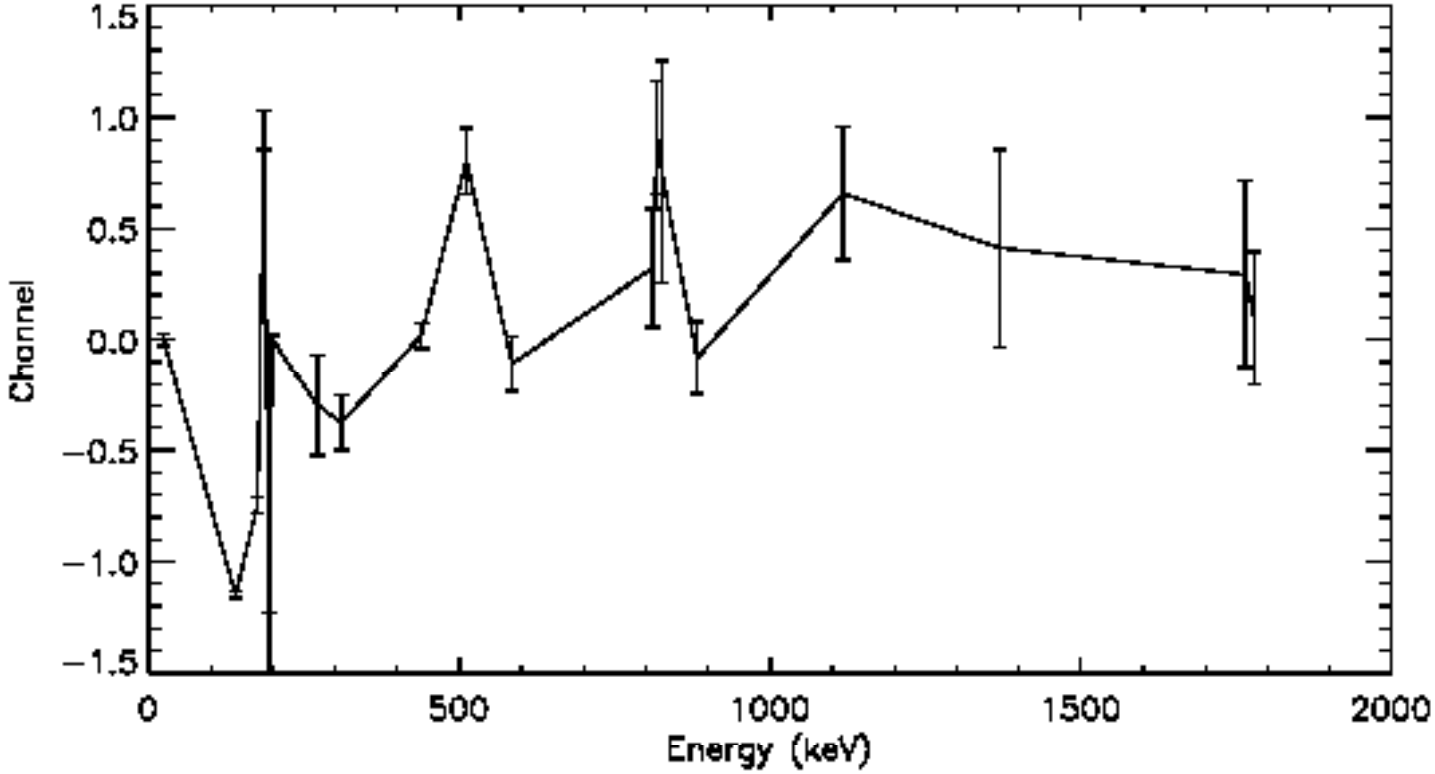

Calibration residuals for the detector 0 (3rd order polynomial).
Calibration lines: 23,43 keV, 198.34 keV, 438.6 keV, 882.35 keV, 1778.9 keV.
Revolution 22.

ENERGY CALIBRATION COEFFICIENTS

Low energy range

DETECTOR NUMBER	A_0	A_1	A_2	A_3
0	0.13566896	1.3739970	-495.23071	63274.922
1	0.13443124	1.4707540	-249.88390	27782.260
2	0.13474136	1.3910645	-428.46790	53293.707
3	0.13365280	2.3179549	-417.54598	50942.319
4	0.13482355	1.4315543	-241.37004	25575.008
5	0.13486428	2.1354298	-427.29725	51991.261
6	0.13442708	1.6446645	-470.73924	58936.306
7	0.13531811	1.4635816	-539.14773	69300.732
8	0.13460487	1.2385193	-425.73204	53775.164
9	0.13461748	1.2595966	-221.96732	22705.352
10	0.13426203	1.5536902	-294.45521	33773.823
11	0.13501858	2.4523628	-349.60258	39990.235
12	0.13531203	1.3453406	-412.49028	50641.204
13	0.13446560	1.2774160	-152.61615	13860.076
14	0.13486408	1.2745028	-372.11223	45596.909
15	0.13470172	1.4552985	-355.34094	42383.997
16	0.13493273	1.0701387	-288.49200	33155.565
17	0.13357310	1.8820558	-273.97205	31331.479
18	0.13488035	1.2443022	-338.93848	41224.183

SPI Team Meeting June 2003 at CESR

Roland Diehl

Instrument Calibration and Background Study

Background Studies

- Karsten Kretschmer, Diego Rodriguez, Andreas von Kienlin, Trixi Wunderer, Roland Diehl

Study:

- Data
  - GCDE Rev's 46-66
- Event Histogramming & Energy Calibration
- Gaussian Fits to Set of Bgd Lines
  - Different Time Scales
  - Different Detectors
  - Different Event Types
  - E,I,σ -> E, counts/sec, σ
- Investigation of Results
  - Peculiarities as Help for Bgd Indentification
  - Correlations among Line Parameters
  - Detector Resolution versus Energy

Background & Spectral Response: Evolution of Line Parameters

- Fitted Line Parameters versus
  - Time
  - Detector
  - …
- Lines
  - 438 keV
  - 511 keV
  - 1107 keV
  - 1117 keV
  - 1124 keV
  - 1138 keV
  - 1764 keV
  - 1779 keV

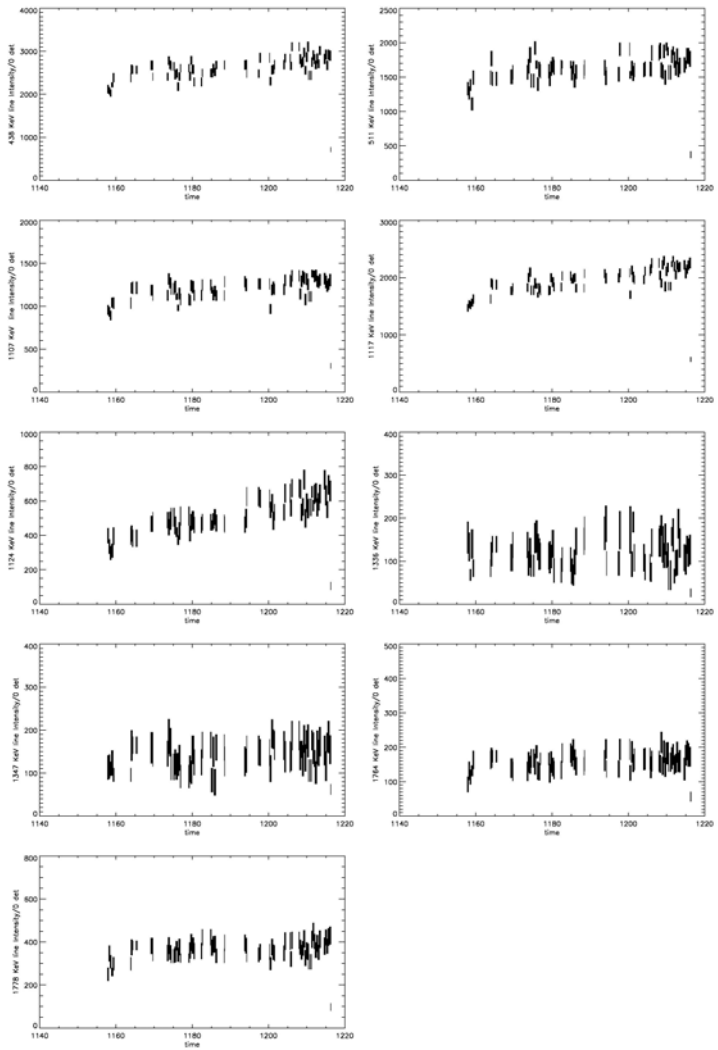

Energy Calibration Checks

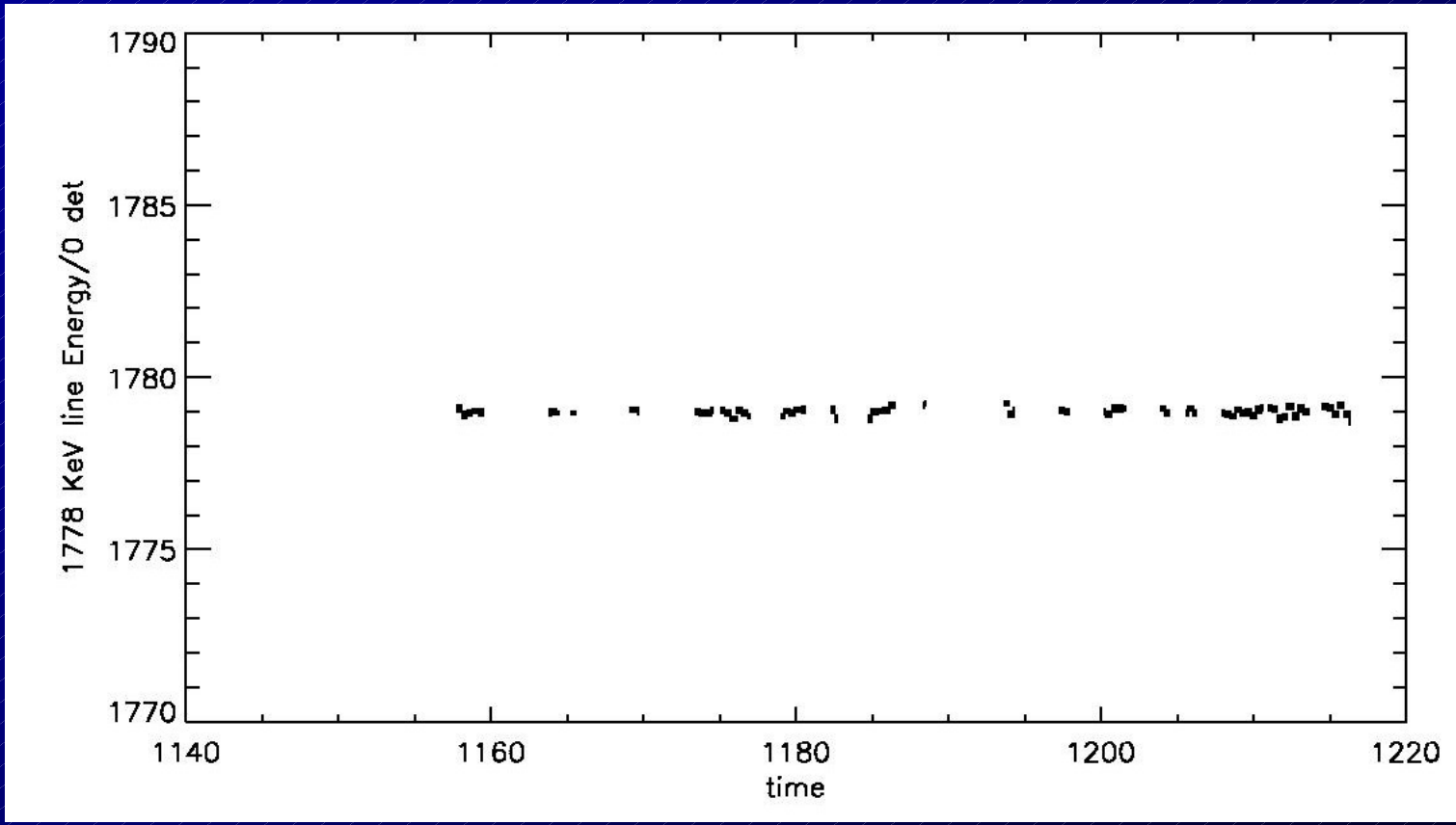

- ☆ Energy Calibration Appears ~Stable
- ☆ Processing ~ok, no Glitches & Outliers

Energy Resolution Checks

- ☆ Line Widths for Many Lines…
  - ☞ Detector Degradation

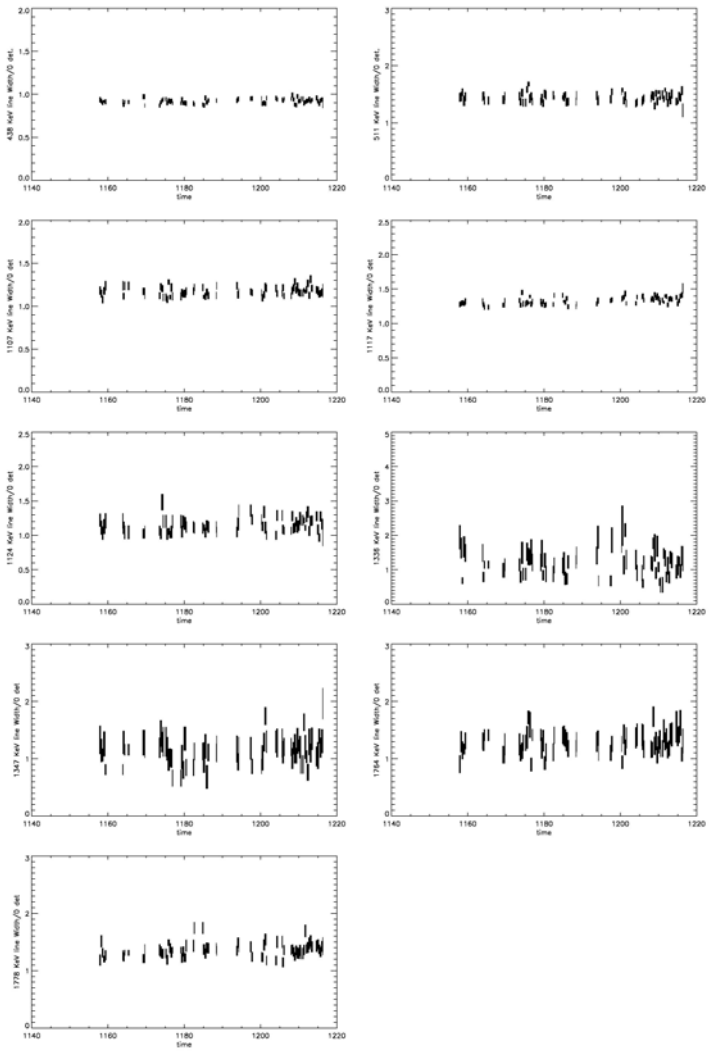

Energy Resolution Checks

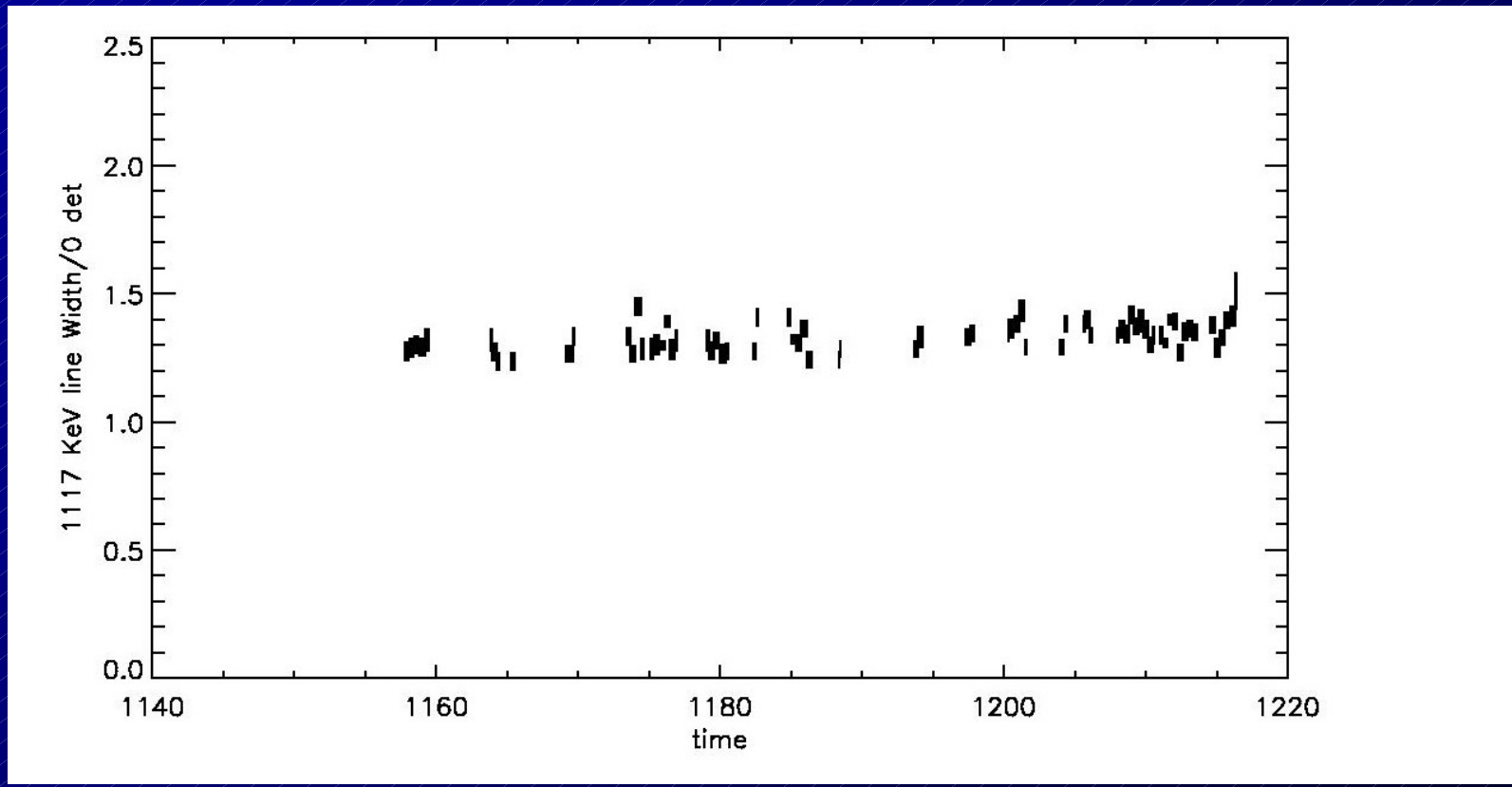

- ☆ Trend from Detector Degradation ~0.216 keV/100d
- ☆ Other Effects Superimposed

Energy Resolution Checks…

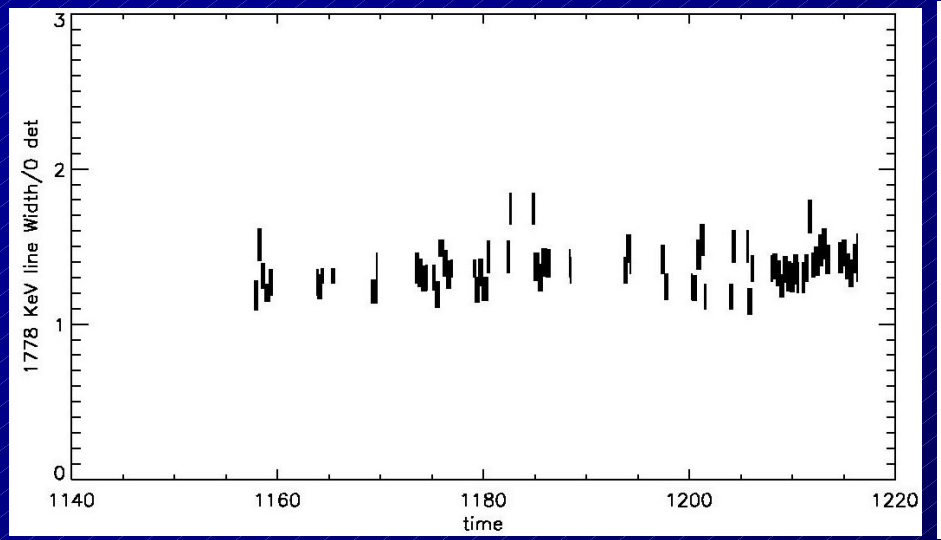

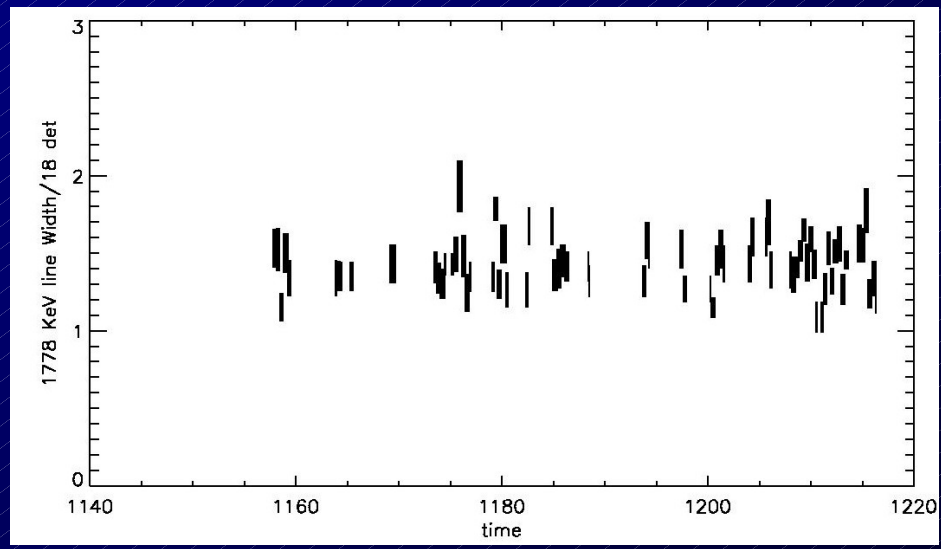

☆ Det 0

Det 18

Energy Resolution: Degradation

Trends: ~ 0.15 keV / 100 days @ 1 MeV

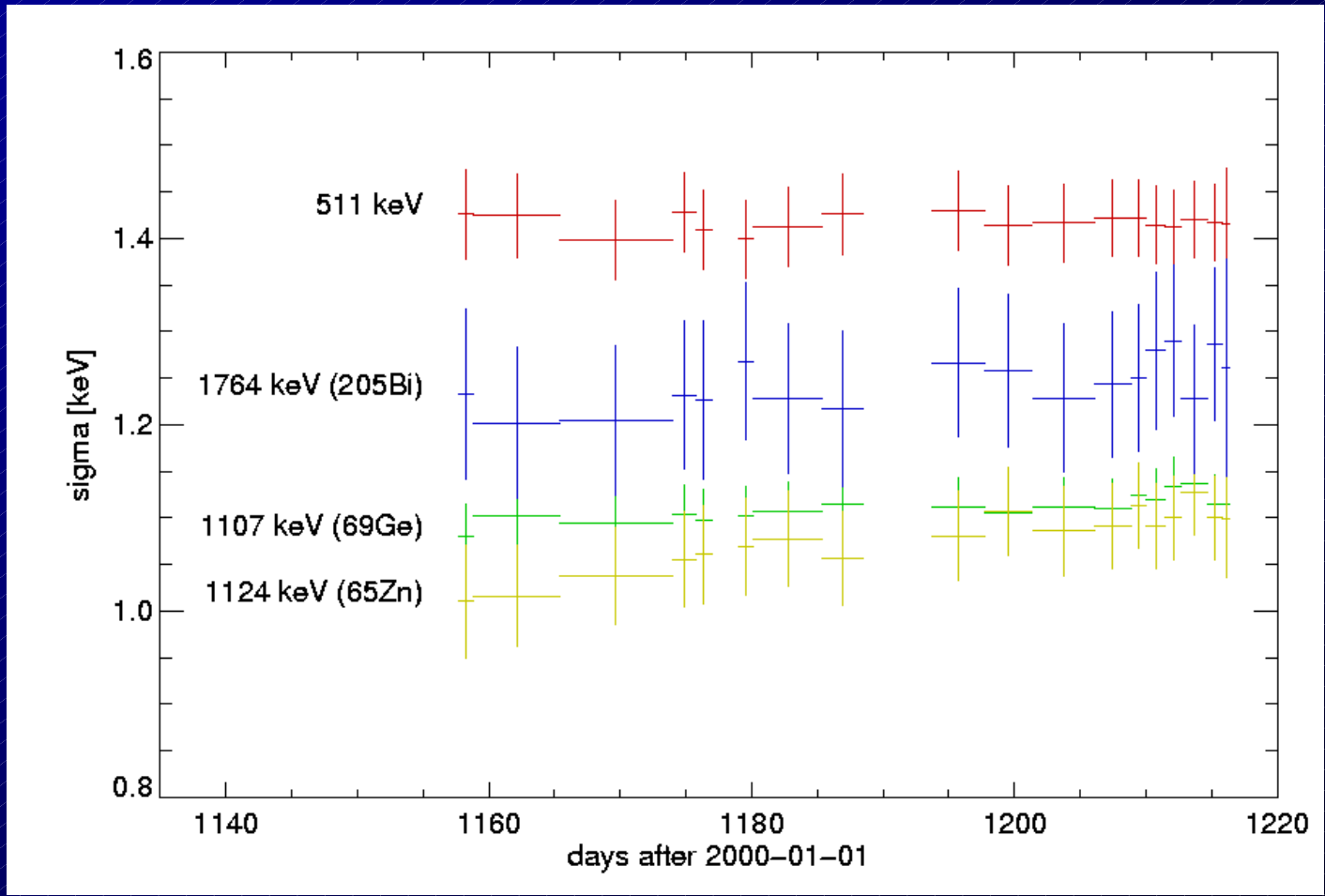

Detector Characteristics: Resolution

- GCDE Fitting of Many Bgd Lines

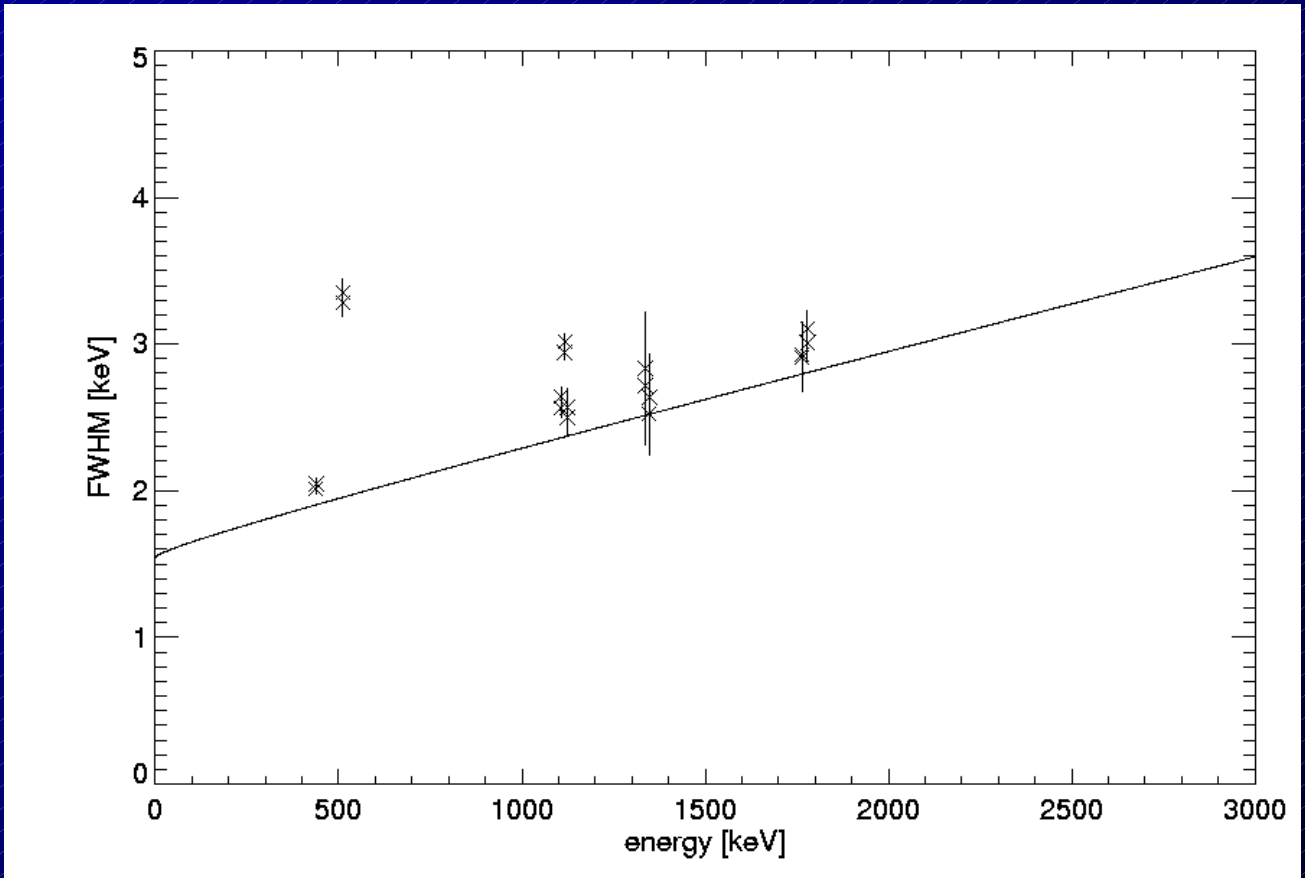

- "Intrinsic" Resolution = Lower Limit
  - Line Blends Tend to Deteriorate Line Widths

Bgd Line Study: more…

☞ See presentation by Karsten Kretschmer

SPI line background

Karsten Kretschmer, MPE Garching

Approach:

- take data from GCDE
- group it into intervals with 24hr exposure
- fit selected regions with 2nd order continuum + gaussian lines

Sample Spectrum and Fit

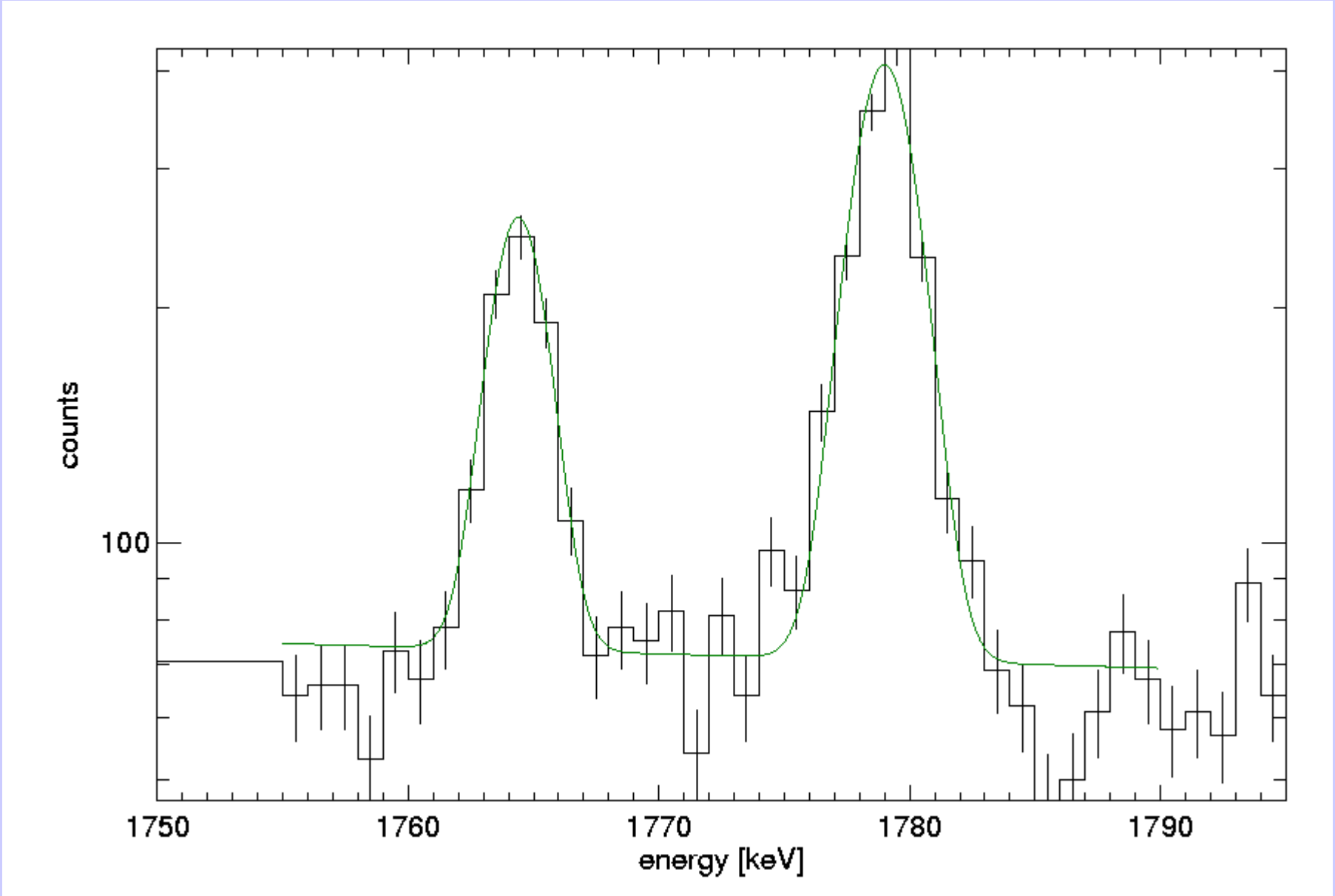

Line Width Evolution

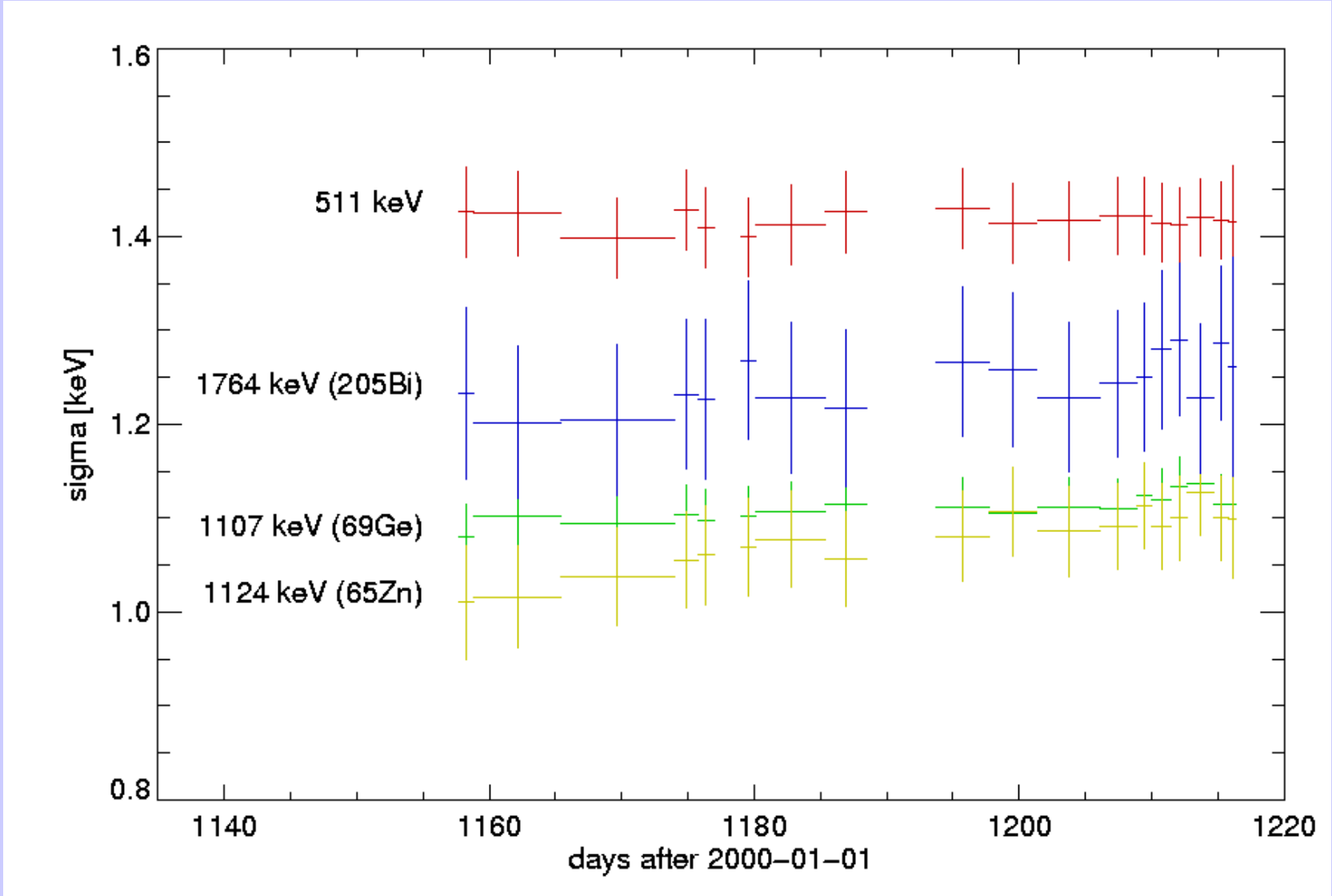

Trends: ~ 0.22 keV / 100 days @ 1 MeV

Line Intensity Correlations – Whole Set

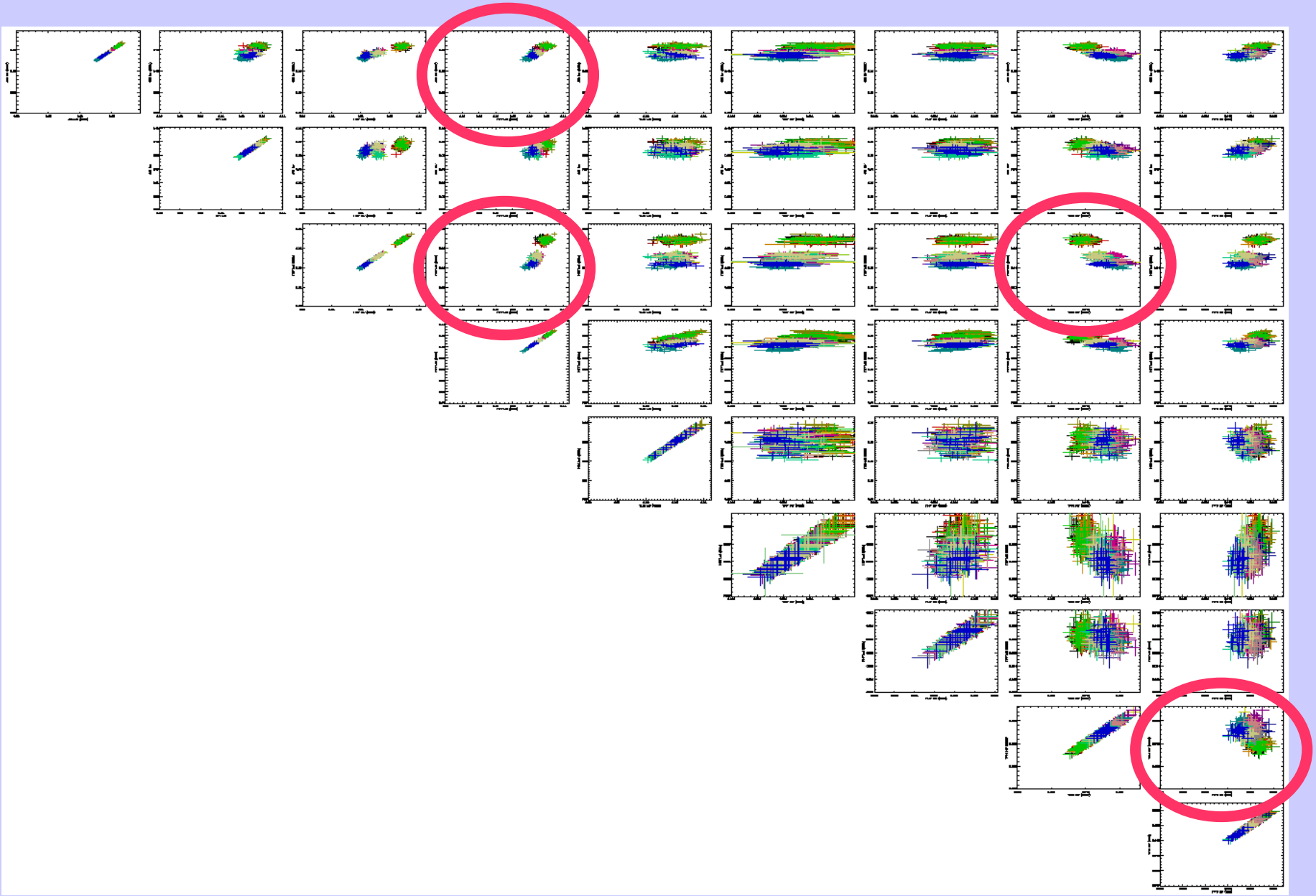

Line intensity correlations – overview

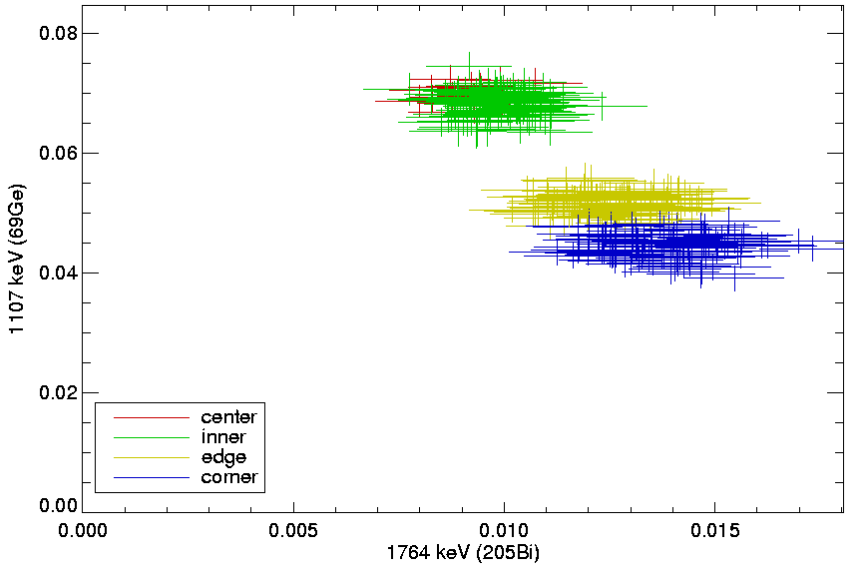

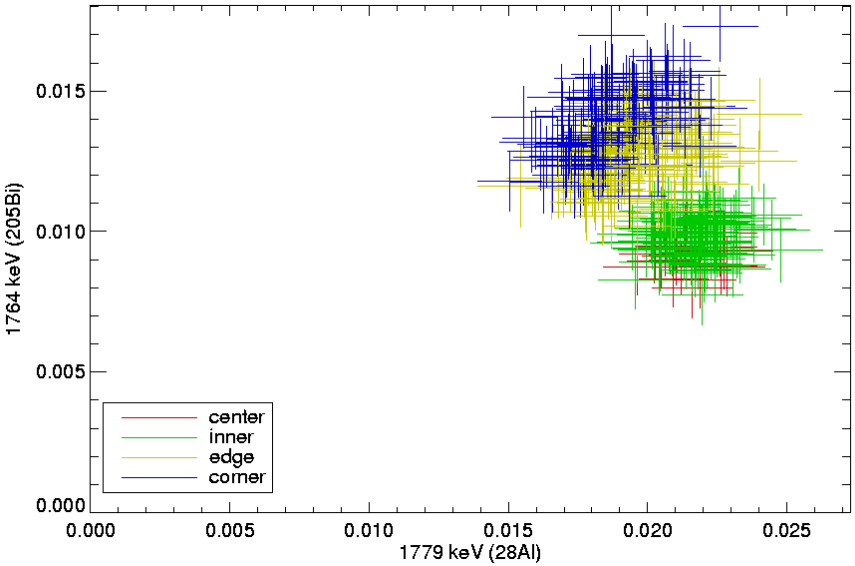

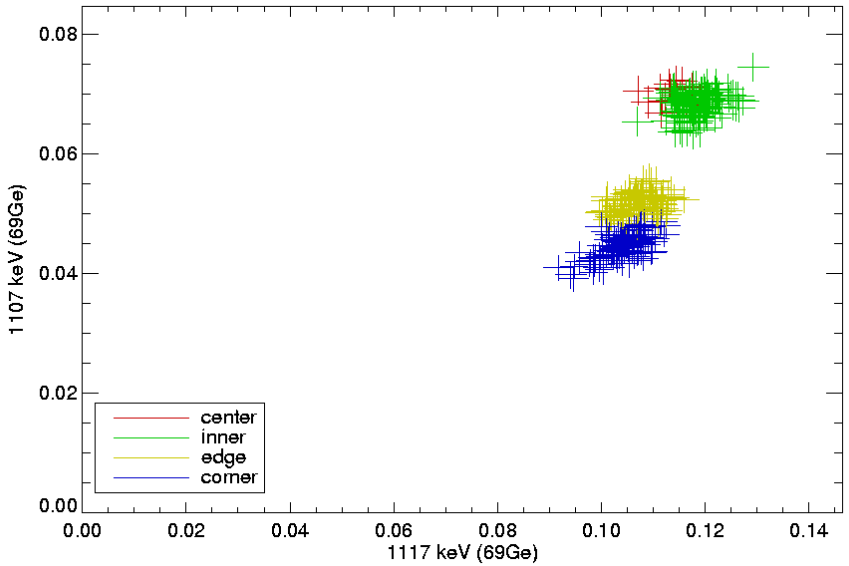

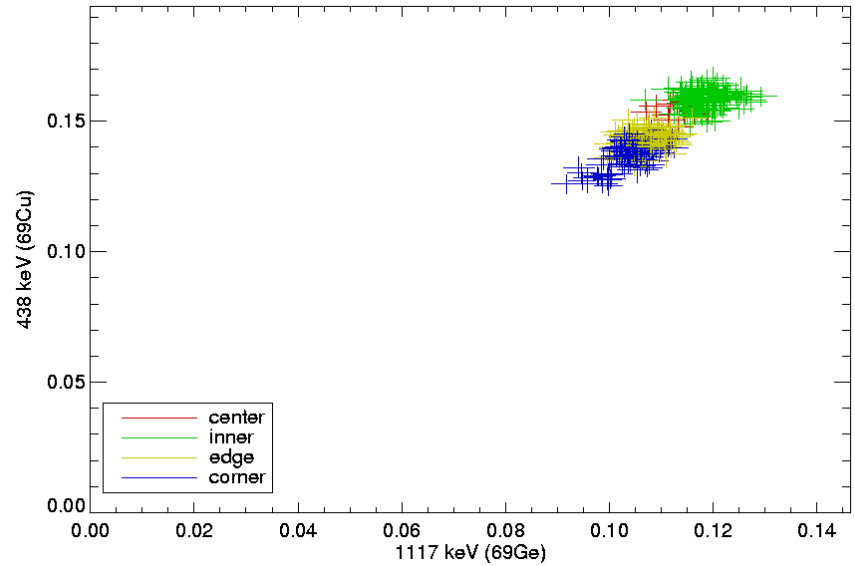

Line correlations 1

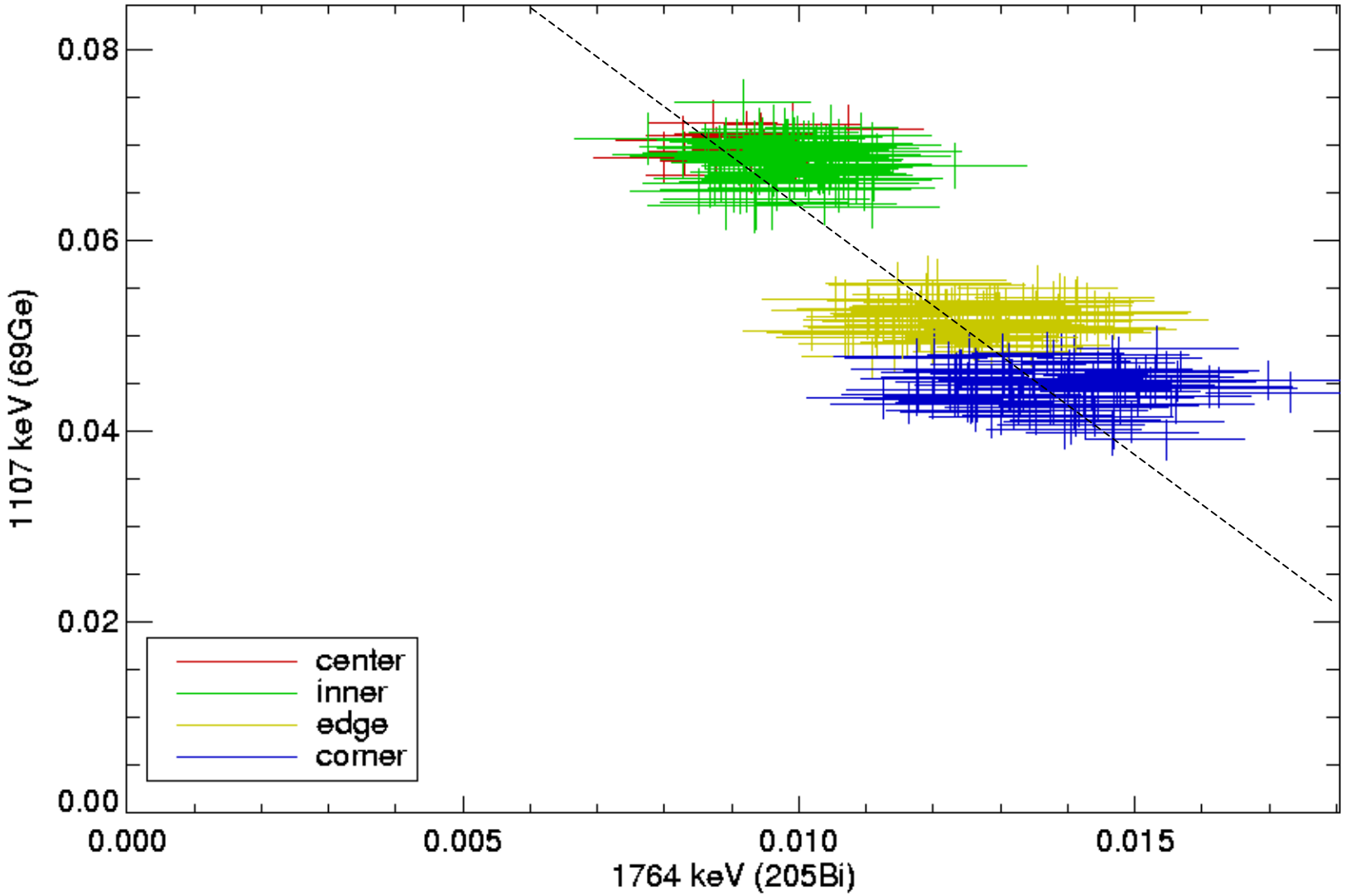

Outer detectors receive more Bi, less Ge Bgd

Line correlations 2

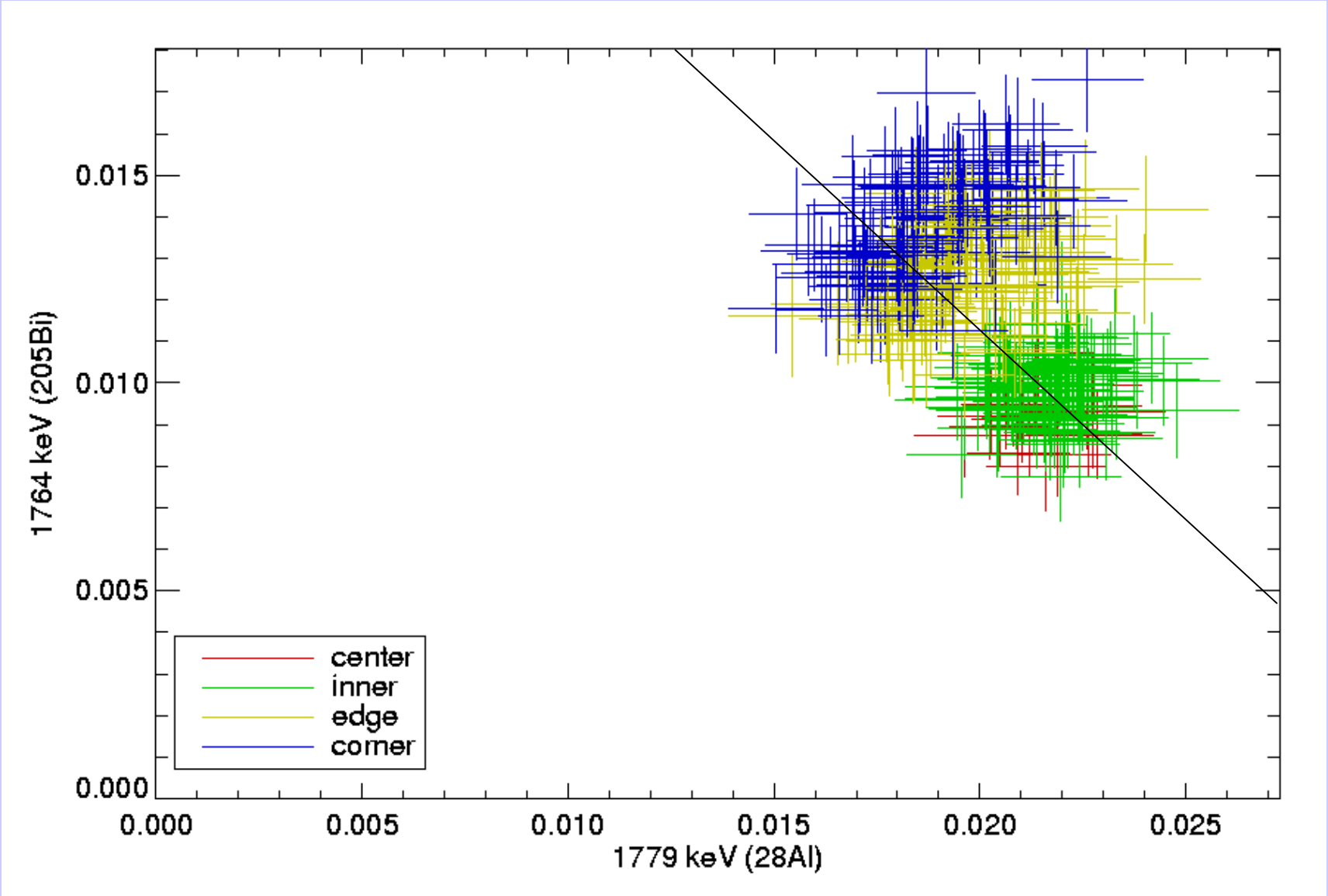

Outer detectors receive less Al, more Bi Bgd

Line correlations 3

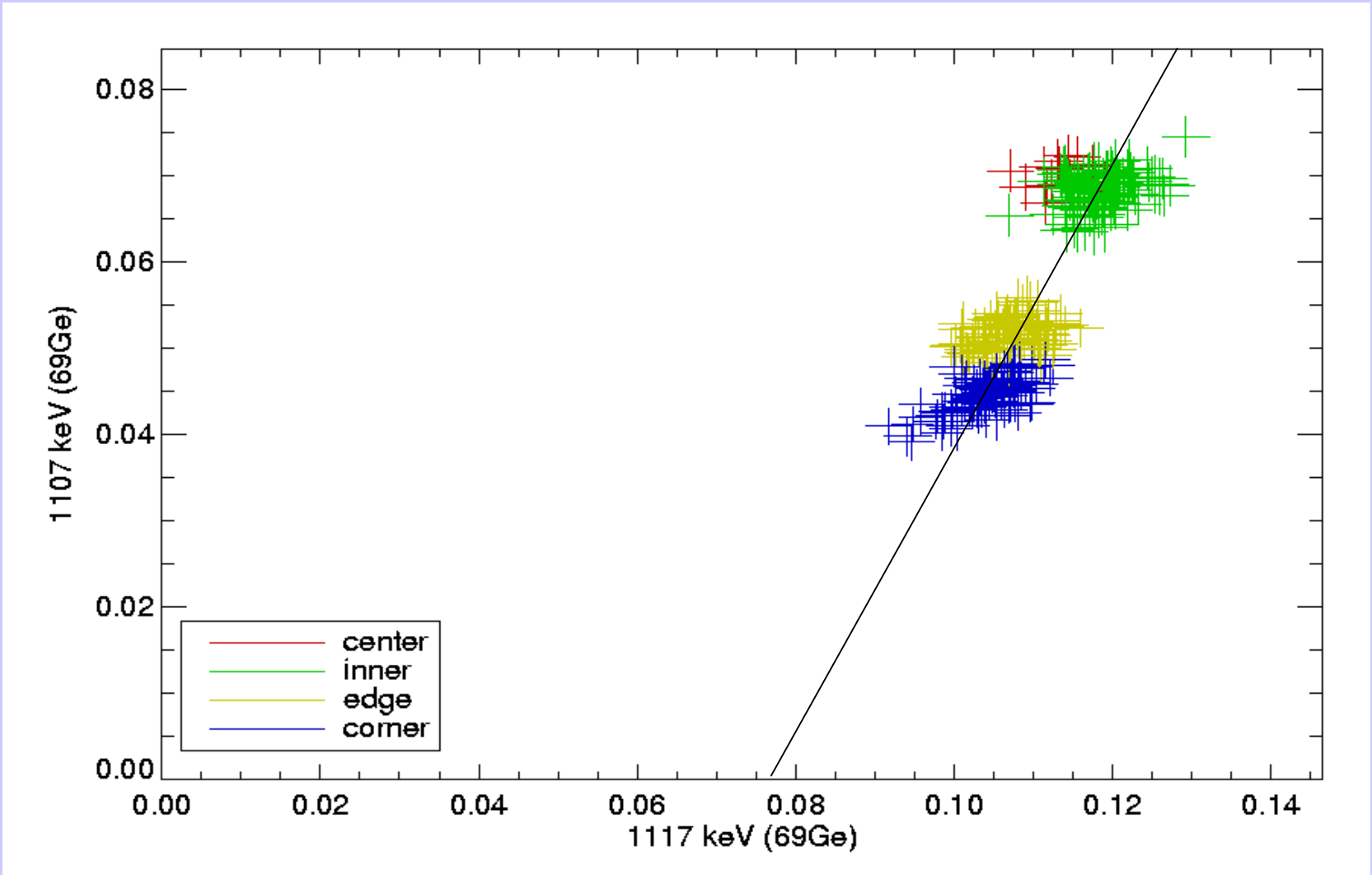

No Strict Proportionality for Ge Bgd

Line correlations 4

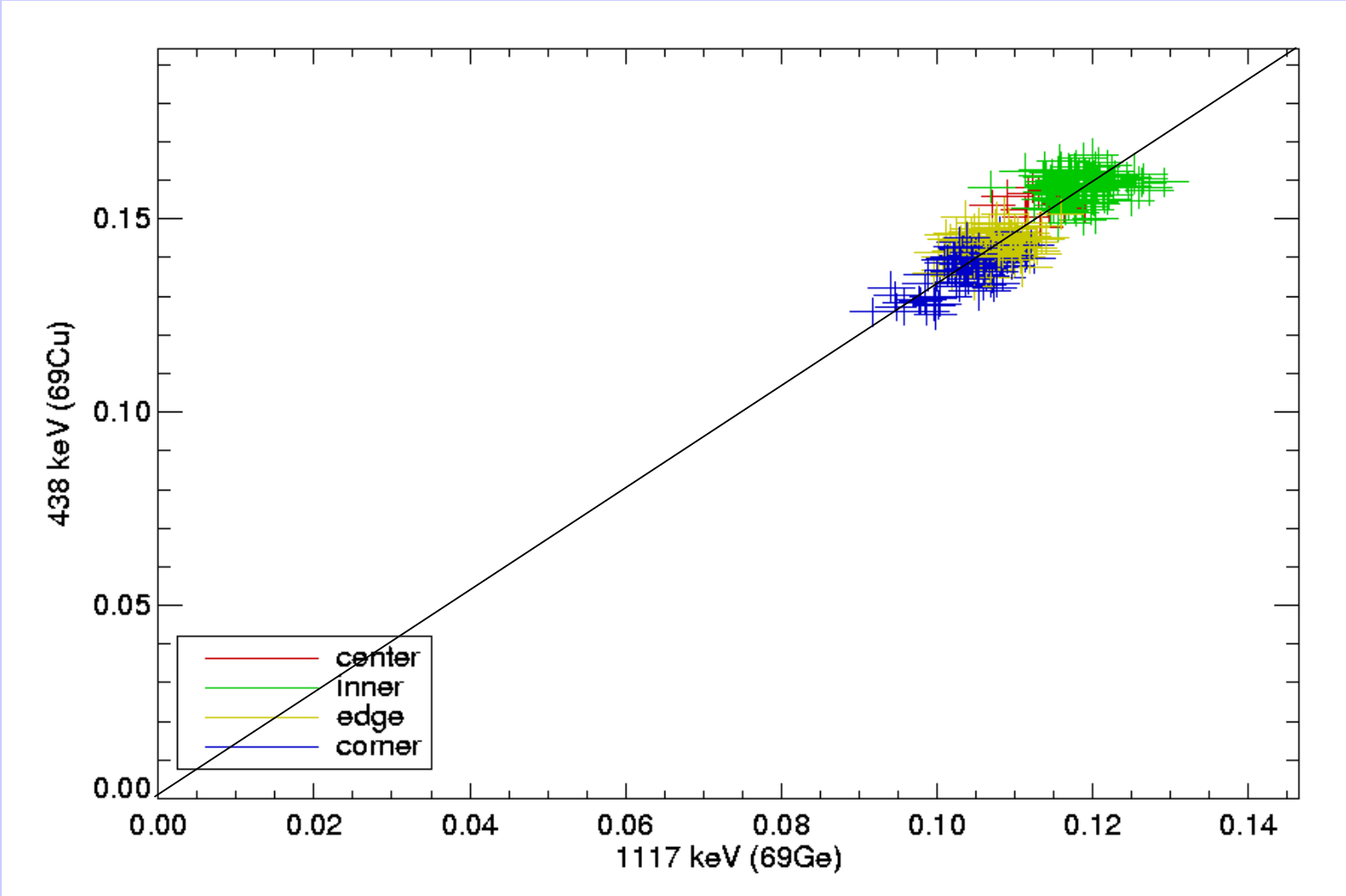

Good Proportionality for Ge and Cu Bgd

Detector position dependence

- Determine BG line count rates per detector
- Distinguish detector types:
  - central (0)
  - inner ring (1-6)
  - edges (7,9,11,13,15,17)
  - corners (8,10,12,14,16,18)
- Count rates depend on solid angle to (unknown) Bgd source

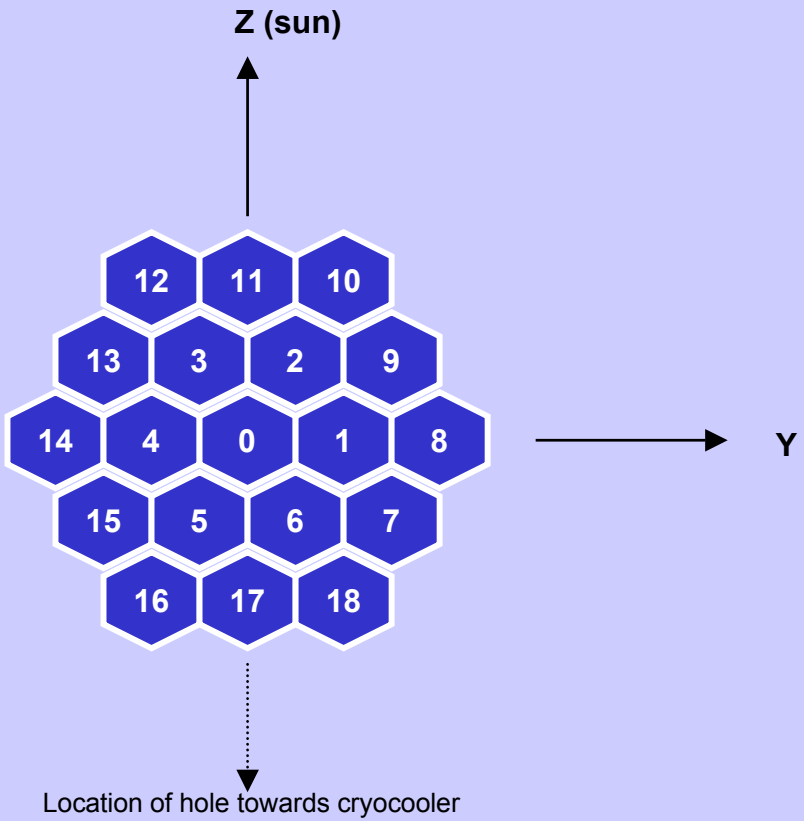

Count rates(line, detector)

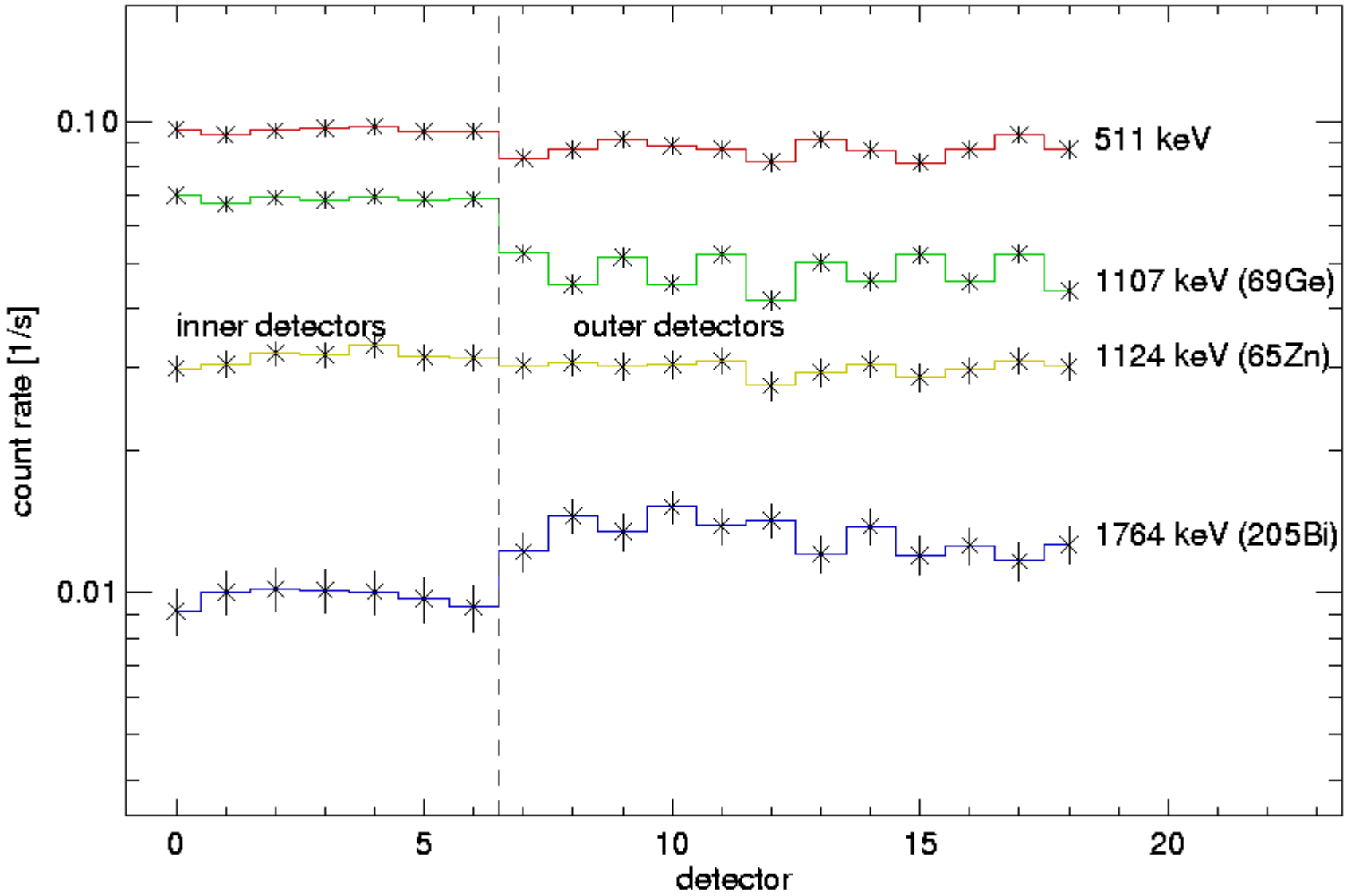

Inner/Outer Detectors Separate Camera/External Bgd Sources

Count rates(line, detector)

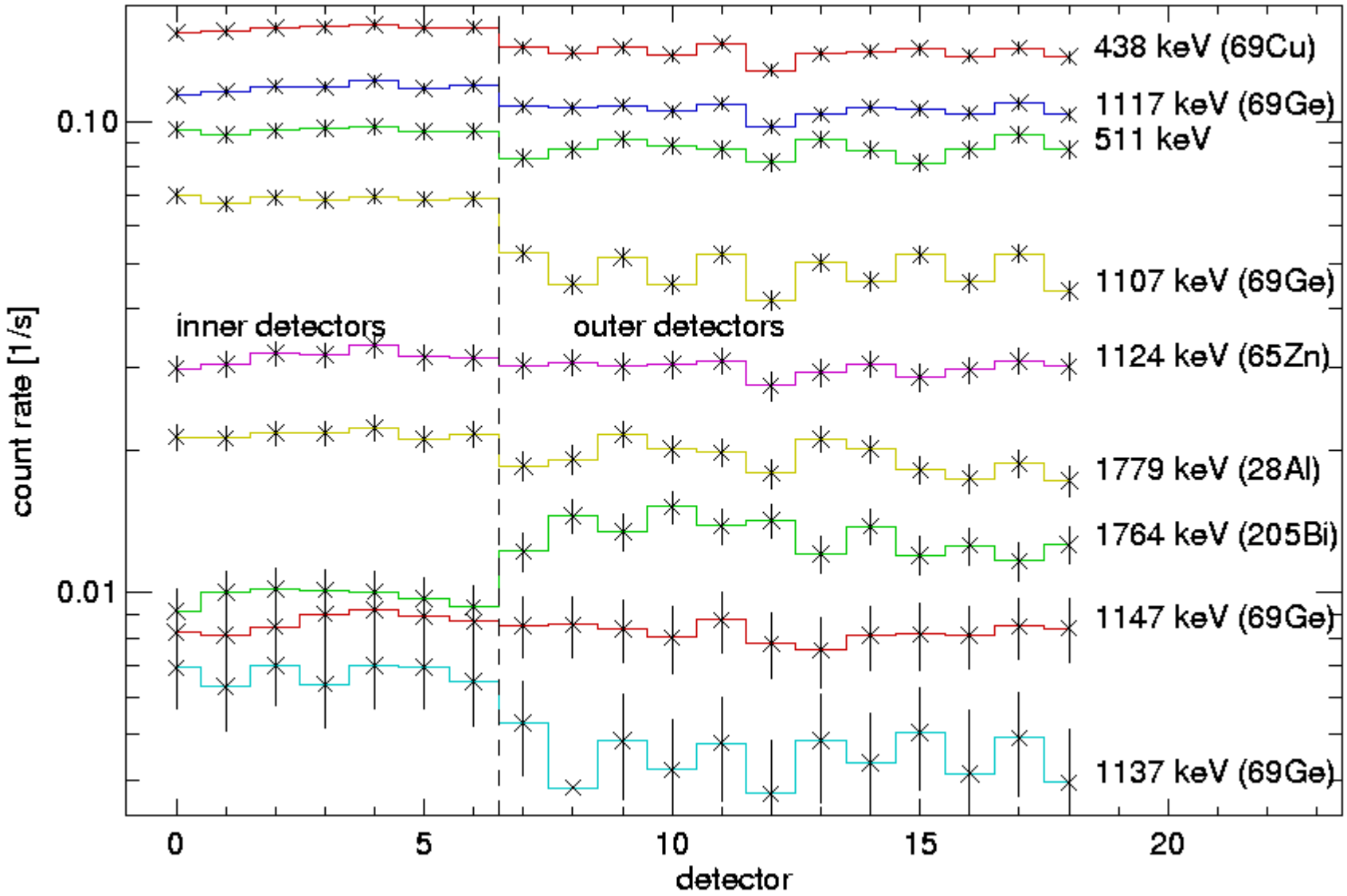

Inner/Outer Detectors Separate Camera/External Bgd Sources

The distribution of SPI background events in lines and continuum for the singles and the multiples

Emrah Kalemci
Steve Boggs
SSL/UCB

Cornelia Wunderer
MPE

Acknowledgment: Pierre J. for his comments and idea of color coding the detector count rates, Georg W. for the line identifications.

Objective

- Our aim is to understand the systematics of the distribution of the multiple events (ME) which is crucial for polarization studies.
- It is important to understand the distribution of single (SE+PE) events to be able to interpret the distribution of ME events.
- We realized that the lines and the continuum behave differently, therefore we characterized them in separate sections. This work may also have importance on understanding SPI background.

Analysis methods

- We analyzed the consolidated data of revolutions 24 and 25 staring observations.
- IDAS was used to obtain livetimes. The channel spectrum was obtained by an IDL program from the raw data. The total good time is ~183 ks.
- Pseudo detectors (PD) 0-18 and 19-60 (SE+PE, and ME) are used.
- For SE+PE, these lines are used: 139.6, 198.4, 309.9, 403.0, 438.6, 511., 584.6, 872.1, 882.5, 911.2, 1021, 1107.4, 1117.4, 1368.7, 1779.0 keV.
- For ME, 139.6, 198.4, 309.9 keV lines are excluded.
- The nuclear lines are fit with a Gaussian plus a line to fit the background.
- All the counts in between visible lines are considered as continuum.

Distribution of ME, lines+continuum

- PDs 51, 52, 53 and 56 have 4-8 % higher count rates than the remaining detectors. These PDs correspond to actual pairs of 8-9, 9-10, 10-11, 13-14.
- Is this excess caused by lines or the continuum?

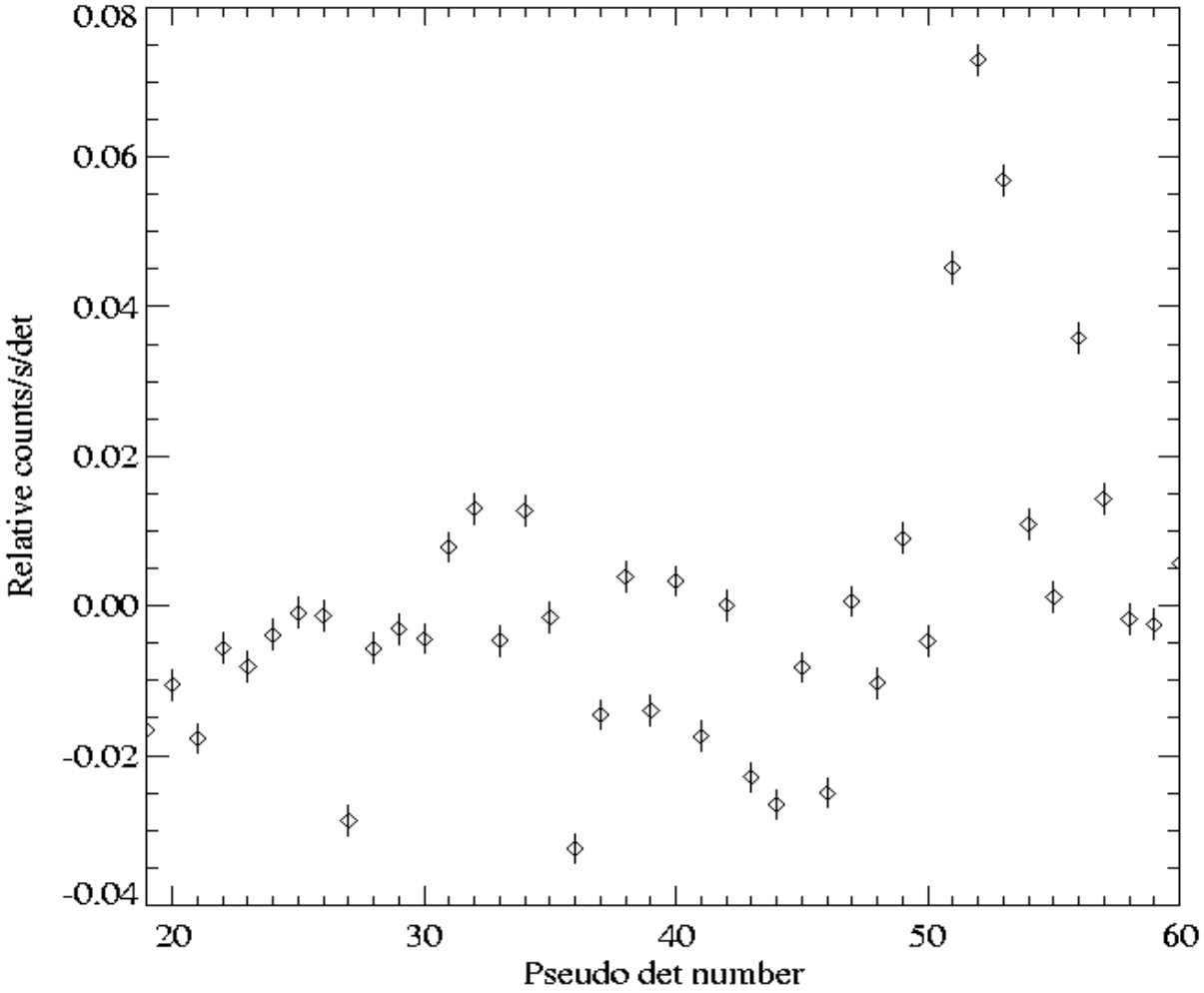

Lines in ME

- Some of the lines (139.6, 438.6, 872.1, 1107.4 keV) in ME have smaller count rates for PDs>49 which correspond outer detector pairs.
- 911.2 keV show an increase for PDs>49
- Remaining lines seem homogeneous.

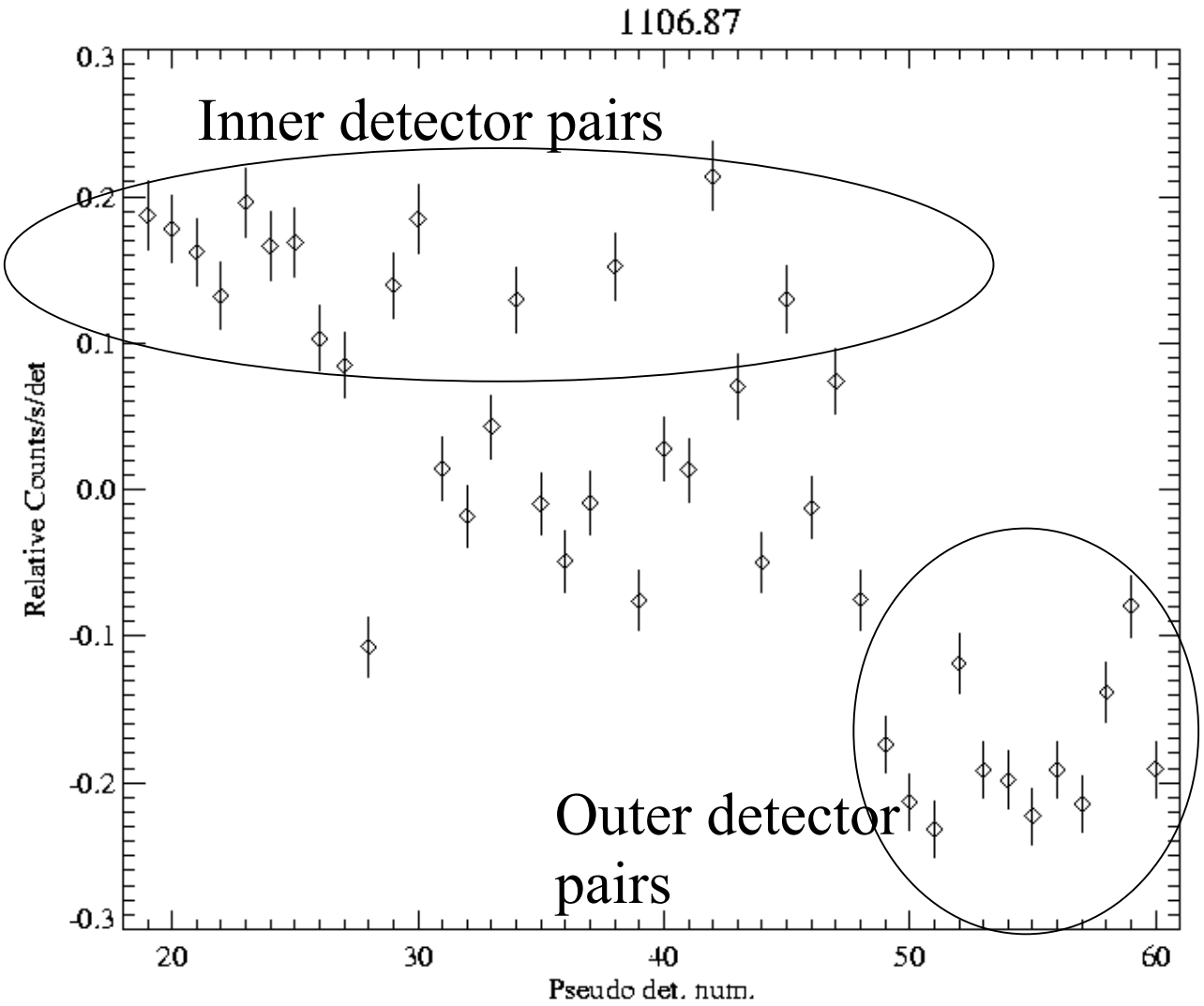

Lines in SE+PE

- Need to understand the distribution in SE+PE to interpret distribution in ME
- For 438.6, 584.6, 872.1, 882,1, 1107.4, 1117.4, and 1779 keV the inner detectors have higher count rates. Among those, for 438.6, 872.1 and 1107.4 keV, not only the difference between inner and outer detectors are substantially high, the outer detector count rates show an alternating behaviour as shown here.
- These lines are originated in the detectors. The photons from these lines have a fair chance of leaving the detector of origin and being captured by a neighbour detector. Therefore the number of counts will increase with increasing number of neighbours.

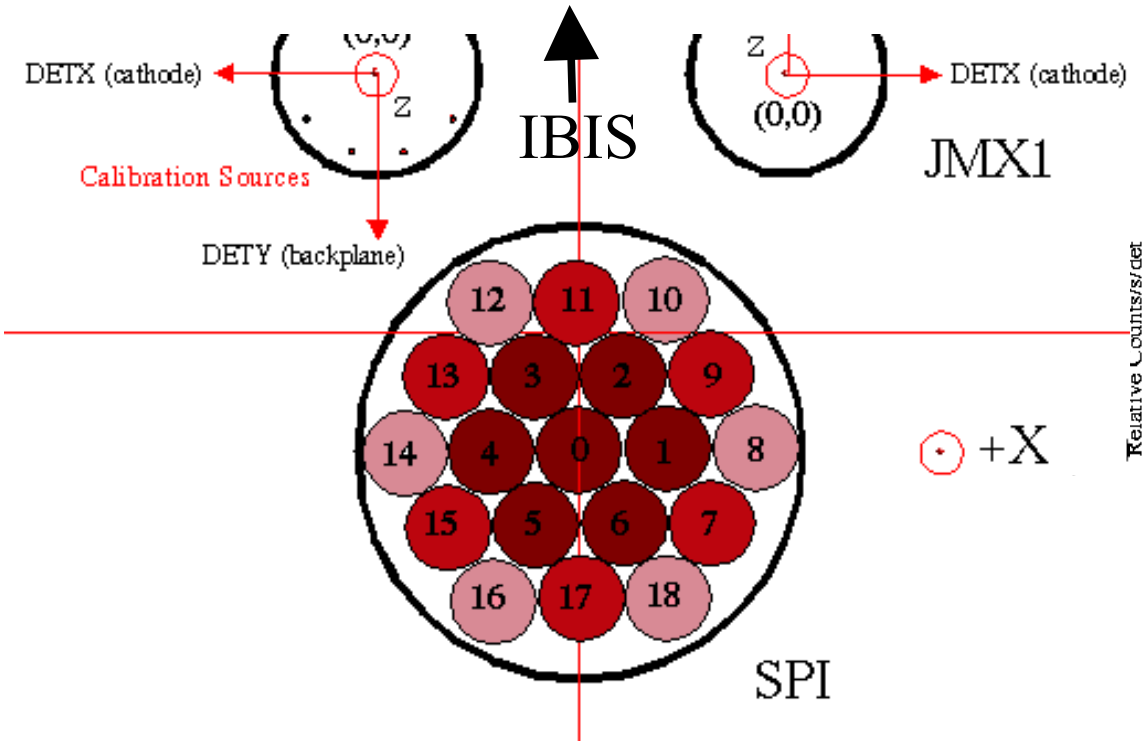

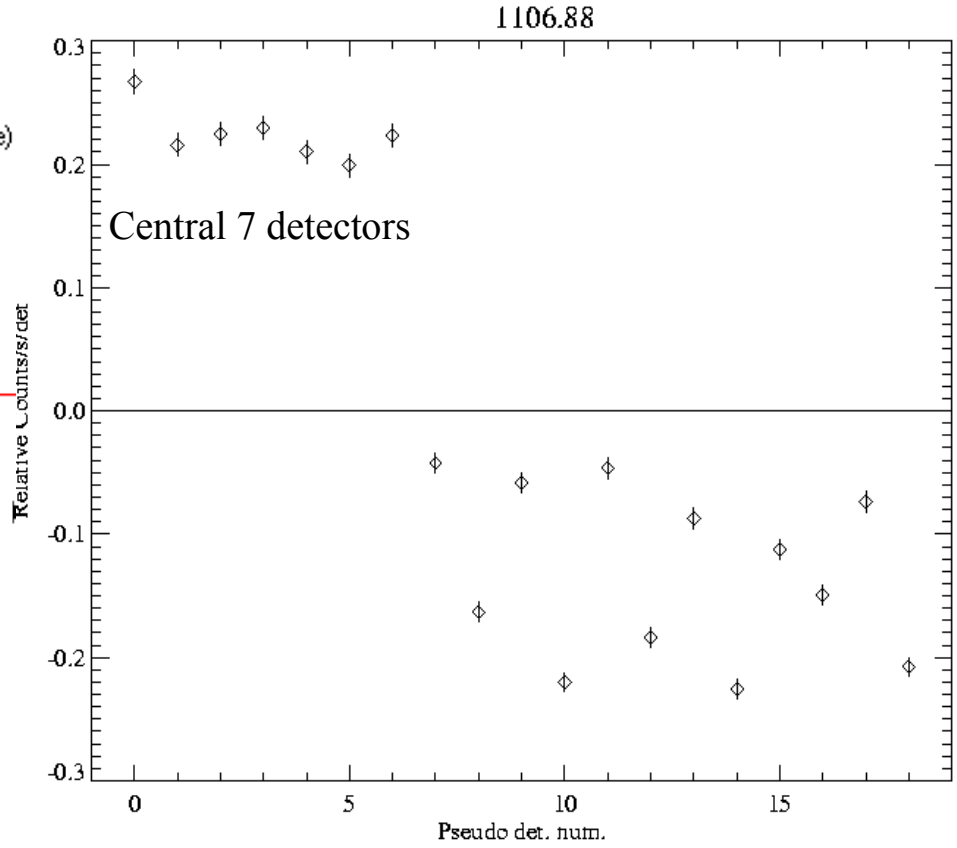

The K photon

- Although for 882.1 keV and 1117.4 keV, the inner detectors have more counts than the outer detectors, the difference is not prominent, and the alternating behaviour at the outer detectors is gone. Yet, the only difference between these lines are the ~10 keV K photon.

1107.4 keV: ^{69}Ge(EC)^{69}Ga

1117.4 keV: ^{69}Ge(EC)^{69}Ga+K

K photon unlikely escapes, so most of the photons from this reaction is captured in the same detector that it originated!

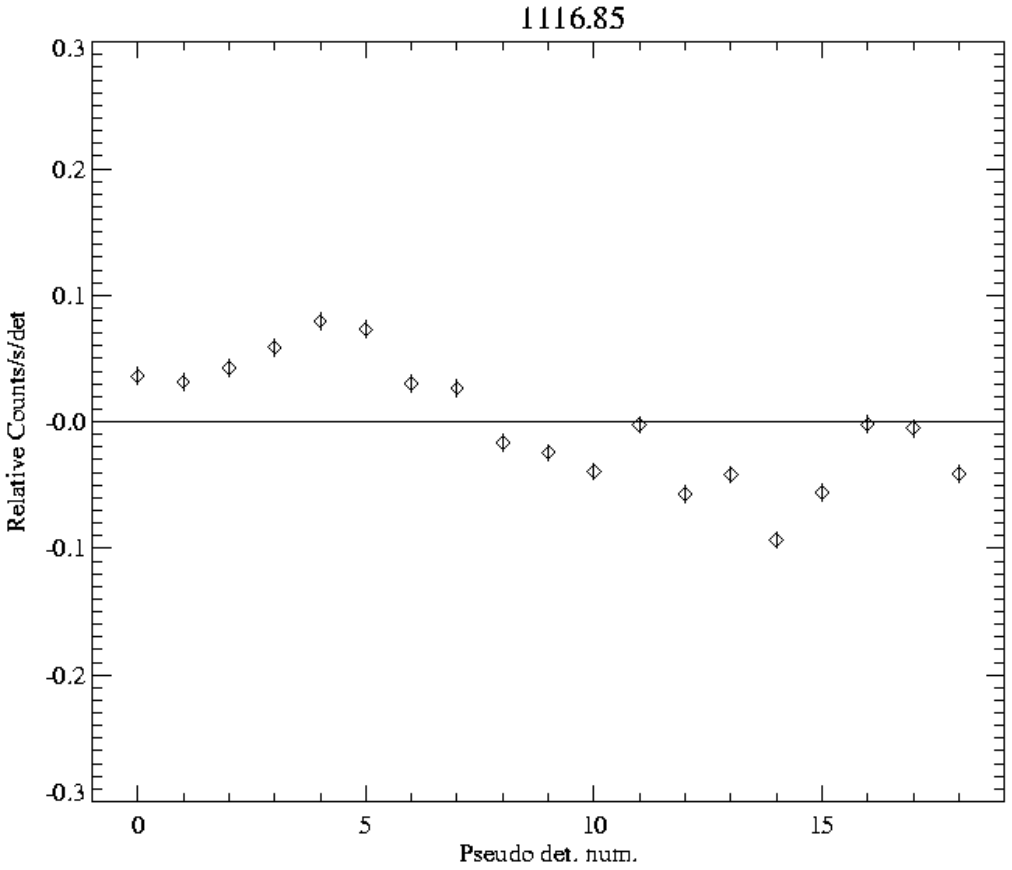

The 911.2 keV line, an outsider?

911.2 keV : ^{228}Ac (β-) ^{228}Th

- Shows opposite behaviour of the previous case, outer detectors have higher count rates, and generally detectors having larger solid angles to the shield have higher count rates: possible origin in the shield or the cryostat?

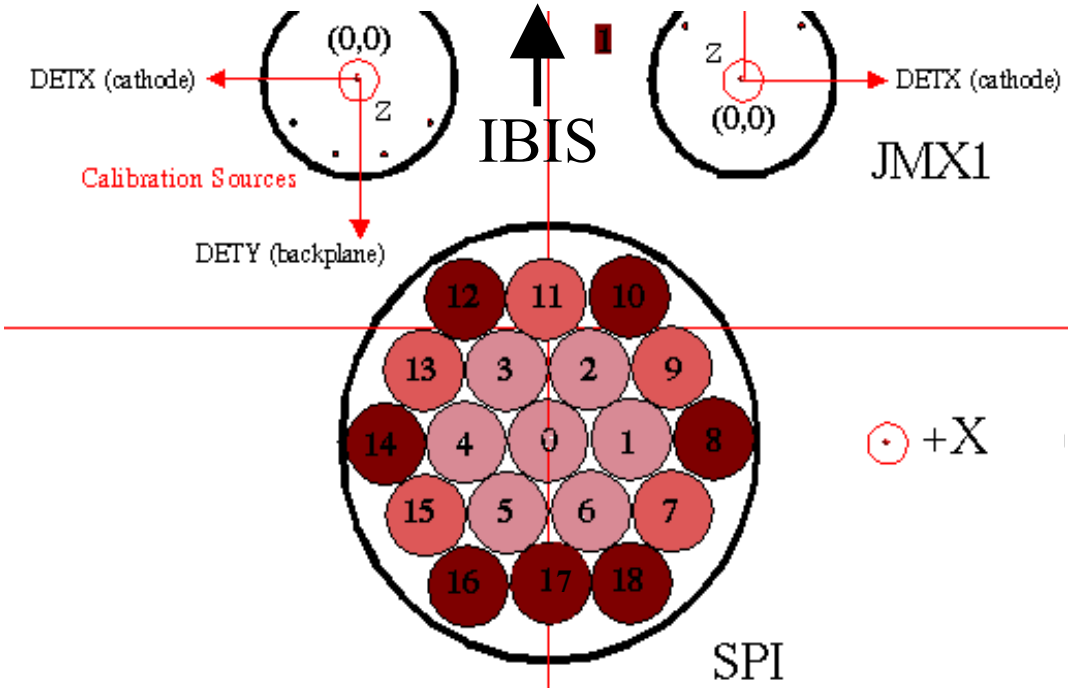

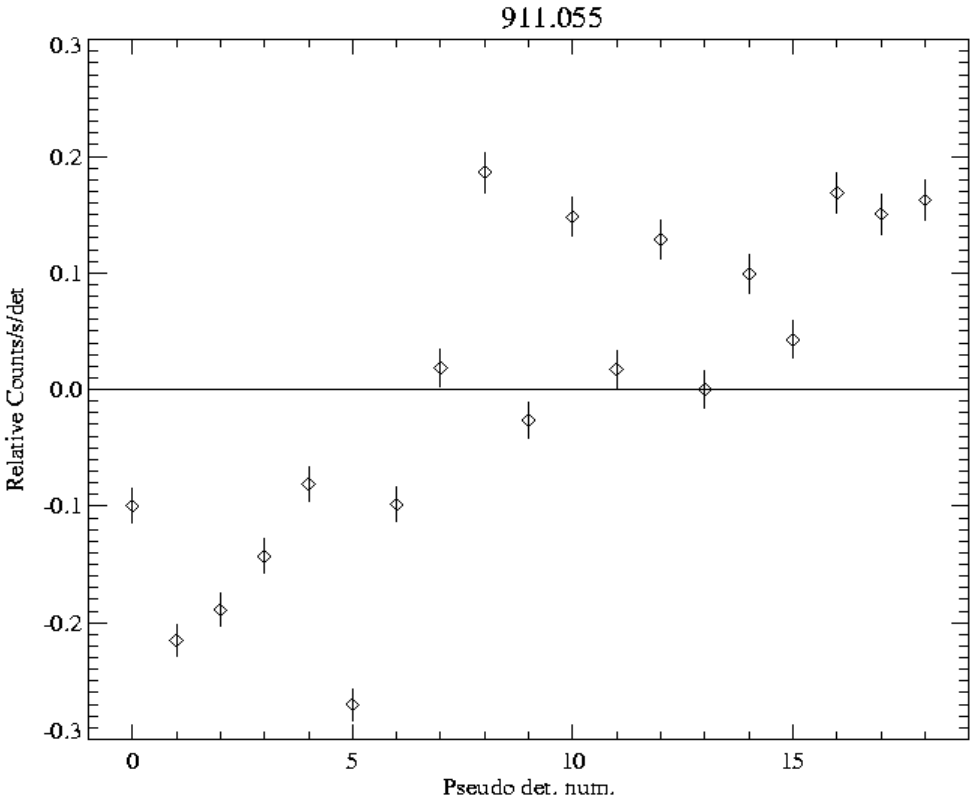

Continuum of SE+PE

- The continuum in SE+PE is energy dependent.
- For the lower energies, it is pretty homogeneous (within 2% except somewhat larger deviations in detectors 14 and 15.)
- For higher energies, there is clear deviation between the inner detectors and outer detectors such that the outer detectors have higher count rates. Det. 14 again seems low. There is also some excess towards IBIS (dets. 8, 9, 10, 11, 12)

Continuum in 20 - 800 keV band

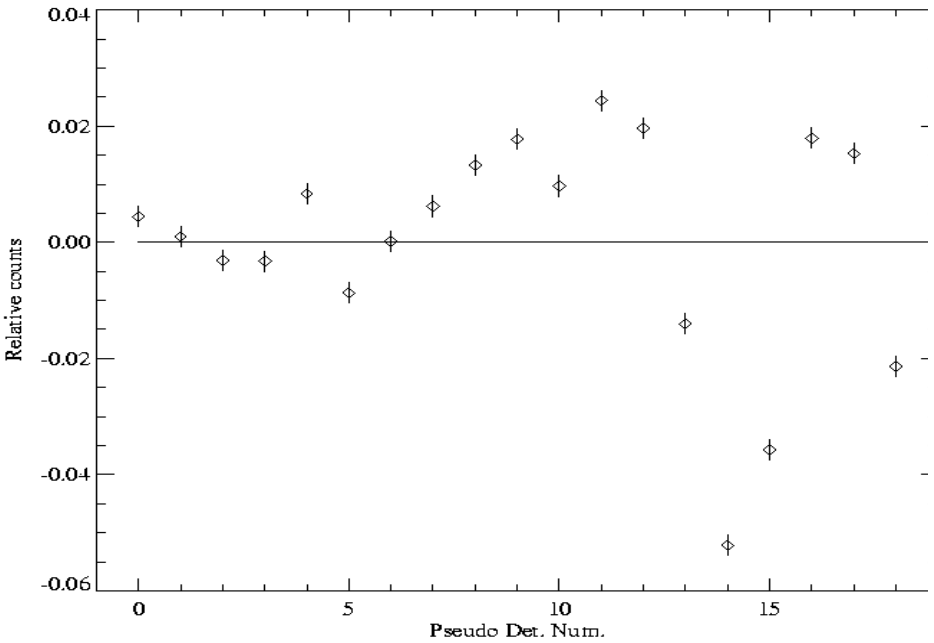

Continuum in 800 keV - 2 MeV

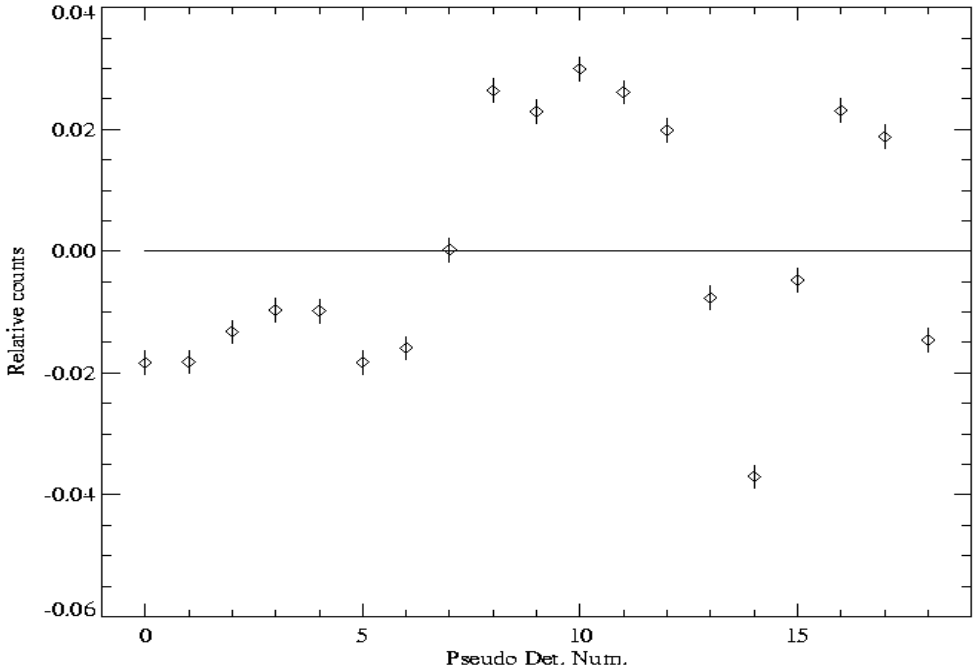

Back to ME continuum

- The distribution of counts in ME lines can be understood by the distribution of counts in SE+PE lines. What about the continuum?
- As in SE+PE continuum, ME continuum is extremely energy dependent. In 20-160 keV, pairs facing IBIS and JEM X has 25%! more counts than the inner pairs. In general, outer pairs have higher counts

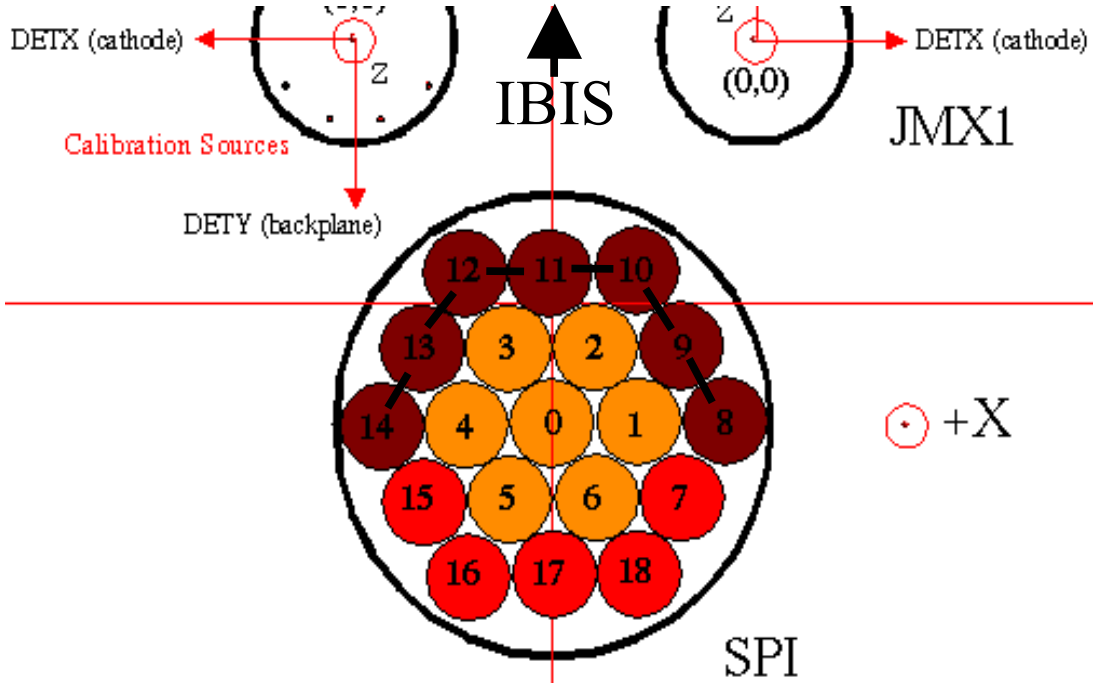

Continuum in ME in 20-160 keV.

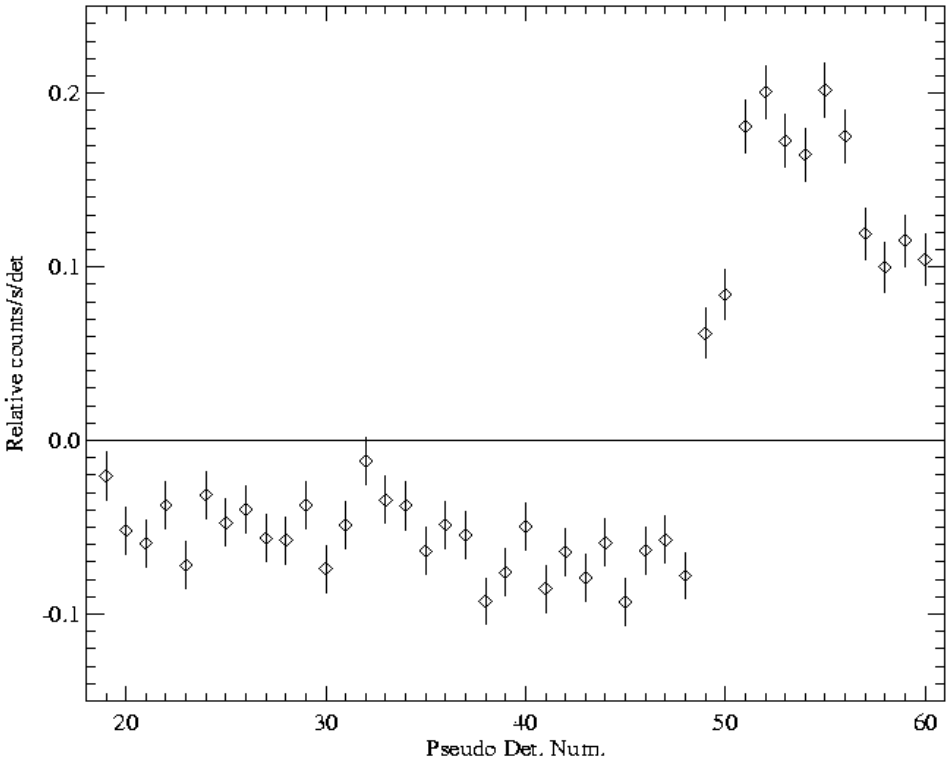

ME Continuum 2

- As energy increases, the difference between inner detector pairs and detectors facing IBIS decreases. For a higher band, the distribution takes the form in the figures below. This distribution is similar to the overall distribution in ME.

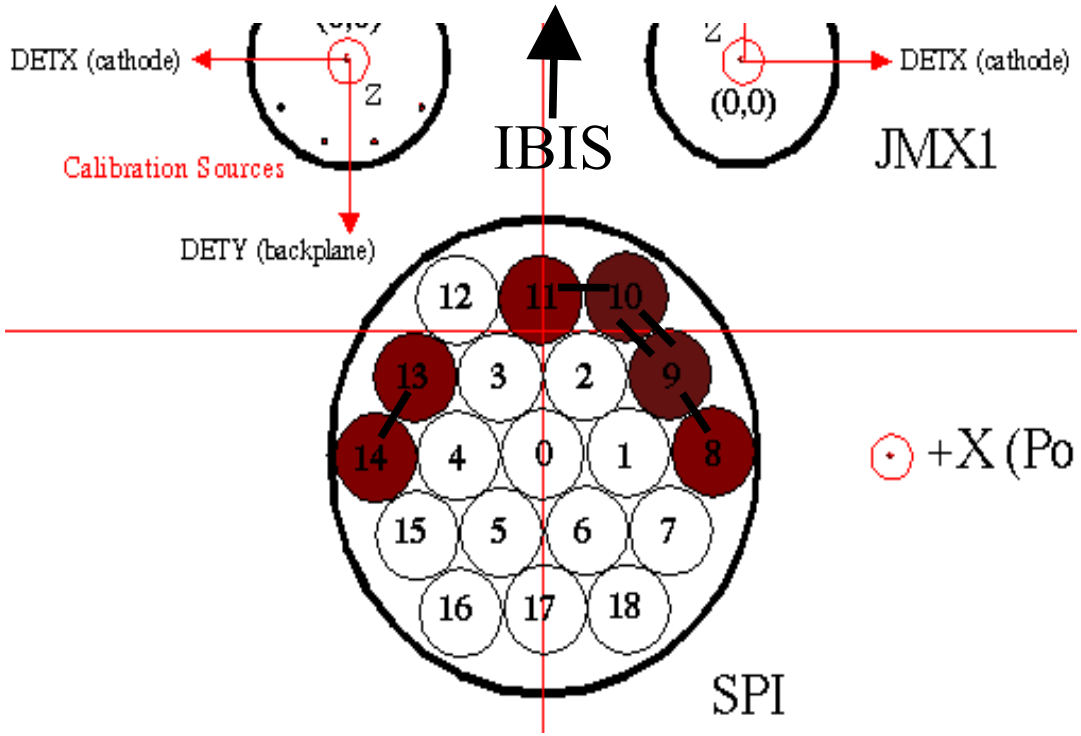

Distribution of ME continuum in 1.4 – 2 MeV

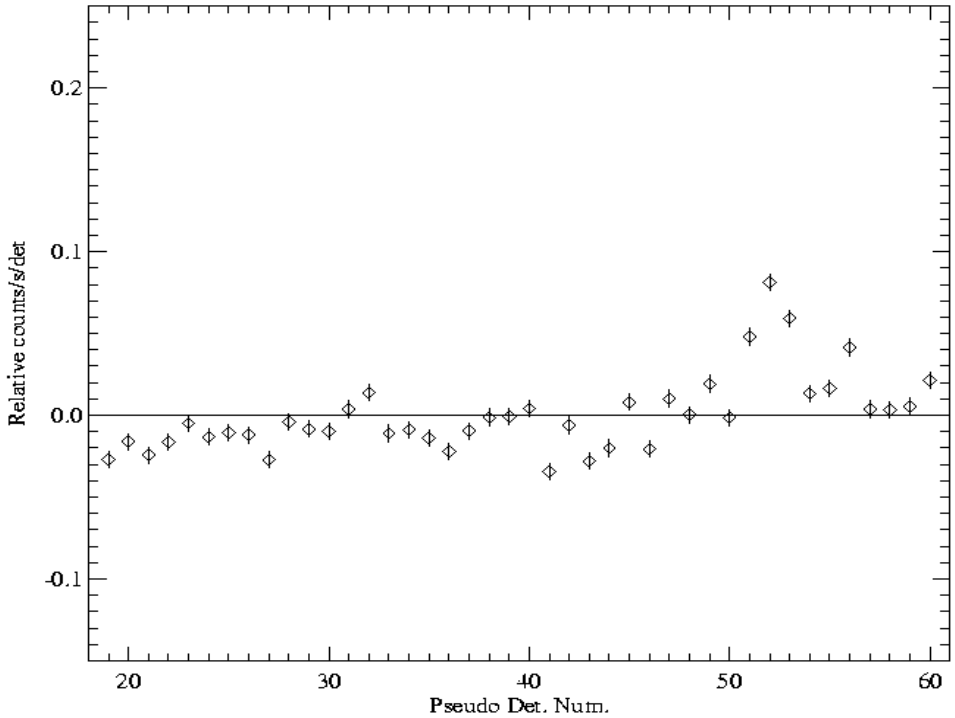

Conclusions, lines

- The distribution of background events in ME has different characteristics for the continuum and the lines, and overall, dominated by the continuum.
- For the distribution of background events in the lines in SE+PE:
  - If the origin is the detectors, and there is fair probability that the photon escaped the detector of origin, than the the number of counts in a detector increases with the number of neighbours (872.1 keV, 1107.4 keV).
  - If there is good probability that the line is captured in the same detector that it originated, then the inner detectors have slightly higher count rates than the outer detectors, and the behaviour of alternating count rates for the outer detectors disappears (882.1 kev, 1117.4 keV).
  - If the origin is outside, the opposite is observed (like 911.2 keV line)
- In general, the distribution of the background counts in the ME lines reflects the distribution in SE+PE lines.

Conclusions, continuum

- The distribution of the continuum events are energy dependent both in SE+PE and ME.
- For SE+PE, the distribution is more homogeneous in the lower energies than that of the higher energies. At higher energies, the inner detectors have lower count rates, and the count rate is slightly higher for detectors 8, 9, 10, 11, 12 facing IBIS and JEM-X detectors. Possible reasons:
  - Increasing contribution of the shield leak photons to the overall background at energies higher than 1 MeV?
- For ME, between 20-160 keV, the count rate is 25% higher for pairs facing the IBIS than the inner pairs! In general outer pairs have higher count rates than the inner pairs. For the 1.4 MeV – 2 MeV band, the distribution becomes homogeneous except PDs 51, 52, 53, 56. Possible reasons:
  - Increased background due to higher number of secondaries coming from the IBIS and JEM X?
  - Weaker shielding facing IBIS? Those two can also explain the distribution of SE+PE continuum.

Distribution of events in several lines I

403.0 keV: 67Ga(EC)67Zn+K

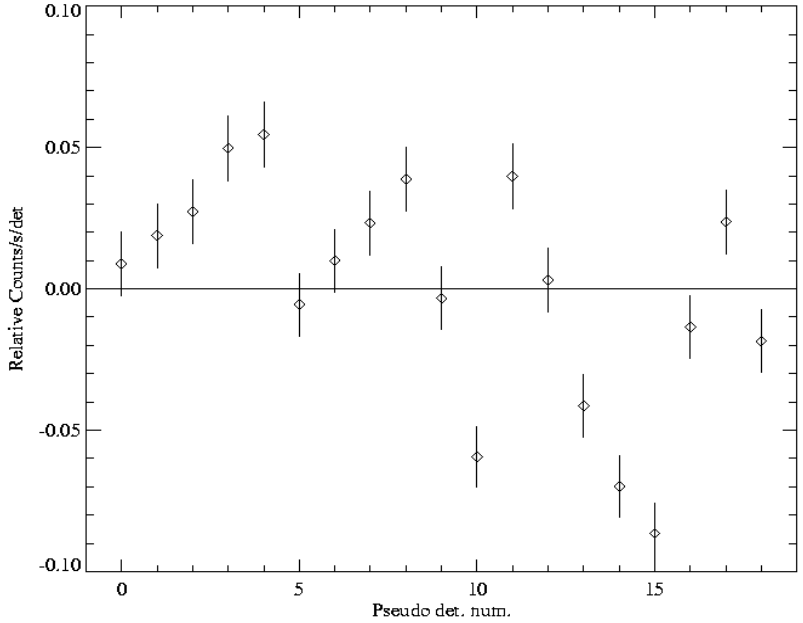

438.6 keV: 67Zn(IT)67Zn

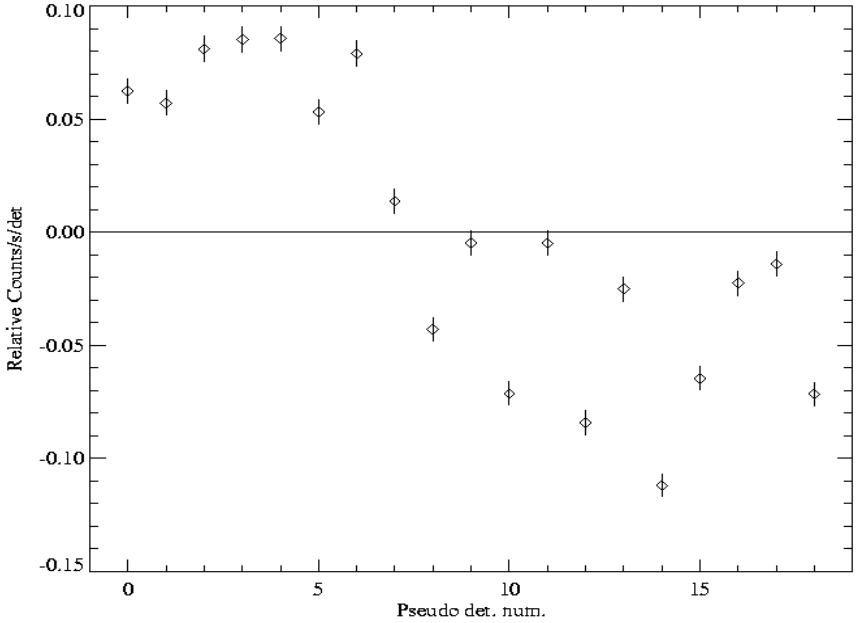

511 keV

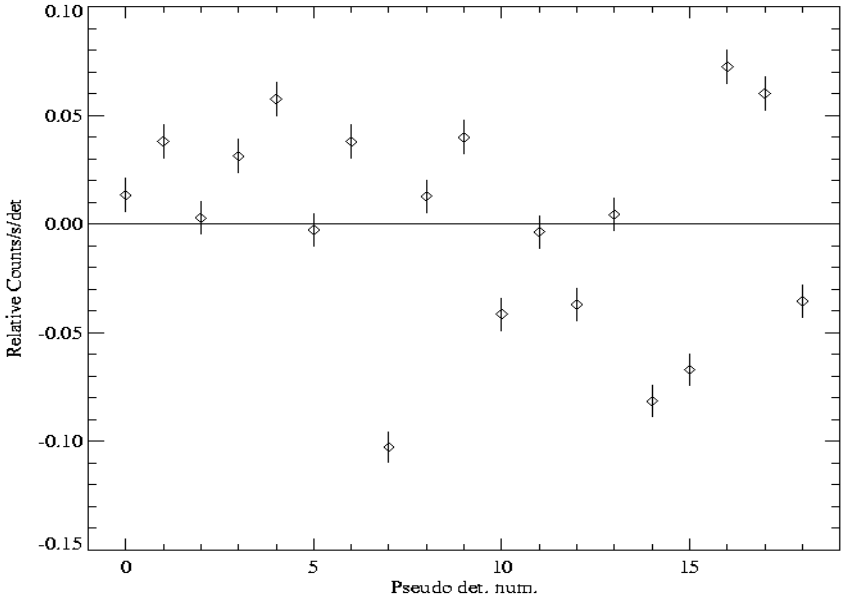

584.6 keV: 69Ge(EC)69Ga+K

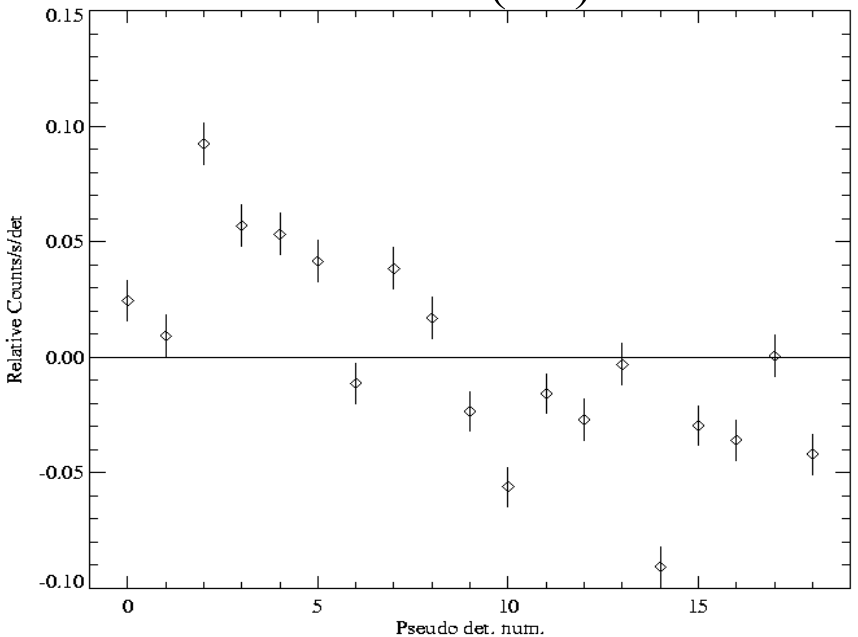

Distribution of events in several lines II

872.1 keV: 69Ge(EC)69Ga

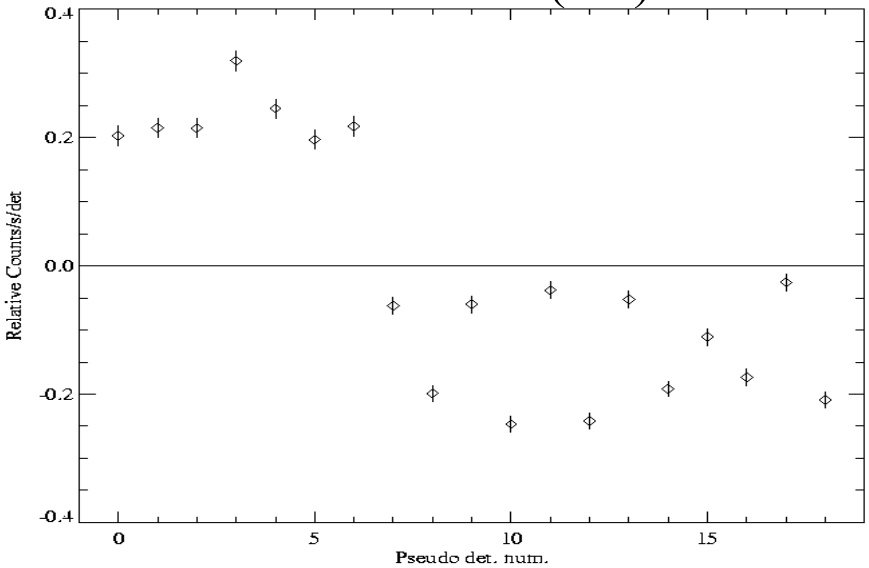

882.5 keV: 69Ge(EC)69Ga+K

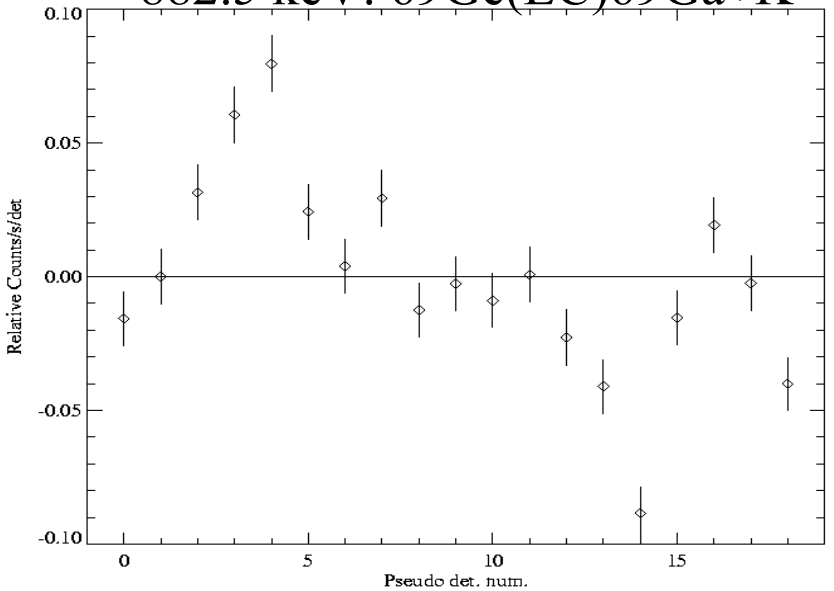

1368.7 keV: 24Na(β-)24Mg

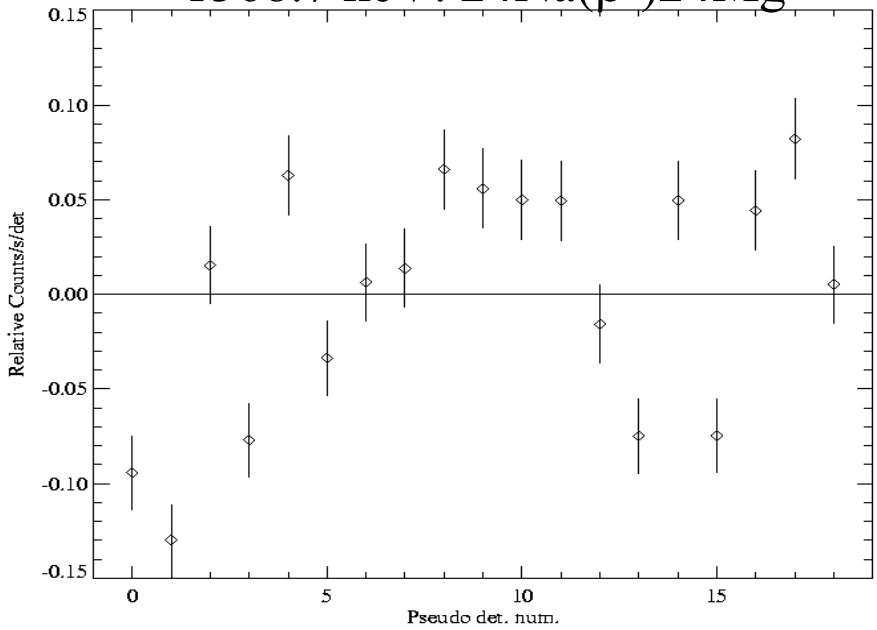

1779.0 keV: 28Al(β-)28Si

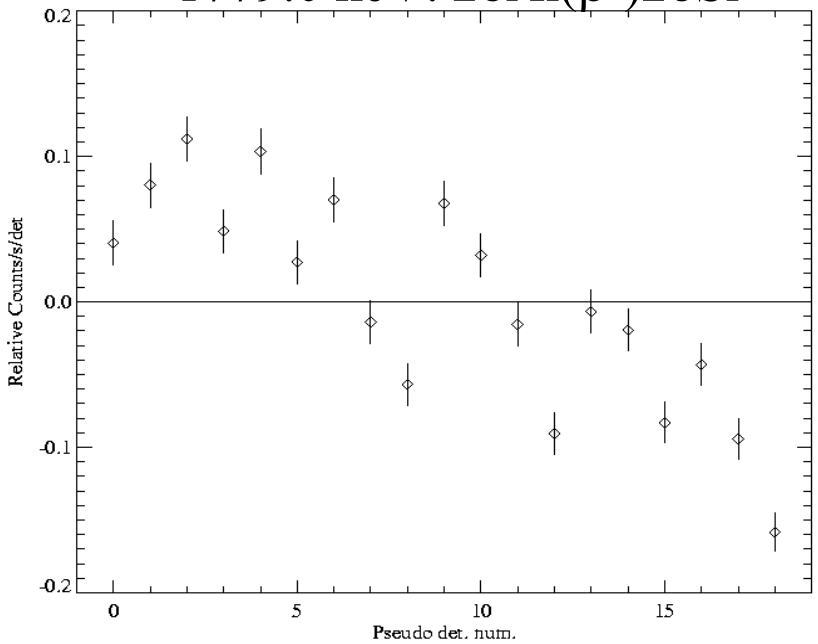

SPI Team Meeting June 2003 at CESR

Roland Diehl

Imaging Spectroscopy Analysis and Checks

GCDE ^{26}Al: ON/OFF Spectral Analysis

Summary:

- ☆ Use Crab Obs as OFF
- ☆ Adjust Resolution Difference

- ☆ Residual Gain Variations, but Small Compared to Cygnus/PV
- ☆ Clear Residual ^{26}Al Line, at ~1809.5 keV, predominantly from 4th Quadrant Data
- ☆ Width ~ Instrumental, < GRIS' Value
- ☆ Multiple-Event Results Unclear

Crab (GCDE) Data Time Dependencies

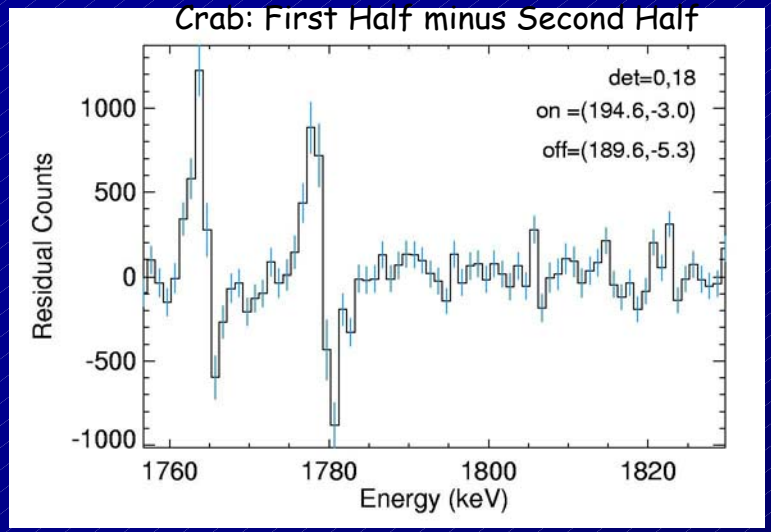

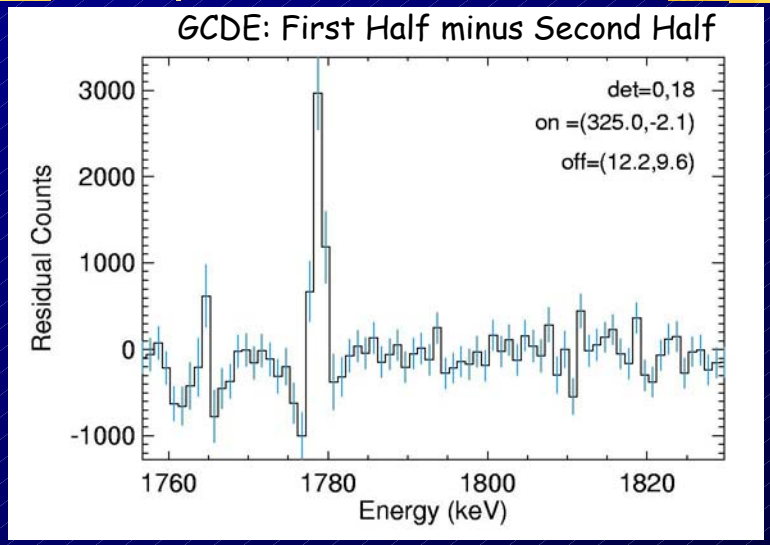

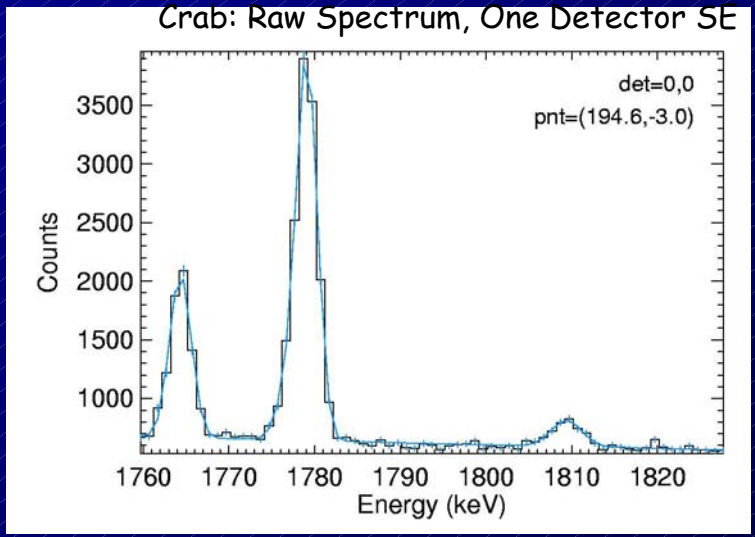

☞"Some" Evolution of Gains and / or Resolutions

- Crab Data: Residuals Very Asymmetric (line shifts)
- GCDE Data: Residuals More Symmetric, but Clear Resolution Degradation (long time interval)

Fitting Crab and GCDE Spectra

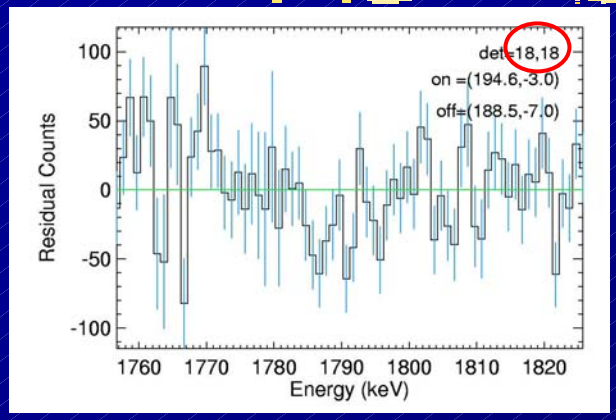

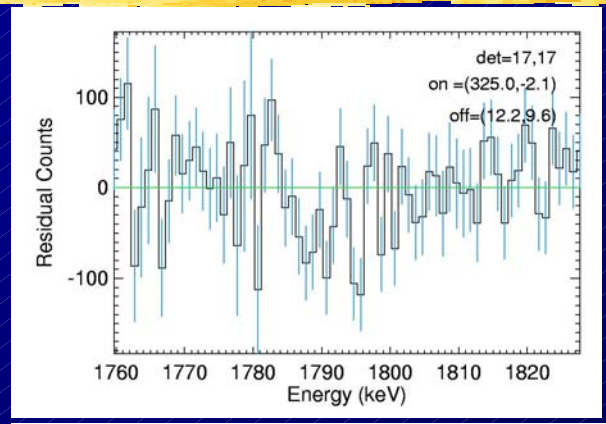

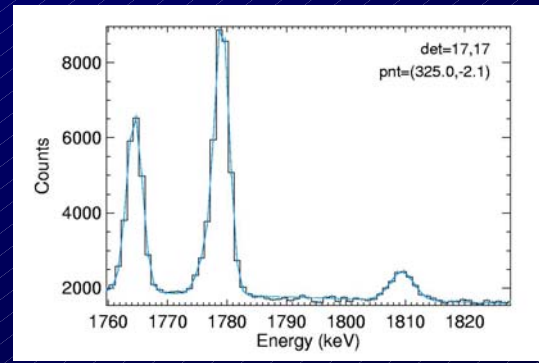

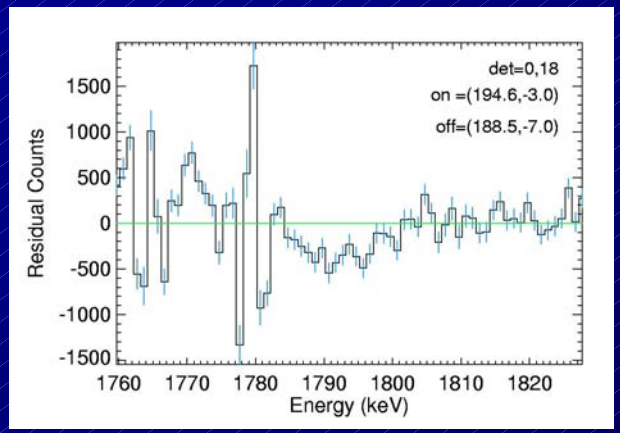

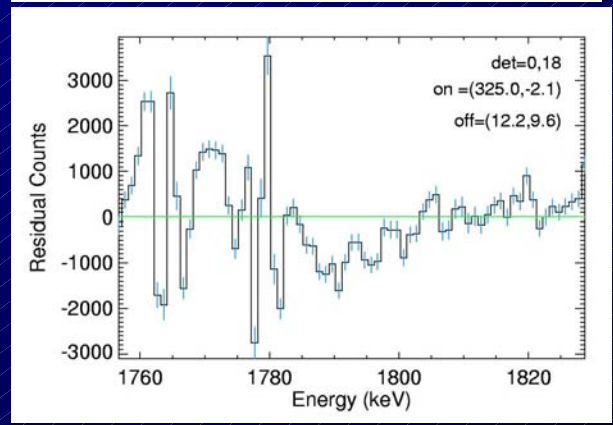

Obs	chisq
Crab det0	1.1
Crab 0-18	9.5
GCDE det 0	1.5
GCDE 0-18	23.4

- Adequate Fits for Single Det's
- Resolution Ratio 1.04…1.07

	centroid	+/-	amplitude	+/-	sigma	+/-	counts	+/-
Crab	1764.345	0.031	1403.644	35.5064	1.2608	0.0317	4435.852	158.2038
ab	1776.908	0.3664	397.5823	128.462	1.3	0	1295.568	418.6085
Crab	1779.124	0.0559	3238.472	87.5673	1.199	0.0334	9732.896	377.7459
Crab	1809.395	0.1693	223.3524	19.4385	1.7887	0.173	1001.442	130.2851
GCDE	1764.361	0.0196	3768.682	55.8745	1.353	0.02	12781.78	267.9284
GCDE	1776.227	0.1494	924.4962	87.5755	1.3	0	3012.579	285.3751
GCDE	1779.135	0.0198	8537.152	79.9648	1.2478	0.0159	26701.9	421.4917
GCDE	1809.48	0.1017	629.4683	26.6233	1.9	0	2997.902	126.7959

GCDE Data, Crab Data Subtracted (ON/OFF)

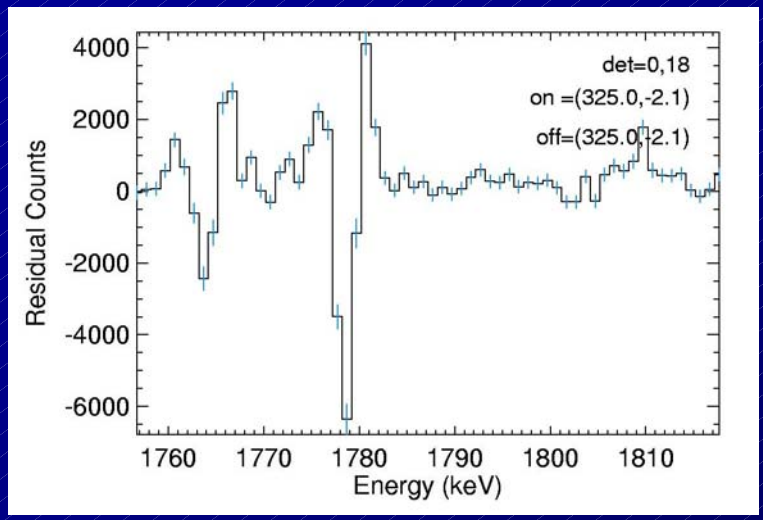

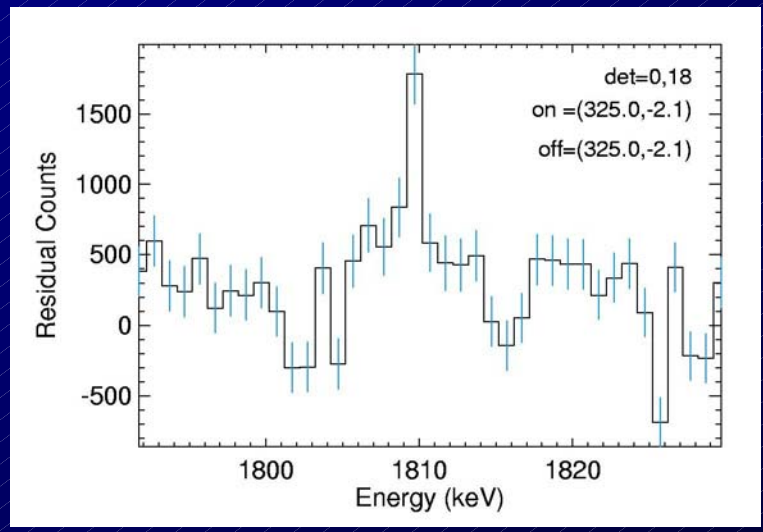

- ☆ Residual Signal Remains
  - ☞ ~2000 SE Counts
  - ☞ Narrow?

GCDE, Resolution-Adjusted OFF

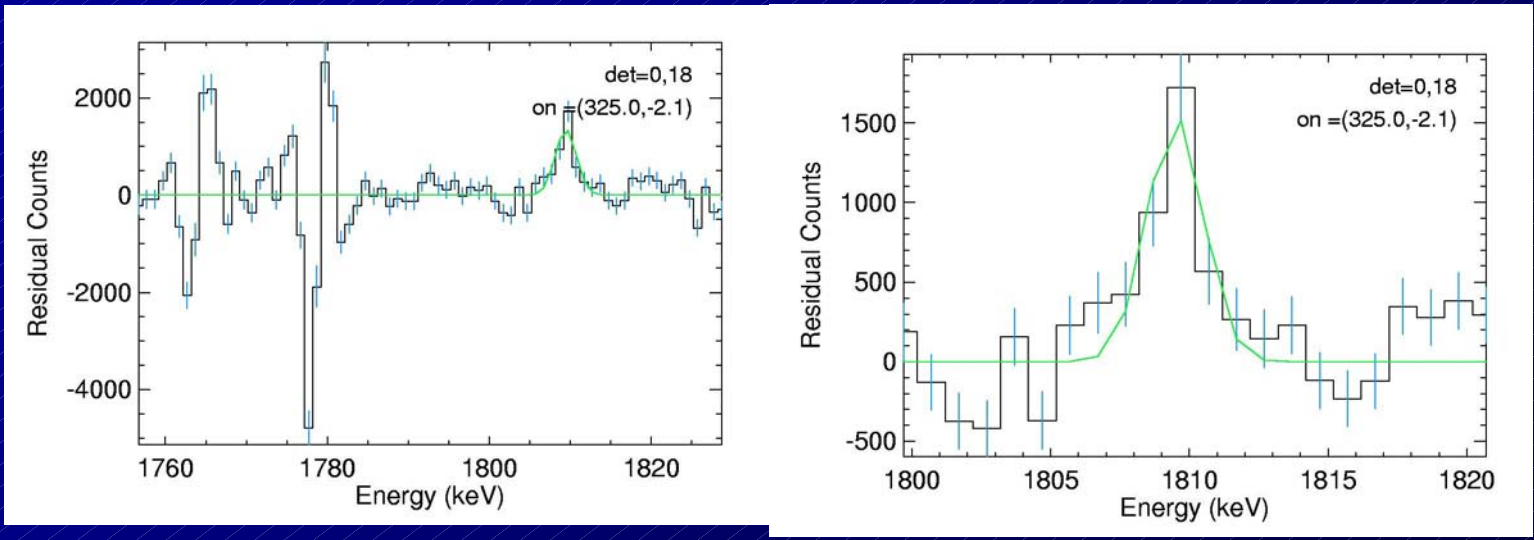

- ☆ Fitting a Resolution-Adjusted OFF Template as Bgd:
  - ☞ Single events only
- ☆ Celestial Residual Remains:
  - ☞ Line Centroid 1809.46 keV
  - ☞ 3912 cnts
  - ☞ FWHM 2.37 keV

Roland Diehl

GCDE, Different Parts

GCDE: 4th - 1st Quadrant

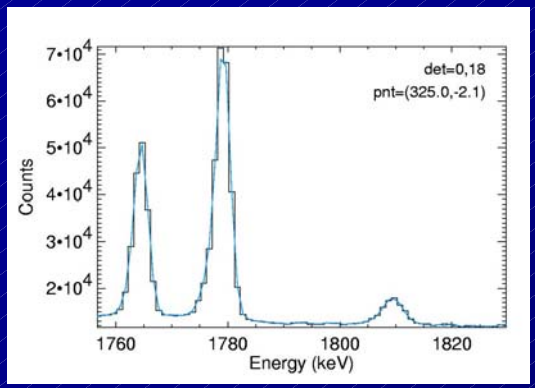

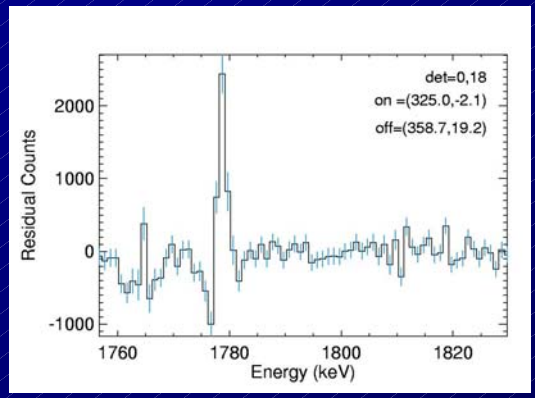

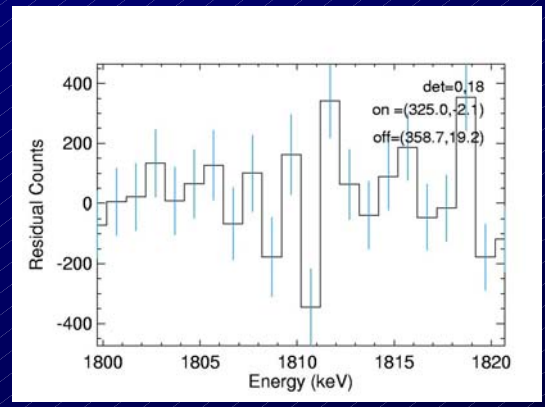

GCDE: 4th and 1st Quadrant: Fitting Residuals from Crab's Resolution-Adjusted Template:

		E	error	I	error	sigma	error	cnts	error
1st quadrant		1809.4974	0.4081	442.5027	87.7367	1.9046	0.4055	2112.537	614.6394
4th quadrant		1809.5226	0.1753	969.1818	151.7788	0.9901	0.1732	2405.307	564.7507

GCDE, ^{26}Al Line Width Illustrations

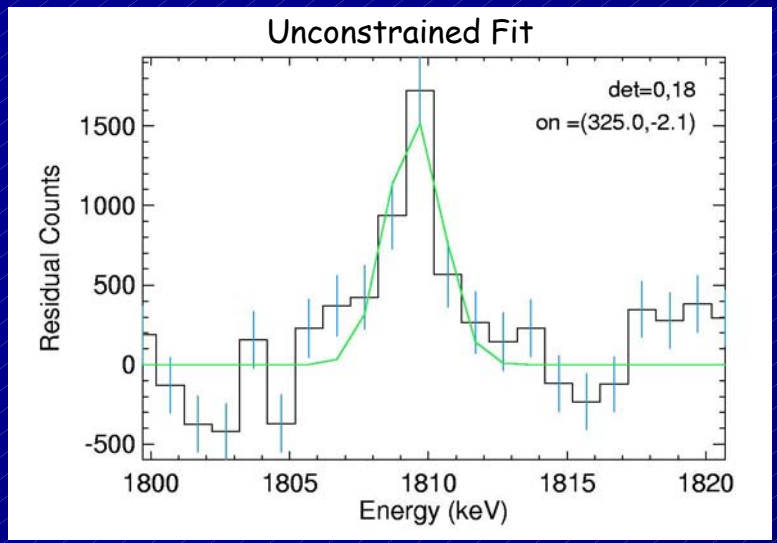

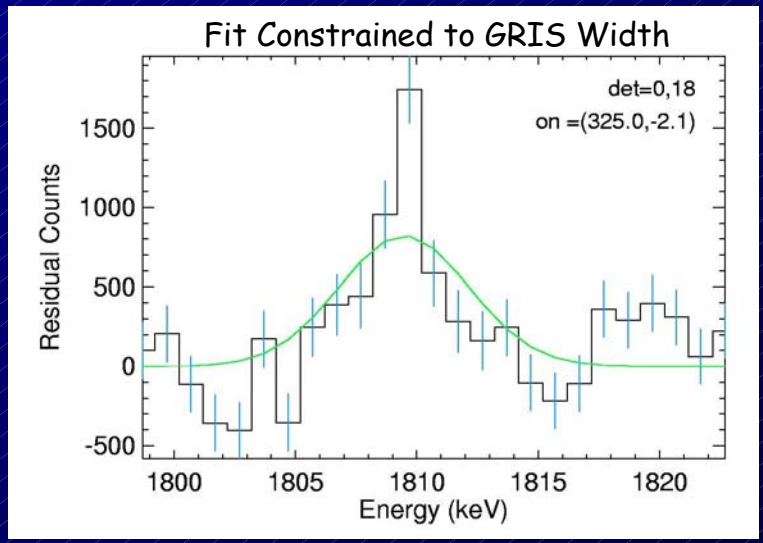

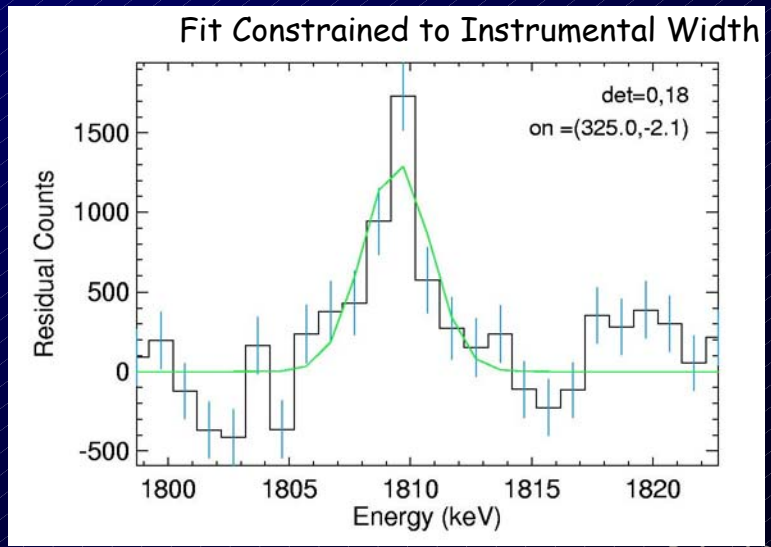

☞"Narrow" Line More Plausible from SE Analysis

Comparisons: SE and ME

	SE	ME
counts	3913	2921
width	1.01	2.36
centroid	1809.5	1808.15

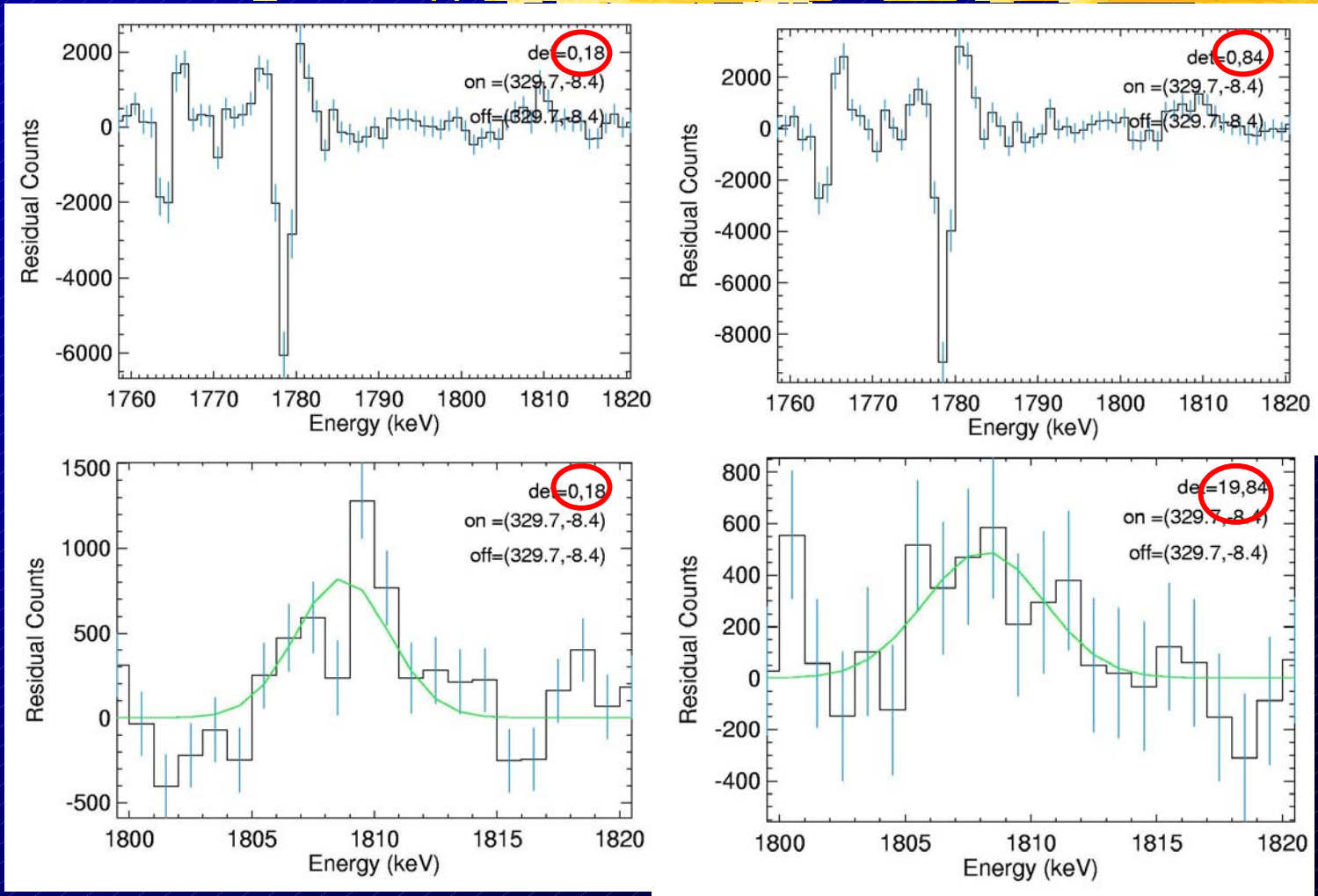

- ☆ SE/ME Analysis ~Feasible; ME: Bgd Leakage?
- ☆ Line Width Not Well-Constrained

GCDE, Resolution-Adjusted OFF

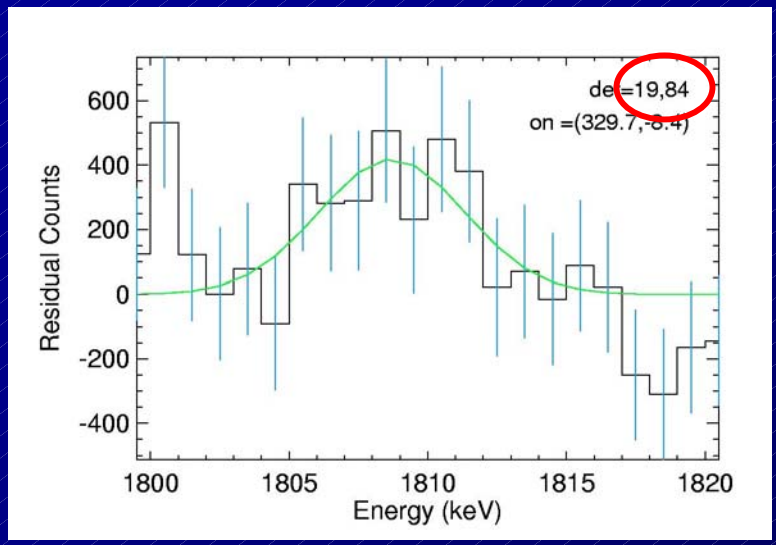

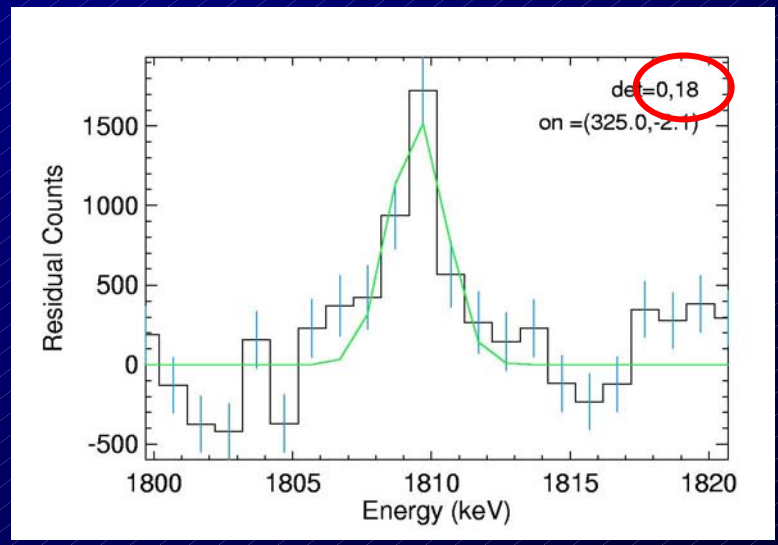

- Multiple Events:
  - Fitting a Resolution-Adjusted OFF Template as Bgd:

- Celestial Residual:
  - Line Centroid 1808.7 keV
  - 2763 cnts
  - FWHM 2.63 keV

- SE:
  - Line Centroid 1809.46 keV
  - 3912 cnts
  - FWHM 2.37 keV

Roland Diehl

^{26}Al Imaging Spectroscopy: SPIDIFFIT

- Compare also C. Wunderer's Presentation (SE), and J. Knödlseder
- ☆ Fitting of
  - Amplitude of Emission Skymap
  - Background Template Normalization per Pointing
- ☆ GCDE (SE+ME Data):
  - Statistics Sufficient to Make Smoothings Uncritical/Unnecessary
  - S/B Discrimination Incomplete -> Positive Amplitudes Throughout

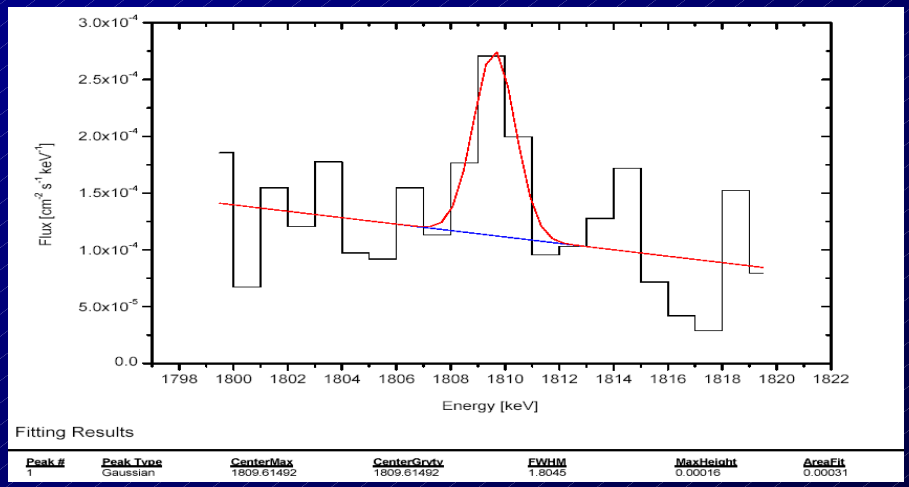

Fitting Results

Peak #	Peak Type	CenterMax	CenterGrvty	FWHM	MaxHeight	AreaFit
1	Gaussian	1809.61492	1809.61492	1.8045	0.00016	0.00031

Centroid 1809.615 keV
Width 1.8045 keV
Intensity 3.1 10^{-4} ph cm^{-2} s^{-1}

- Clear Detection, Line Width ~Instrumental

511 keV Imaging Spectroscopy: SPIDIFFIT

☞ See also CESR Presentations

☆ GCDE, SE+ME Analysis, COBE Sky Intensity Model

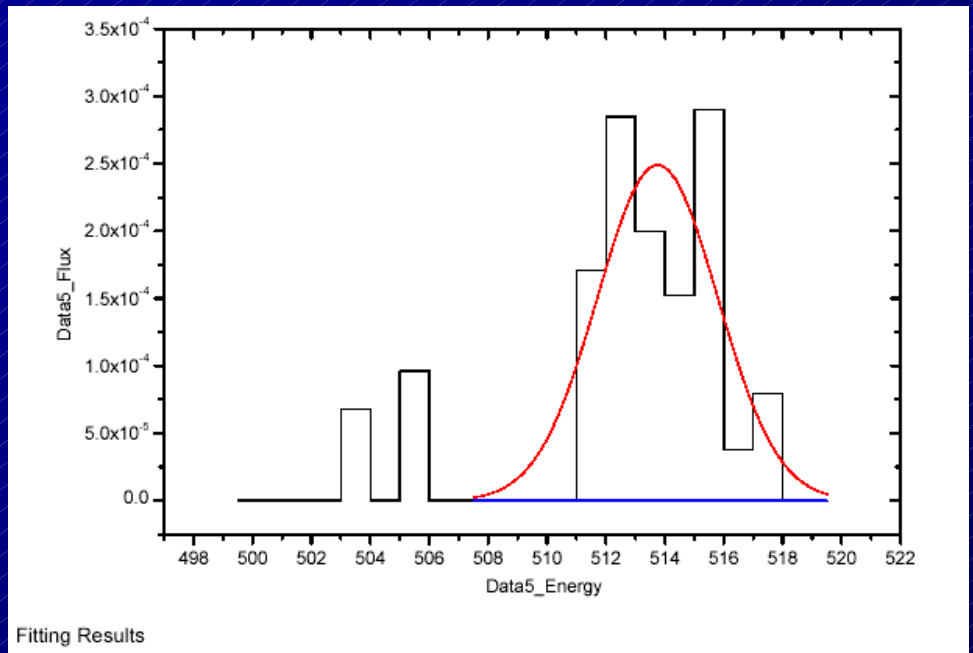

Fitting Results

Peak #	Peak Type	CenterMax	CenterGrvty	FWHM	MaxHeight	AreaFit
1	Gaussian	513.75266	513.75266	4.79694	0.00025	0.00127

Centroid	513.75 keV
Width	4.80 keV
Intensity	1.27 10^{-3} ph cm^{-2} s^{-1}

Search for ^{60}Fe with Imaging

-> Presentation Lichti

- ☆ Test COBE Dust Emission Spatial Emission Model
- ☆ GCDE Data and Analysis as for ^{26}Al ON/OFF
- ☆ SE+ME
- ☆ ^{60}Fe->^{60}Co Lines: 1173.237 and 1332.501 keV

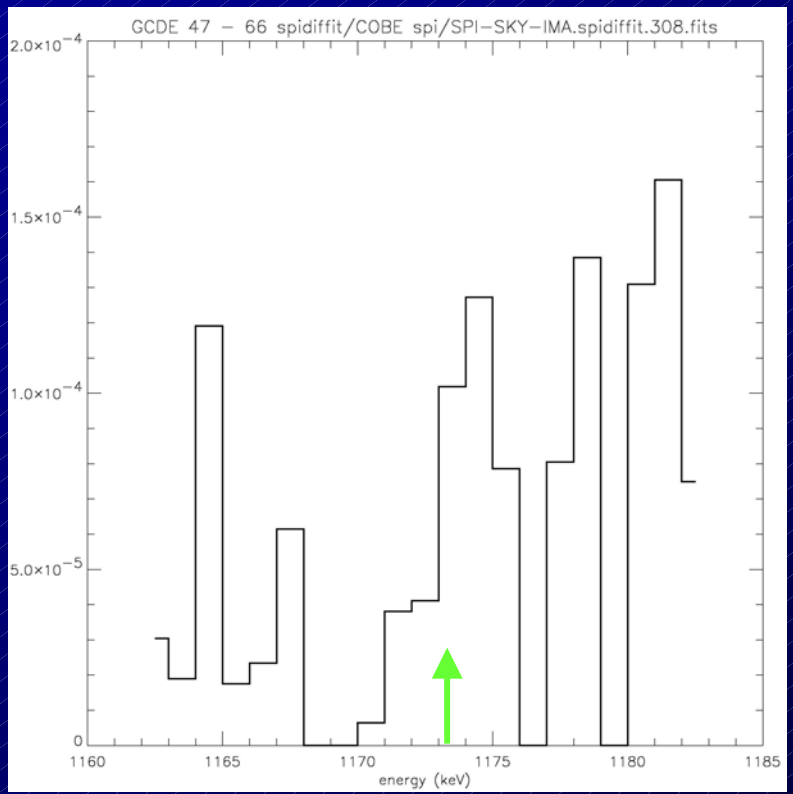

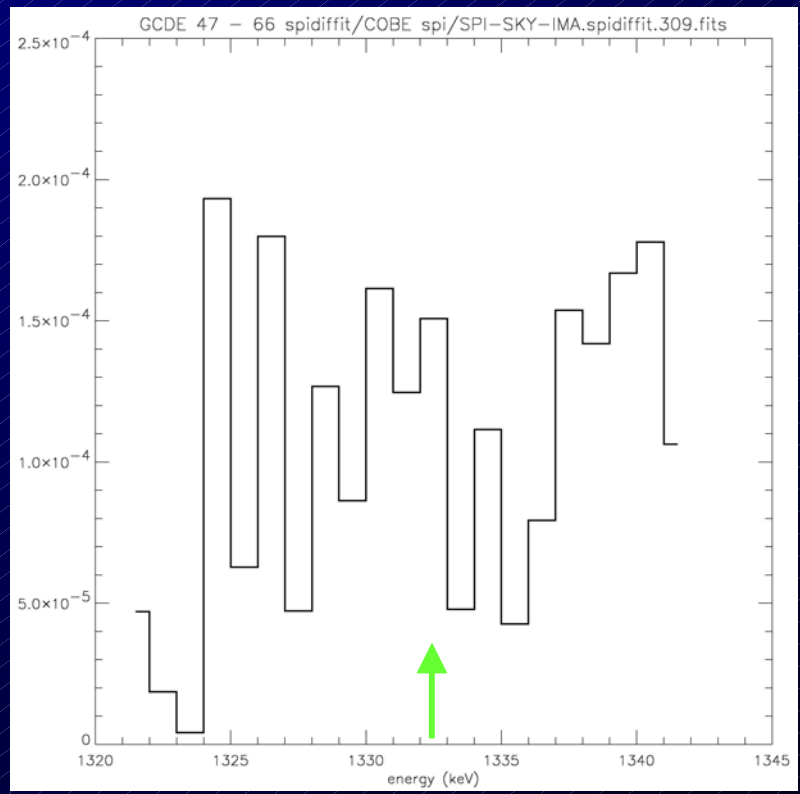

INTEGRAL FoV - GRBs:

Status of analysis / Papers

SPI Co-Is Meeting, Toulouse
Andreas von Kienlin MPE

Distribution of the FoV GRB data to different PIs Status of the analysis

GRBs:

- GRB021125 → Pino Malaguti
- GRB021219 → Sandro Mereghetti
- GRB030131 → IBIS: Sandro Mereghetti (open time) SPI: Lorraine Hanlon
- GRB030227 → Sandro Mereghetti (public data)
- GRB030320 → Andreas von Kienlin
- GRB030501 → OMC
- GRB??????
- Summary of SPI analysis results in:
  - "INTEGRAL Spectrometer SPI's GRB detection capabilities"
  - (GRBs detected inside SPI's FoV and with the anticoincidence sub system ACS)
  - For A&A special issue, PI: Andreas

Distribution of the FoV GRB data to different PIs
Status of the analysis

GRB021125:

- A&A special issue, PI: Pino Malaguti
  - Status of paper: Pino is writing his first draft
  - SPI-input from Volker Beckmann und Andreas v. K. on 5.6.03
  - SPI-Team Co-authors: Peter v. Ballmoos, Volker Beckmann, Gerry Skinner, Andreas v. K
- SPI-analysis results of GRB021125 will be used in the SPI-GRB A&A special issue.
- Status of analysis:
  - SPI was set into „low TM-mode“ (only on-board spectra and SCHK-data)
  - GRB localization only with SPI SCHK-data possible
  - Extraction and use of ACON onboard spectra possible
    - Problem of 30 min time shift (NRT/CONS) has to be solved !

Distribution of the FoV GRB data to different PIs
Status of the analysis

GRB021219:

- A&A special issue, PI: Sandro Mereghetti
  - Status of paper: Sandro is writing his first draft
  - SPI-input from Volker Beckmann und Andreas v.K. on 19.5.2003.
  - SPI-input from Laurent Bouchet ?
  - SPI-Team Co-authors: V. Beckmann, Laurent Bouchet, Andreas v. K
- SPI-analysis results of GRB021219 will be used in the SPI-GRB A&A special issue.
- Status of analysis:
  - SPI was set into „low TM-mode“ (only PSD-, ME-events and SCHK-data)
  - GRB localization only with SPI SCHK-data possible
  - GRB localization with PSD und ME not possible (only a flux can be derived)
  - up to now no spectrum

Distribution of the FoV GRB data to different PIs
Status of the analysis

GRB030131:

- First „open time“ GRB
- IBIS-data: open time proposal PI: Sandro Mereghetti
- SPI-data: open time proposal PI: Lorraine Hanlon
- „quick publication“ of PI: Sandro Mereghetti
  - SPI-input: up to now NO ?!
  - No Co-authors from SPI-team
- Dublin-group will contribute their analysis results to the SPI-GRB A&A special issue
- Status of analysis:
  - GRB occurred during slew !! (analysis of slew data not possible with standard ISDC-tools)
  - MPE: up to now no access to the data
  - Volker Beckmann is supporting the Dublin group

Distribution of the FoV GRB data to different PIs
Status of the analysis

GRB030227:

- ApJ, accepted, 15.05.2003 PI: Sandro Mereghetti
  - INTEGRAL + XMM data
  - SPI-input from Volker Beckmann, Andreas v. Kienlin and Laurent Bouchet
  - SPI-Team Co-authors: V. Beckmann, A. von Kienlin, V. Schönfelder, J.P. Roques, L. Bouchet
- SPI-analysis results of GRB030227 will be used in the SPI-GRB A&A special issue.
- Status of analysis:
  - SPI localization obtained
  - PL-spectrum
  - „hard-to-soft“ evolution

Distribution of the FoV GRB data to different PIs
Status of the analysis

GRB030320:

- A&A special issue, PI: Andreas von Kienlin
  - Status of paper: Andreas is writing his first draft ….
  - Co-authors: TBD
  - IBIS-input von Sandro Mereghetti und Diego Gotz
- SPI-analysis results of GRB030320 will be used in the SPI-GRB A&A special issue.
- Status Analyse:
  - GRB occurred near to „zero coding“
  - GRB will be analyzed with new response (14)
  - Localization and extraction of GRB spectrum possible

Distribution of the FoV GRB data to different PIs Status of the analysis

GRB030501:

- 5.5.2003 inquiry to Niels Lund: „asked to determine its ownership“
  - Ownership: OMC
- Paper under preparation (Journal: ??)
  - SPI data analysis and contribution by Volker Beckmann
  - SPI-Team Co-author: V. Beckmann
  - Secret analysis of data by Andreas v. Kienlin
  - Use of SPI-analysis results of GRB030501 in SPI-GRB A&A special issue ???

GRB0303501 secret analysis results

- "line feature at ~ 200 keV", width 20 – 30 keV
- Caused by
  - bad handling of ONTIME ??
  - bad background handling of SPIROS
  - background caused by the GRB itself ??

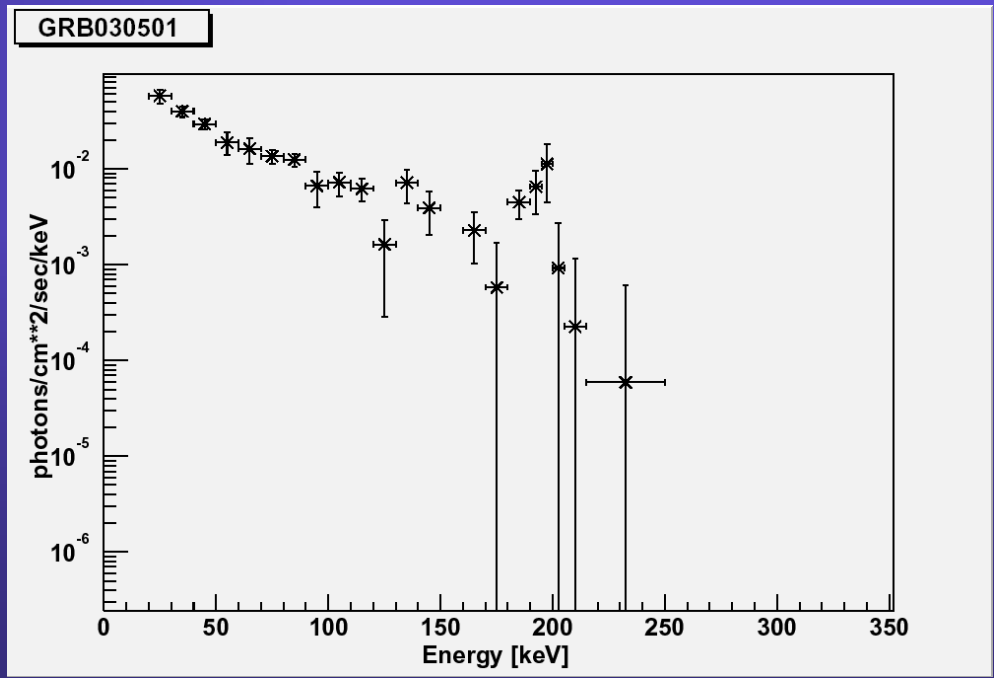

...sults

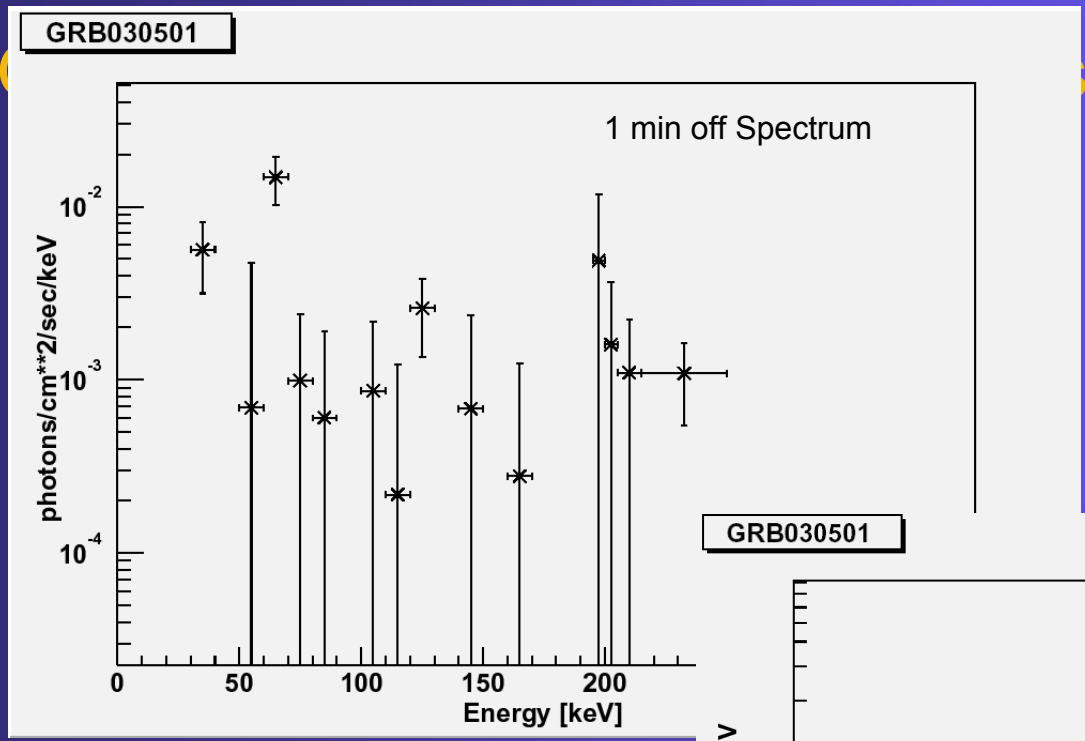
GRB030501
1 min off Spectrum
photons/cm**2/sec/keV
10^-2
10^-3
10^-4
0
50
100
150
200
Energy [keV]

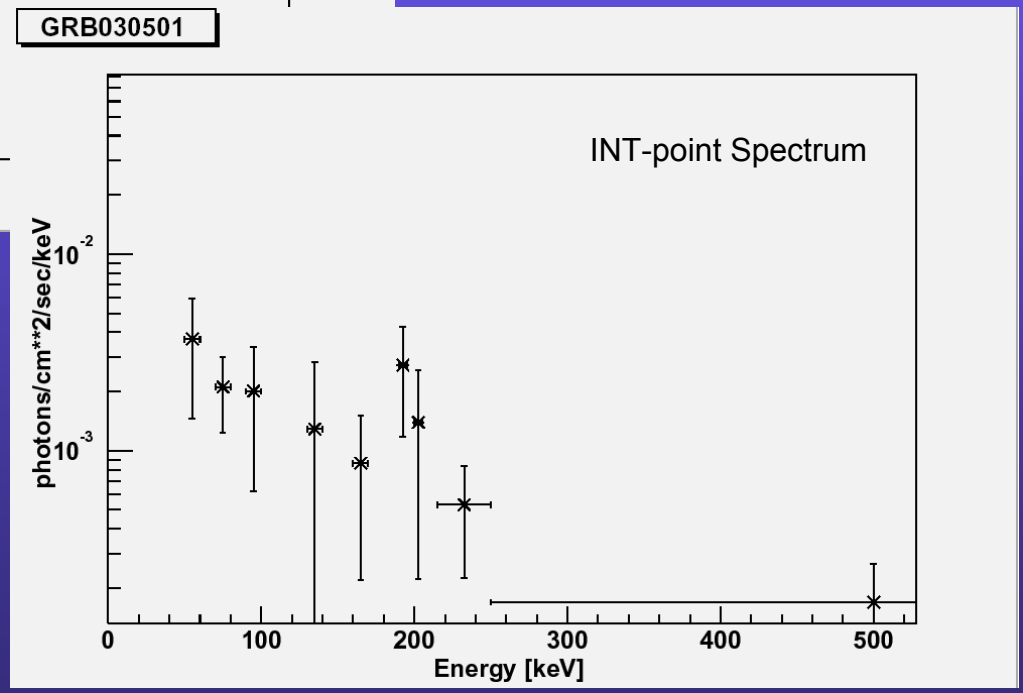
GRB030501
INT-point Spectrum
photons/cm**2/sec/keV
10^-2
10^-3
0
100
200
300
400
500
Energy [keV]

Gamma-Ray Bursts observed with the SPI instrument

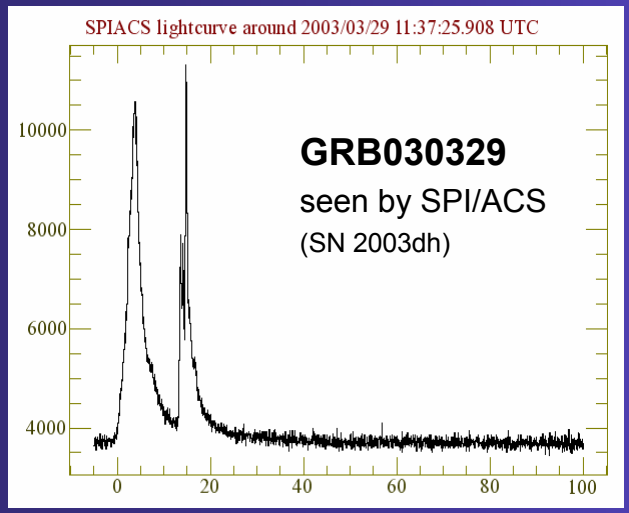

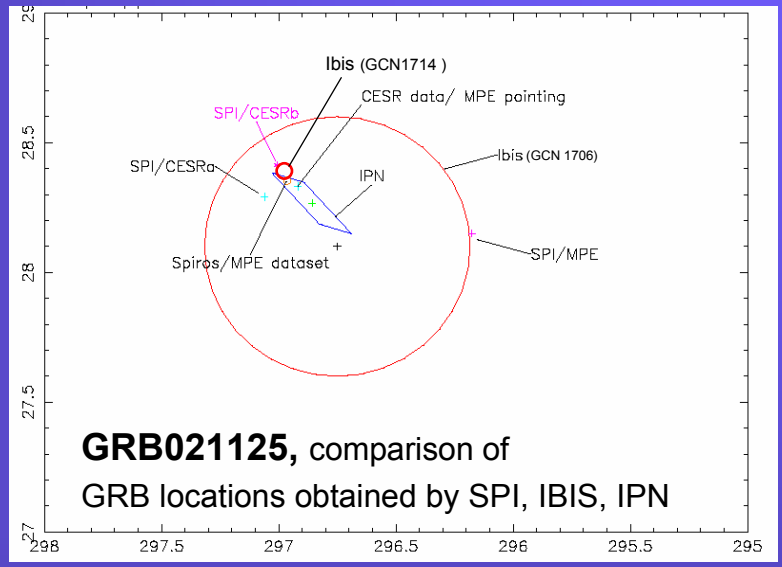

- GRBs detected within SPI's FoV
  - Since launch: 6 GRBs
  - SPI/FoV GRB detection rate: ~ 1 GRB/month
- GRBs detected with SPI/ACS
  - First 4 months of mission:
    - 90 GRB candidates
    - ~40 % confirmed by other instruments (IPN, HETE)
  - ACS GRB detection rate:
    - ~0.75 GRBs/day
    - ~0.3 confirmed GRBs/day

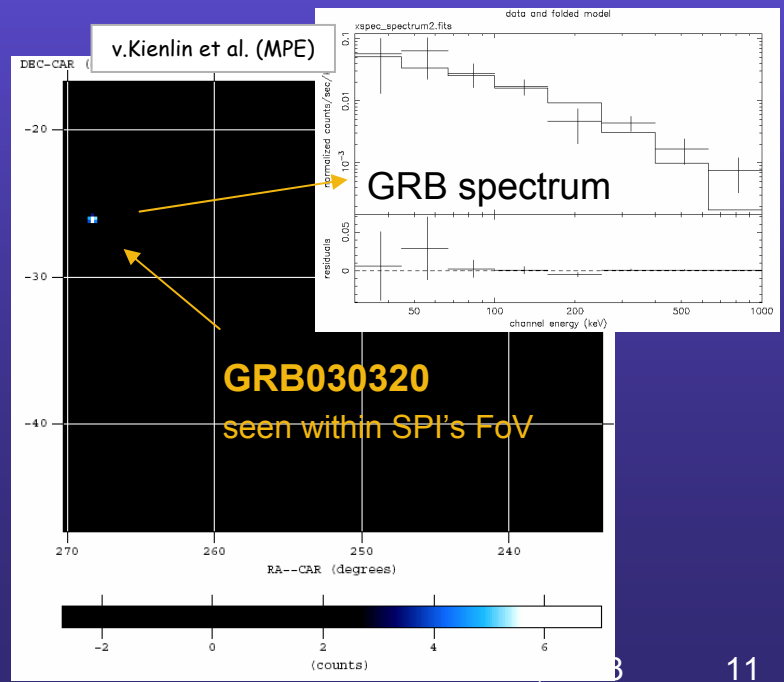

INTEGRAL special issue contribution: "INTEGRAL Spectrometer SPI's GRB detection capabilities"

Status:

- Preparation meeting on April 1, in Garching (1 day before last SPI Co-Is meeting)
- First draft written, including contributions from:
  - Arne Rau → ACS GRBs
  - Sandrine Deluit → ACS GRBs
  - Volker Beckman → GRB030227
- Still inputs needed from
  - V. Beckmann → "Analysis methods for GRBs", (GRB030501???)
  - L. Hanlon → GRB030131
  - ….
- Co-authors (current list):
  - A. von Kienlin, V. Beckmann, S. Deluit, L. Hanlon, G. Lichti, A. Rau, J.-P. Roques, V. Schönfelder, A. Strong, TBD, TBD, TBD

Diffuse Galactic Continuum Emission

Studies with INTEGRAL/SPI

A. Strong, MPE,

SPI Team Meeting/Toulouse

June 2003

Diffuse emission analysis:

long-term: imaging with e.g. maximum entropy (cf COMPTEL)
but not yet enough data
can anyway do spectroscopic analysis only via *spatial model fitting*

-> model fitting approach

maximum-likelihood fit to linear sum of components:
* sources
* tracers of diffuse emission (COBE, HI, CO, COMPTEL ....)

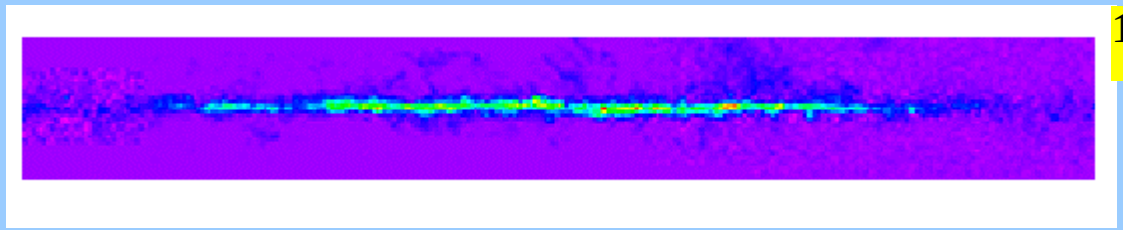

^{12}CO

* instrumental background
explicit time-dependence determined in fitting.
Background: template from 'empty field'"" observations:
fixes detector ratios; level per pointing is free.
Method will work if (and only if) detector background ratios are ~time-independent. *OFF data used: Rev 12+13.*

Spidiffit:

$$\text{counts} = \sum_{\text{model components}} \theta_m * \text{skymap}_m * \text{IRF} + \sum_{\text{pointings}} \theta_{m'} * \text{background-template}$$

Model components: using *gensky* and input survey maps.
Background assumed to have same form for each pointing, scaled in intensity

Form template taken from 'OFF' observations, summed over OFF pointings: *spioffback.*

Fit: *maximum likelihood* using NAG routine, with first derivatives.
Maximum found fast and to good accuracy, $d\log L / d\theta_m = 0$
Background factors 0.8 -1.2 : variation ~ expected.

Parameter distributions, errors: Bayesian MCMC method, seems to give reliable values.
Explicitly includes all correlations between parameters.
Start with ML solution, typically 10^5 samples.
Method details in *spidiffit* manual. ISDC delivered (not most recent version)

GCDE diffuse spectral fitting

35 log E ranges 15 – 1000 keV
singles only
background template from rev 12+13

spidiffit
time dependence free
HI+ CO + 4 sources, all free spectra

HI

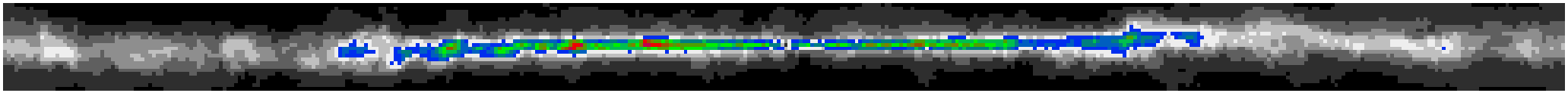

CO

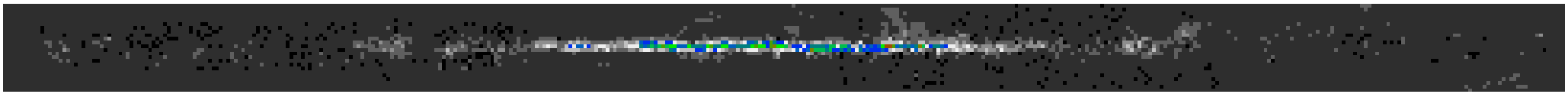

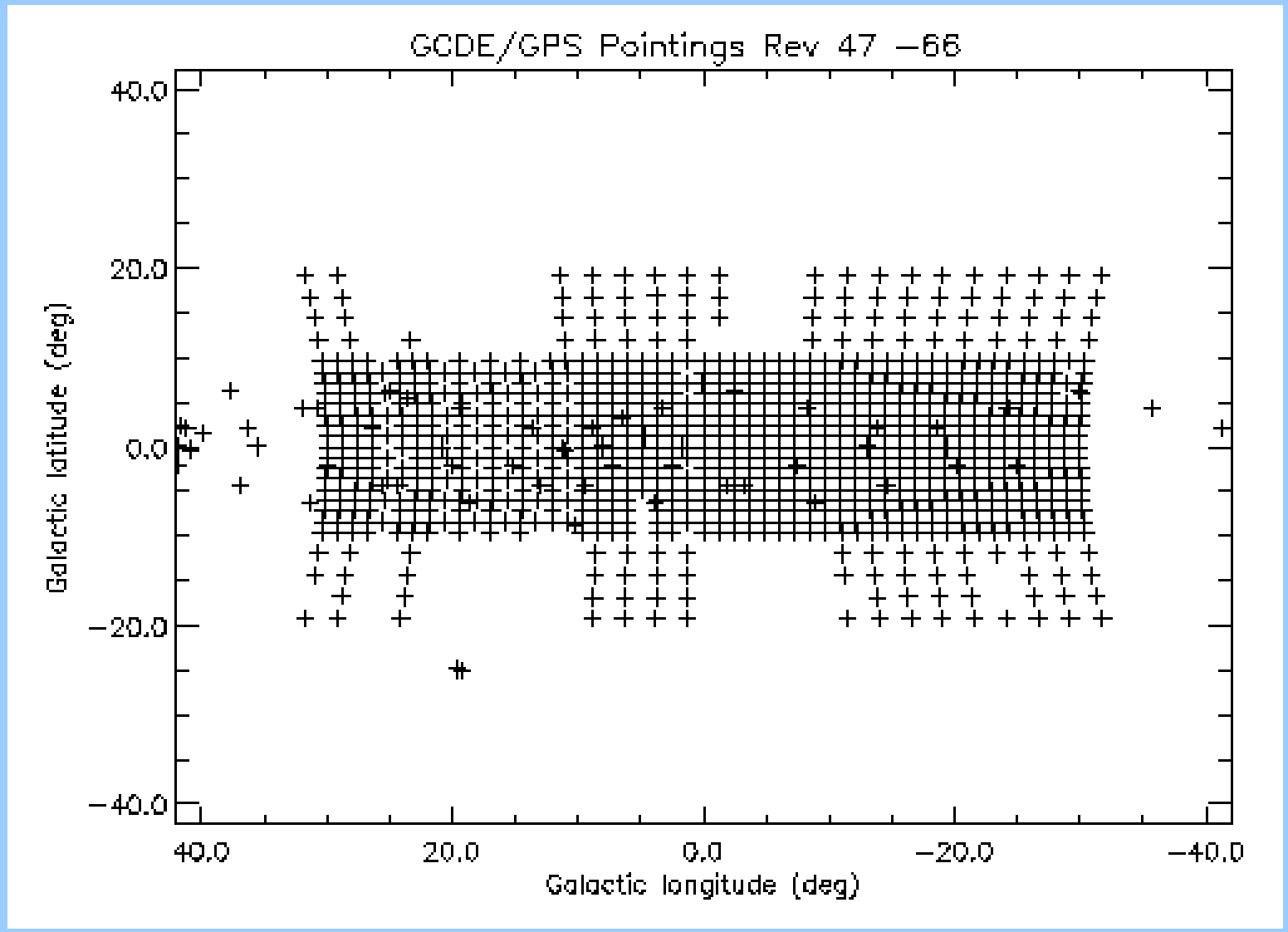
GCDE/GPS Pointings Rev 47 –66
40.0
20.0
0.0
–20.0
–40.0
Galactic latitude (deg)
40.0
20.0
0.0
–20.0
–40.0
Galactic longitude (deg)

GCDE Rev 47-66 Singles
spidiffit HI+ CO

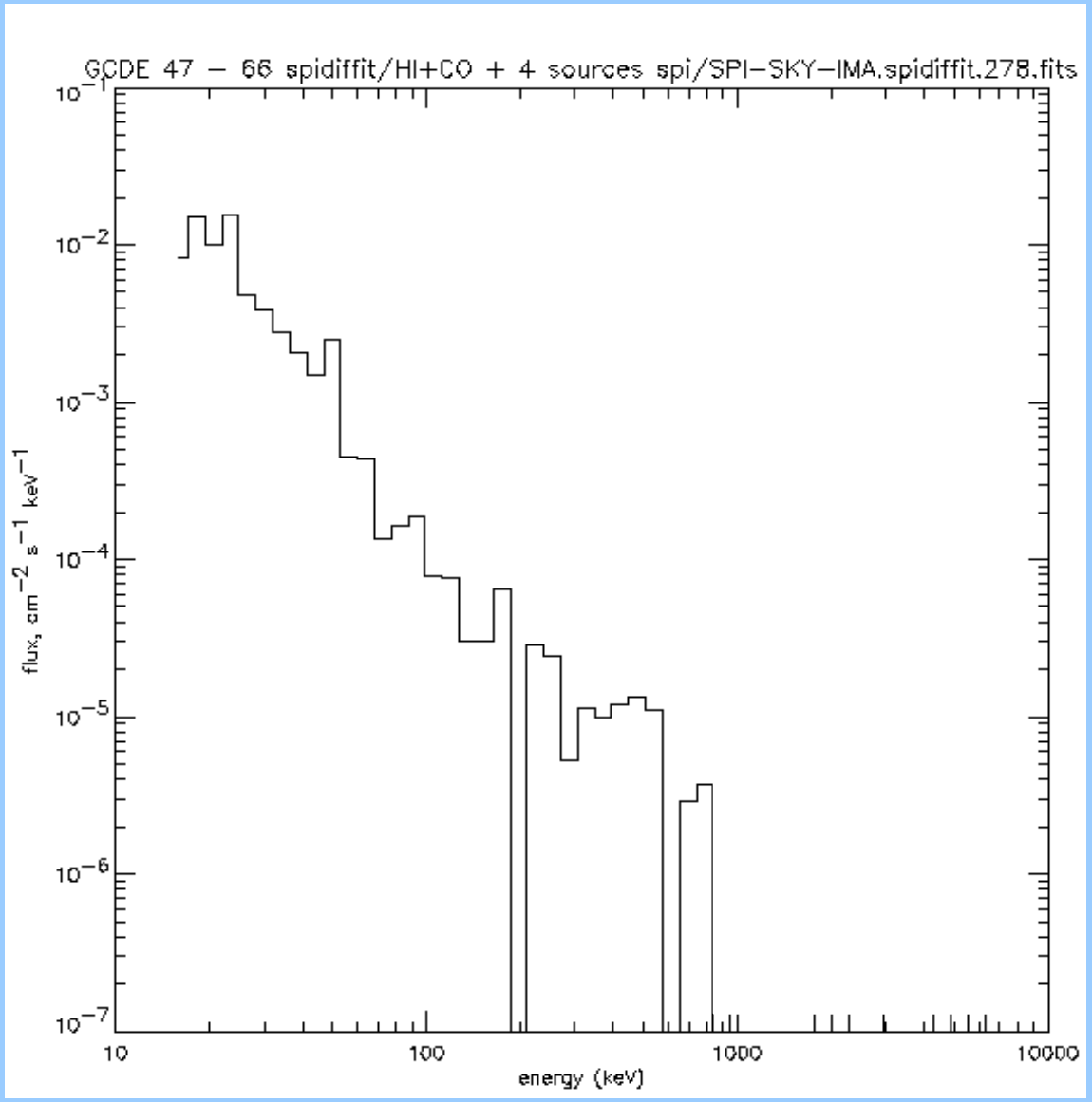

Kinzer et al. 1999, 2001
OSSE
l=b=0

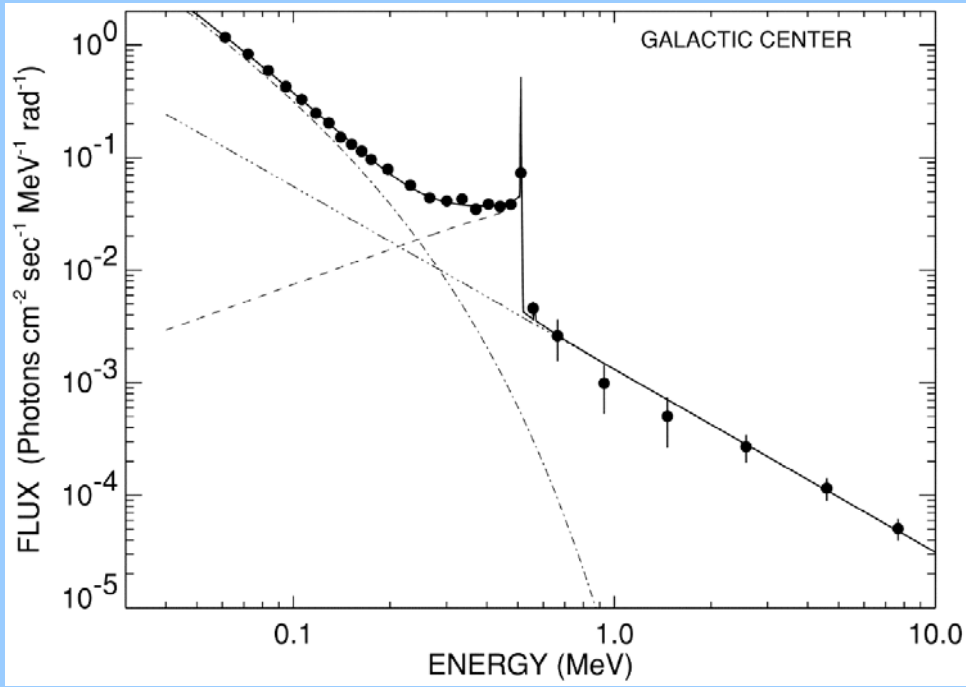

Valinia et al. 2000
RXTE, OSSE
diffuse emission l ~ 33º

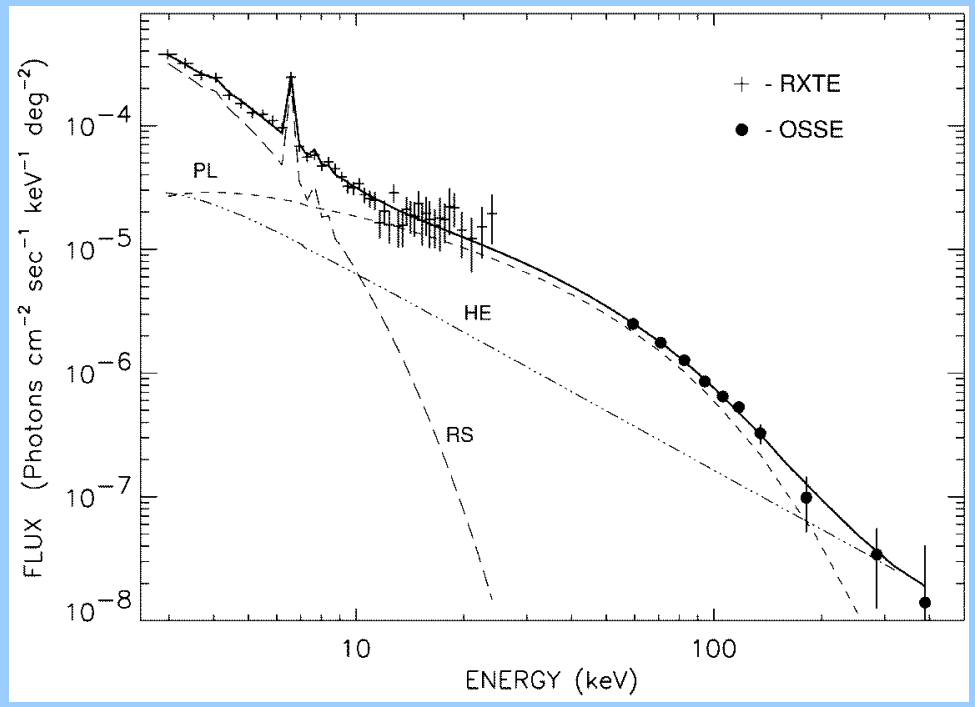

GCDE Rev 47-66 Singles
spidiffit HI+ CO

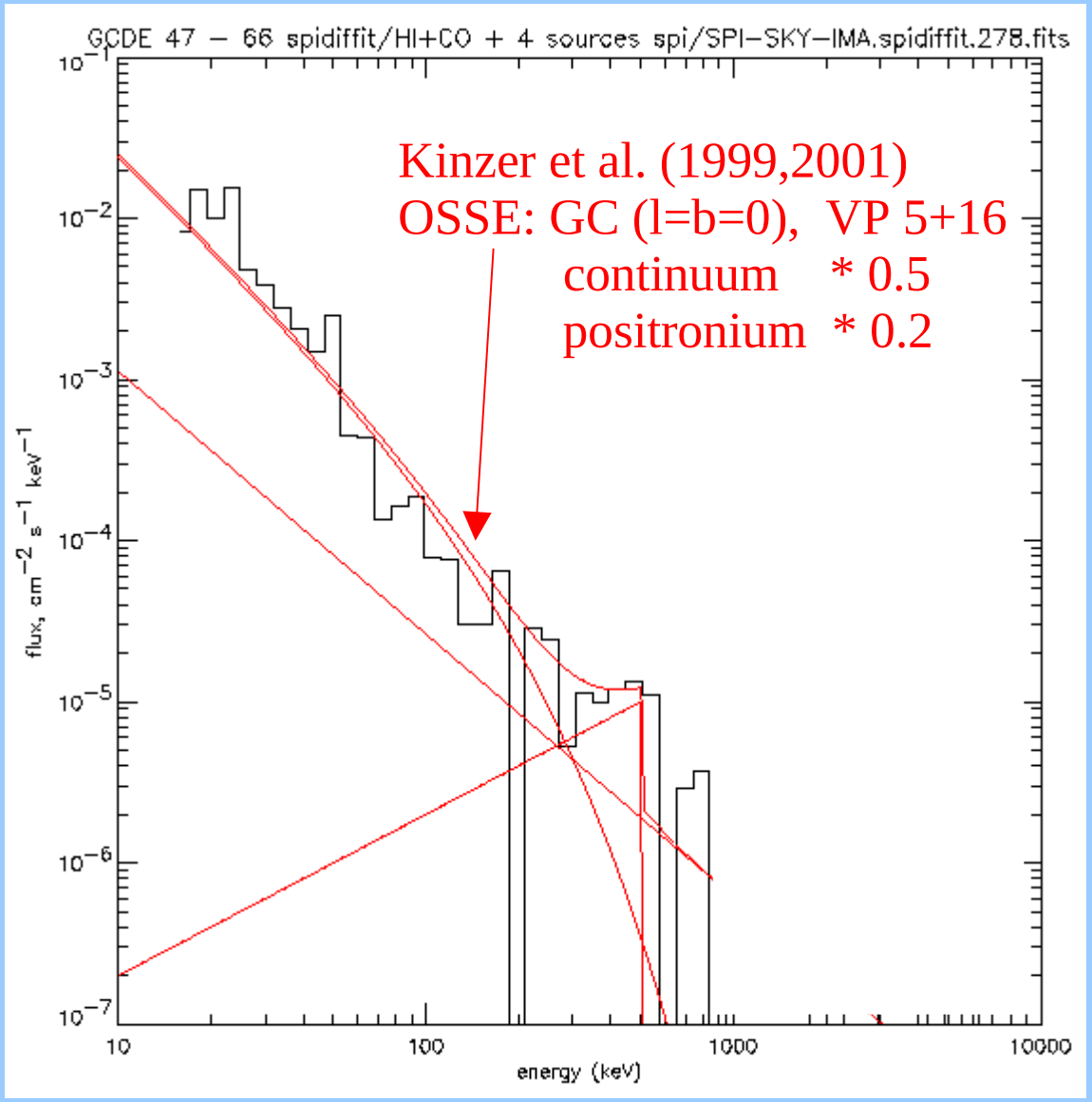

GCDE Rev 47-66 Singles
spidiffit HI+ CO

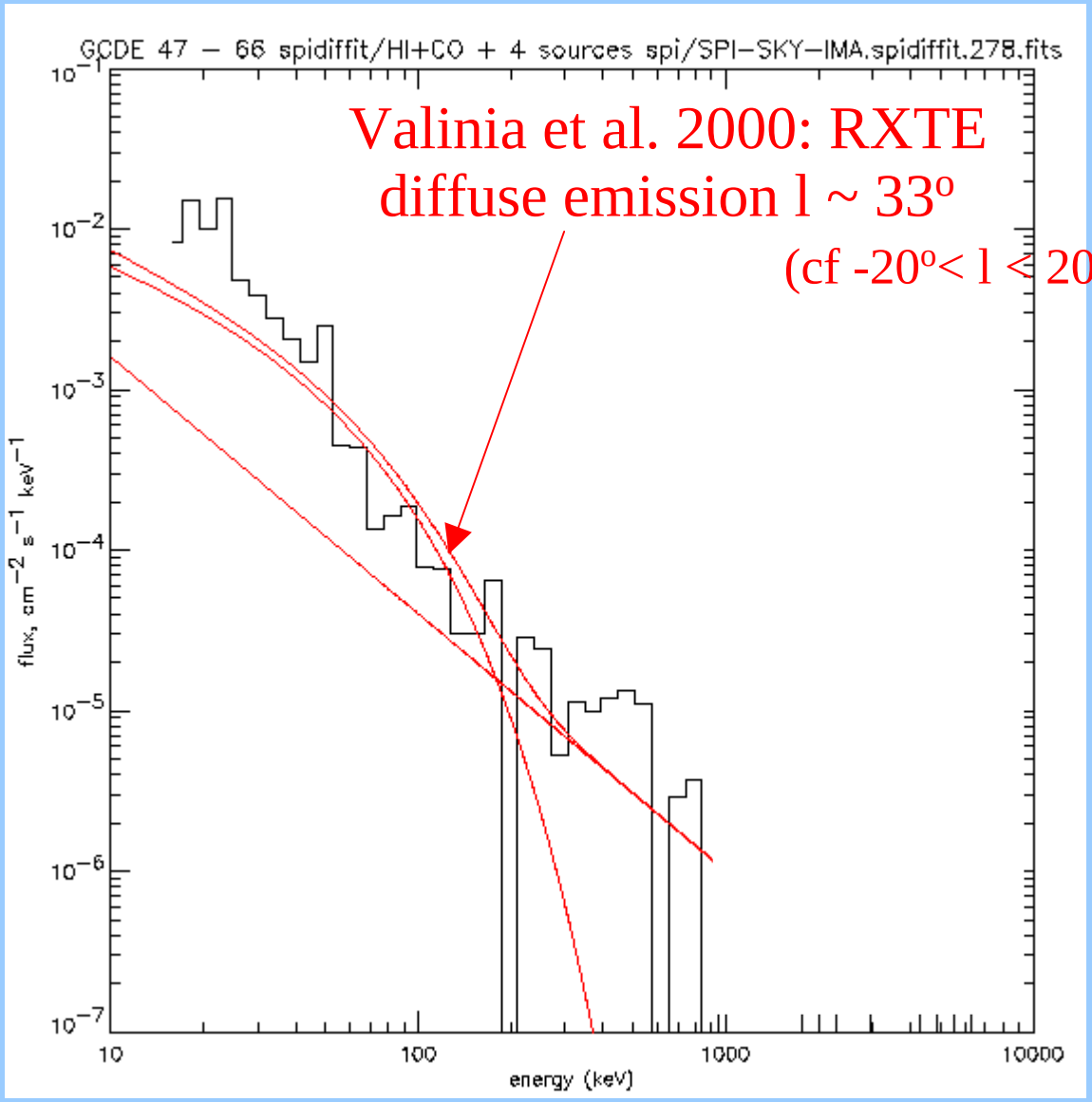

Separate components more noisy, but sum is robust

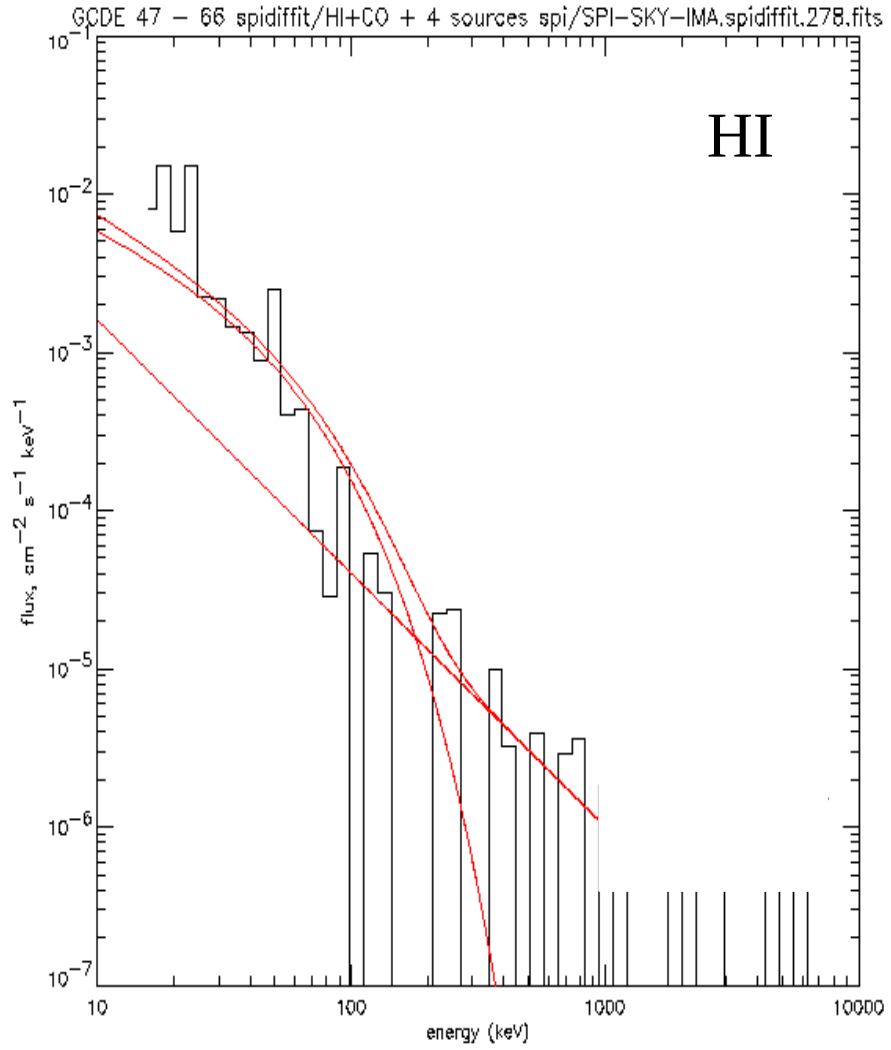

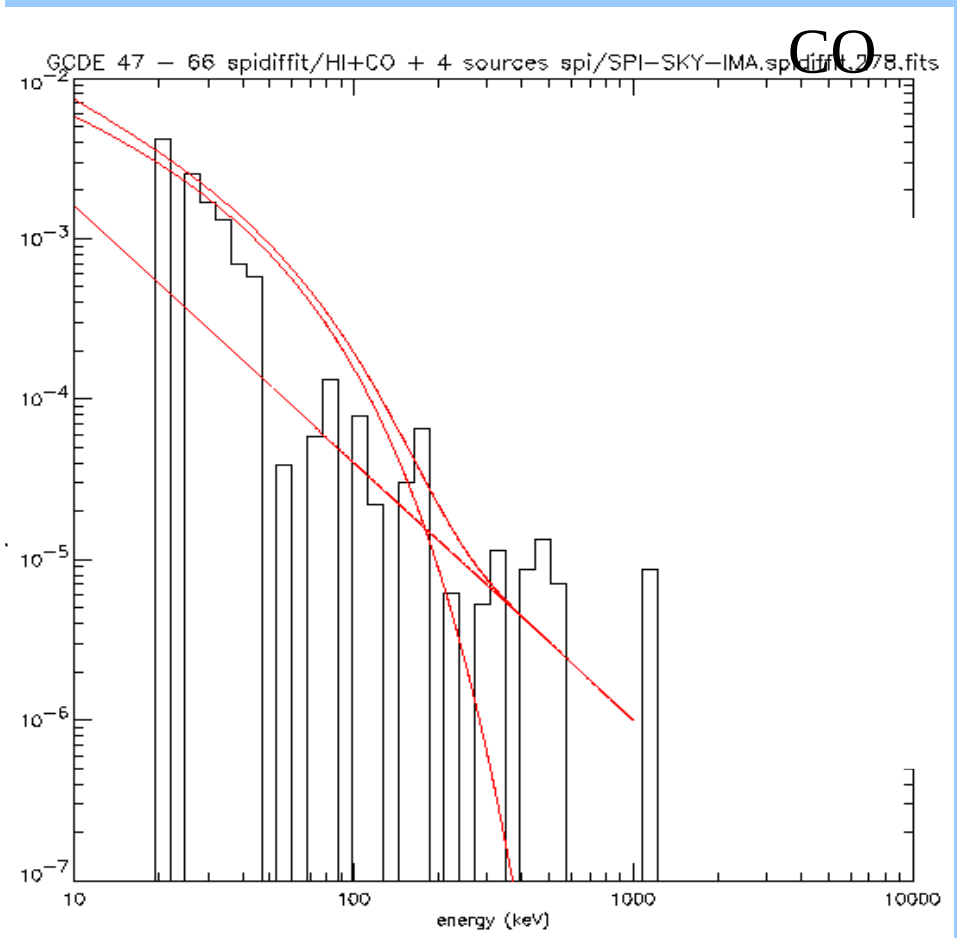

GCDE Rev 4 7 - 6 6 spidiffit source spectra

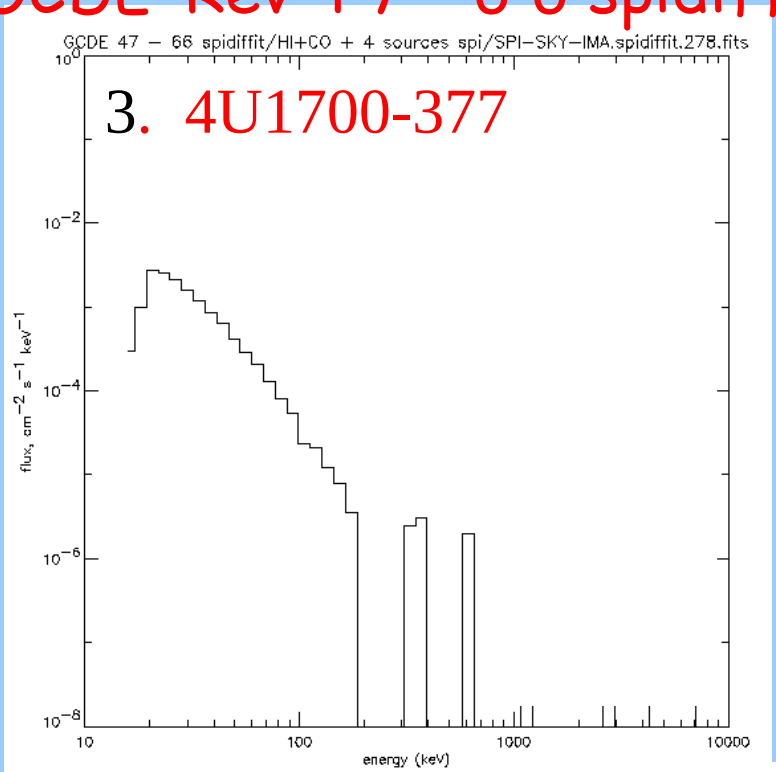

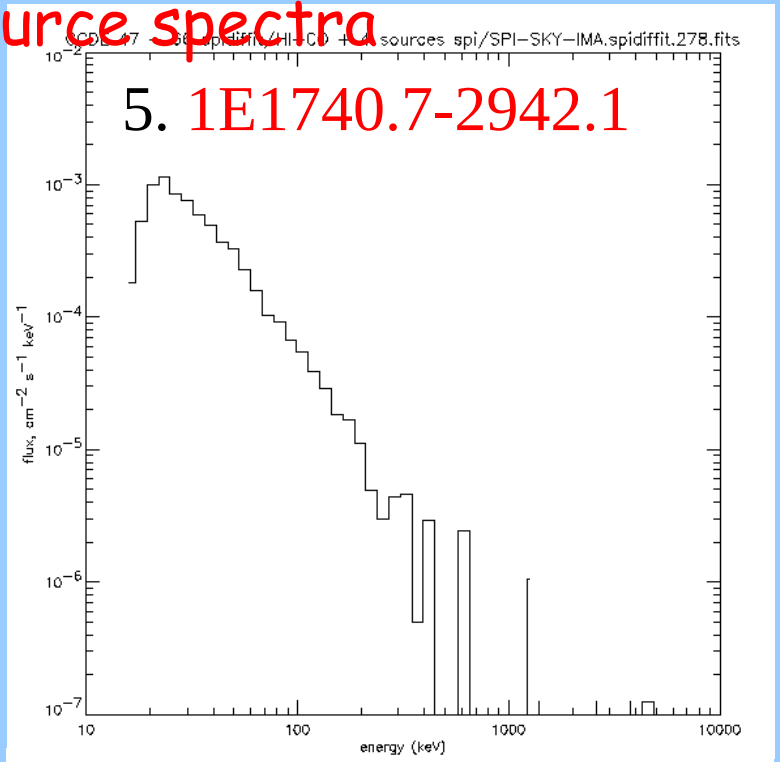

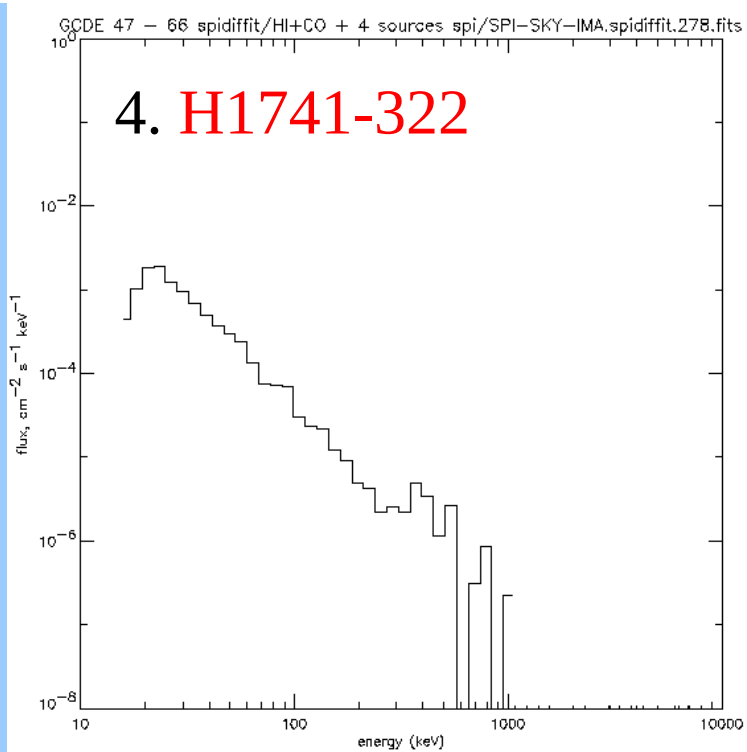

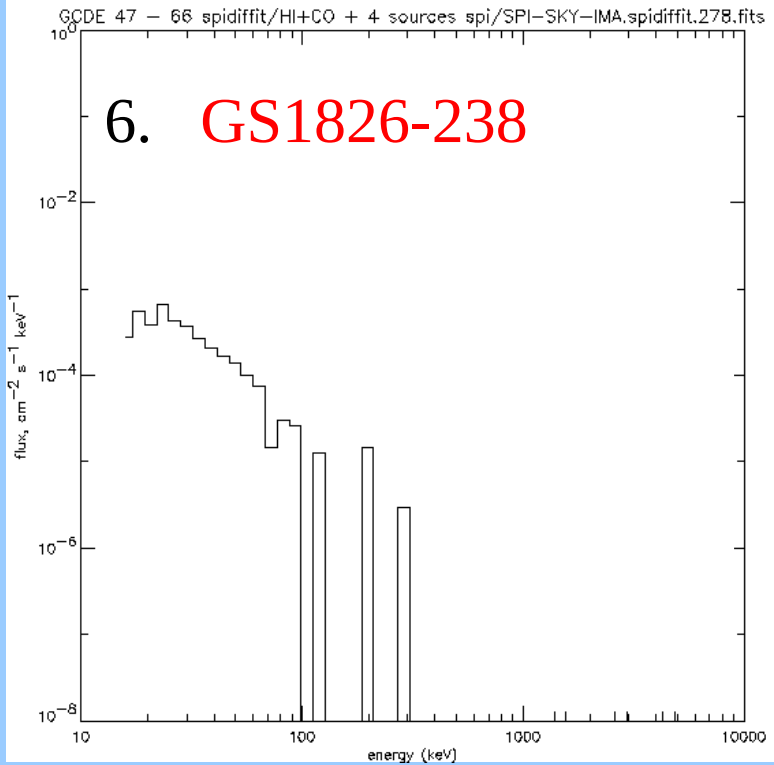

GCDE spectrum HI + CO + sources

HI + CO only

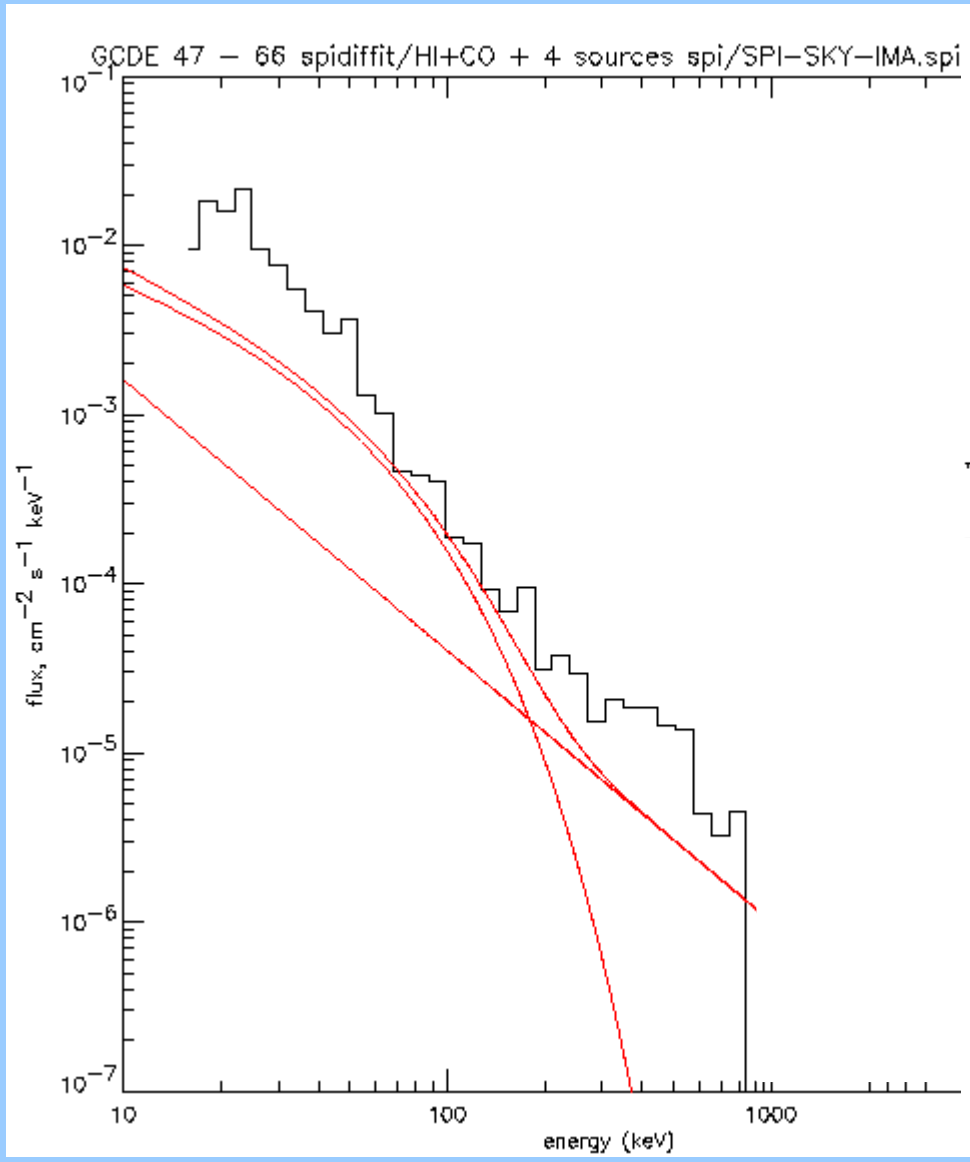

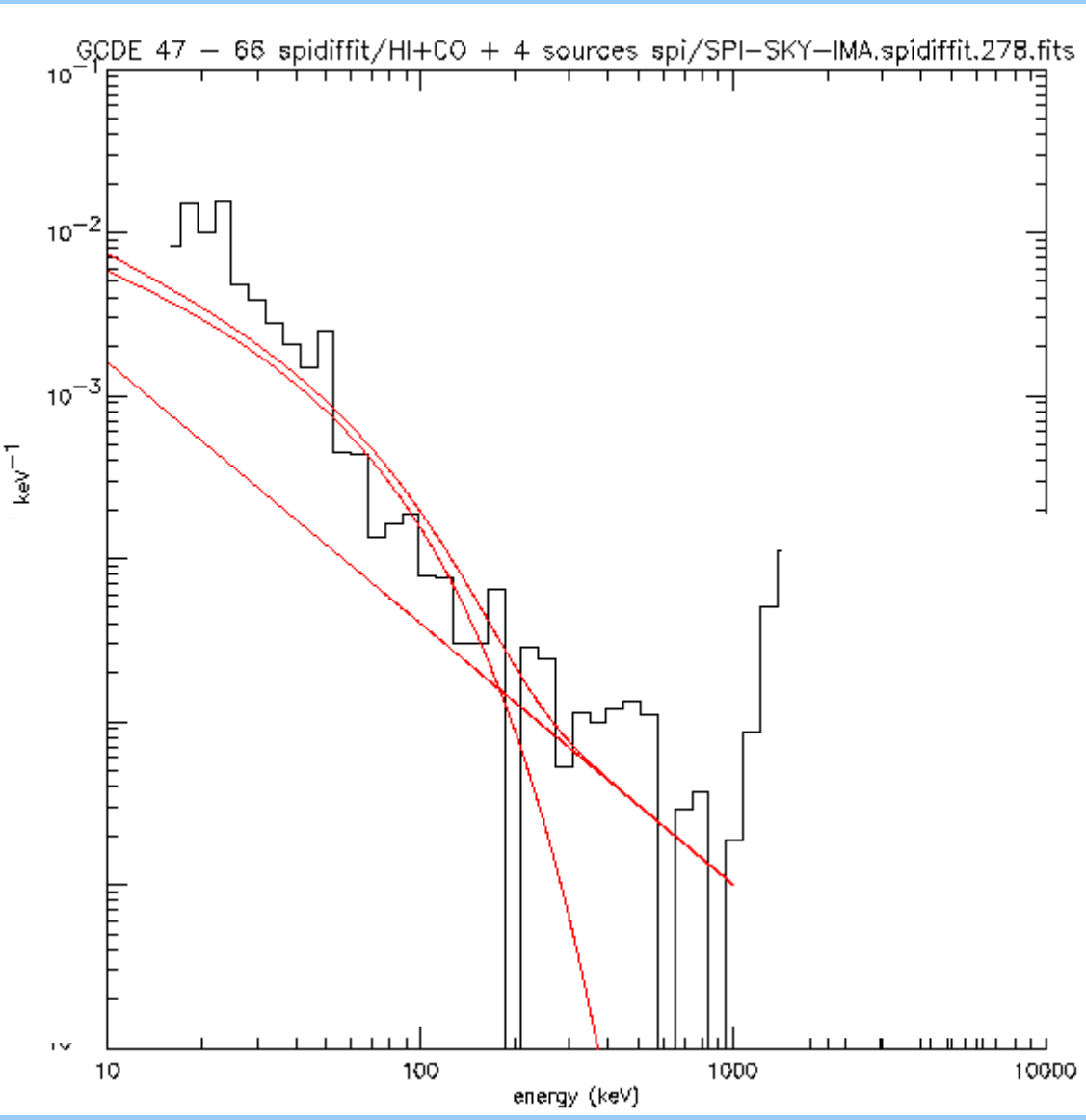

HI+ CO

Summed sources

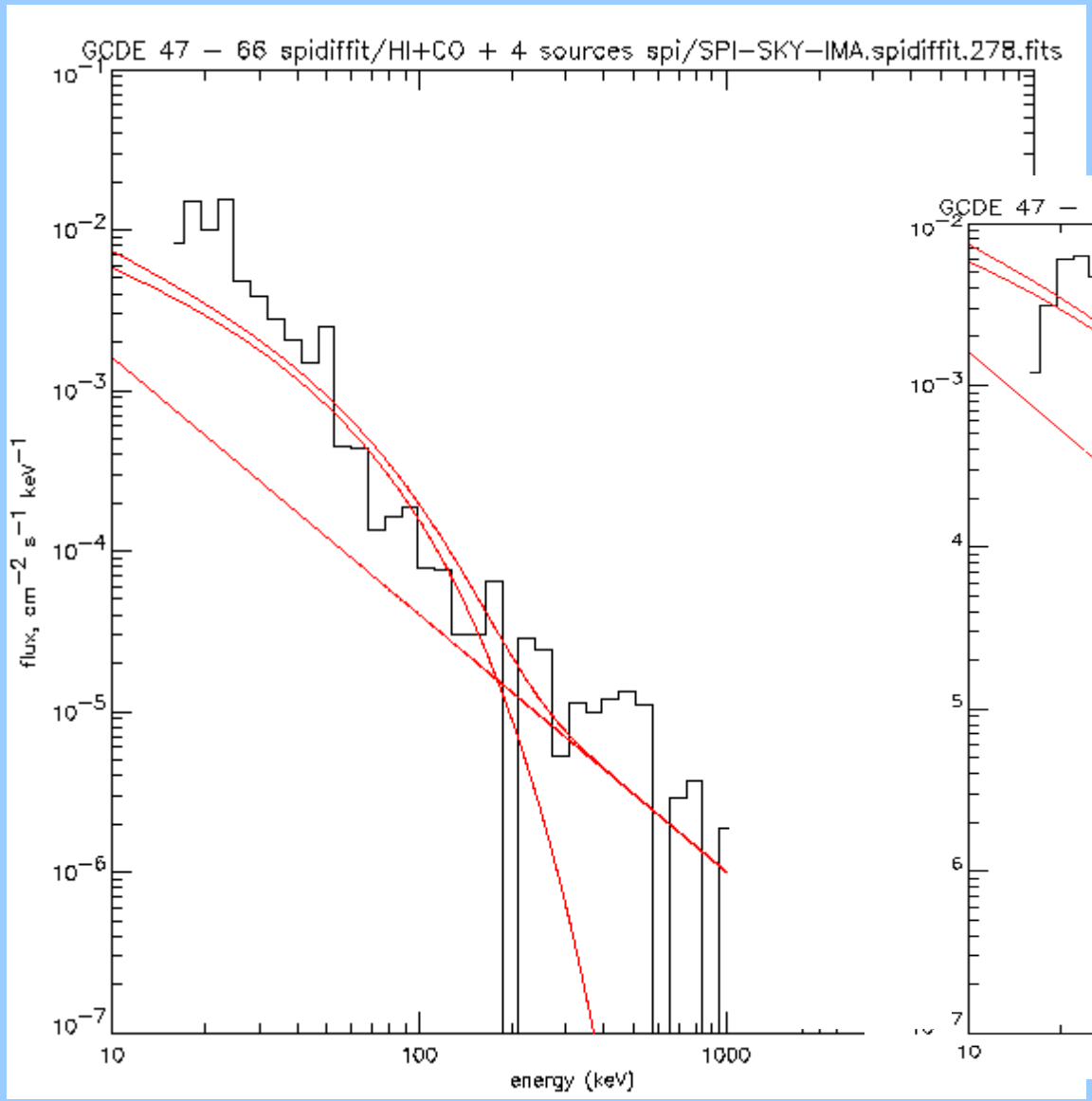

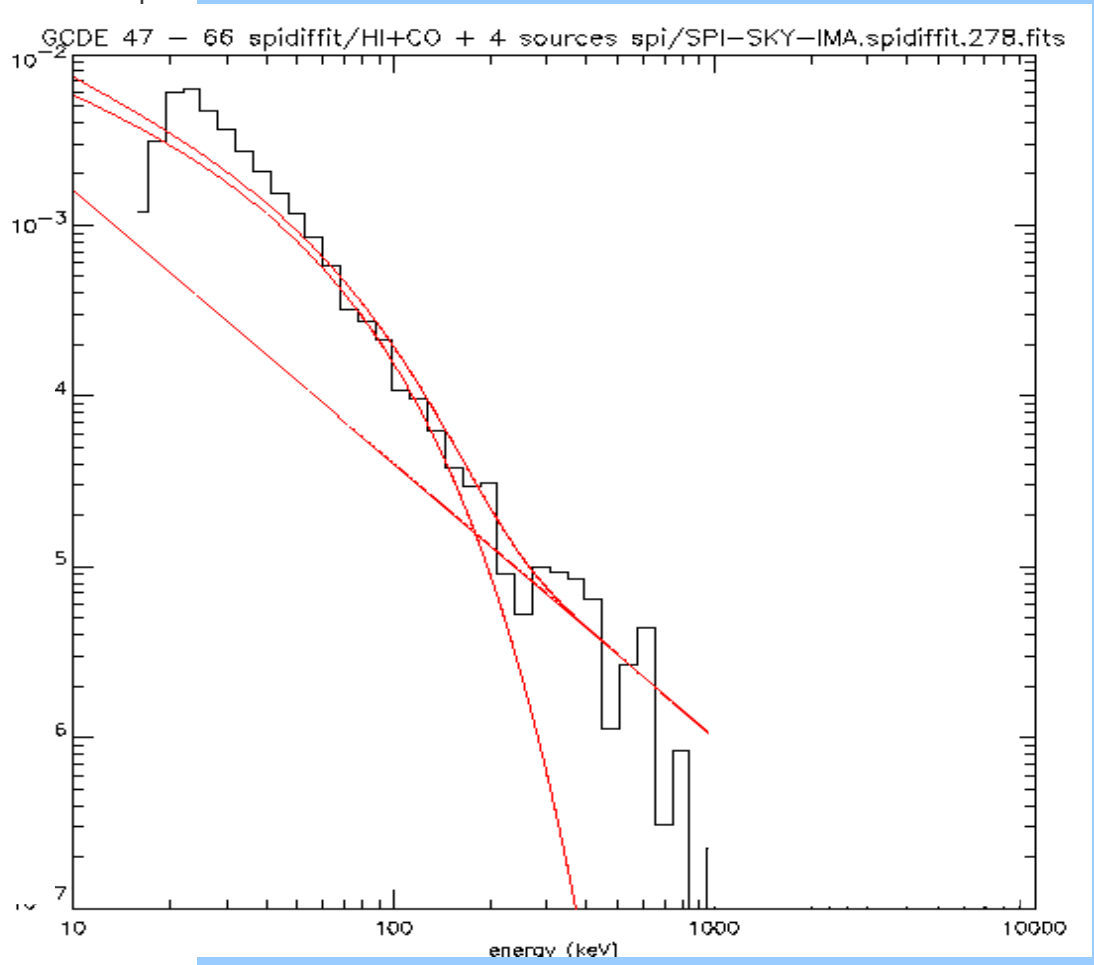

Next steps:

analyse consolidated data

include multiples

identify more sources and include in fitting

add skymap model for positronium

tune energy binning

compare models

combine GCDE, GPS, PV phase data to get
~ full Galactic plane map

Activate RSci group

spiskymax images from GCDE

Rev 47-66, singles

15 - 40- 100- 200 -400- 700 -1200- 2500 keV

background: *spioffback*, rev 12 + 13
spidiffit -> time dependence
spiskymax: detector ratios free

15-40 keV

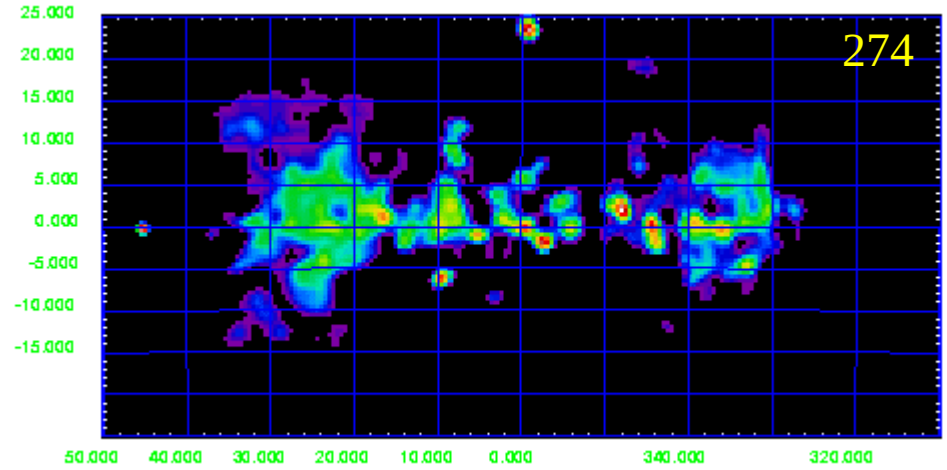

200-400 keV

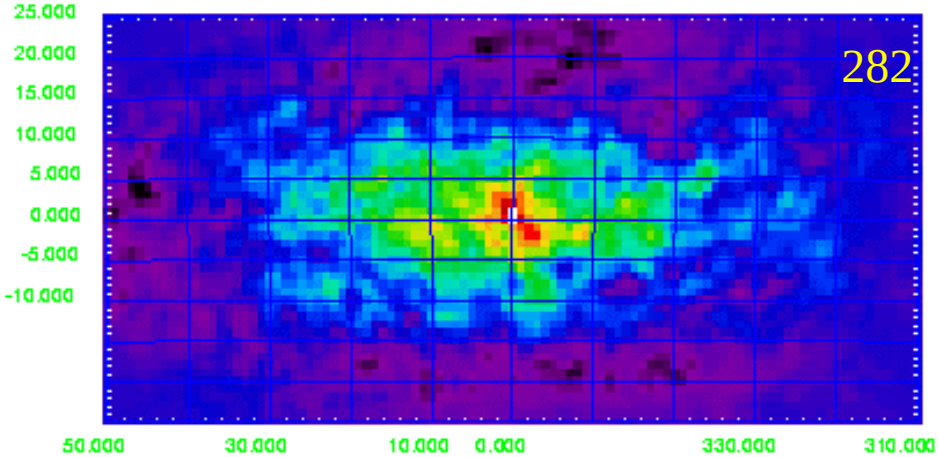

40-100 keV

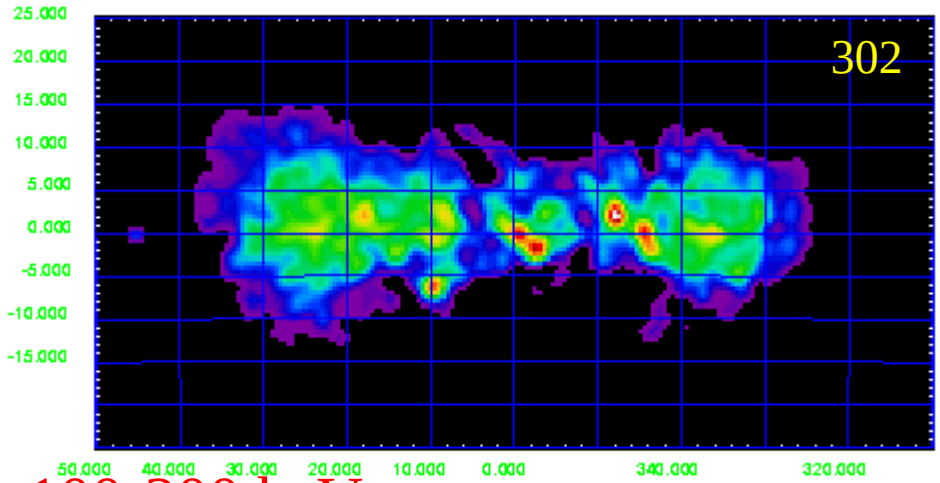

400-700 keV

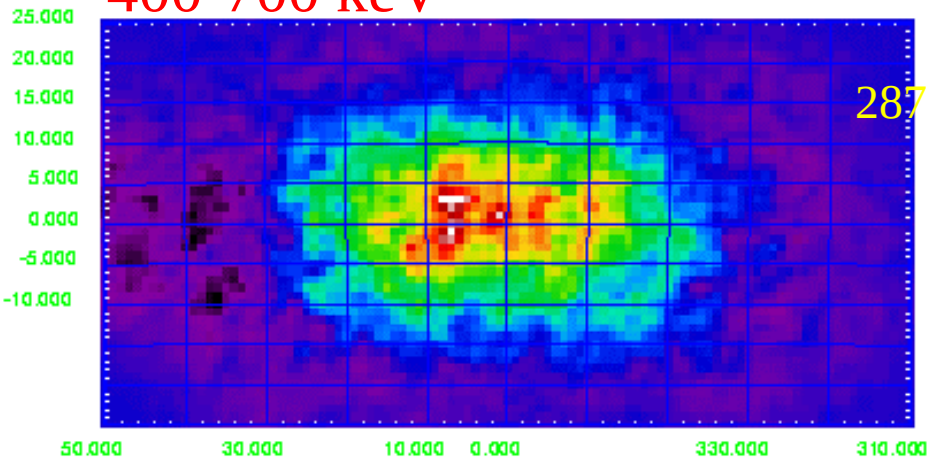

100-200 keV

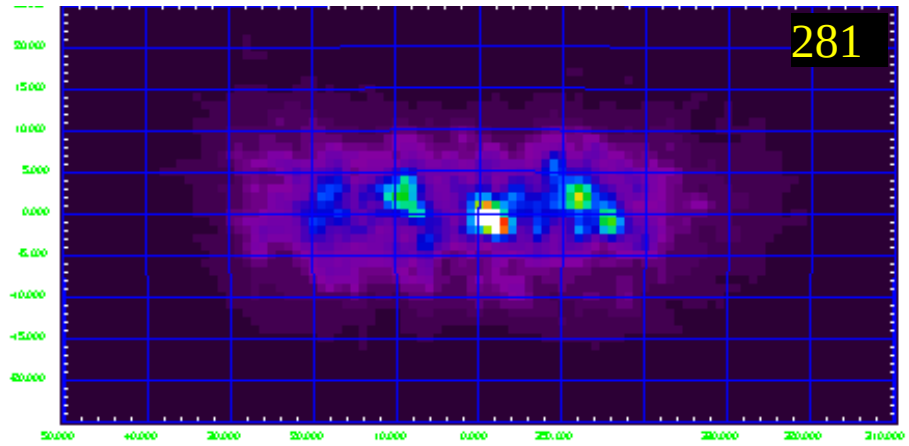

700-1200 keV

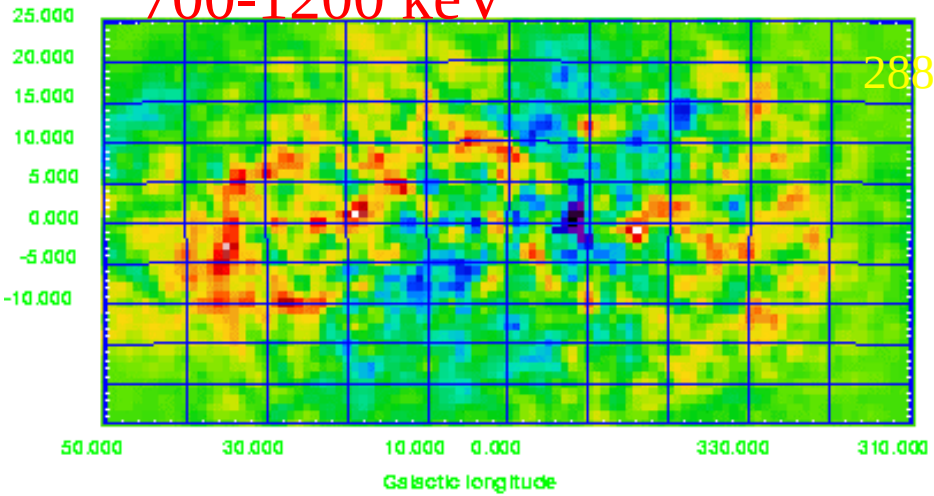

GCDE 15 – 40 keV

spiskymax

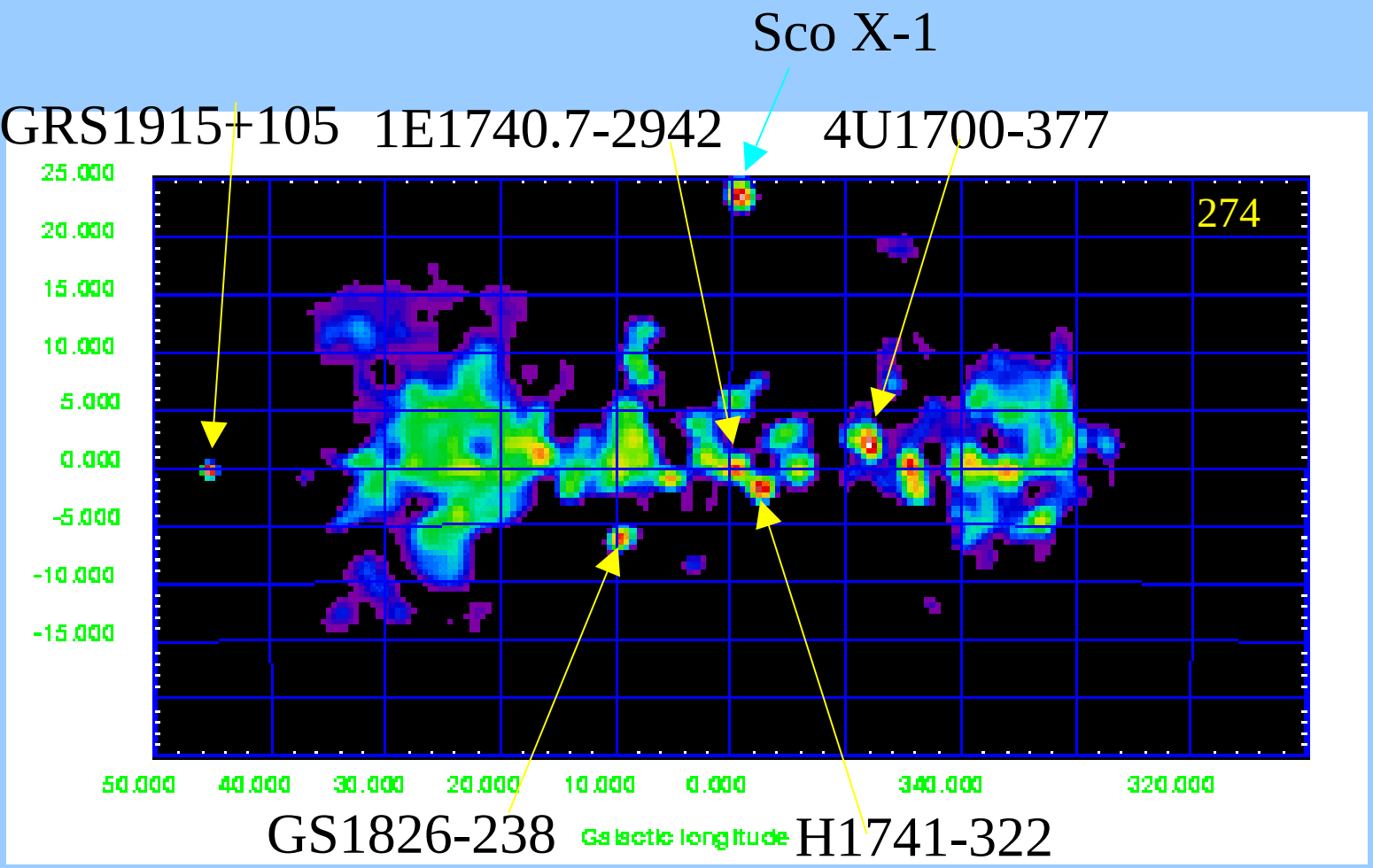

GCDE 40 – 100 keV

spiskymax

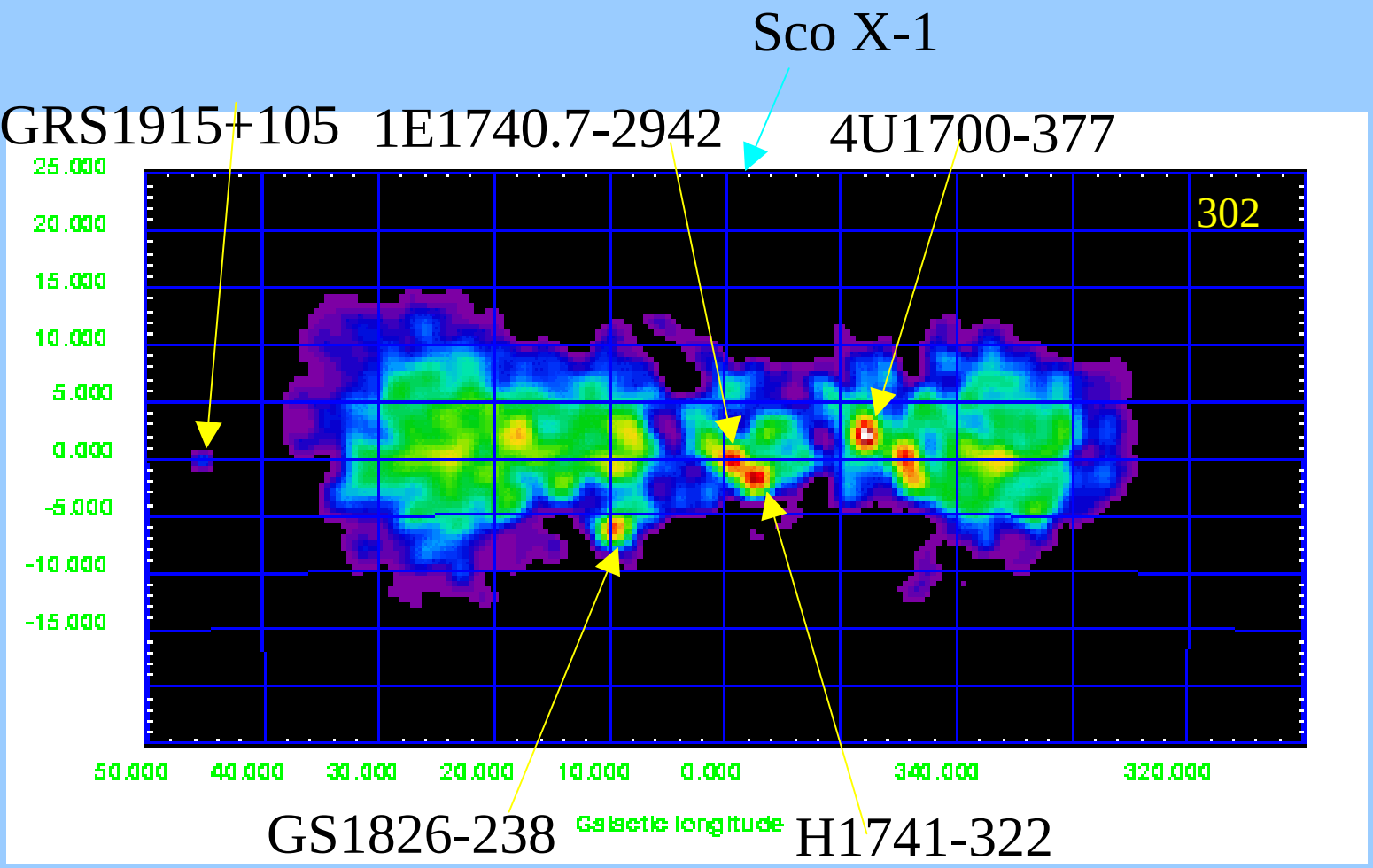

700-1200 keV

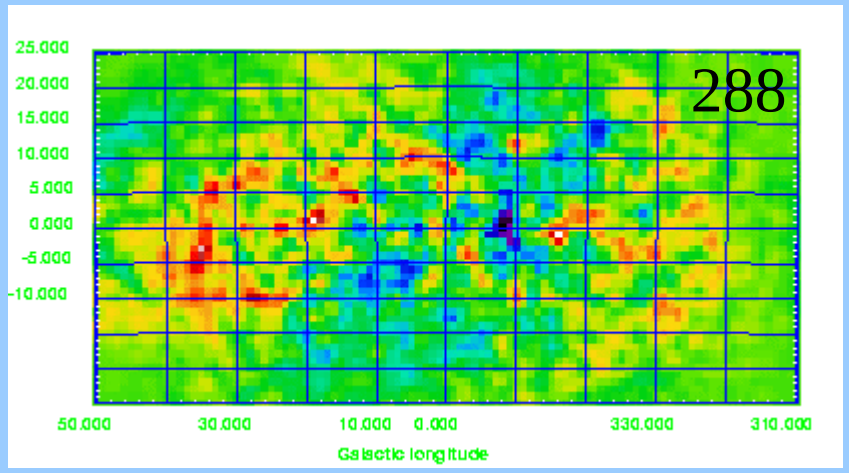

1200-2500 keV

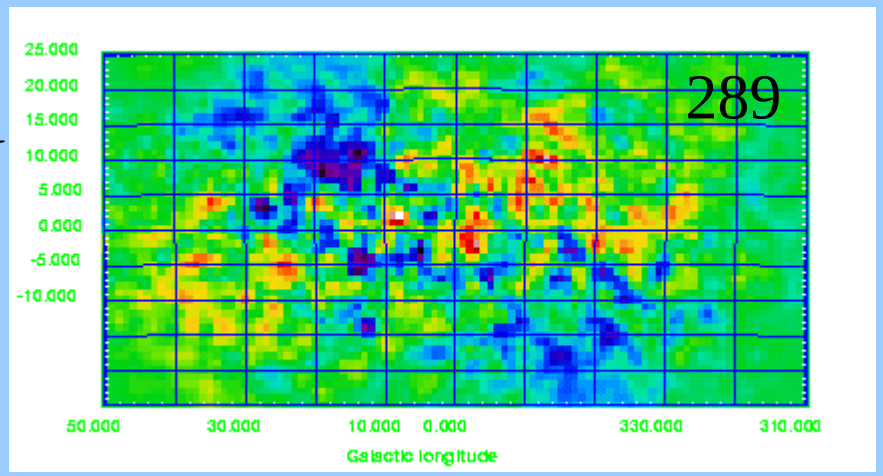

INTEGRAL:

GCDE investigations with SPIROS

Line Sources in ^{44}Ti ??

Andreas von Kienlin MPE

Search for ^{44}Ti-line point sources (GCDE)

- γ-ray lines from SNRs: Cas-A, RX J0852.0-4622
  - COMPTEL: 1.157 MeV ^{44}Ti line with fluxes (2 to 4) $\cdot 10^{-5}$ ph/cm^{2}s
- Prospect of SPI:
  - "measure line profiles from both objects"
  - "… find further, so far unknown SNRs with SPI"
- SPI narrow line sensitivity
  - 68 keV ~ $1 \cdot 10^{-4}$ ph/cm^{2}s → sensitivity degraded, due to strong background line complex at 54-67 keV
  - 78 keV ~ $4 \cdot 10^{-5}$ ph/cm^{2}s
  - 1.157 MeV ~ $4 \cdot 10^{-5}$ ph/cm^{2}s
- For SNR expansion velocities of ~ 3000 km/s:
  - At 78 keV: astrophysical line width in the order of the instrumental energy resolution
  - At 1.157 MeV: broadened line of ~ 25 keV expected
    - ⇨ degradation of SPI's line sensitivity by a factor of about $\times$ 3
- Research topic 3.1 of core program (PIs V.Schönfelder, P. Jean): SPI survey @ 44Ti energies and new sources from survey in 3rd and 4th quadrants

Search for ^{44}Ti-line point sources (GCDE)

- Method used:
  1) Use of ISDC standard SW tools: SPIROS (SPISKYMAX, SPIDIFFIT)
  2) GCDE event binning (SEs + MEs):
     - 50 – 110 keV in 1 KeV bins → 44Ti line @ 78.4 keV
     - 1100 - 1205 keV in 1 keV bins → 44 Ti line @ 1157 keV
  3) Free search for point sources with SPIROS in different energy bands and of different widths
     - 28 - 48 keV IBIS sources → search for keV continuum sources
     - 77 - 80 keV 10 sources → search 78.4 keV Ti-line source
     - 82 - 90 keV 10 sources → neighboring energy band
     - 1155 - 1159 keV 5 sources → search for 1157 keV Ti-line source
     - 1152 -1162 keV 5 sources → search in broader energy band
     - 1100 - 1800 keV 5 sources → search for MeV continuum sources
  4) Comparison of obtained point sources locations
     - continuum source / line source
     - Ti “low” / Ti “high” energy band
     - Energy band of expected line source / neighboring energy bands
  5) Extraction of point source spectra in SPIROS spectral mode
  6) Use SPIDIFFIT with point source model to confirm sources found with SPIROS

SPIROS - search for 5 sources in 77 – 80 keV

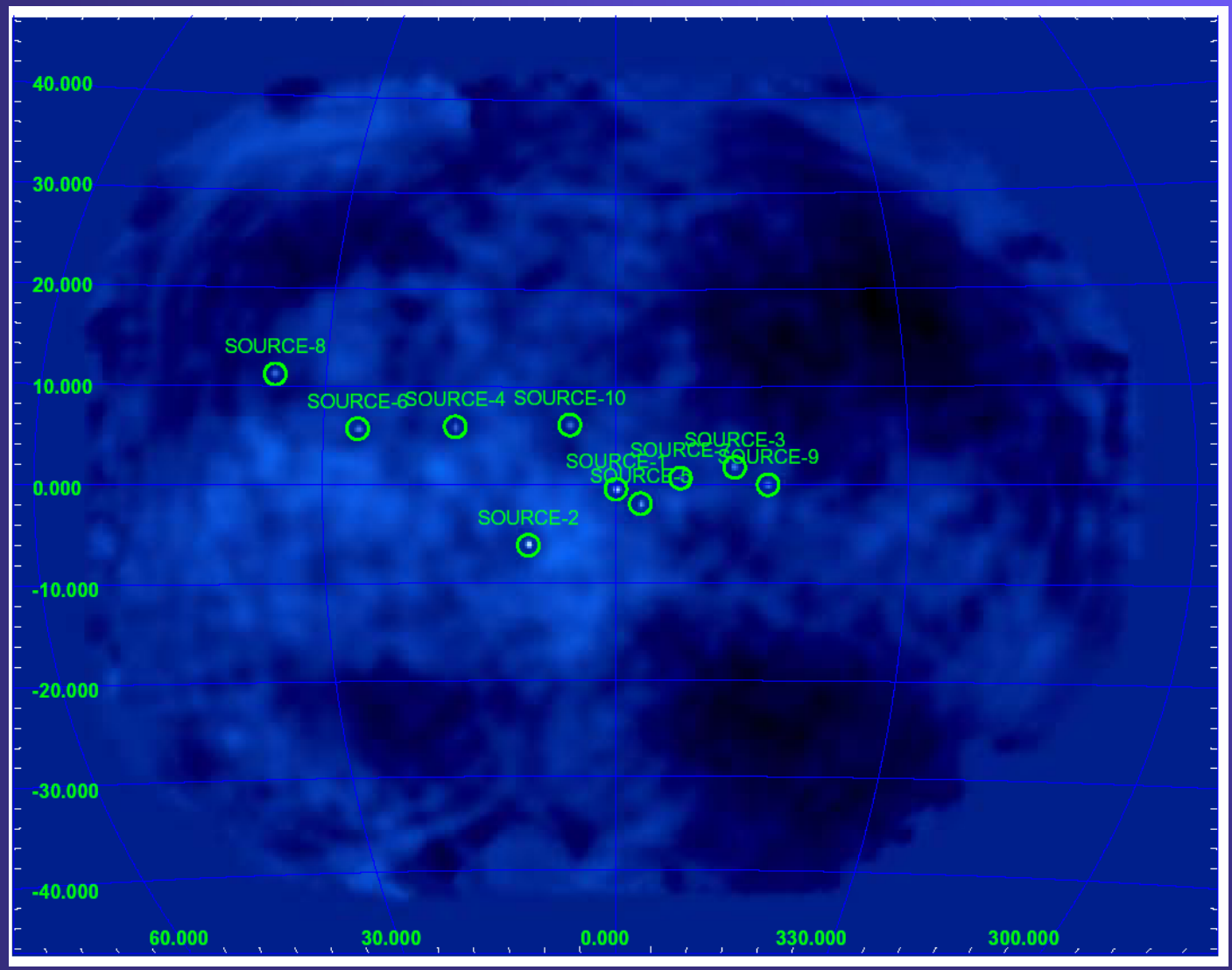

SPIROS - search for 5 sources in 77 – 80 keV

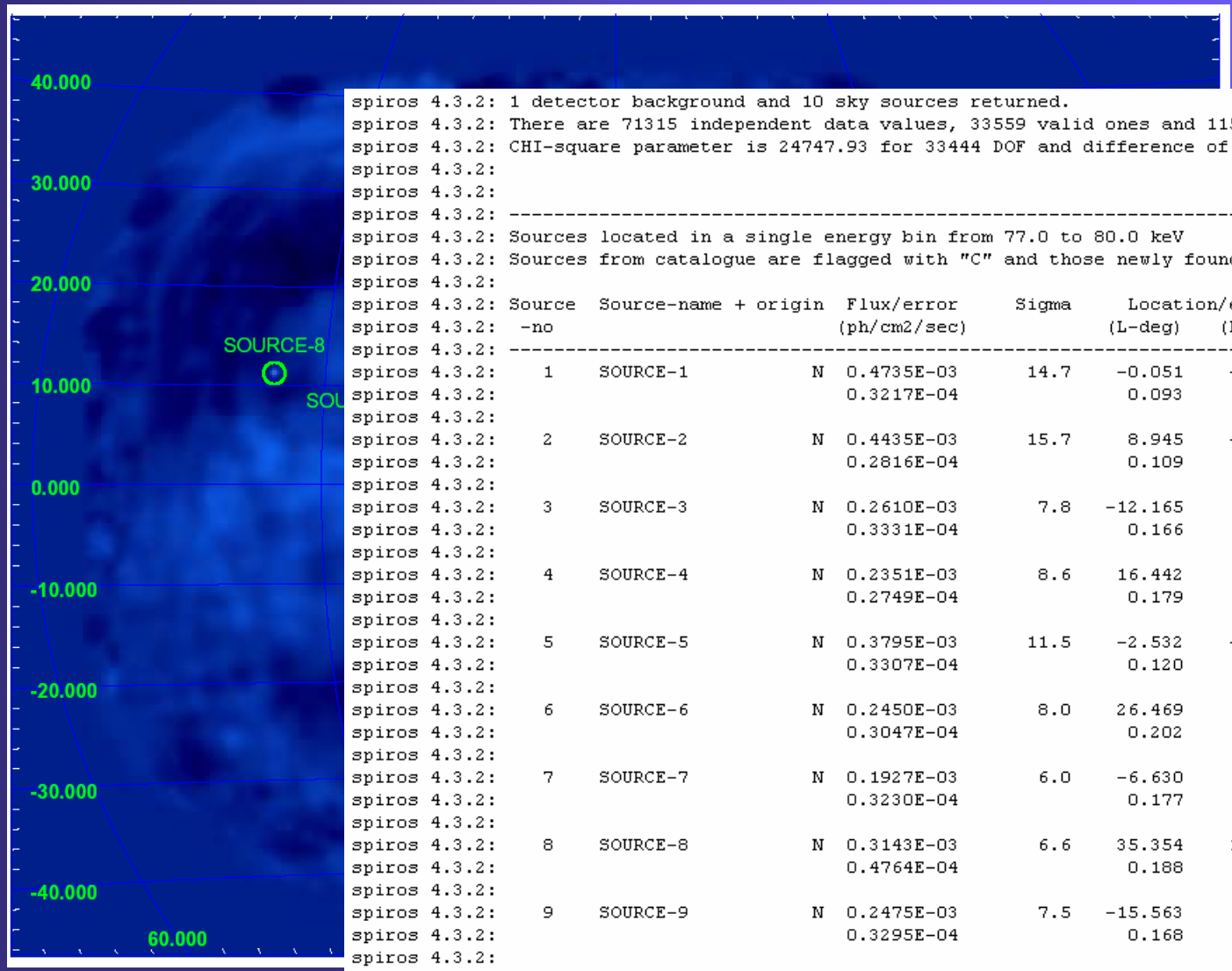


```
spiros 4.3.2: 1 detector background and 10 sky sources returned.
spiros 4.3.2: There are 71315 independent data values, 33559 valid ones and 115 solution variabl
spiros 4.3.2: CHI-square parameter is 24747.93 for 33444 DOF and difference of -33.62 stdev.
spiros 4.3.2:
spiros 4.3.2:
spiros 4.3.2: ------------------------------------------------------------------------------
spiros 4.3.2: Sources located in a single energy bin from 77.0 to 80.0 keV
spiros 4.3.2: Sources from catalogue are flagged with "C" and those newly found with "N"
spiros 4.3.2:
spiros 4.3.2: Source  Source-name + origin  Flux/error     Sigma     Location/error      Width
spiros 4.3.2:  -no                          (ph/cm2/sec)            (L-deg)   (B-deg)    (deg)
spiros 4.3.2: ------------------------------------------------------------------------------
spiros 4.3.2:    1    SOURCE-1           N  0.4735E-03     14.7    -0.051    -0.405     0.000
spiros 4.3.2:                               0.3217E-04              0.093     0.132
spiros 4.3.2:
spiros 4.3.2:    2    SOURCE-2           N  0.4435E-03     15.7     8.945    -6.133     0.000
spiros 4.3.2:                               0.2816E-04              0.109     0.108
spiros 4.3.2:
spiros 4.3.2:    3    SOURCE-3           N  0.2610E-03      7.8   -12.165     1.801     0.000
spiros 4.3.2:                               0.3331E-04              0.166     0.138
spiros 4.3.2:
spiros 4.3.2:    4    SOURCE-4           N  0.2351E-03      8.6    16.442     5.920     0.000
spiros 4.3.2:                               0.2749E-04              0.179     0.179
spiros 4.3.2:
spiros 4.3.2:    5    SOURCE-5           N  0.3795E-03     11.5    -2.532    -1.894     0.000
spiros 4.3.2:                               0.3307E-04              0.120     0.151
spiros 4.3.2:
spiros 4.3.2:    6    SOURCE-6           N  0.2450E-03      8.0    26.469     5.701     0.000
spiros 4.3.2:                               0.3047E-04              0.202     0.162
spiros 4.3.2:
spiros 4.3.2:    7    SOURCE-7           N  0.1927E-03      6.0    -6.630     0.720     0.000
spiros 4.3.2:                               0.3230E-04              0.177     0.214
spiros 4.3.2:
spiros 4.3.2:    8    SOURCE-8           N  0.3143E-03      6.6    35.354    11.202     0.000
spiros 4.3.2:                               0.4764E-04              0.188     0.184
spiros 4.3.2:
spiros 4.3.2:    9    SOURCE-9           N  0.2475E-03      7.5   -15.563     0.023     0.000
spiros 4.3.2:                               0.3295E-04              0.168     0.248
spiros 4.3.2:
spiros 4.3.2:   10    SOURCE-10          N  0.1902E-03      6.6     4.686     6.122     0.000
spiros 4.3.2:                               0.2896E-04              0.192     0.217
spiros 4.3.2:
```

SPIROS - 10 sources in 77 – 80 keV

comparison with sources found by IBIS

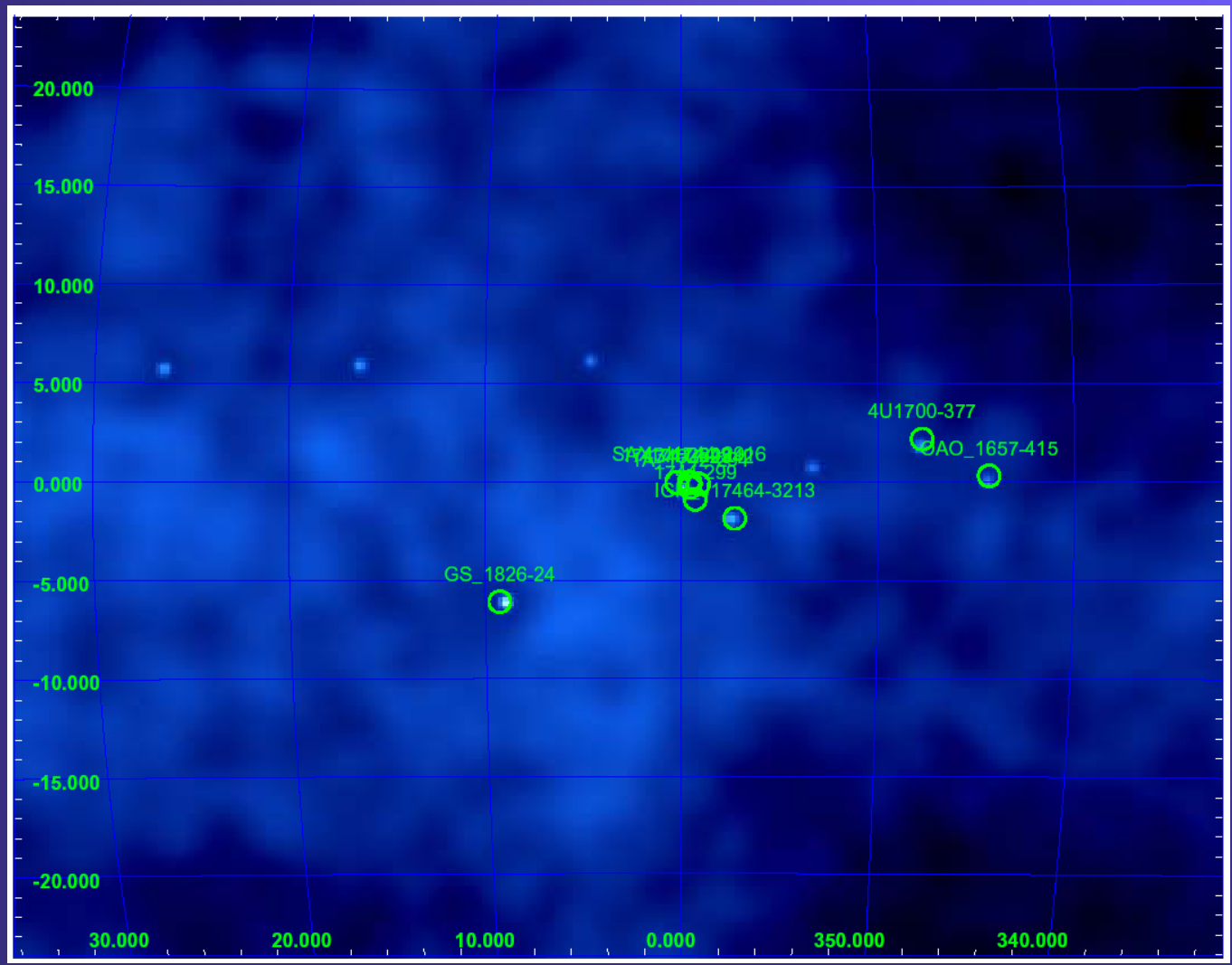

Ge detector 3 spectrum of rev44

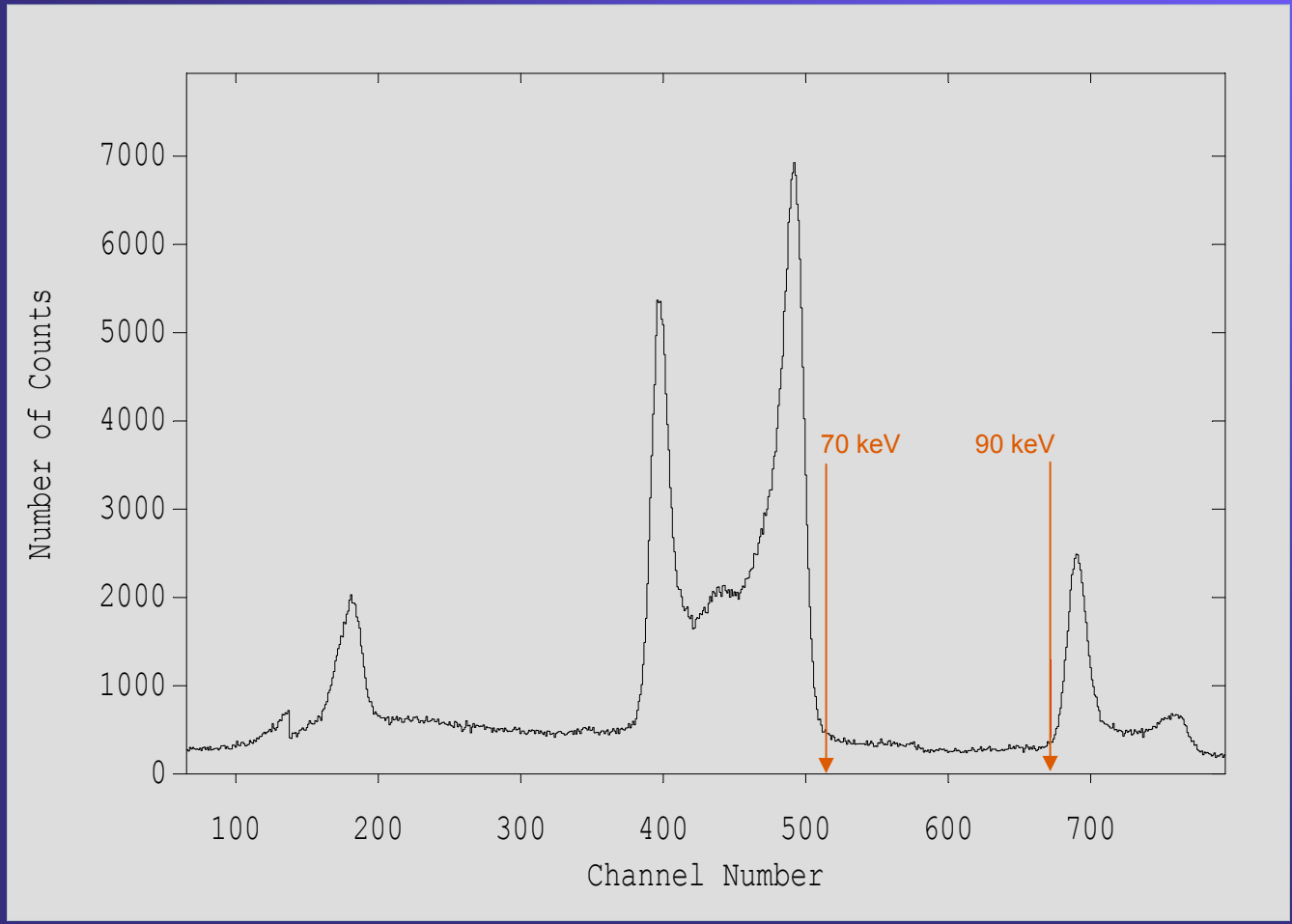

SPIROS - spectra of sources in 77 – 80 keV

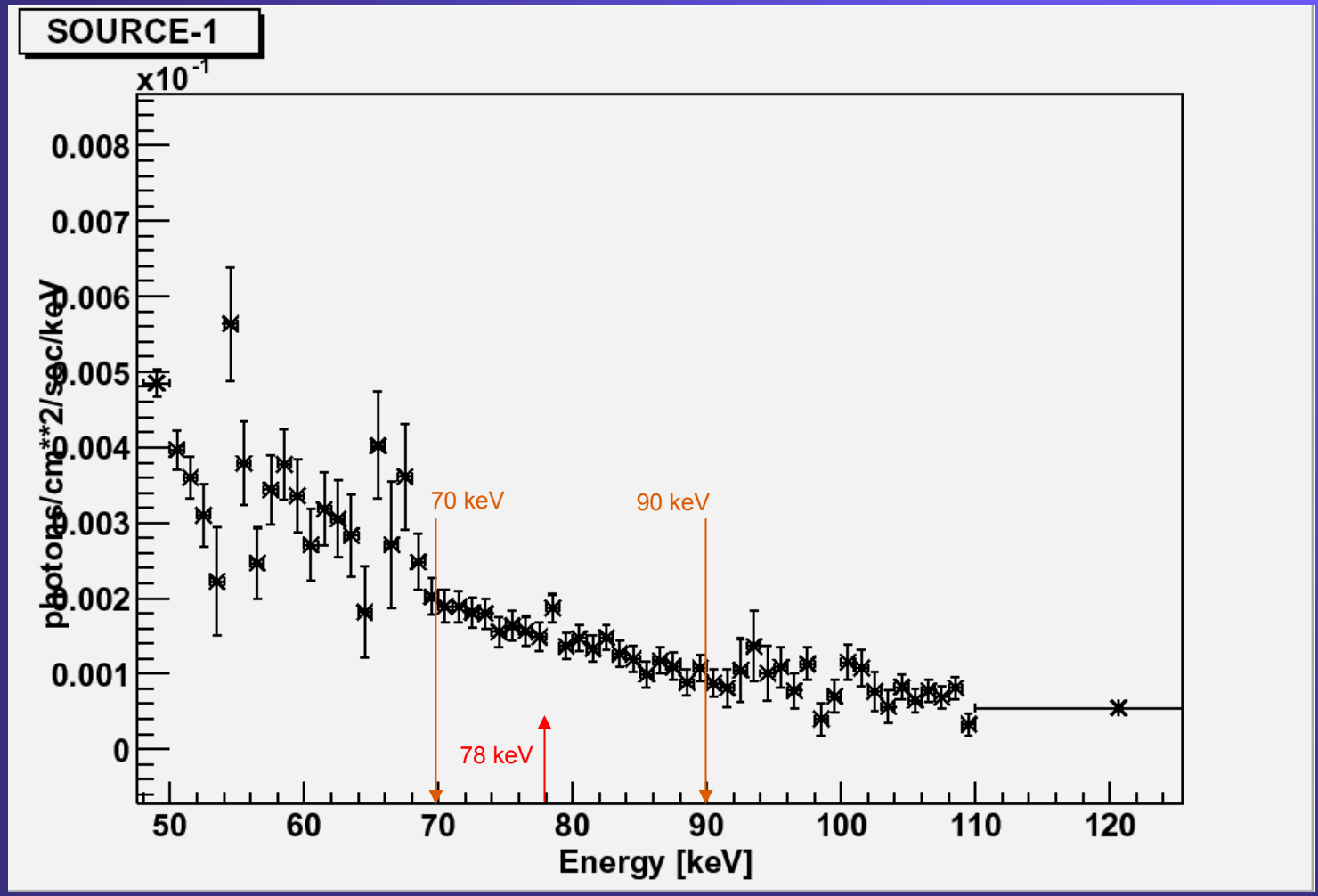

SPIROS - spectra of sources in 77 – 80 keV

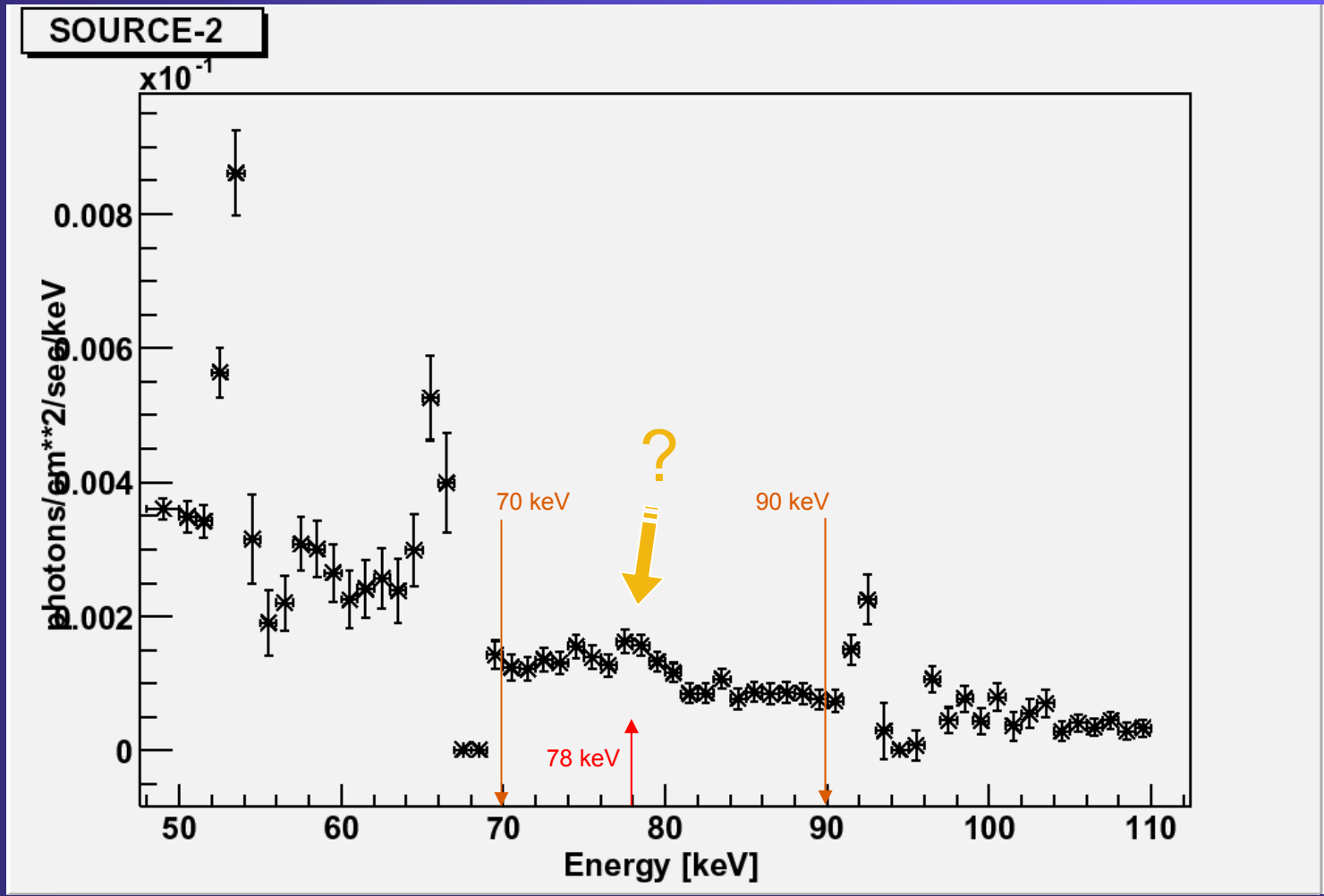

SPIROS - spectra of sources in 77 – 80 keV

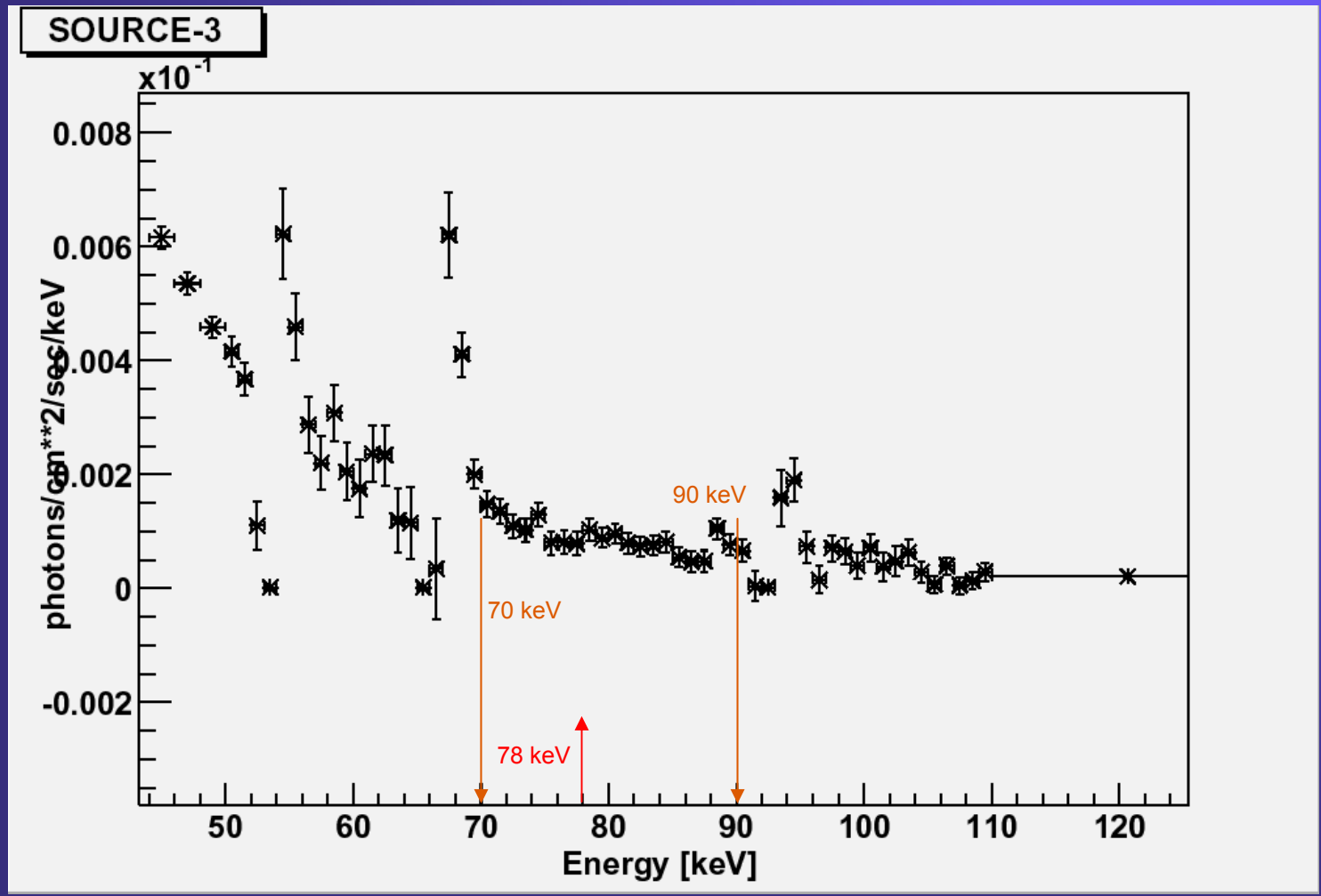

SPIROS - spectra of sources in 77 – 80 keV

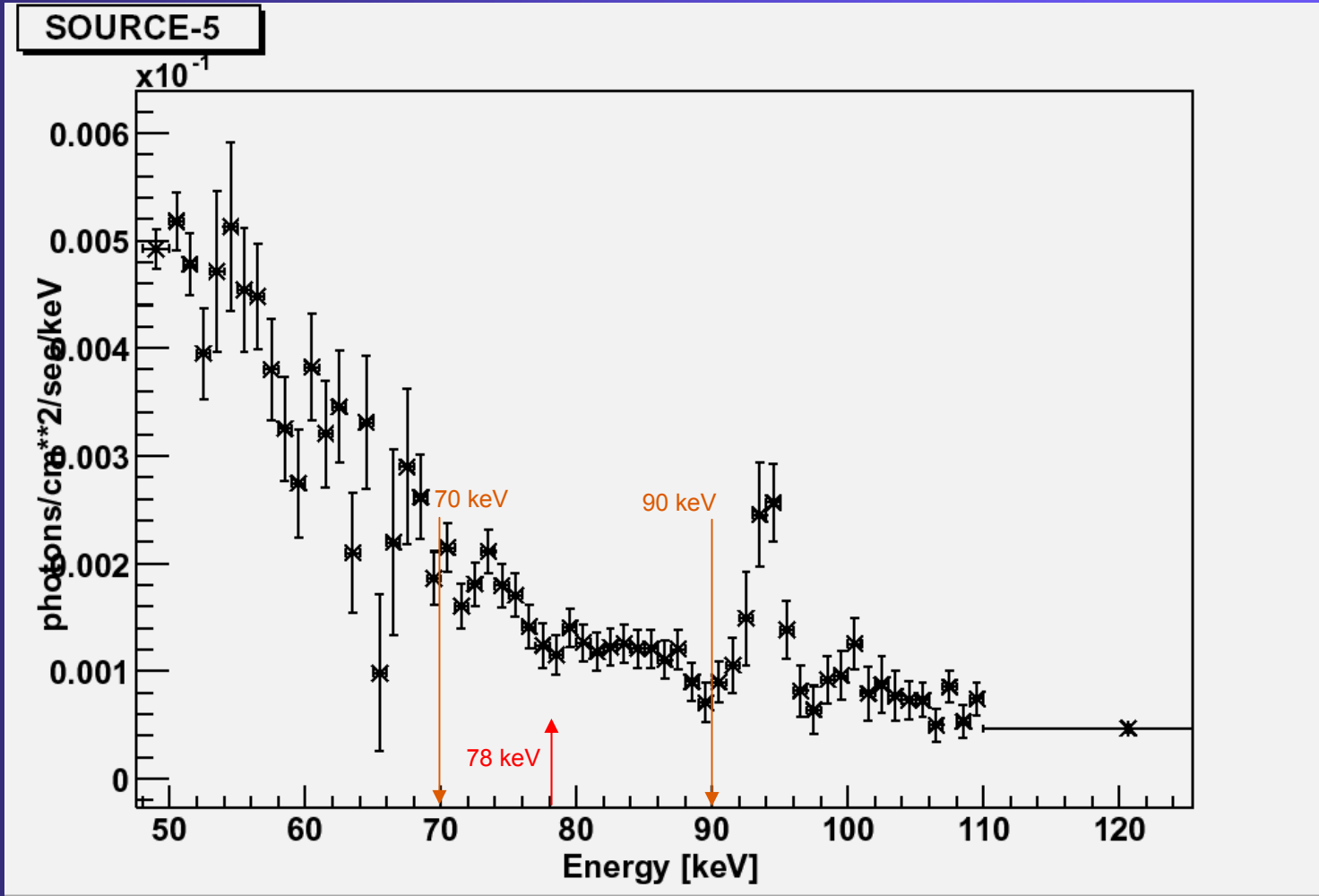

SPIROS - spectra of sources in 77 – 80 keV

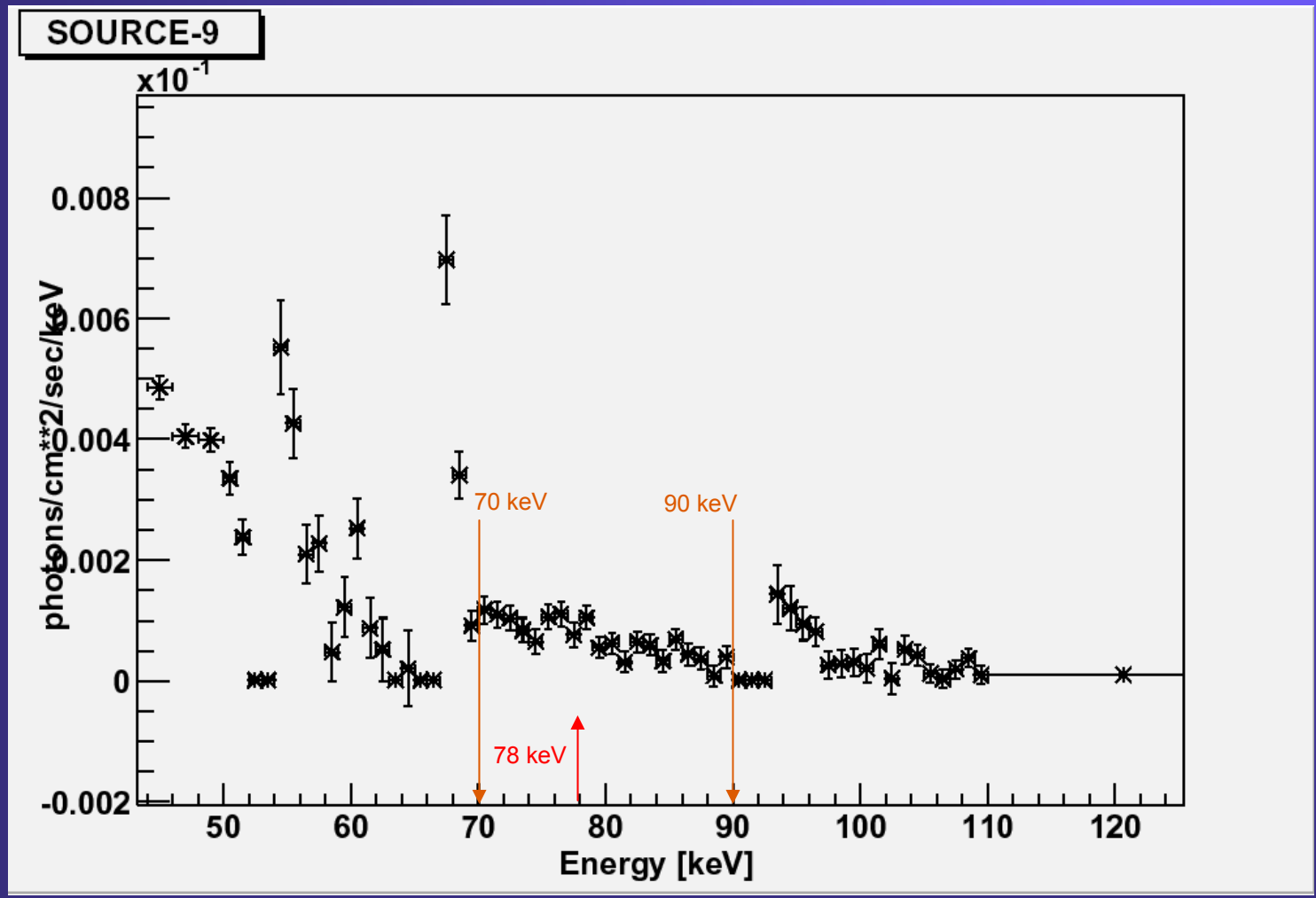

Spectra of Sources 2 with SPIROS and SPIDIFFIT

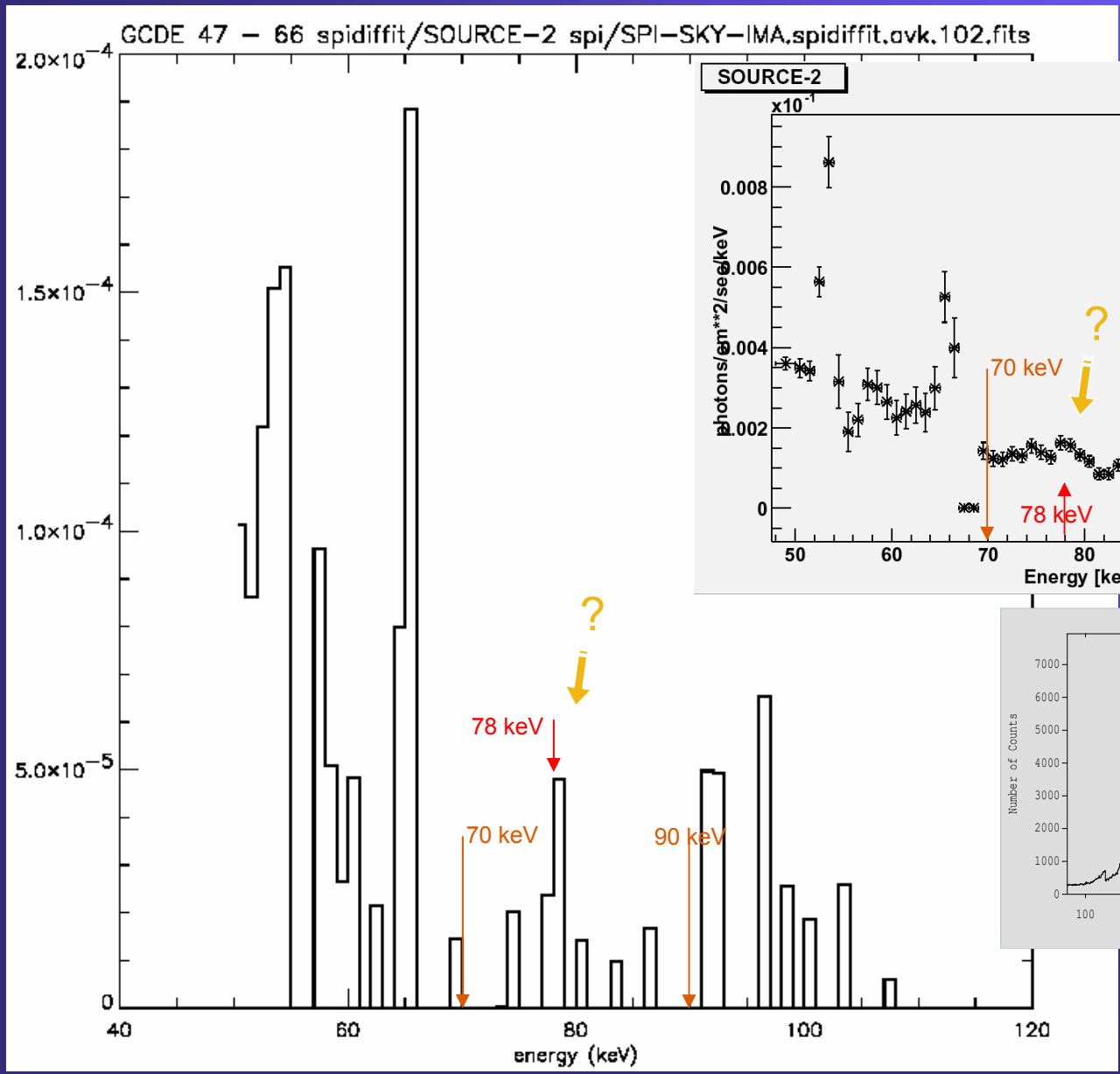

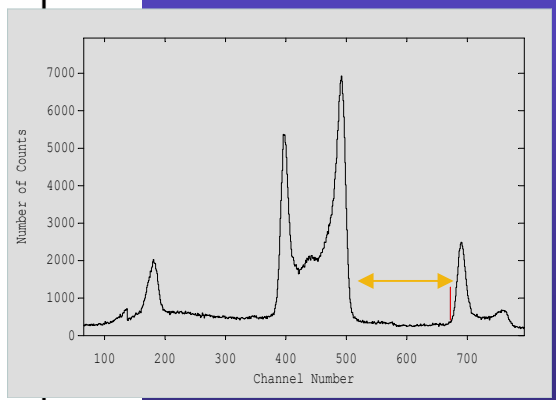

SPIROS - search for 5 sources in 1100-1800 keV

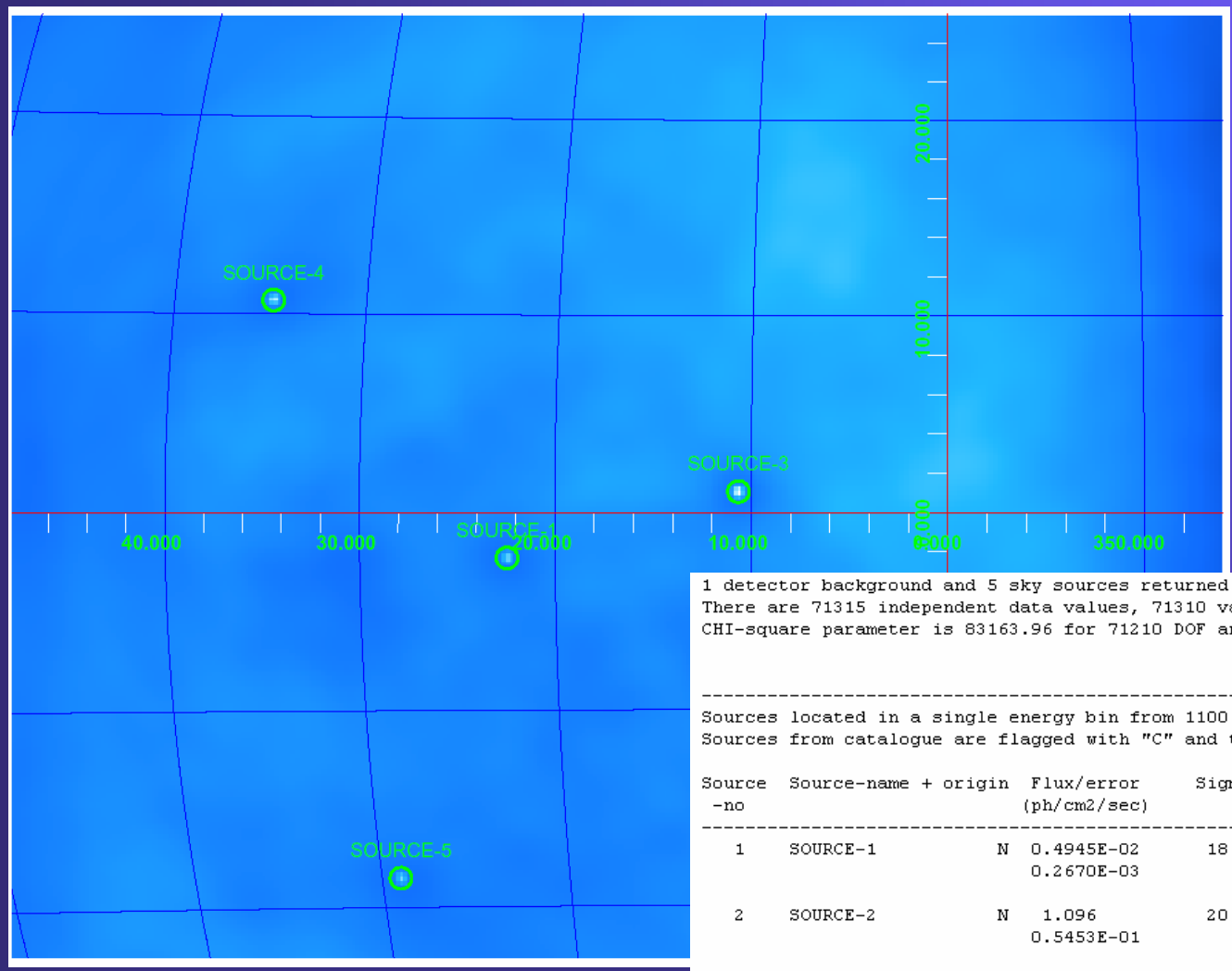

1 detector background and 5 sky sources returned.
There are 71315 independent data values, 71310 valid ones and 100 solution variables.
CHI-square parameter is 83163.96 for 71210 DOF and difference of 31.68 stdev.

Sources located in a single energy bin from 1100.0 to 1801.0 keV
Sources from catalogue are flagged with "C" and those newly found with "N"

Source -no	Source-name + origin		Flux/error (ph/cm2/sec)	Sigma	Location/error (L-deg)	(B-deg)	Width (deg)
1	SOURCE-1	N	0.4945E-02	18.5	22.460	-2.292	0.000
			0.2670E-03		0.122	0.083	
2	SOURCE-2	N	1.096	20.1	56.568	-17.227	0.000
			0.5453E-01		0.204	0.333	
3	SOURCE-3	N	0.7448E-02	28.4	10.653	1.062	0.000
			0.2618E-03		0.107	0.116	
4	SOURCE-4	N	0.9648E-02	23.3	34.859	10.686	0.000
			0.4142E-03		0.081	0.093	
5	SOURCE-5	N	0.9256E-02	19.2	29.016	-18.496	0.000
			0.4818E-03		0.107	0.122	

SPIROS - 5 sources in 1100-1800 keV

comparison with sources found by IBIS

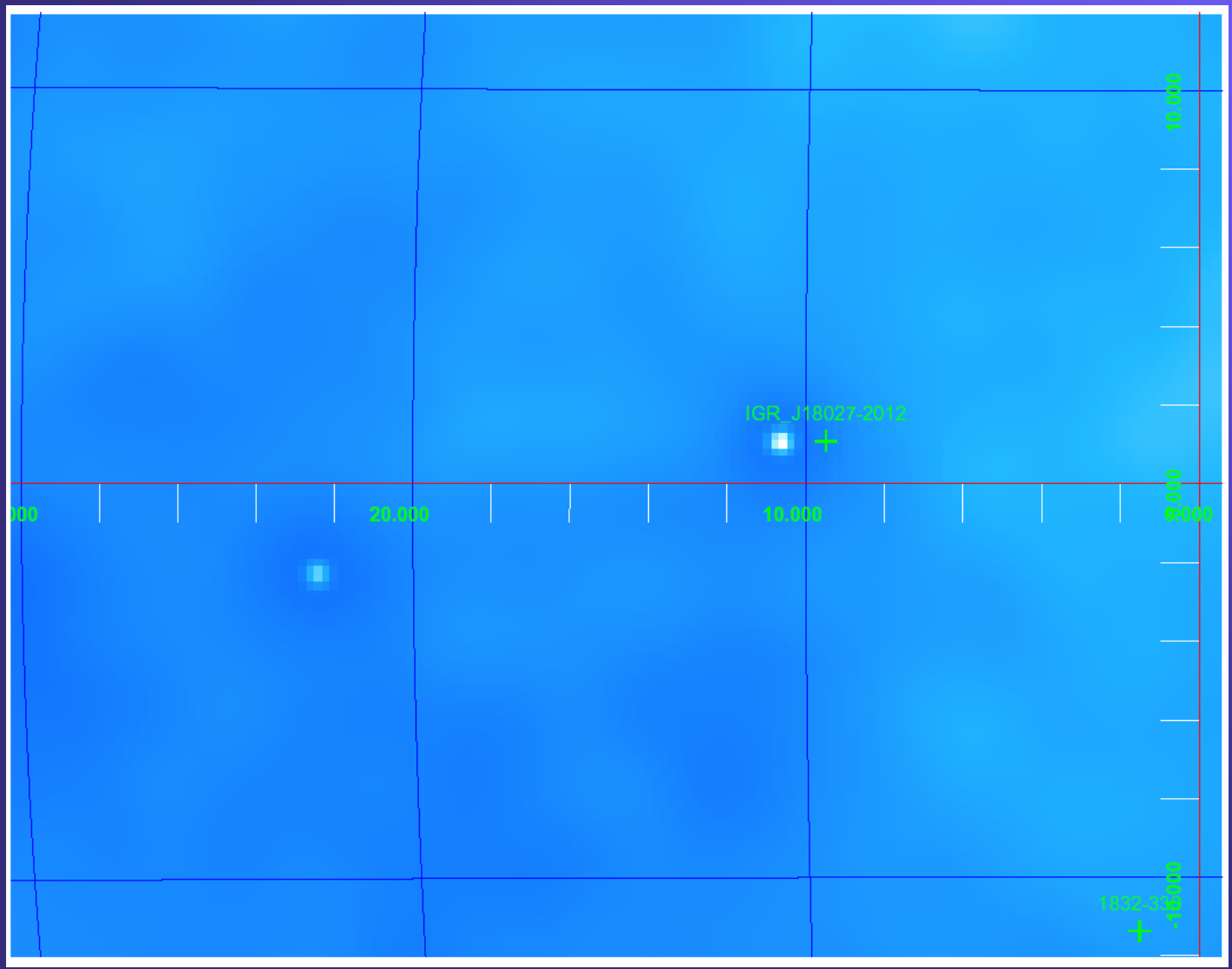

SPIROS - search for 5 sources in : 1152-1162 keV

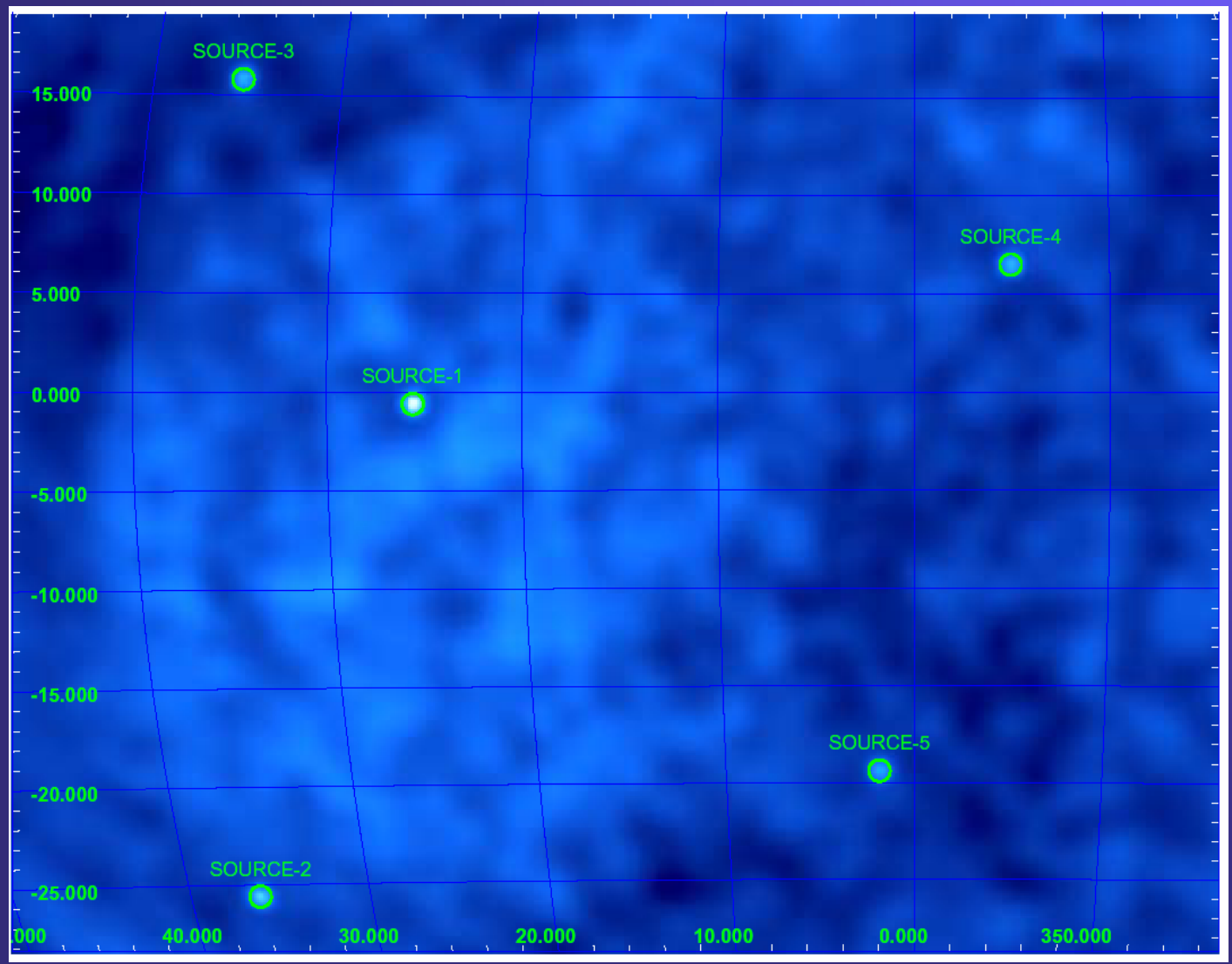

SPIROS - search for 5 sources in : 1152-1162 keV

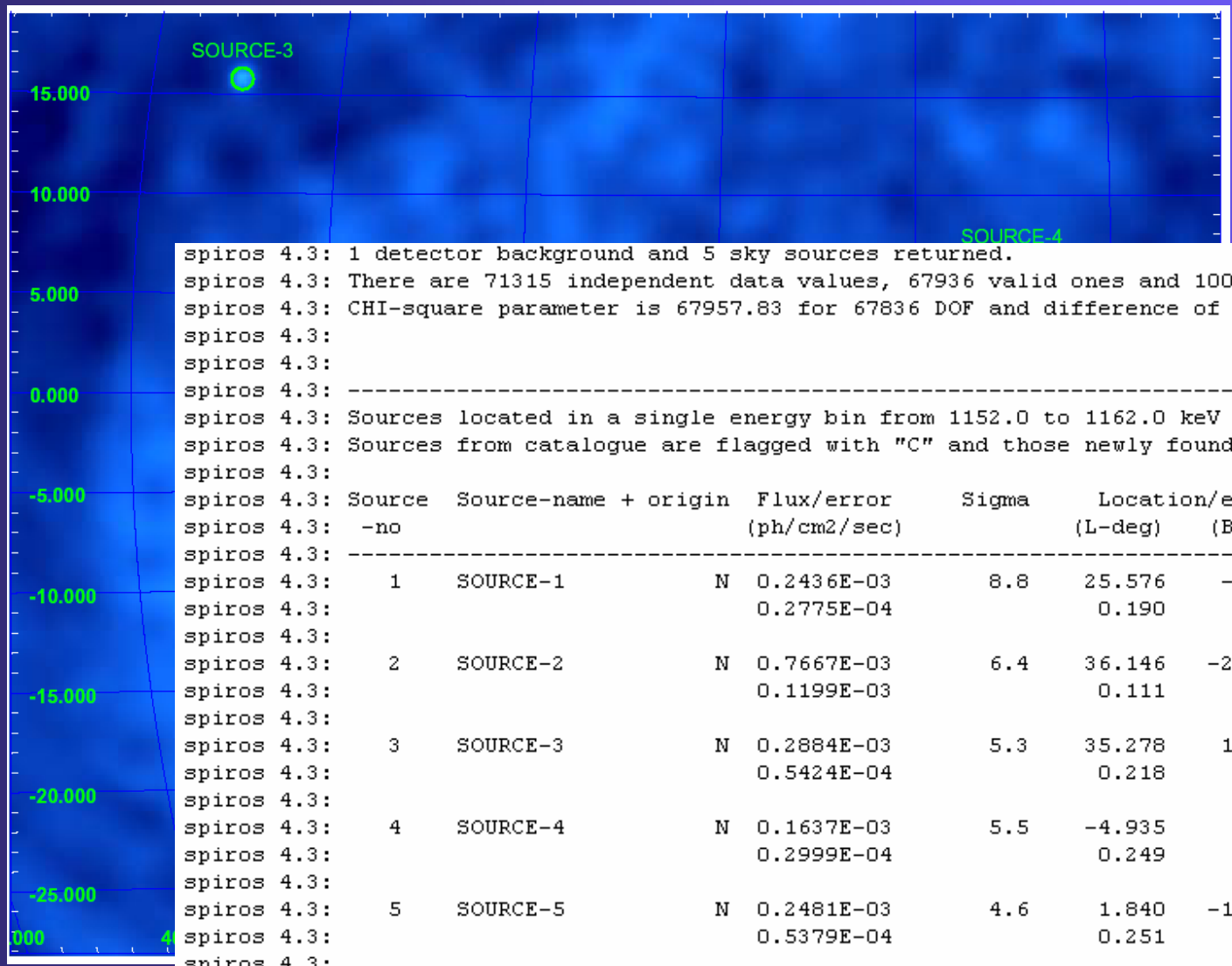


```
spiros 4.3: 1 detector background and 5 sky sources returned.
spiros 4.3: There are 71315 independent data values, 67936 valid ones and 100 solution variables.
spiros 4.3: CHI-square parameter is 67957.83 for 67836 DOF and difference of 0.33 stdev.
spiros 4.3:
spiros 4.3:
spiros 4.3: ------------------------------------------------------------------------------
spiros 4.3: Sources located in a single energy bin from 1152.0 to 1162.0 keV
spiros 4.3: Sources from catalogue are flagged with "C" and those newly found with "N"
spiros 4.3:
spiros 4.3: Source  Source-name + origin  Flux/error     Sigma     Location/error      Width
spiros 4.3:  -no                         (ph/cm2/sec)           (L-deg)   (B-deg)     (deg)
spiros 4.3: ------------------------------------------------------------------------------
spiros 4.3:    1    SOURCE-1           N  0.2436E-03      8.8    25.576    -0.606     0.000
spiros 4.3:                               0.2775E-04             0.190     0.262
spiros 4.3:
spiros 4.3:    2    SOURCE-2           N  0.7667E-03      6.4    36.146   -25.602     0.000
spiros 4.3:                               0.1199E-03             0.111     0.110
spiros 4.3:
spiros 4.3:    3    SOURCE-3           N  0.2884E-03      5.3    35.278    15.785     0.000
spiros 4.3:                               0.5424E-04             0.218     0.252
spiros 4.3:
spiros 4.3:    4    SOURCE-4           N  0.1637E-03      5.5    -4.935     6.489     0.000
spiros 4.3:                               0.2999E-04             0.249     0.228
spiros 4.3:
spiros 4.3:    5    SOURCE-5           N  0.2481E-03      4.6     1.840   -19.371     0.000
spiros 4.3:                               0.5379E-04             0.251     0.308
spiros 4.3:
```

SPIROS - 5 sources in 1152-1162 keV
comparison with sources found in 1100 – 1800 keV

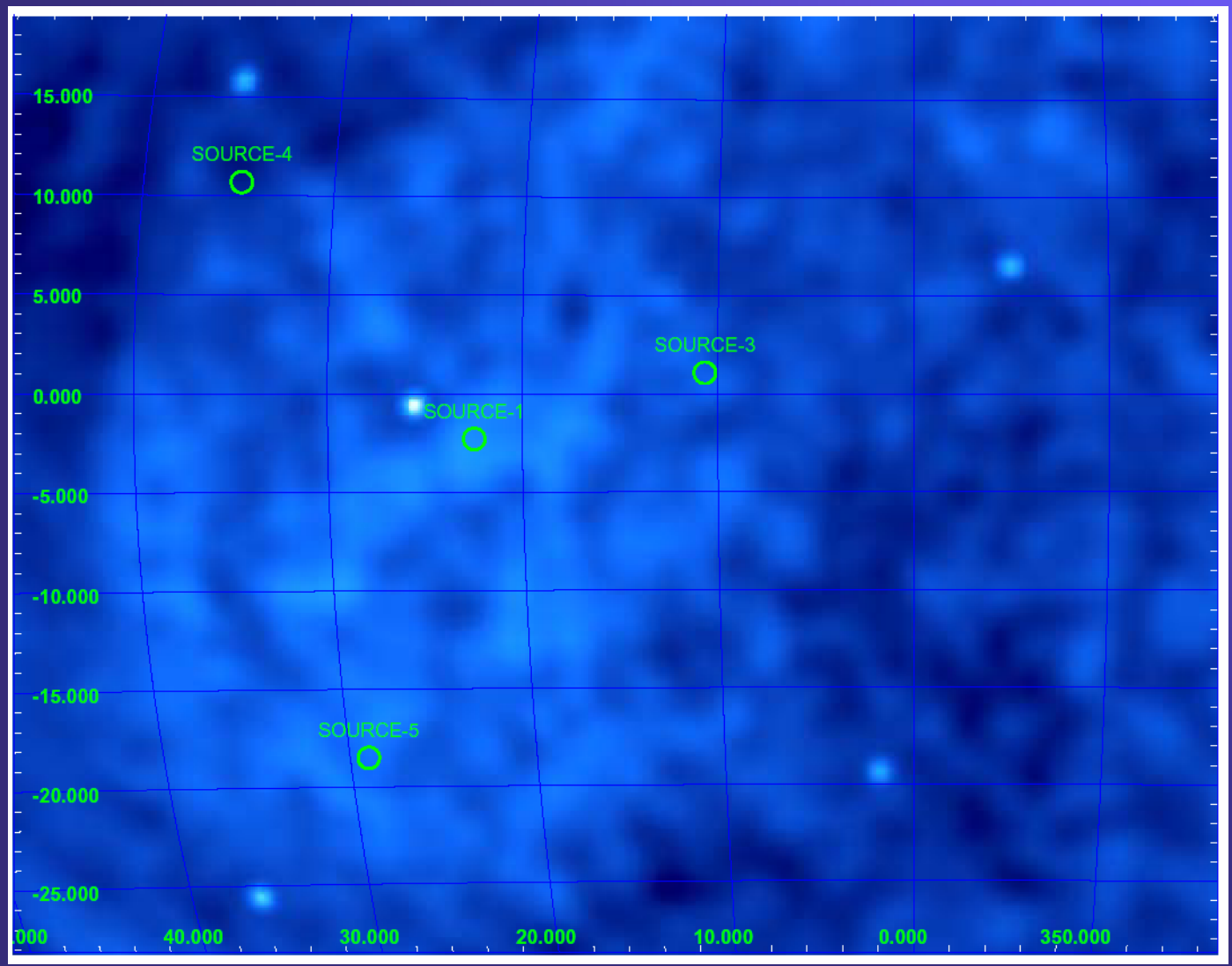

Looking for ^{60}Fe in the GCDE

-

via ^{26}Al

(according the RHESSI announcement of ^{60}Fe detection at the Seeon meeting, ^{60}Fe should be visible at ~ 15% intensity of the 1809 flux ....)

Energy Calibration

- Used 7 Lines for energy calibration – optimized for the 500keV – 1.8 MeV range (following G. Weidenspointner)

438.6 keV	584.5 keV	882.5 keV
1014.4 keV	1124.5 keV	1368.6 keV
	1779.0 keV	

- The whole study uses single events only so far, since the not-quite-understood energy calibration < 200 keV is likely to cause problems with a good calibration of multiple events at all energies!
- Quadratic energy calibration determined & applied in the ISDC gaincor.

„The Plan“

- ^{26}Al should be clearly detectable in the full GCDE
- „learn“ on ^{26}Al, then look for ^{60}Fe emission using the same method(s)

- (so far) emphasis on the model fitting approach *spidiffit* by A. Strong;
  background from *spioffback* (determines detector ratios) and *spiback*/DFEE (gives time evolution)

- For ^{60}Fe, Giselher Lichti is looking at „light bucket“ (on/off) methods – using the same datasets

First Steps

- Spidiffit w/ COBE map, background from spioffback (Crab rev. 43-45), analyze rev. 46-63 (w/o 48,50,58) turned out wrong energy calibration on rev. 62-63
- Again, using only rev 46-61: better ;-)
- So far, so good ....

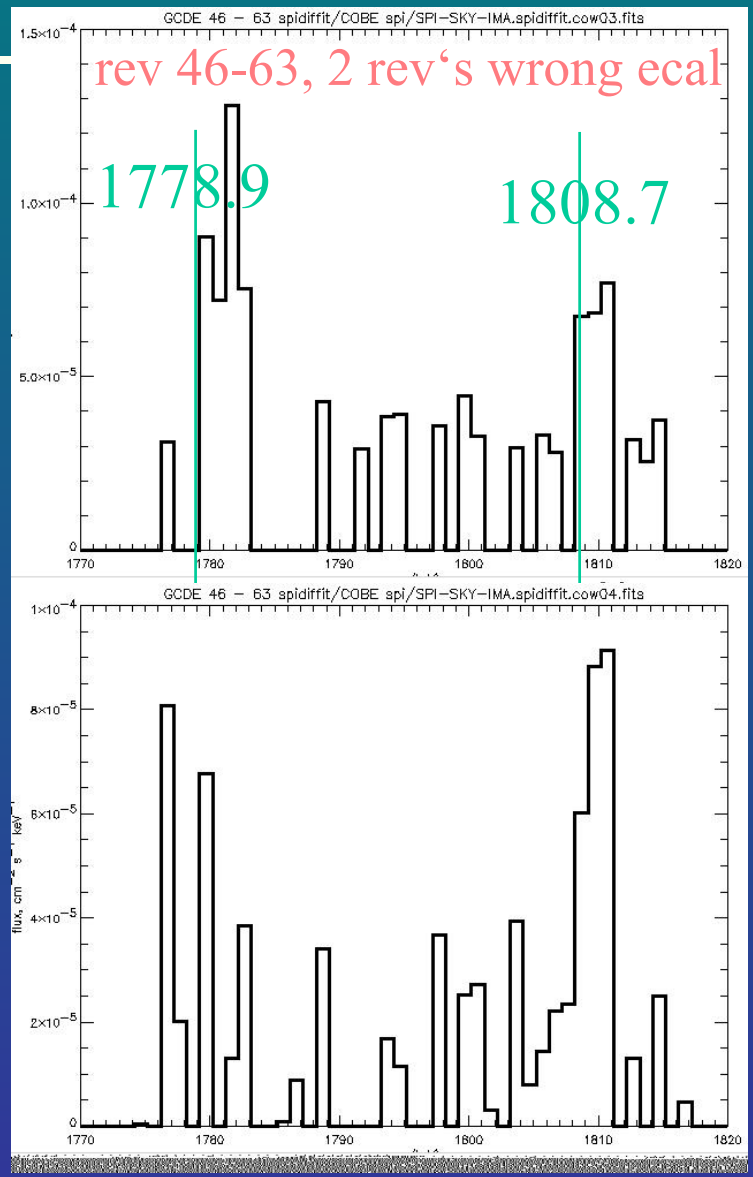

More: Rev 46-61

- Reduction of bg in 1778.9 keV line suggests Al signal above residual from background feature; flux level reasonable
- Attempt at the 1173 keV line (identical meth.)

So with ~ ¼ of the data there's possibly something ...

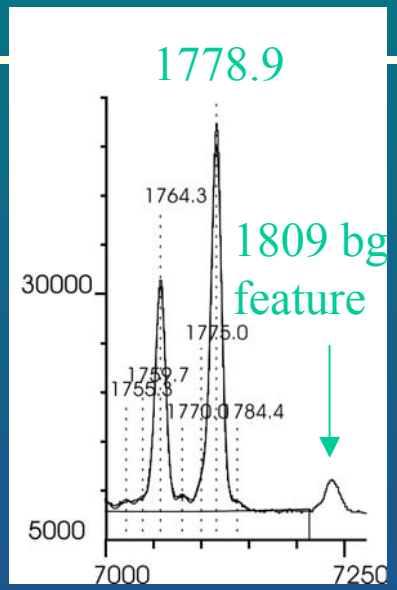

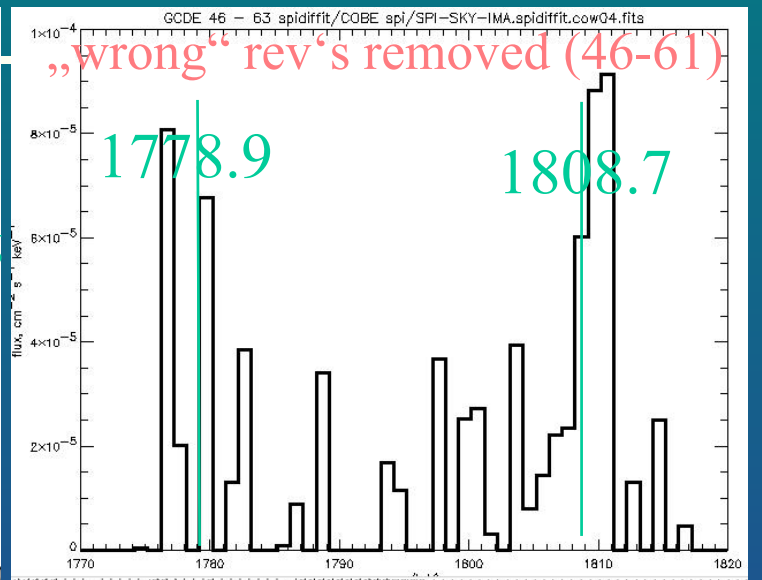

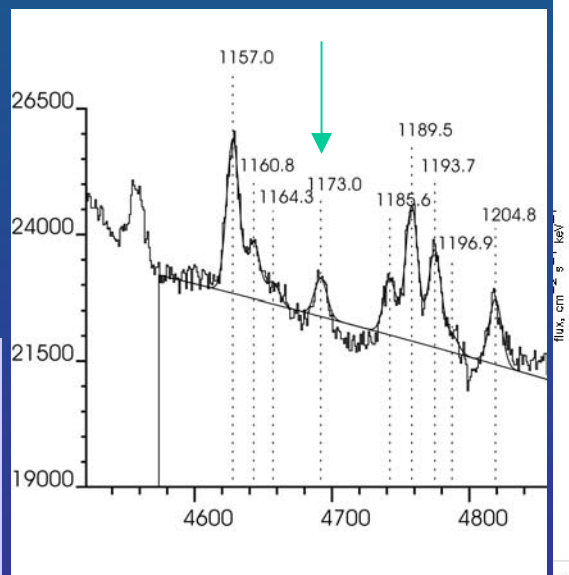

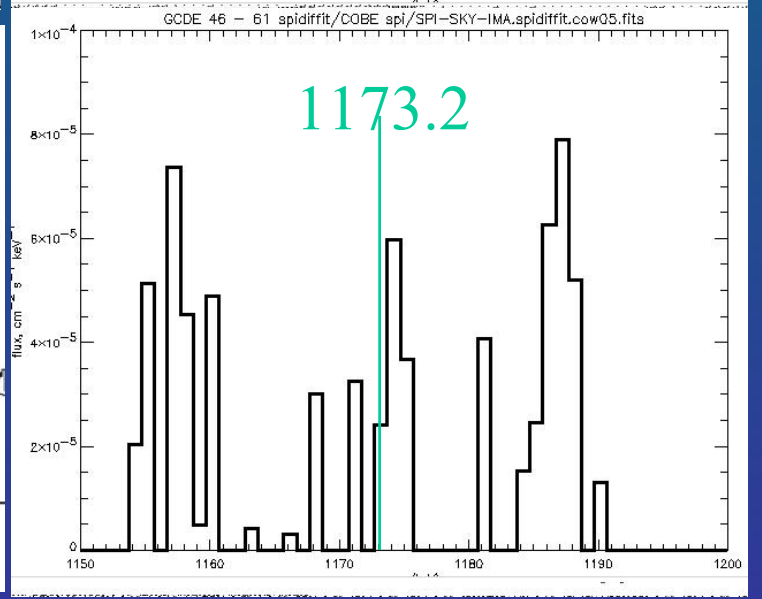

Use all „det 0-18“ data rev 46-66

- Results get worse !
  Full GCDE does not reveal 1809 at all if one takes the jitter at 1782-1803 keV as measure of uncertainty...

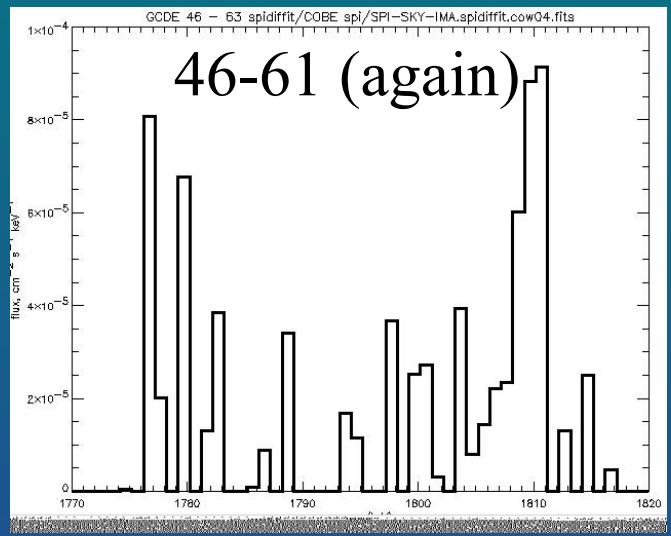

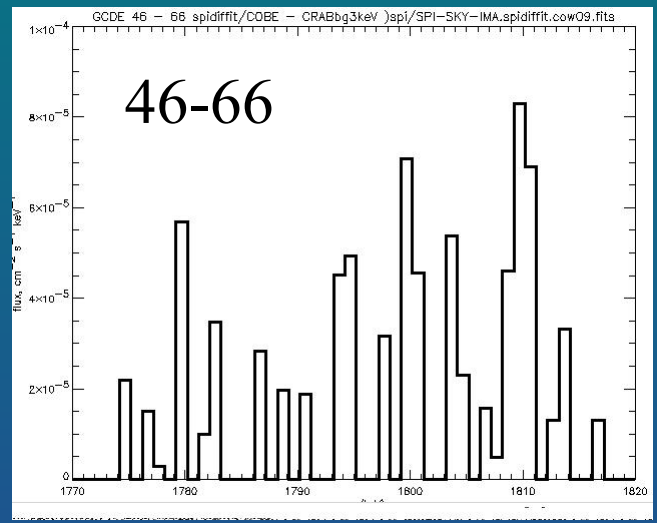

- rev 62-66 alone

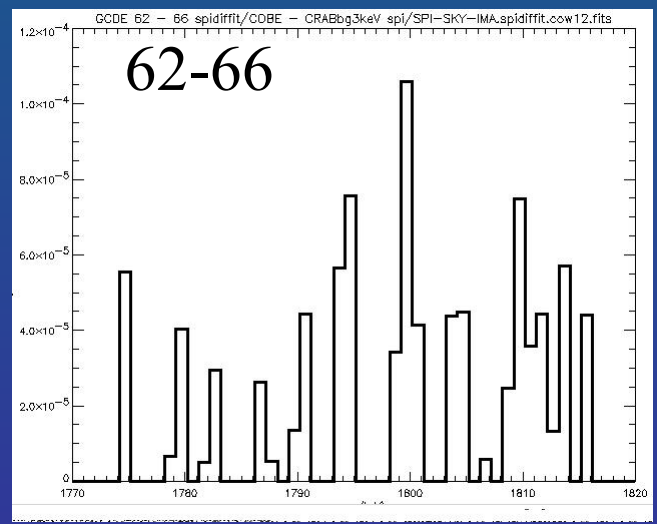

Findings

- Omitting a single revolution from the 62-66 block does not help – not a short time frame „to blame“
- *spioffback* allows averaging over several bins in background for better statistics – tried 1,3,5 keV but does not make difference for det 0-18 as enough counts are available
- Results using COMPTEL (maxent) Al map as template rather than the COBE map do not change much

- Tried a time-dependent background method as well (*spiback*/DFEE), 19 det rates relative to each other are free to vary here (19 free par‘s per energy bin). – Spectral shape no „better“, generally Al flux levels lower.

Next Steps

- For *spioffback*, get BG measurements from later revolutions
  (agreement from PIs obtained, technical method at ISDC to be found ;-(( )
- Understand how the „line feature“ around 1800 keV appears in the later-revolution reconstructions
  (need even better energy calibration? Other explanation?)
- Use J. Knödlseder‘s software and spidiffit/spiback and spidiffit/spioffback on the same data to better understand differences/systematics

- Other good suggestions welcome ;-)

This is definitely *work in progress* ...

Search for the Galactic ^{60}Fe Line (preliminary!)

Giselher Lichti, Andreas von Kienlin &
Cornelia Wunderer

Used Data & Analysis Tool

- Data of the GCDE were used:
  - Orbits: 47 – 60 (without 48, 50 & 58)
    - Pointings: 0 – 838
    - Total exposure time: ~2 000 000 s
  - Background from the Crab observations:
    - Pointings: 0 - 265
- Data selection
  - all single events (detectors 0 – 18)
  - all multiple events (detectors 19 – 84)
- Line-fitting software of Roland Diehl was used
  - after background subtraction a line was fitted at the two ^{60}Fe lines

Fit-Energy Ranges & Calibration

- The following fit-energy ranges around the two ^{60}Fe lines (at 1173.24 keV and 1332.5 keV) were used:
  - 1150 – 1195 keV
  - 1320 – 1342 keV
- The energy calibration of Cornelia Wunderer was used.
- Counts were normalized to the fit-region counts

Spectra of 1173.2 keV Line

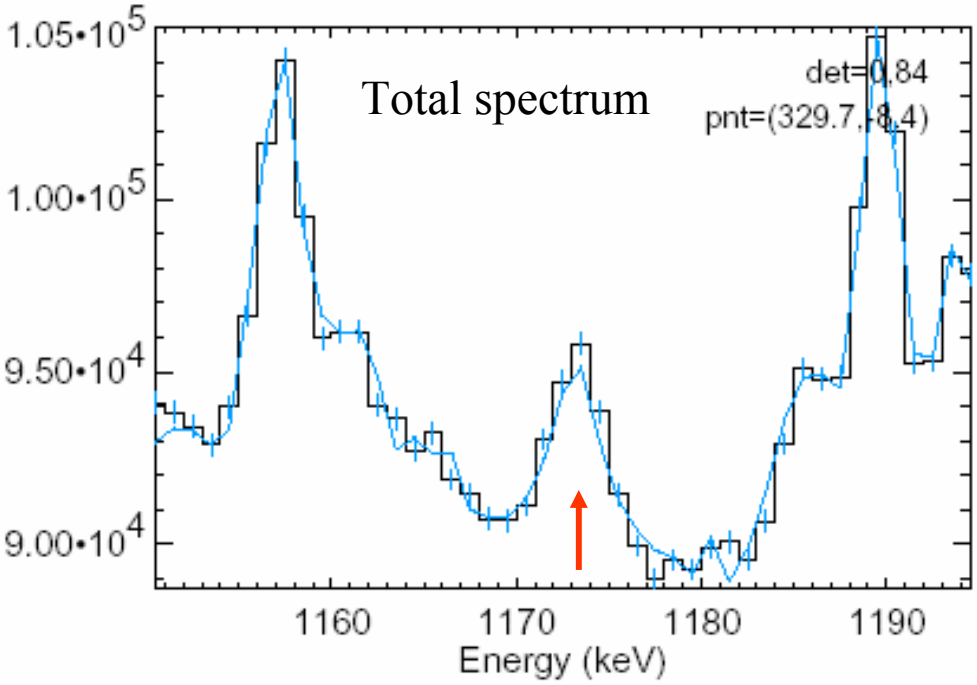

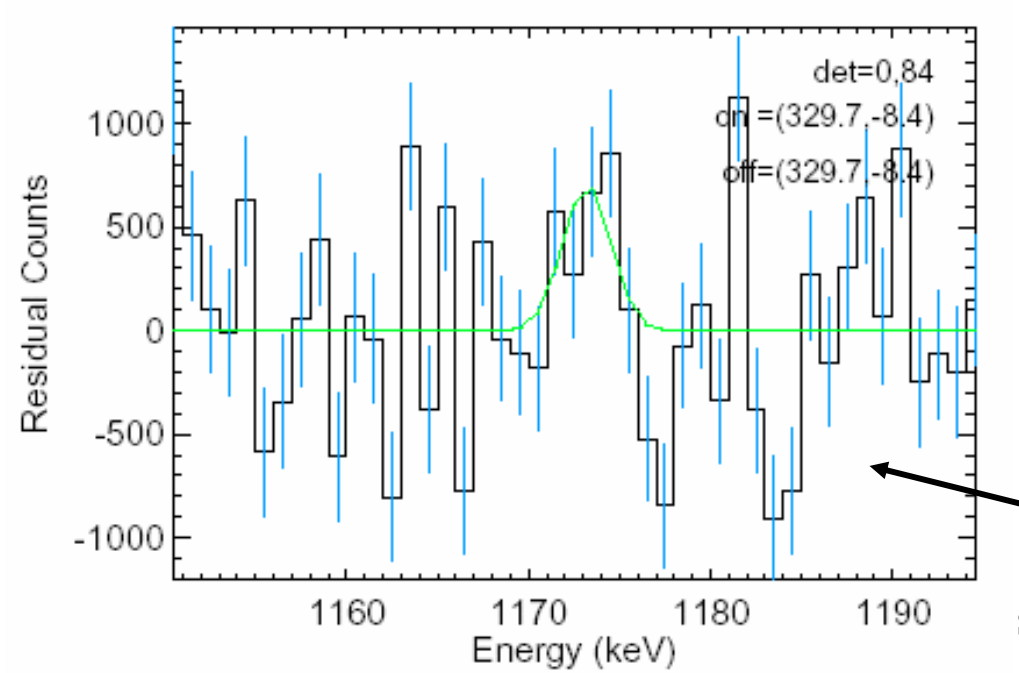

Background counts: ~$5.6 \cdot 10^5$

Source counts: ~1151 ➔

signal-to-background ratio: ~0.2%

signal-to-noise ratio: 1.54

Background-subtracted spectrum

Spectra of 1332.5 keV Line

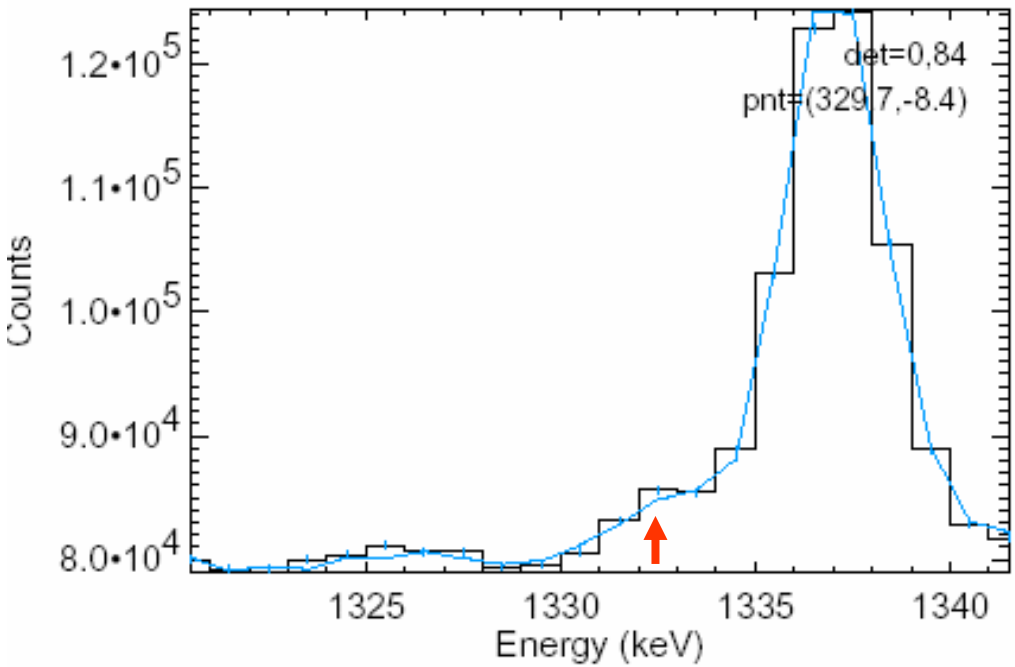

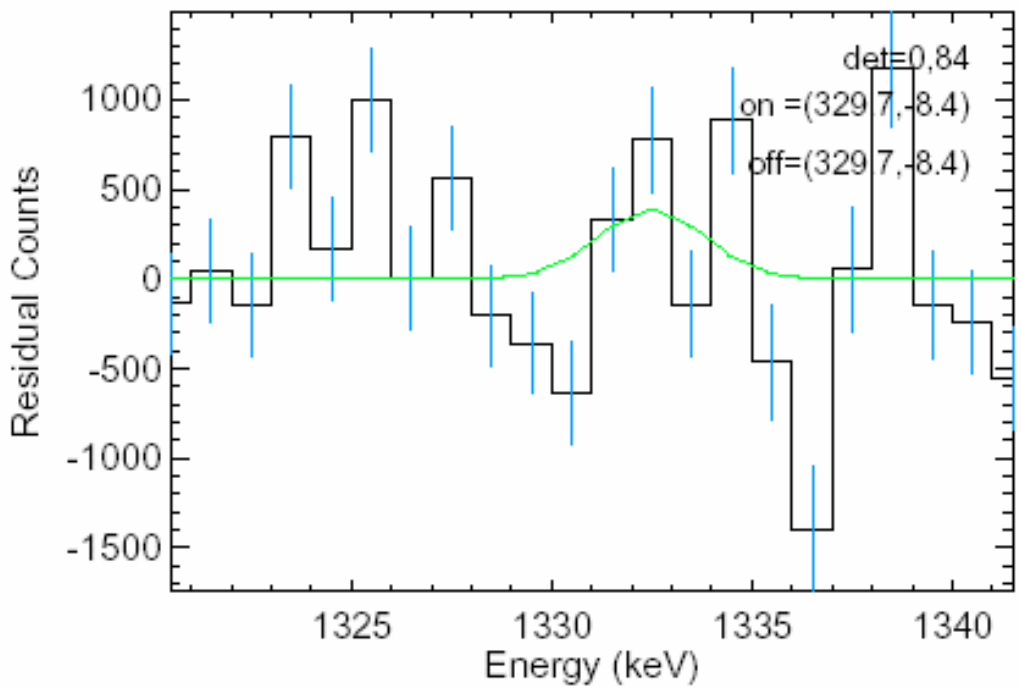

Line is obviously not visible, but a Gaussian can be fitted to the data!

Results

- The neighbouring background lines subtracted perfectly (after applying a normalization factor of ~2)
- At the iron lines a small positive excess remained
- Gaussian lines were fitted to these excesses:
  - 1173.24 keV ($\chi_{red}^2 = 2.8$):
    - Integrated counts: (1151 ± 625) cts/s $\Rightarrow 1.8\ \sigma$
    - Amplitudes: $712 \pm 252 \Rightarrow 2.8\ \sigma$
  - 1332.5 keV ($\chi_{red}^2 = 3.9$):
    - Integrated counts: (638 ± 350) cts/s $\Rightarrow 1.8\ \sigma$
    - Amplitudes: $391 \pm 215 \Rightarrow 1.8\ \sigma$
- Adding the results yields in total **2.5 σ**

Coarse Comparison with ^{26}Al Line Intensity

- ^{26}Al counts (singles & multiples): ~4500
- Efficiencies:
  - ^{26}Al: ~22%
  - ^{60}Fe: ~28%
- ^{60}Fe counts (singles & multiples): ~894
- Calculation of ratio:
  - (894 * 0.22)/(4500 * 0.28) = 0.156
- Surprisingly the data yield the expected ^{60}Fe/^{26}Al ratio of ~ 15% (making at least one theorist happy!)

Conclusions

- No detection of the ^{60}Fe lines is claimed here.
- However hints for ^{60}Fe-line emission are found.
- more data and a refined analysis are obviously needed!
- Plan is to look for the lines with singles only.
- Plan is to add the two background-subtracted spectra and derive the significance.

1173.2 keV Line (single events from AvK with Crab Background from AvK)

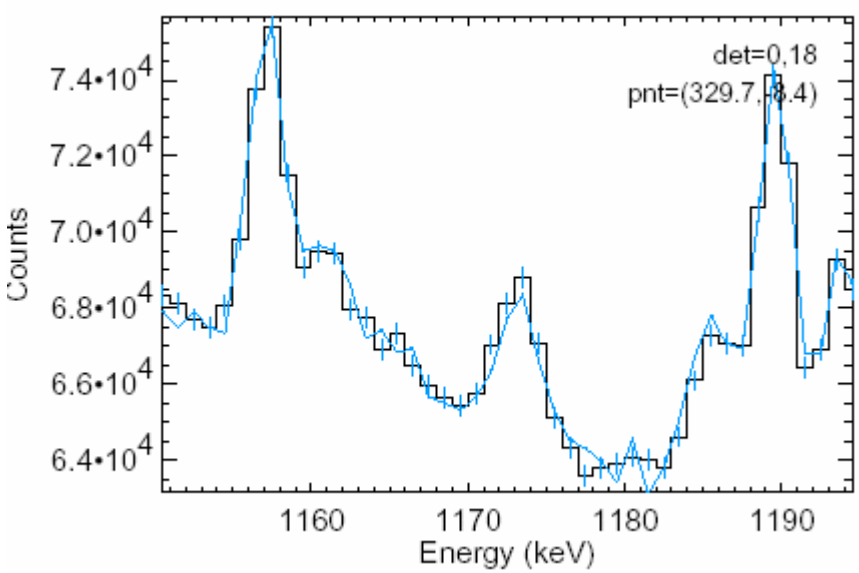

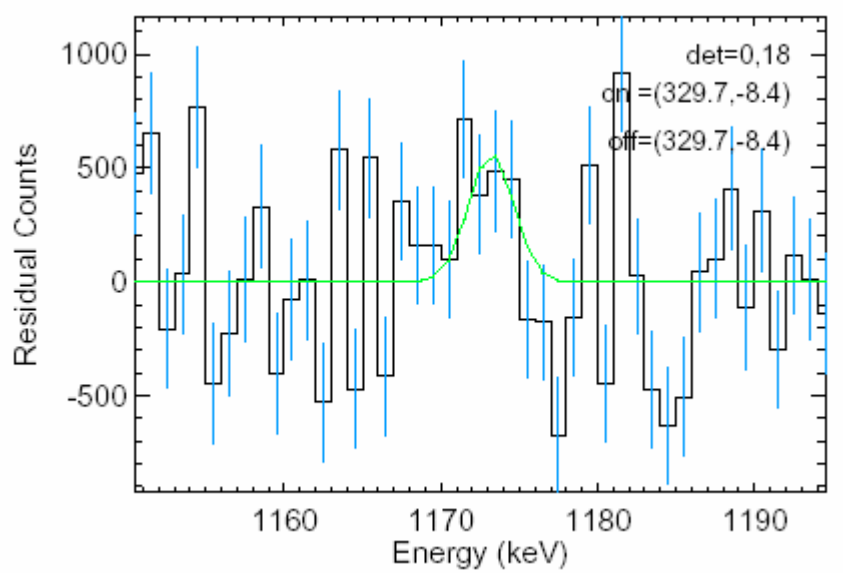

<u>Fit results:</u> $\chi_{red}^2 = 2.3$

Position: fixed at 1173.2 keV

Amplitude: 565 ± 204

Width: 1.42 keV (fitted)

Integrated counts: 1005 ± 555

Significance = 1.81 σ

1173.2 keV Line (single events from CW with Crab Background from CW)

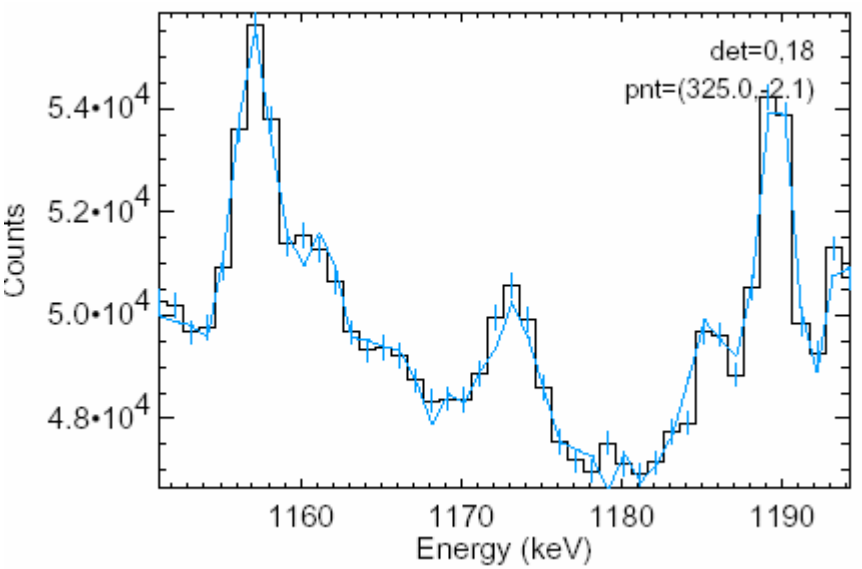

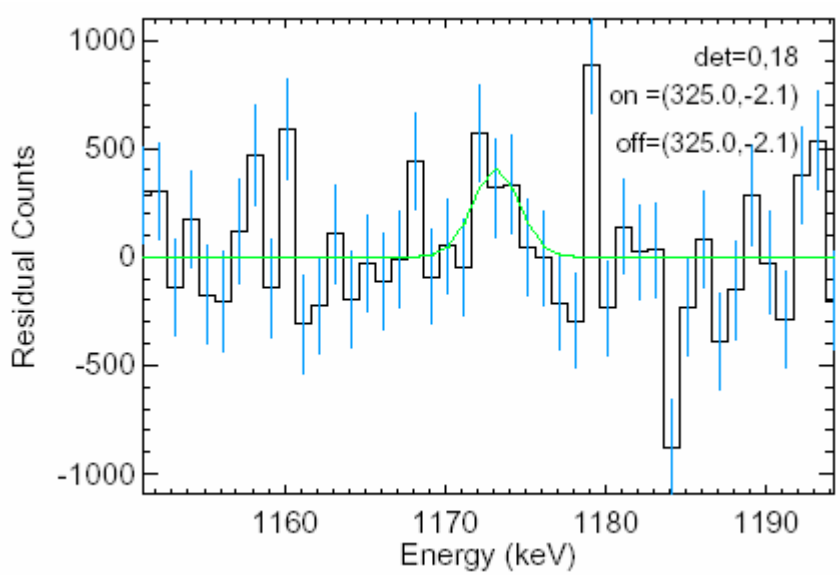

Fit results: $\chi_{red}^2 = 1.9$

Position: fixed at 1173.2 keV

Amplitude: 405 ± 150

Width: fixed at 1.42 keV

Integrated counts: 1443 ± 533

Significance = 2.71 σ

Stability of ^{69}Ge(EC)^{69}Ga Background Line at 1336.9 keV

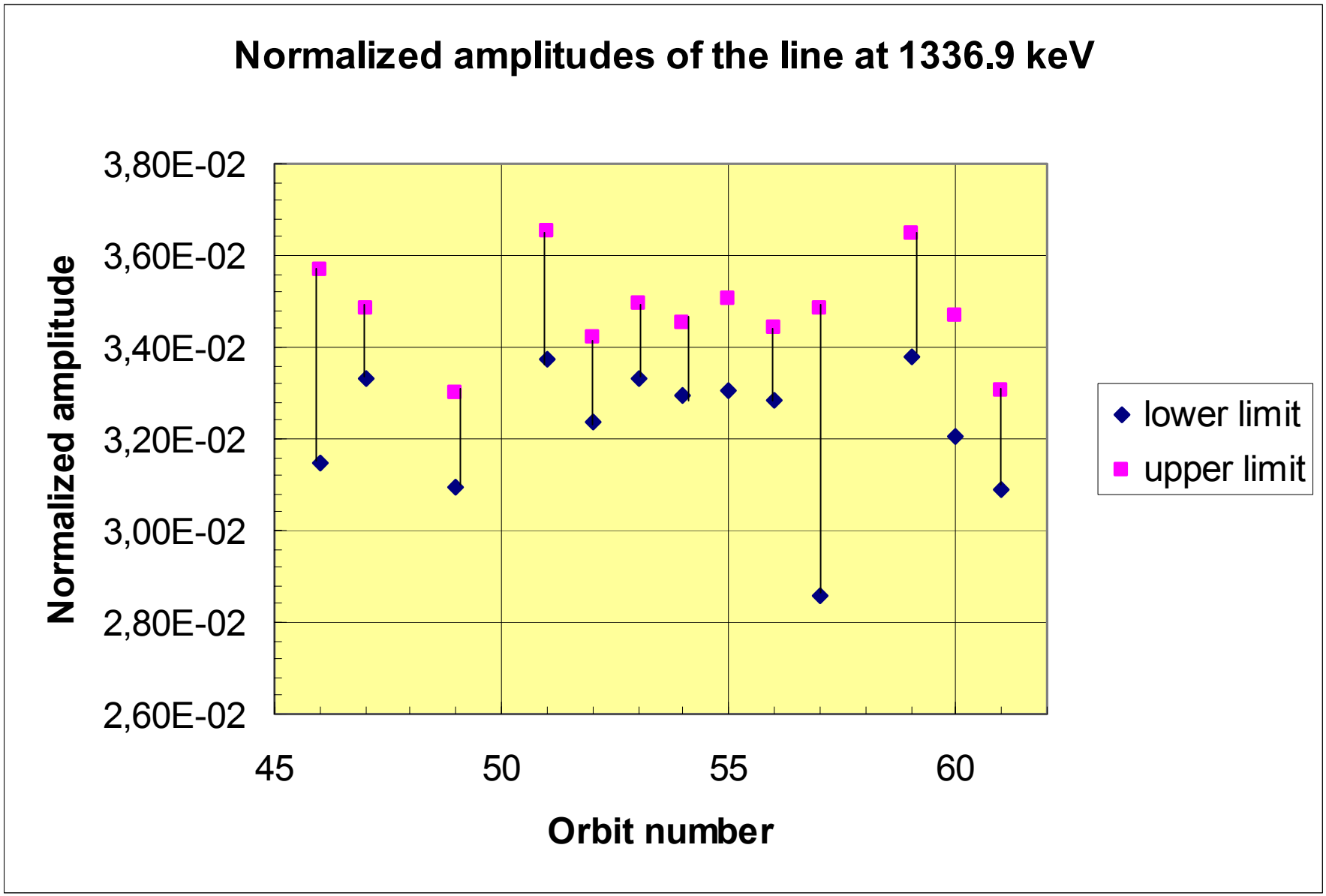

Spectra

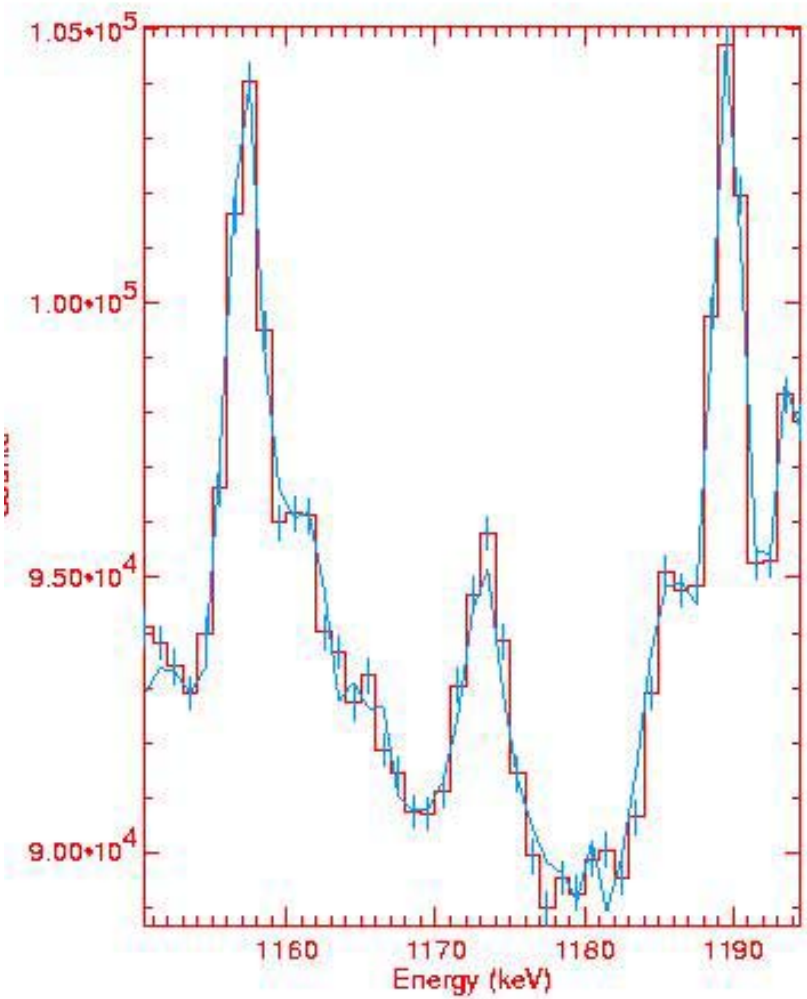
1.05•10^5
1.00•10^5
9.50•10^4
9.00•10^4
1160
1170
1180
1190
Energy (keV)

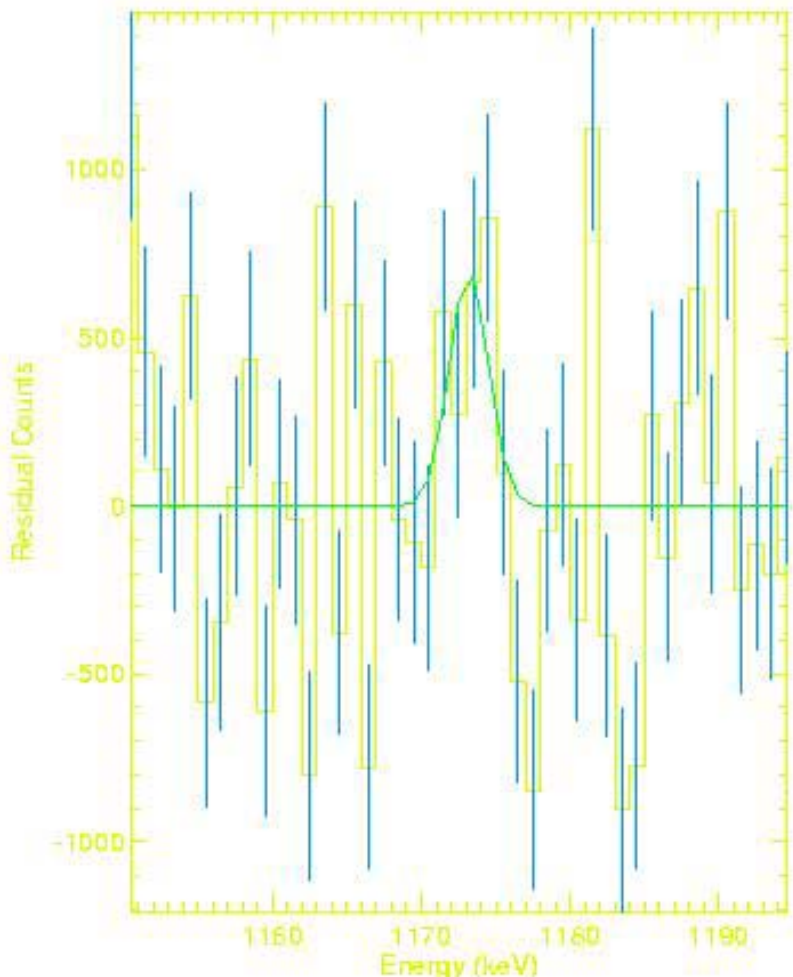
Residual Counts
1000
500
0
-500
-1000
1160
1170
1180
1190
Energy (keV)

Diffuse gamma-ray line emission from the Galaxy

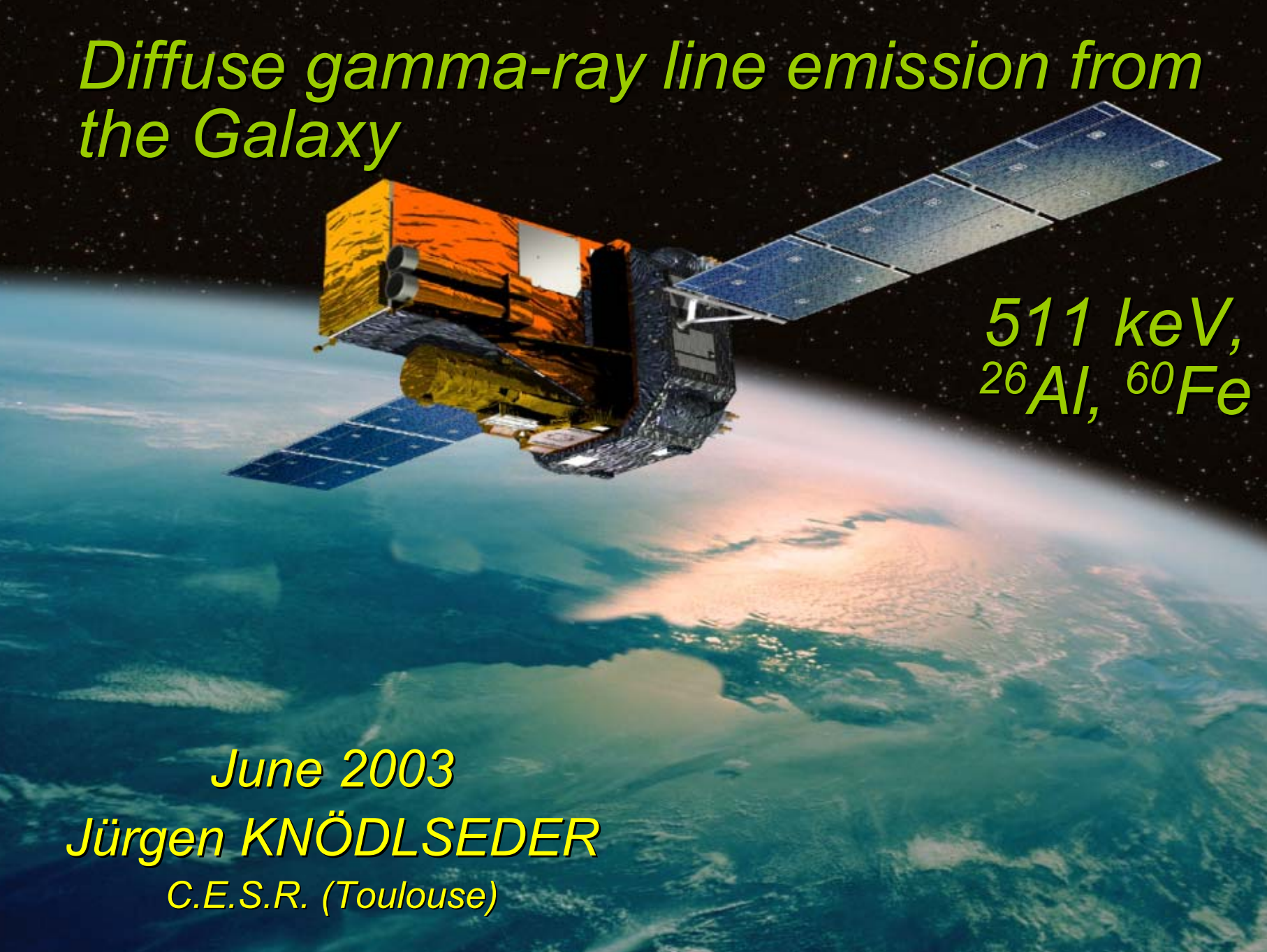

511 keV,
^{26}Al, ^{60}Fe

June 2003

Jürgen KNÖDLSEDER
C.E.S.R. (Toulouse)

Analysed data

Galactic centre region (GCDE) :

- Revolutions 47 - 66
- Detector averaged ONTIME : 1703 ks
- Pointings : 1215

Empty field observations :

- SN1987A : Revolutions 27-29, 33-35
  Detector averaged ONTIME : 718 ks

- Crab : Revolutions 43-45 (excluding revolution 42 due to strong temp. variation)
  Detector averaged ONTIME : 450 ks

Energy calibration :

- idem to last CoI meeting

1809 keV spectrum

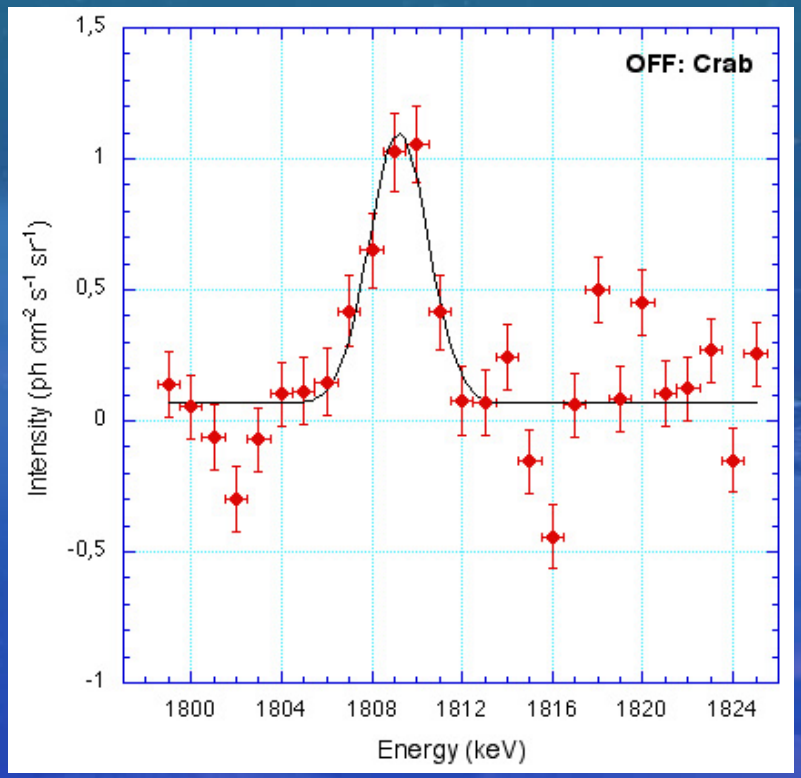

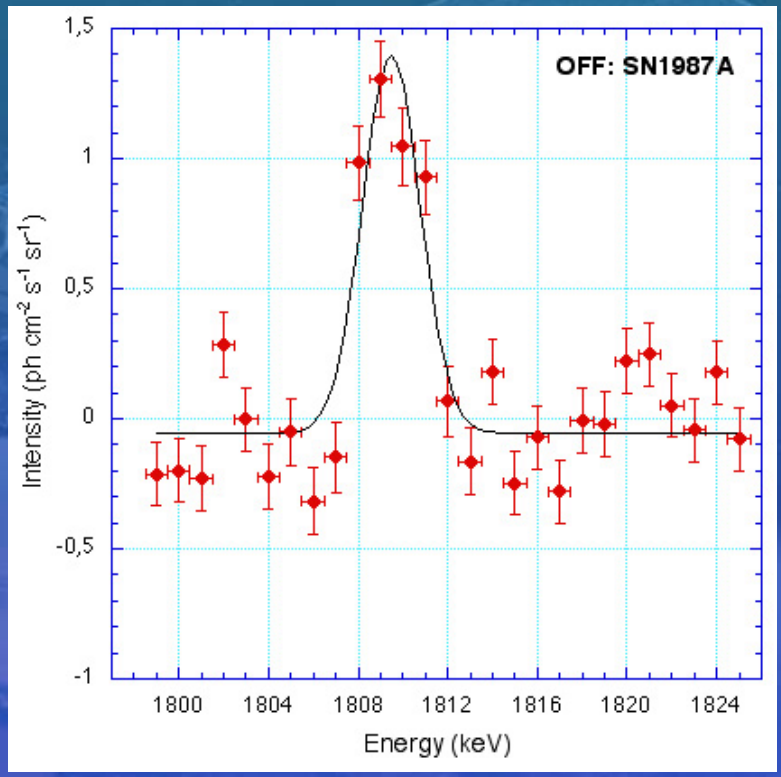

Fixed background model (GEDSAT) :

- Detection significance : 10.7 / 12.8 σ (OFF: Crab / SN)
- DIRBE 240 μm flux : (3.4 / 4.7 ± 0.4) 10^{-4} ph cm^{-2} s^{-1} sr^{-1}
- Position : 1809.2 / 1809.5 ± 0.2 keV
- FWHM : 3.1 / 3.0 ± 0.4 keV

Degradation corrections

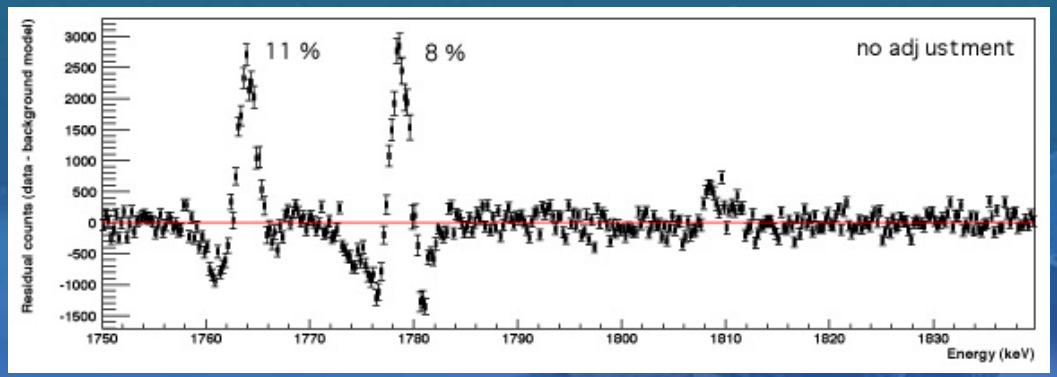

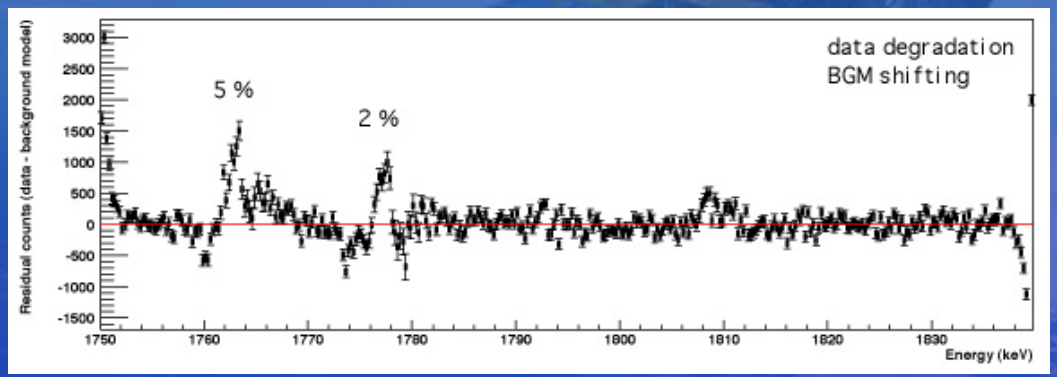

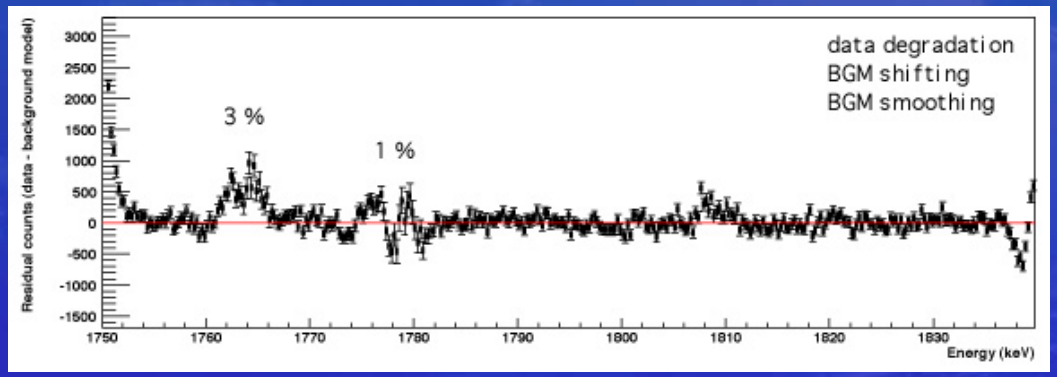

1809 keV

ON : GCDE

OFF : SN1987A

- Degradation using exponential function
- Linear shift of OFF data
- Gaussian smoothing of OFF data
- Optimisation using Chi-squared statistics on total spectrum over energy interval 1755 - 1790 keV

Degradation corrections

1809 keV

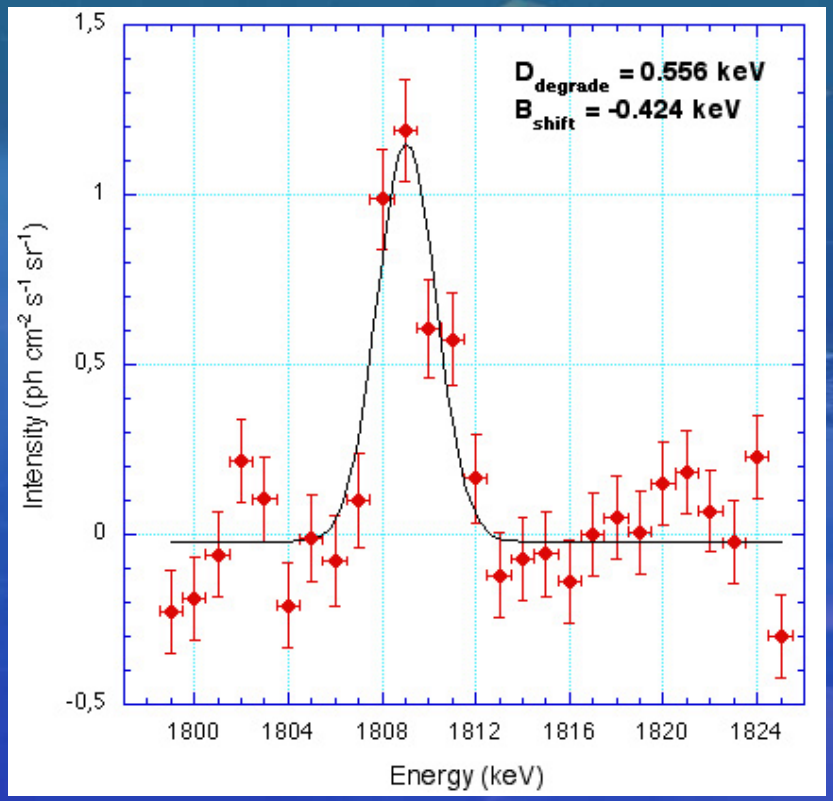

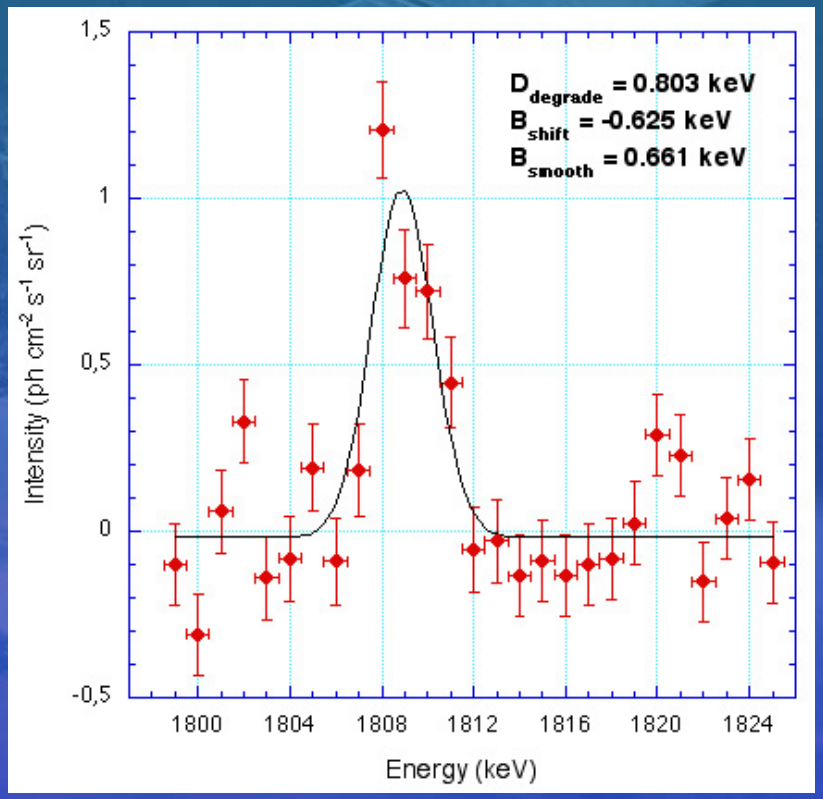

	no	D_{deg}, B_{shift}	D_{deg}, B_{shift}, B_{smooth}
Scaling	4.7 ± 0.4	3.7 ± 0.4	3.5 ± 0.4
Position	1809.5 ± 0.1	1809.1 ± 0.2	1808.9 ± 0.2
FWHM	3.0 ± 0.3	3.0 ± 0.4	3.2 ± 0.4

Background model fitting

1809 keV

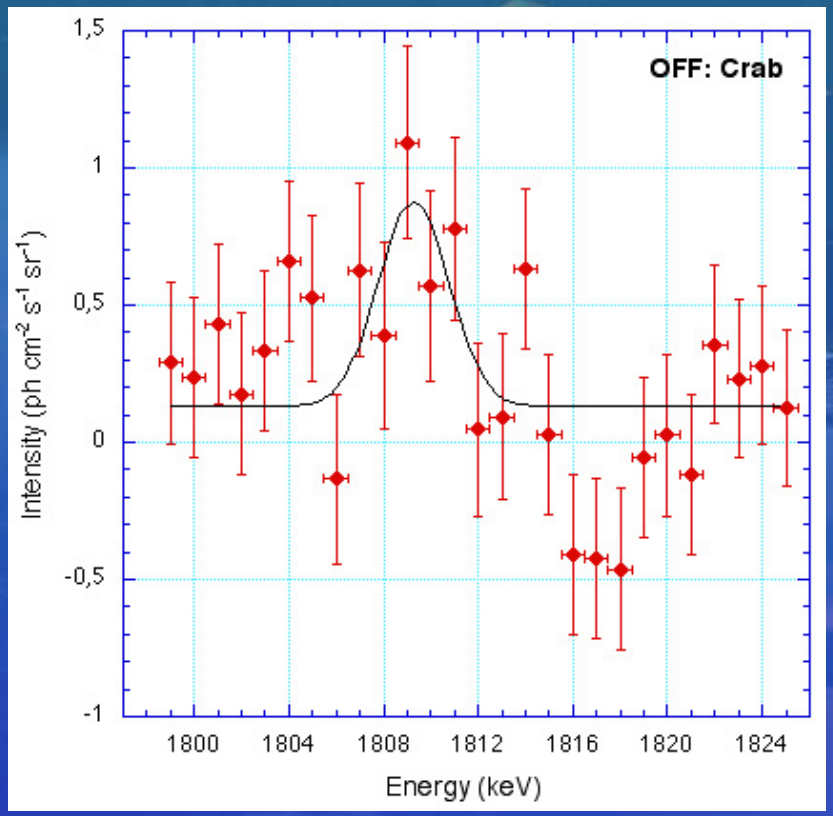

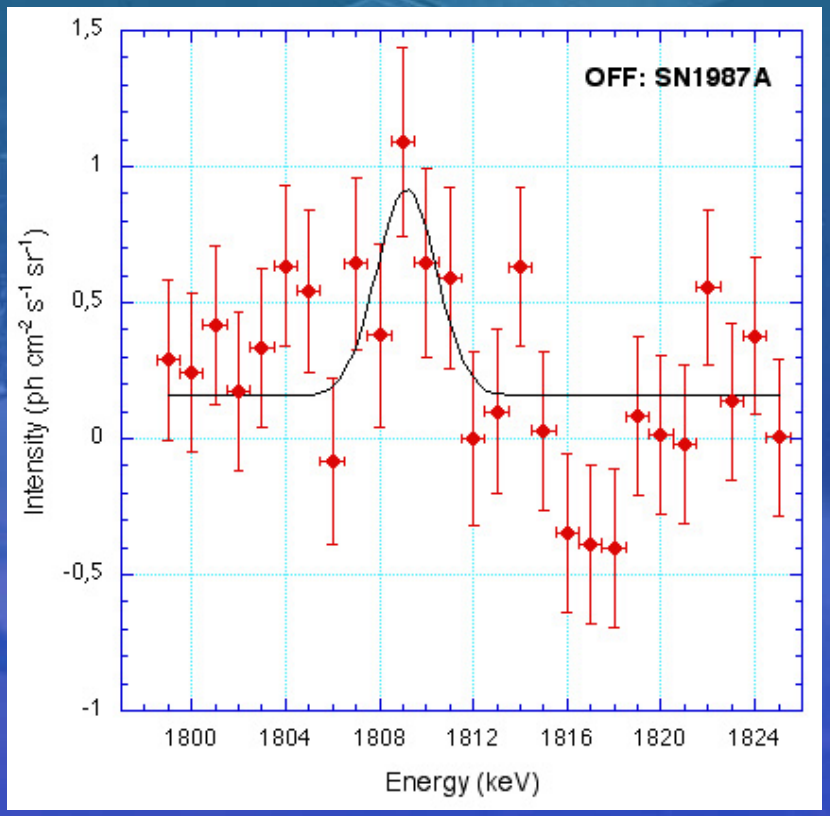

- one scaling factor for each energy bin and background model component
- result (basically) independent of OFF observation (only relative detector rate fixed)
- no significant line detection anymore

Background model fitting

511 keV

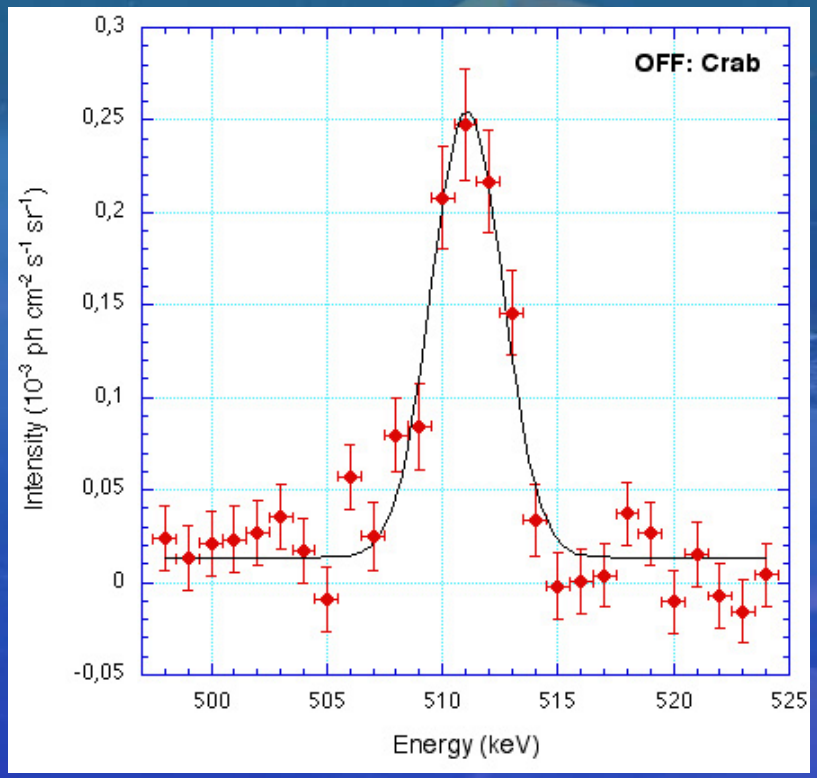

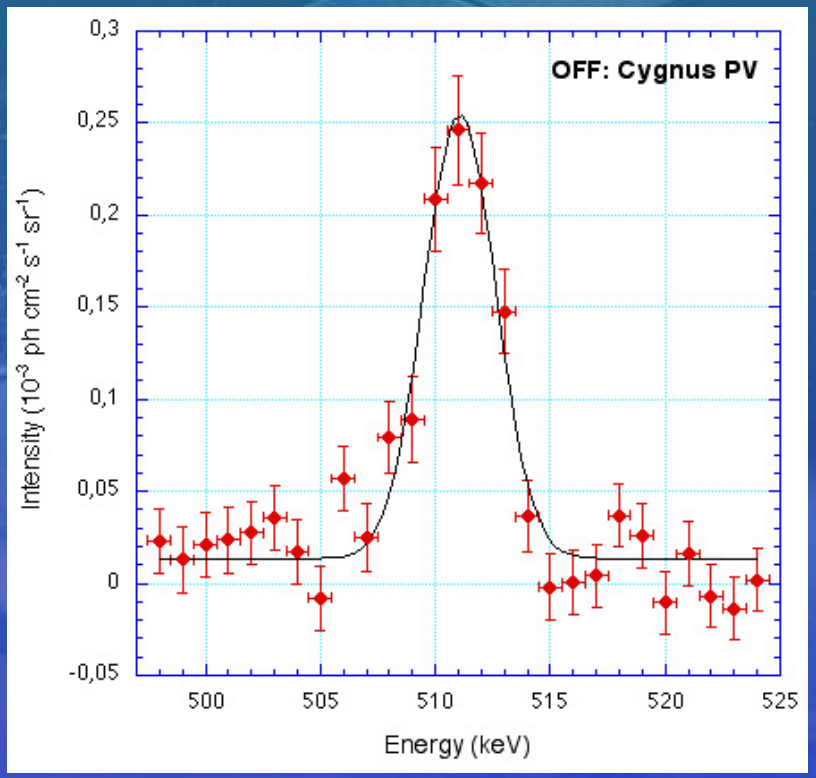

- Gaussian 10° FWHM (best fitting model)
- significance reduction by about a factor of 2
- FWHM : 3.7 ± 0.4 (±0.1) keV (systematic error from different OFF and different sky models)
- good Chi-squared (P ~ 0.5)

Background model fitting

1809 keV

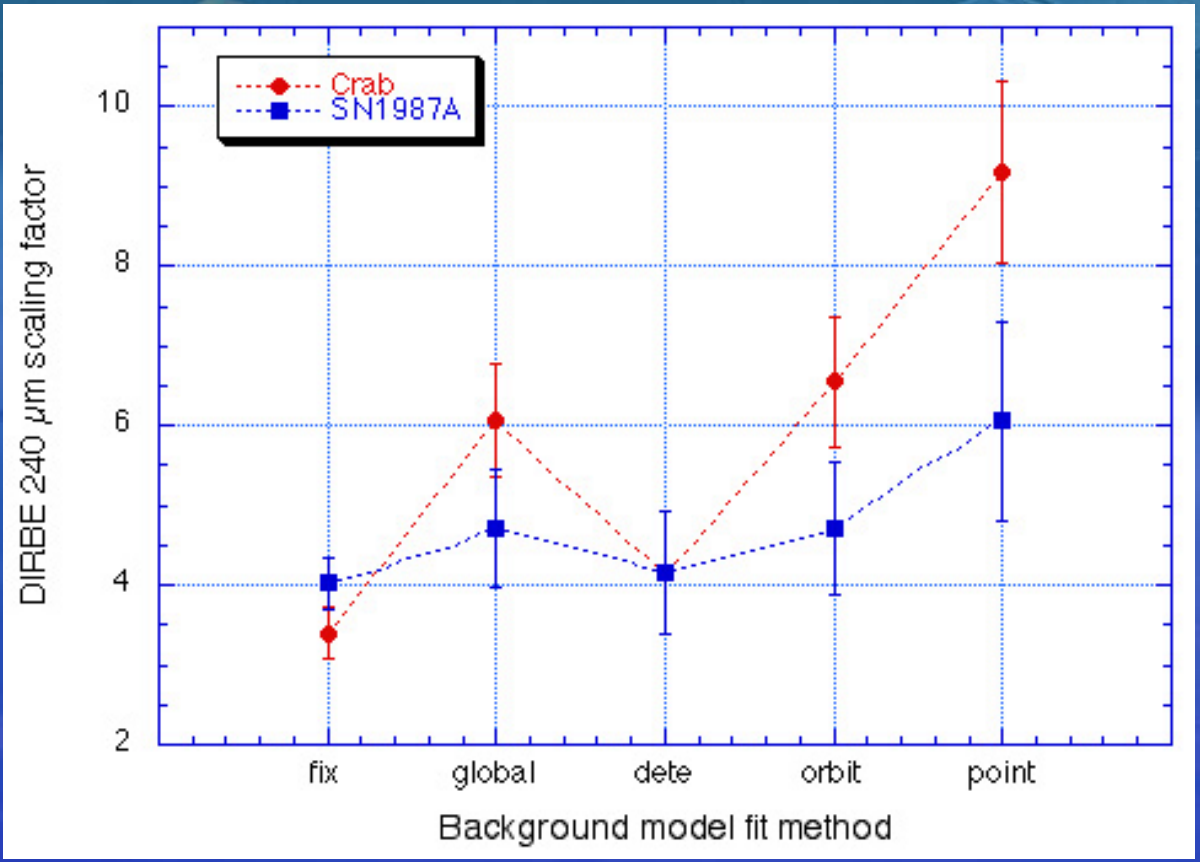

Background model uncertainties :

- up to 40% flux variations for different OFF observations
- result dependent of fit method (⇒ systematic uncertainties)

Background variations

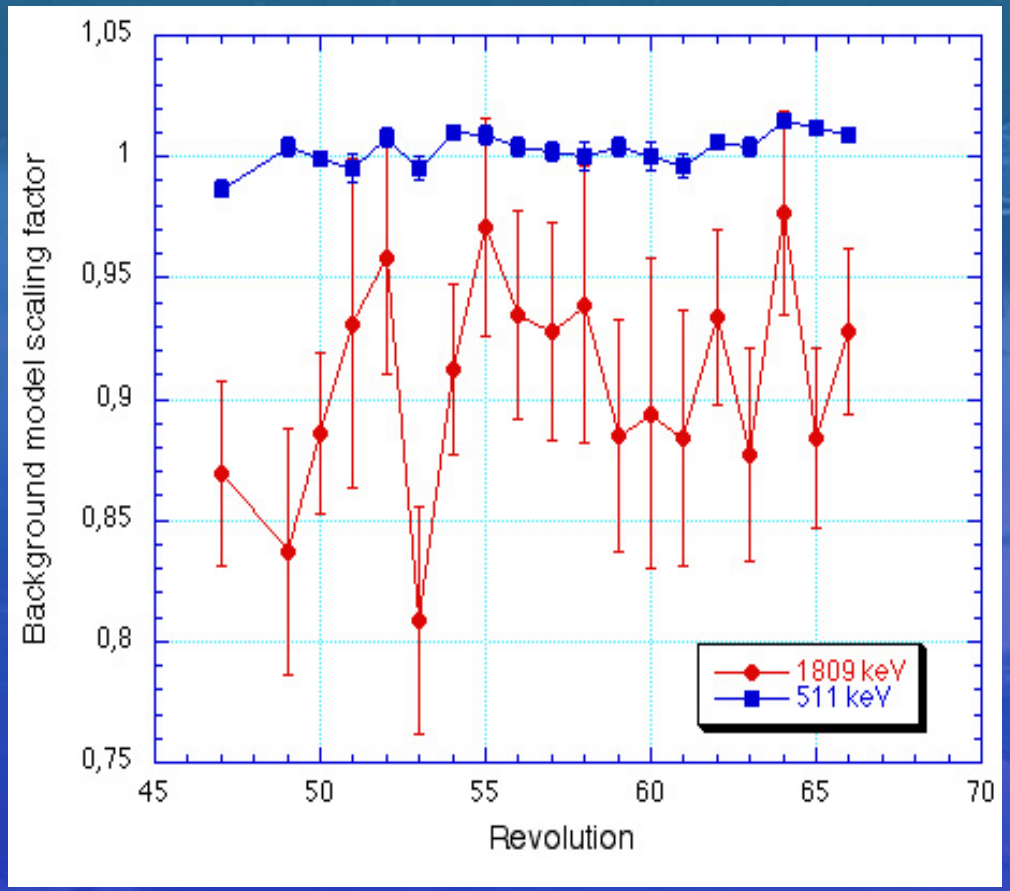

Background variation studies suggest a residual variation (w/r GEDSAT) with orbit ⇒

one BGM scaling factor per orbit

- 511 keV : Gauss 10° FWHM
  significant variation,
  modest uncertainties (≤ 2 %)
- 1809 keV : DIRBE 240 µm
  large uncertainties (up to 20 %)

Morphology determination

511 keV

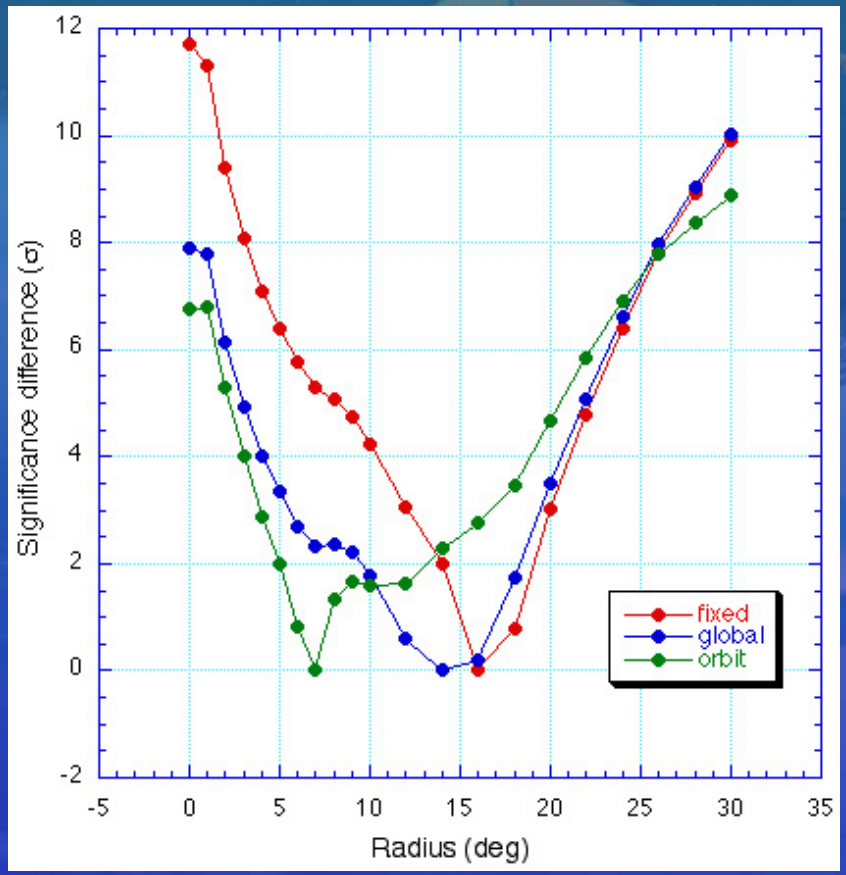

circular uniform disk fitting vs BGM fitting method

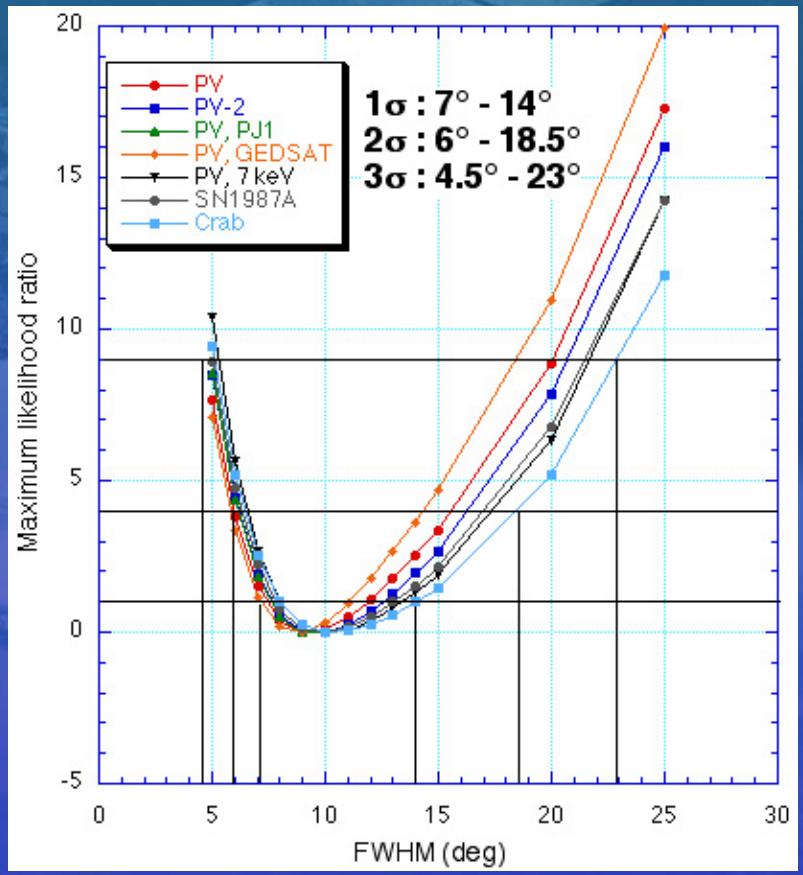

Gaussian fitting (1 factor per orbit)

1173 keV spectrum

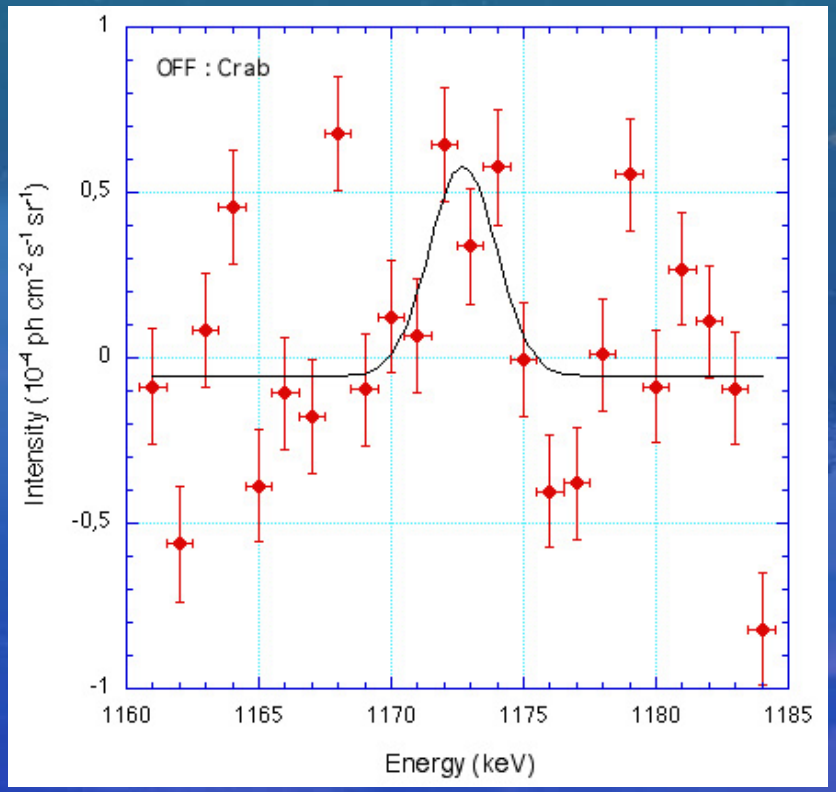

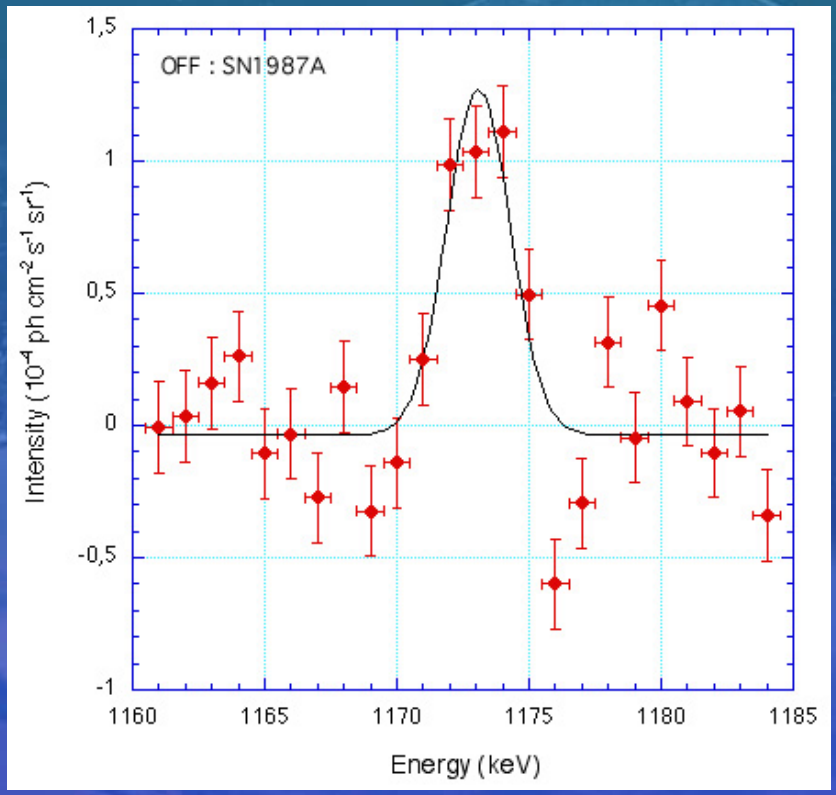

Fixed background model (GEDSAT) :

- DIRBE 240 µm flux : (2.0 / 3.9 ± 0.5) 10^{-4} ph cm^{-2} s^{-1} sr^{-1}
- Position : 1172.7 ± 0.3 / 1173.1 ± 0.2 keV
- FWHM : 3.0 ± 0.8 / 2.8 ± 0.4 keV

1333 keV spectrum

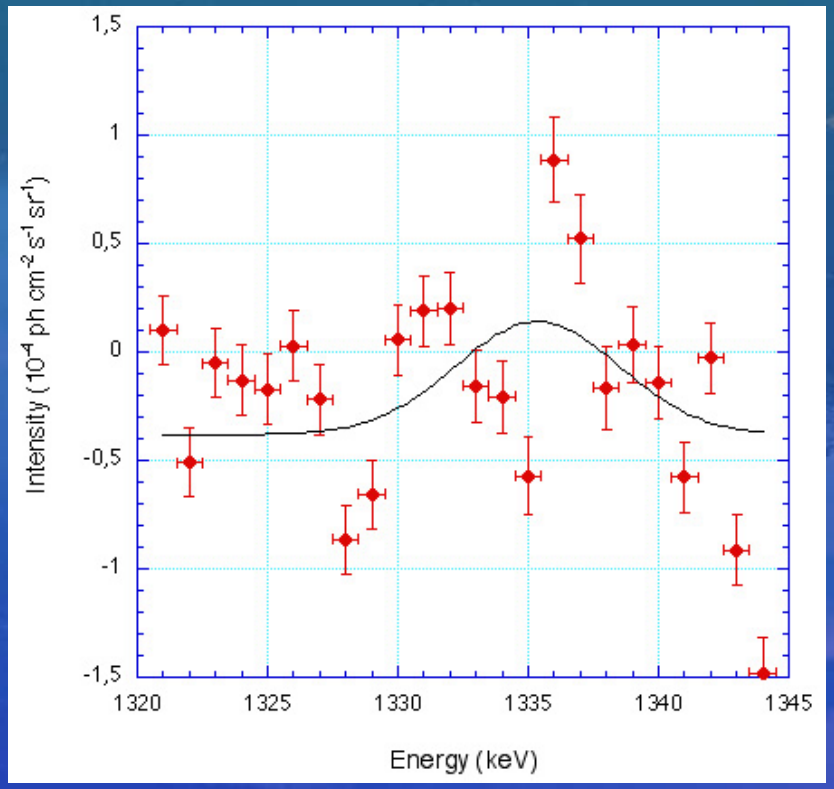

OFF: Crab

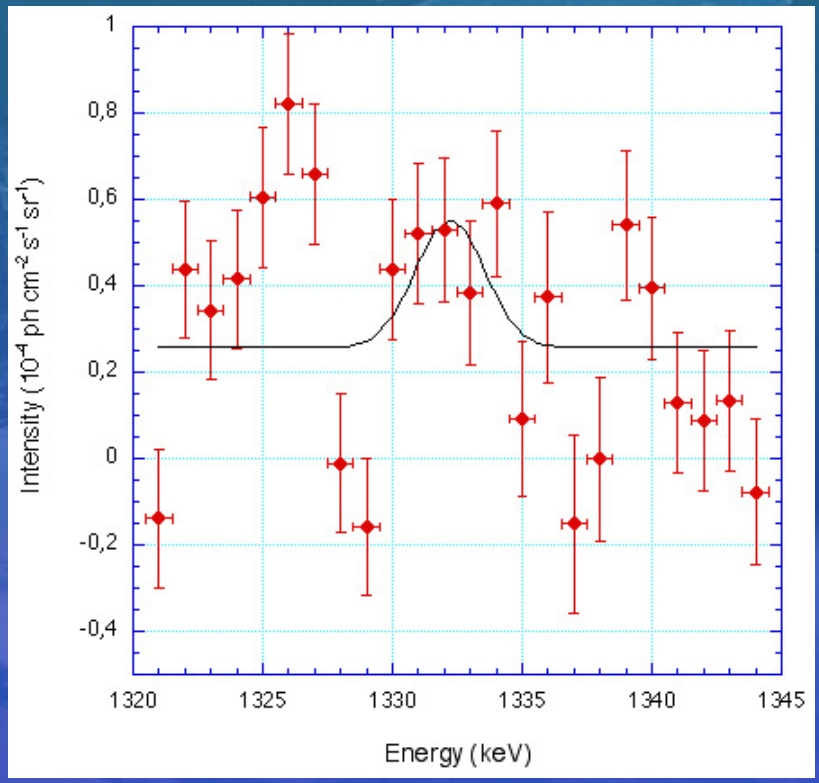

OFF: SN1987A

Fixed background model (GEDSAT) :

- DIRBE 240 μm flux : (4.1 ± 1.2 / 1.0 ± 0.5) 10^{-4} ph cm^{-2} s^{-1} sr^{-1}
- Position : 1335.4 ± 0.6 / 1332.2 ± 0.7 keV
- FWHM : 7.4 ± 1.9 / 3.1 ± 1.8 keV

Conclusions

- **1809 keV**

  Fixed background model :
  Position : 1809.1 ± 0.2 keV (± 0.2 keV)
  FWHM : 3.2 ± 0.4 keV (± 0.1 keV)
  Flux : (3.5 ± 0.4) (±0.1) 10^{-4} ph cm^{-2} s^{-1} from central steradian

  Uncertainties : absolute flux value, spectral shape

- **511 keV**

  Introduction of moderate number of free parameters reduces systematic uncertainties in the analysis (see P. Jean presentation)
  Morphology : one global scaling factor per orbit
  Spectroscopie : one global scaling factor for each of the background model components and energy bins

- **1173 & 1333 keV**

  No evidence for signal so far, yet only crude analysis (no systematics assessed).
  3σ statistical error (SE+PE only, single line) : 1.1 10^{-4} ph cm^{-2} s^{-1} sr^{-1} (31% 1809 keV flux)
  2σ upper limit (SE+PE only, single line) : 0.8 10^{-4} ph cm^{-2} s^{-1} sr^{-1} (21% 1809 keV flux)

Galactic 511 keV emission

- Data analysis
- Background models
- Morphological study
- Spectral analysis
- Conclusion

Data analysis

- GCDE & GPS
  - revolutions 47 - 66
  - ONTIME ~ 1667 ks

- Pointings

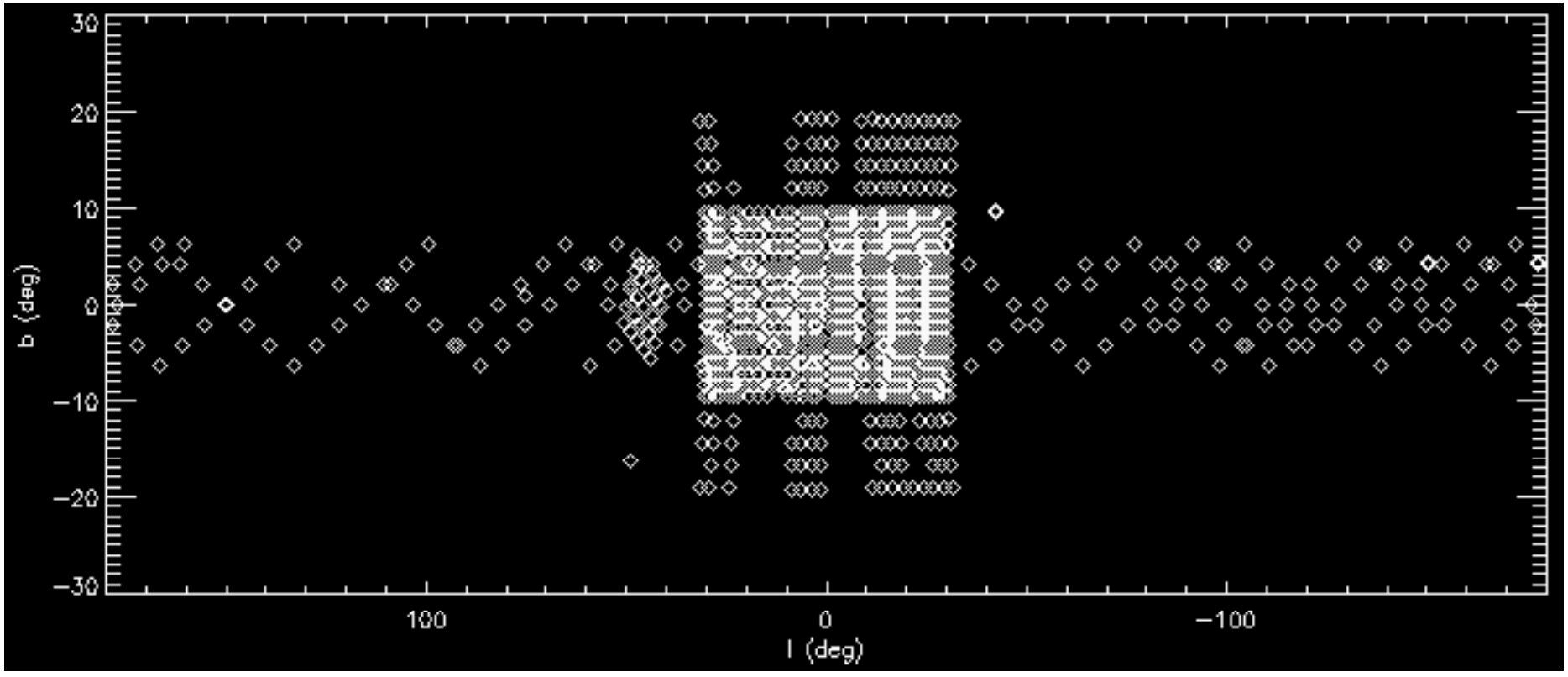

Data analysis

- Exposure

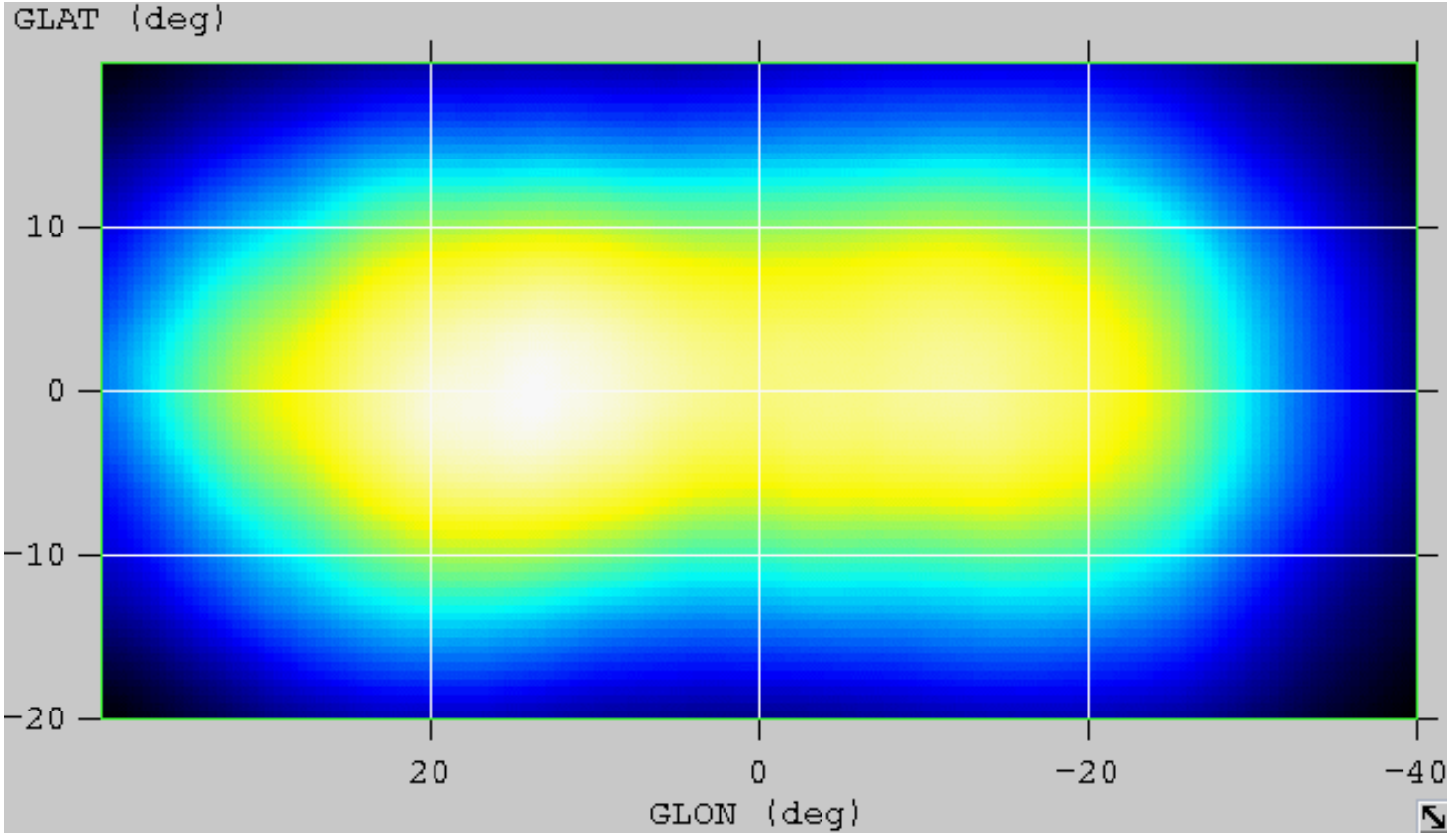

- Energy calibration:
  - linear, performed for each orbit
  - 438.64 keV (^{69}Zn), 1107.01 keV (^{69}Ge), 1778.97 keV (^{28}Al)
  - accuracy <0.05 keV at 511 keV

  => average instrumental resolution : 2.16 keV

Background model

- Two components:
  - $b_{line,d,p,e}$ = line from an OFF observation scaled by $GEDSAT_{d,p}/\langle GEDSAT_{OFF,d}\rangle$
  - $b_{cont,d,p,e}$ = mean continuum from ON observation modulated by $GEDSAT_{d,p}/\langle GEDSAT_{ON,d}\rangle$

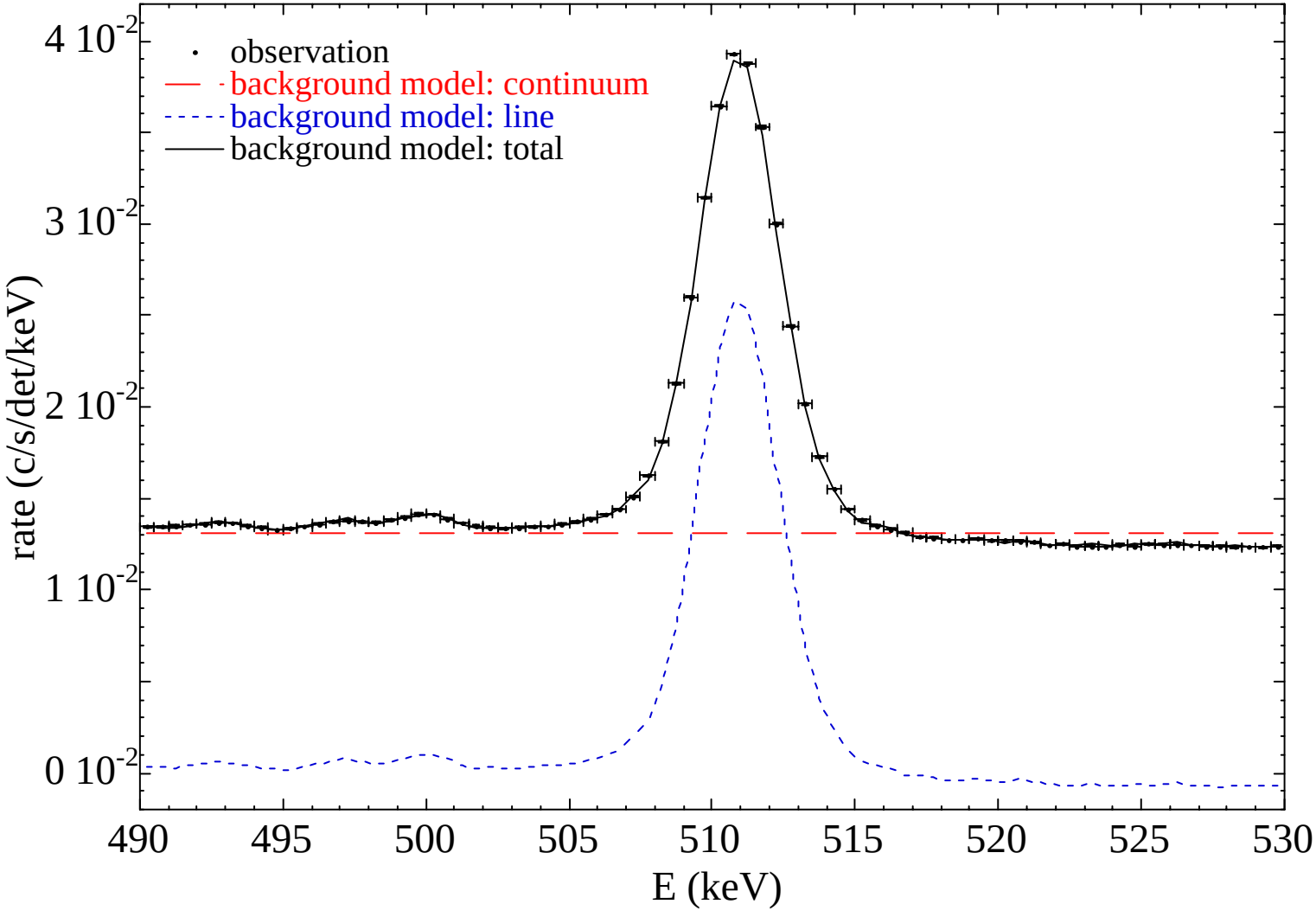

Background model

- OFF observations :
  - rev. 19-25 : PV phase (Cyg)
  - rev. 27-29 & 33-35 : LMC - SN87A
  - rev. 43-45 : Crab

- Systematics: tests performed on OFF data show that using the background model as an absolute model leads to up to ~2% of systematic error

- Solution: fit background model scaling factors to the data

  - for morphological study : $b_{line,p,d,e} \rightarrow \alpha_{orbit}\, b_{line,p,d,e}$

  - for spectral study : $b_{line,p,d,e} \rightarrow \alpha_{e}\, b_{line,p,d,e}$
    $b_{cont,p,d,e} \rightarrow \beta_{e}\, b_{cont,p,d,e}$

Morphological study

- Richardson-Lucy

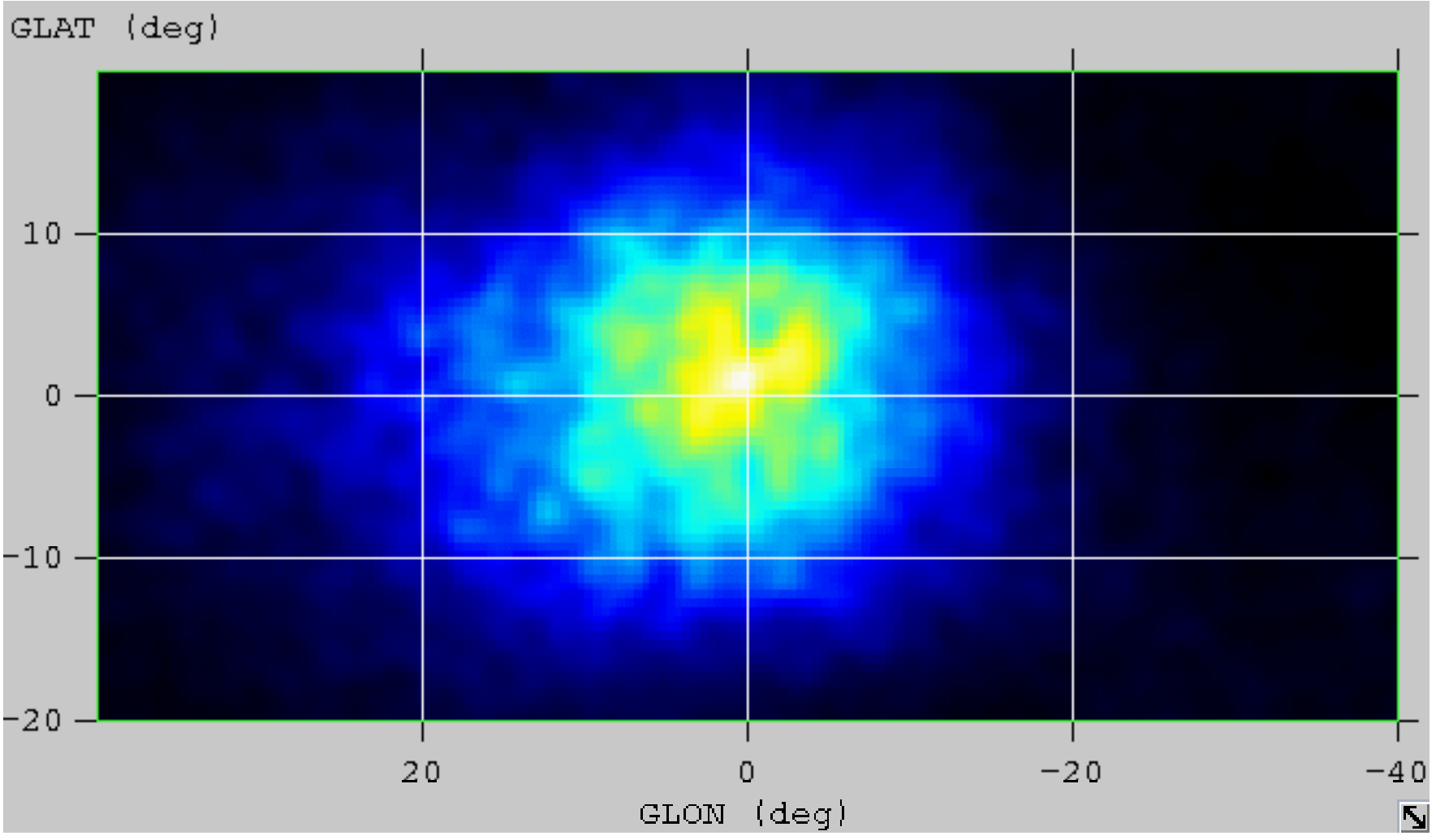

Morphological study

- Model fitting with gaussian spatial distributions

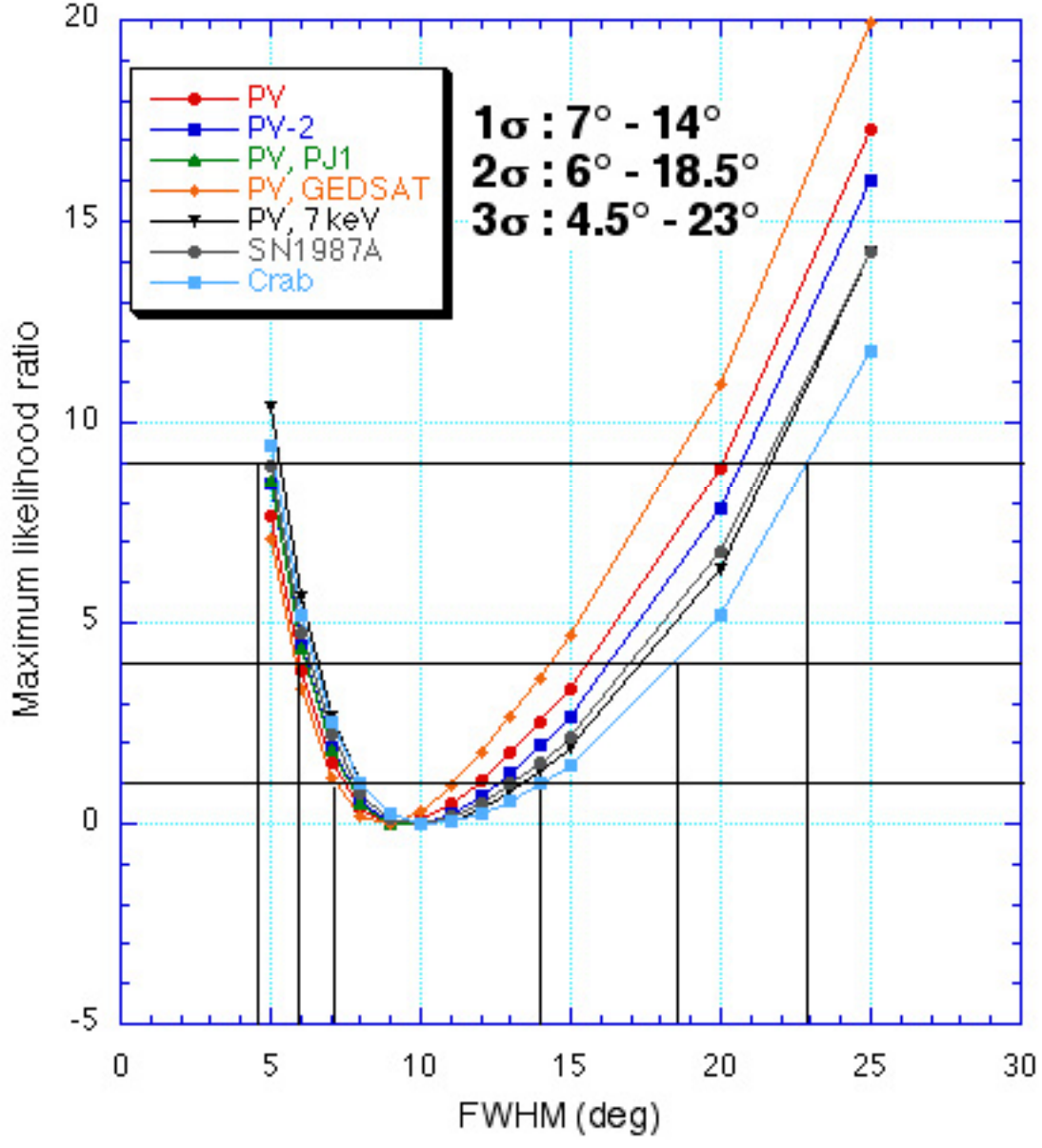

Morphological study

- Model fitting : a centered gaussian of 10° FWHM

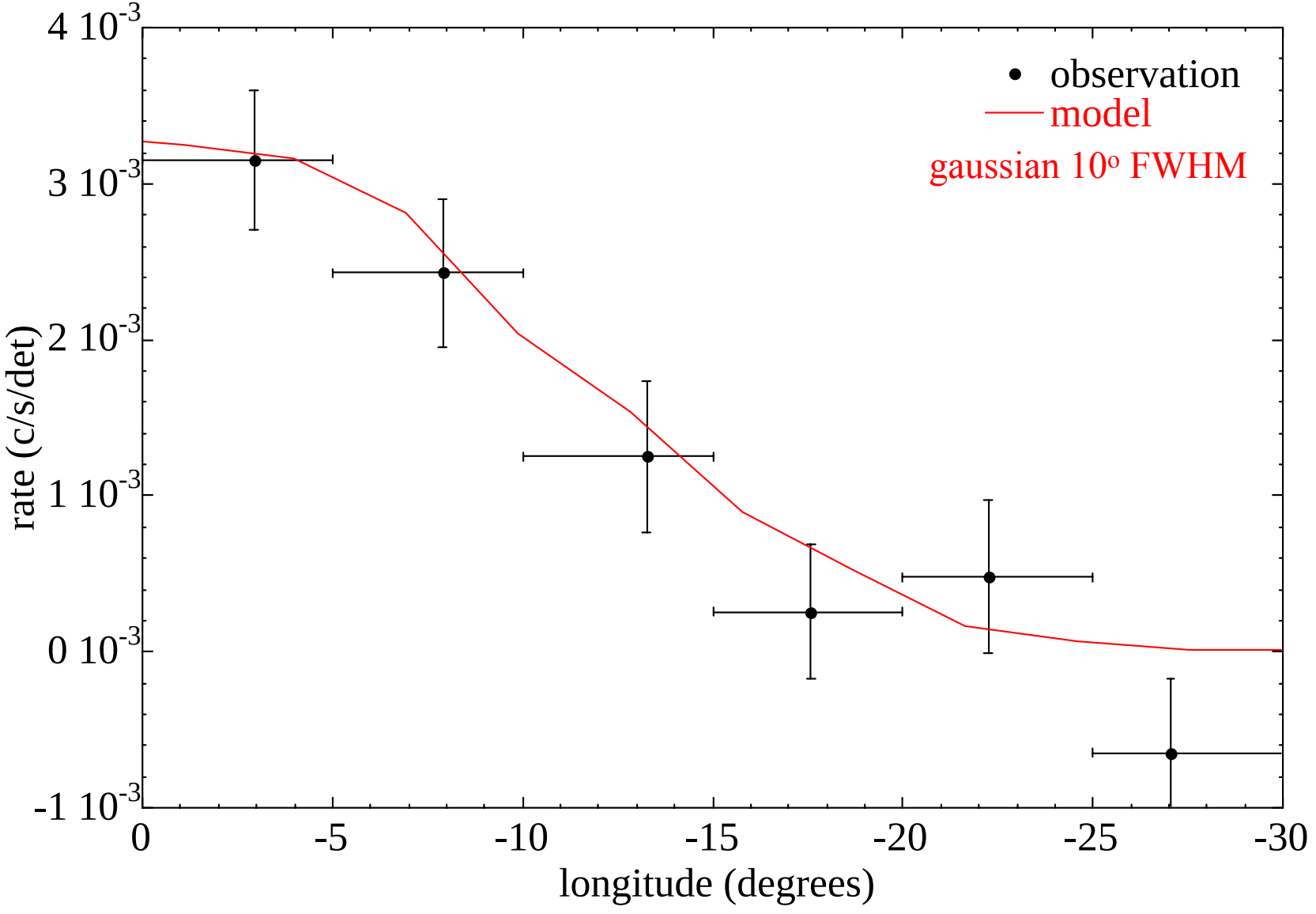

Spectral study

- model fitting assuming a gaussian spatial distribution (FWHM = 10º)

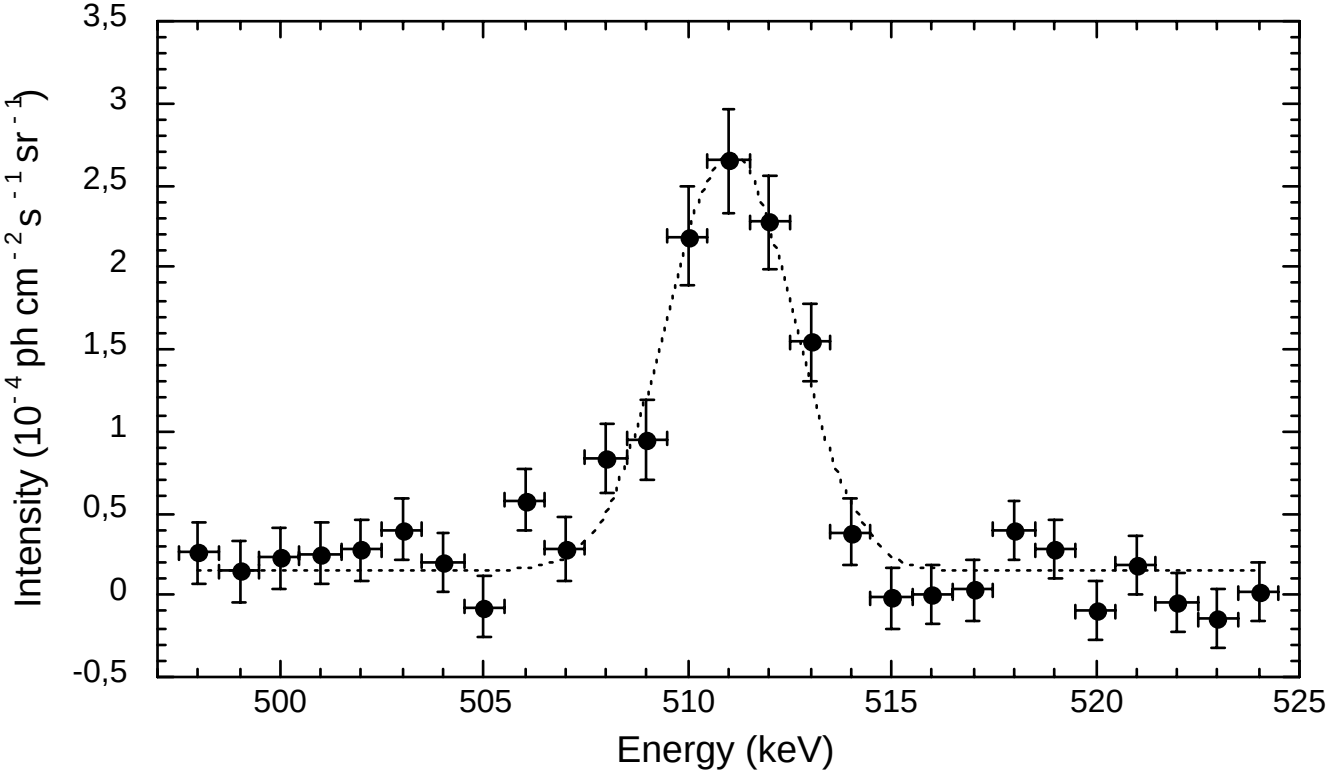

- Results taking into account ’uncertainties ’ in spatial distributions

flux:	$(0.99\ ^{+0.47}_{-0.21})\ 10^{-3}$	photons s^{-1} cm^{-2}
width:	$(2.95\ ^{+0.45}_{-0.51})$	keV (FWHM)
line position:	$(511.06\ ^{+0.17}_{-0.19})$	keV

Conclusion

instrument	year	flux $[10^{-3}\ ph\ cm^{-2}\ s^{-1}]$	centroid $[keV]$	width (FWHM) $[keV]$	references
HEAO-3[a]	$1979-1980$	1.13 ± 0.13	510.92 ± 0.23	$1.6^{+0.9}_{-1.6}$	Mahoney *et al.* 1994
GRIS[b]	1988 *and* 1992	0.88 ± 0.07		2.5 ± 0.4	Leventhal *et al.* 1993
HEXAGONE[b]	1989	1.00 ± 0.24	511.33 ± 0.41	$2.90^{+1.10}_{-1.01}$	Smith *et al.* 1993
TGRS[c]	$1995-1997$	1.07 ± 0.05	510.98 ± 0.10	1.81 ± 0.54	Harris *et al.* 1998
SPI	2003	$0.99^{+0.47}_{-0.21}$	$511.06^{+0.17}_{-0.19}$	$2.95^{+0.45}_{-0.51}$	this work

[a] assuming a point source.
[b] flux in the field of view (17° and 18° for GRIS and HEXAGONE respectively).
[c] gaussian-shape source (FWHM 30°).

- Spatial distribution :
  - compact source in the GC excluded
  - extension 6^o - 18^o FWHM (gaussian shape)

- Further work :
  - study of background at 511 keV (-> model)
  - spatial distributions from earlier measurements
  - galactic distributions
  - positronium...